Development of Composites for Bone Repair

Thesis submitted by

Kirsty Alexandra Iskrzycka Main

For the degree of

Doctor of Philosophy

Eastman Dental Institute

Division of Biomaterials and Tissue Engineering

University College London

256 Grays Inn Road

London

WC1X 8LD

2013

DECLARATION

I, Kirsty Alexandra Iskrzycka Main confirm that the work presented in this thesis is my own. Where information has been derived from other sources, I confirm that this has been indicated in the thesis.

ACKNOWLEDGMENTS

Firstly I would like to thank my supervisor Dr. Anne Young, for giving me seemingly limitless time, patience and guidance throughout the project. Dr. Juha-Pekka Nuutinen and everyone else at Ozics for making the research possible and providing inspiration and direction.

A special thanks to Dr. Graham Palmer, Dr. Wendy Xia and Dr Nicky Mordan for their technical support and to Dr. Vehid Salih, Dr. Ensanya Abou-Neel and Prof. Peter Revell for all their help and invaluable experience with in-vivo work.

I would like to thank Prof. Jonathan Knowles for his support in the department.

I am grateful to all past and present students and staff of BTE department for academic support and friendship over the past four years.

Finally I would like to thank my family and friends for their support without which I would not have been able to complete this body of work.

ABSTRACT

Current bone repair materials can be too stiff compared to native bone and with insufficient strength for load bearing applications often with brittle fracture behaviour. In addition they can have unacceptably high polymerization shrinkage and decline in strength with time. This thesis describes the development of chemical cure, silica reinforced dimethacrylate composites and discusses their viability as alternatives for bone repair. The intended applications of these composites include hip fracture screw augmentation and vertebroplasty

Characterization and comparison of cement materials was central to this thesis. The handling of the materials was assessed qualitatively via repeated delivery and mixing whilst the rate and degree of cure was determined from Fourier Transform Infrared (FTIR) spectroscopy. This cure data was used with composition to calculate and compare the volumetric shrinkage of materials. Biaxial testing gave the fracture behaviour, flexural strength and Young's modulus of cements.

The properties of several existing bone cement materials (including composite cements Cortoss and Comp06 and PMMA cements Palacos R and Simplex P) were compared using the techniques above.

Subsequently a variety of (di)methacrylate monomers, silica fillers and silica and polymer fibres were screened, and monomer and filler systems selected for further testing.

The levels of each component in the selected systems were varied systematically and the effects on trends in mechanical properties were quantified. The interaction between level of initiator and the chosen monomer system was investigated and the polymerization reaction described in terms of kinetic theory.

It was found that PPG DMA, combined with UDMA and HEMA monomers, and silane treated silica glass particles and fibres could produce materials that cured more

extensivley than existing bone cements (69 – 97 % methacrylate conversion compared to 86 % and 64 % for Palacos and Cortoss respectively). A PPG DMA composite achieved a flexural strength of 93 MPa that was maintained even after 20 weeks storage in hydrated conditions, unlike Cortoss declined in strength by 40 % following hydrated storage. Maintainance of good mechanical properties is essential for load bearing applications. This PPG DMA composite had a stiffness of 2.2 GPa, whilst PMMA cements and Cortoss had Young's moduli 1.6 and 3.4 GPa respectively. Moreover these materials were found to perform well in-vivo in a lapine femoral condyle model.

Table of Contents

LIST OF ABBREVIATIONS

ATR FTIR	Attenuated total reflectance fourier transform spectroscopy
BFS	Biaxial Flexural Strength
BHT	Butylated hydroxy toluene
BisEMA	Ethoxylated bisphenol-A dimethacrylate
BisGMA	Bisphenol A glycidyl methacrylate
BP	Benzoyl Peroxide
DDMA	1-10 decanediol dimethacrylate
DMPT	Dimethyl para toluidine
E	Young's Modulus
EDX	Energy dispersive X-ray
HEMA	Hydroxyethyl methacrylate
IFD	Initiator factorial design
MCPM	Monocalcium phosphate monohydrate
MicroCT	X-Ray Microtomography
MMA	Methyl methacrylate
PETA	Pentaerythritol tetraacrylate
PFC	PPGDMA fibre composite
PLR	Powder to liquid ratio
PMMA	Poly(methyl methacrylate)
PPGDMA	Poly (propylene glycol)425 dimethacrylate
PPGMMA	Poly(propylene glycol) 300 monomethacrylate
Raman IR	Raman infrared spectroscopy
SEM	Scanning electron microscopy
TEGDMA	Tri(ethylene glycol) dimethacrylate
Tg	Glass transition temperature

UDMA	Urethane dimethacrylate
XRF	X-ray fluorescence
βTCP	Beta-tricalcium phosphate

LIST OF TABLES

LIST OF FIGURES

1 Introduction and Literature Review

In the following sections different bone cement materials and applications will be introduced as motivation for this project. The composition and shortfalls of selected cement materials will be described and a review of the literature surrounding research into their development will be presented. Through this introduction the scope and aims of this project will be defined.

1.1 Bone Cement: Definition and History

Definition

Bone cements are a class of synthetic materials that are implanted into the body to repair damaged bone. In this thesis, a bone cement is defined as a paste-like material that is implanted whilst soft, to repair bone tissue in a range of applications, which then cures within the body. Bone cements can either remain within the body for many years (non-degradable) or be broken down by biological processes and replaced by new bone growth (degradable). Bone cements should not be confused with bone grafts; in which bone tissue (either from the patient or another human or animal source) is used to repair bone defects. Bioactive glasses are also not considered bone cement materials. Non-degradable bone cement materials will be the focus in this thesis, neither bioactive glass nor bone grafts will be covered.

History

One of the first reported instances of using a non-biological material to repair bone was by Dressman in 1892, using plaster of Paris (1). Poly(methyl methacrylate) (PMMA) has been used historically as an acrylic ‘glass’ being used extensively in World War II in windshields of aircraft and submarines. Following this Charnley noticed that PMMA was biologically inert as servicemen wounded with PMMA shrapnel did not show any adverse biological response to the material. He encouraged the use of methyl

methacrylate resins in orthopaedic surgery from the 1940's onwards (2,3). Since this time PMMA has been established as a major medical material with a huge number of applications including, but not limited to, bone repair, contact lenses, denture and impression materials in dentistry. Although the prevalence of PMMA in orthopaedics and dentistry is clear different types of bone cement have emerged.

1.2 Applications and Materials

There are a variety of cement materials available for various applications. In this section a selection of these applications and materials will be summarized. This is by no means an exhaustive list but is intended to highlight the most prevalent indications of common bone cement materials. The incidence of each usage will also be discussed.

Calcium phosphate based cements and PMMA resin cements have both been used to reconstruct bones in craniofacial and other skeletal defect surgeries (1,4).

In cases where sections of bone are missing, such as following bone tumour excision or the bone trauma/defects mentioned above, acrylic bone void filler materials have been used (2,5). These materials can be loaded with antibiotic drugs in the case of infection (3).

Total Joint arthroplasties commonly use PMMA cements to anchor joint prostheses (2–4).

More recently, Osteoporotic vertebral fractures have been stabilized with (PMMA) cements (2–4).

The numbers affected by bone cancer or requiring bone reconstruction following osteomyelitis or trauma and the relative risks of developing osteoporosis are varied. It is estimated that over 3000 people will be diagnosed with bone cancer in the US in 2013 (6). The number of people hospitalized by osteomyelitis was over 51 000 from

1993 - 2000. Whilst the estimated numbers requiring bone reconstruction following trauma were around 500 000 annually in the US in 2005 (7). Around 1 in 5 / 1 in 2 (Men/Women) over 50 years in age in England and Wales will develop an osteoporotic fracture (8). Although these statistics are a mixture between absolute numbers and relative risks, and are therefore not directly comparable, it is clear that osteoporotic fractures are the most prevalent of these conditions. Furthermore, the increasing elderly population (8) means that vertebral fracture numbers and the incidence of hip and knee implant requirements are escalating.

1.3 Project Motivation

When looking at the numbers of patients affected in each treatment case it was clear that osteoporotic fractures are the most prevalent. As such, bone cement development for applications involving the treatment of osteoporotic fractures was chosen as the main motivation for this project.

1.4 Current Bone Cement Treatments for Osteoporotic Fractures

In the previous sections, the main indications of bone cement were summarized and osteoporotic fracture applications were defined as the motivation for this project. This section will introduce the current bone cement treatment strategies for two of the most common osteoporotic fractures in more detail. Furthermore some treatment options, which are not currently common practice, are suggested as improvements on current methods. Finally the requirements of successful bone cement materials in each of these applications will be discussed.

1.4.1 Vertebral Fractures

Vertebroplasty is the name given to the procedure in which vertebral fractures are stabilised by percutaneous injection of bone cement. This method was first introduced in 1987 using PMMA cement (9). More recently composite bone cements have been introduced (5,9–11).

The following key properties for a successful vertebroplasty cement material were defined by Heini and Berlemann (9):

- Injectable
- Easy to handle
- Radiopaque
- Sufficient viscosity to prevent leakage prior to cure
- Constant viscosity before cure, curing time sufficient to allow implantation.
- Sufficient strength/stiffness to restore mechanical properties of vertebrae (both compressive and bending strengths must be sufficient to carry the loads applied to the material and at the bone/cement interface in the implanted site) (12).

Some of the problems with vertebroplasty cements are discussed in section 1.5.

1.4.2 Femoral Neck Fractures

Traditionally, femoral fractures are fixed by replacing the femur head with a prosthesis, which must be held in place with surgical cement in a total joint replacement (TJR). Screws and plates are used to treat femoral neck fractures in healthy bone, but do not work well with osteoporotic bone. Screw augmentation with bone cement can overcome this.

Canulated screws on their own only attach to the bone at the ends. As the bone is weak the screw cannot get any purchase and the surrounding bone is often damaged. Systems involving screws, and augmented with bone cement come some way to increasing the contact area between implant and bone and improving the stability of the fracture (13,14).

When the femoral head is replaced with a prosthesis, bone cement is used as a grout to anchor the prosthesis into place and transfer loading between prosthesis and bone (3). The bone cement increases the contact area between the prosthesis and bone

tissue, by mechanical interlocking, making it more suitable for osteoporotic patients with low quality bone.

Requirements for cements for screw augmentation and TJR are as follows:

- Sufficient strength and stiffness to carry applied loads (15) without damaging weak host bone.
- Viscosity /composition that enables good mechanical interlock with bone
- Radiopaque
- Easy to handle and implant.
- Curing rates that facilitate implantation.

In addition to the above, there are British standard (ISO 5833 - 2002) and ASTM standard (ASTM F 451-08) specifications for acrylic bone cements. In these standards the following requirements are stipulated:

ISO 5833

Bone cements should be supplied in sterile packaging. Setting time should be between 6.5 – 15 minutes for syringe deliverable cements and 3 – 15 minutes for hand mixed materials with a maximum curing temperature of 90 °C. The compressive strength should be over 70 MPa, with bending strength over 50 MPa and stiffness over 1.8 GPa. Cement viscosity should be such that intrusion is more than 2 mm. Stability such that following storage at 23 °C for one hour, viscosity should not increase by more than 10 %.

ASTM

The material when removed from its package should be sterile. Setting time should be 5 – 15 minutes with a maximum temperature rise of 90 °C. Compressive strength should be more than 70 MPa. After heating for 48 hours at 60 °C, the viscosity of the liquid should not increase by more than 10%.

The test methods for determining the above are specified in each standard.

1.5 Currents Cements: Description and Disadvantages

Throughout this thesis, the properties of bone cement materials are split into five categories:

- Composition
- Handling
- Cure: curing times and rates; and degree of conversion
- Shrinkage and heat generation
- Mechanical properties: strength, stiffness, fracture behaviour and fatigue response.

As described previously bone cements are paste-like materials that set within the body. As part of this research project is concerned with characterization of the setting chemistry of cement materials, firstly, this section will describe the setting mechanism of two classes of bone cement (PMMA cements and composite cements) currently used for treatment of osteoporotic fractures along with dental composites. Following this these materials will be described according to the above categories with some of their disadvantages followed by a summary of their key components. After this some of the key modifications made to PMMA and composite materials will then be addressed.

Bone cements are paste-like materials composed of a liquid phase and a solid powder phase. A composite is generally defined as a material that has physically distinct phases that differ in either material or form like concrete or carbon fibre composites. As will be seen in the following sections the two main groups of bone cements described (poly(methyl methacrylate) and composite cements), strictly speaking are both composites; in that they both consist of a liquid phase, solid reinforcing phase and often a radiopacifying phase. For the purposes of this thesis poly(methyl methacrylate) cements are not termed ‘composites’ because the main constituents (liquid and

reinforcing phase) are different forms of organic material, whereas so called 'composite' cements consist of phases of different form and material; the liquid phase is organic and the reinforcing phase is inorganic.

1.5.1 Free Radical Polymerization

The bone cements introduced below are a mixture of liquid and powder phases in proportions that result in a paste. The liquid phase is monomer molecules that contain one (or more) methacrylate groups that contain a carbon to carbon double bond (C=C). Chemical initiators are included; these are small compounds that form free radicals with a short half life. Initiator radicals can be stabilized either chemically or with exposure to light of the correct frequency (16). The mechanism by which these materials harden and cure is free radical addition polymerization during which free radicals generated by the initiator system attack the liquid monomer C=C double bond, breaking it open to create a monomer free radical that can bond to other monomer free radicals creating a polymer chain.

Reaction Mechanisms

An inhibited dimethacrylate polymerization mechanism can be represented by (17)

$A + B \xrightarrow{k_d} 2I^{\bullet}$ Initiation

$I^{\bullet} + M \longrightarrow M^{\bullet}$

$M_n^{\bullet} + M \xrightarrow{k_p} M_{n+1}^{\bullet}$ Propagation

$M_n^{\bullet} + Z \xrightarrow{k_z} M_n + Z^{\bullet}$ Inhibition

$I^{\bullet} + M_n \longrightarrow M_n^{\bullet}$

$M_n^{\bullet} + M_m \xrightarrow{k_c} M_{n+m}^{\bullet}$ Crosslinking

$$M_n^{\bullet} + M_n^{\bullet} \xrightarrow{k_t} P$$

Termination

For monomethacrylates (like PMMA) crosslinking does not apply. As can be seen from the above mechanisms, initiation is either when an initiator free radical ($I^{\bullet}$) or a monomer free radical ($M^{\bullet}$) interacts with a monomer molecule, creating a monomer free radical that can either go on to create more radicals or join a polymerzation chain. This chain formation is called propagation. Often bone cements include an inhibitor to prevent polymerization during storage. In the inhibition step free radicals are neutralized and prevented from causing further polymerization. For termination, the above assumes a general case where chain radicals are consumed in pairs to produce dead polymer. k_d, k_p, k_z, k_c, and k_t are rate constants for initiation, propagation, inhibition, crosslinking and termination. During propagation, diffusion becomes difficult due to the decreased mobility of the growing polymer chains, and termination (diffusion controlled) reactions are prevented; the rate of polymerization increases rapidly (autoacceleration). These simplified mechanisms assume that monomers in bone cements all have similar polymerization rates and can copolymerize. A simplified schematic of free radical polymerization can be found in Figure 1-1.

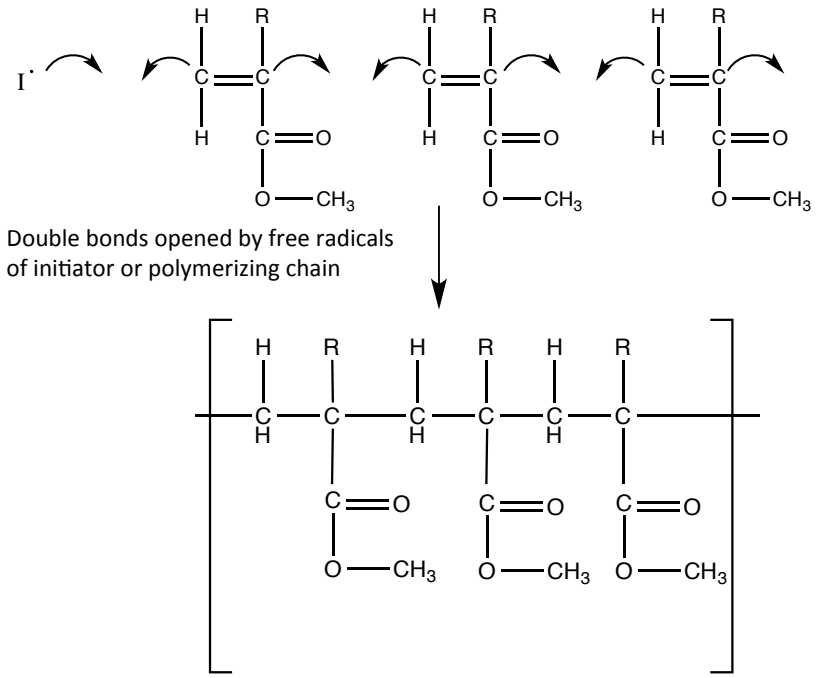

Figure 1-1 Free radical polymerisation reaction schematic. Initiator free radical (I•) attacts double bonds in methacrylate group to create monomer free radical – which can in turn create more monomer free radicals and polymerize to form a polymer chain. In the case of PMMA cements R is CH_3. For dimethacrylates, two methacrylate functional groups are present and crosslinking is possible.

1.5.2 PMMA Cements

Composition

PMMA cements contain methyl methacrylate (MMA) monomer liquid (Figure 1-2) and pre-polymerized PMMA powder (2). There are many poly(methyl methacrylate) cements available with a range of compositions and additives. Typical PMMA cements contain liquid methyl methacrylate monomer (MMA) with pre-polymerised beads of poly(methyl methacrylate) as filler with a radiopacifier of barium sulphate or zirconium dioxide (18). PMMA cements have a chemical initiator system usually incorporating; Benzoyl Peroxide (BP) initiator and Dimethyl-para-toluidine (DMPT) accelerator. The benzoyl peroxide radicals are stabilised by the DMPT accelerator; following mixing, the polymer beads in some PMMA cements can dissolve in the monomer and a solid

composite is formed via chemically induced free radical polymerization of the monomer liquid forming an interpenetrating network with the dissolved polymer.

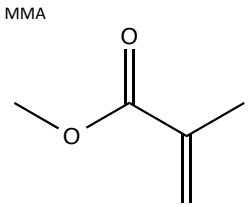

Figure 1-2 Molecular structure of methyl methacrylate monomer.

The inclusion of barium sulphate as a radiopacifier has been reported to encourage bone resorbtion (18,19) whilst the toxicity of the accelerator DMPT and initiator BP have also caused concern (18,20). Bone resorption can lead to cement loosening (21).

PMMA cements often contain antibacterial agents to prevent deep infection following TJR. There have been some concerns raised that inclusion of antibacterial agents, particularly aqueous based, can detrimentally affect curing and mechanical properties. It has been found, however, that when incorporated at the correct level by the manufacturer that there are no adverse effects (22).

Handling

PMMA cements are supplied to the surgeon as a powder and a liquid that must be mixed in the operating room prior to use.

Hand mixing of powder and liquid components has been identified as producing PMMA cements with poorer mechanical properties than mechanically/vacuum mixed cements (23) and could be responsible for a reduction in sterility (24). It has also been reported that the scatter of strength results for hand mixed cements is larger than for mechanically mixed materials (15,25) whilst differences in skill and technique of cement preparer has been shown to result in cements of varying porosity (26). Increasing porosity can decrease the strength and modulus of PMMA cements

(23,27,28). There are concerns also about the exposure of the mixing technician to methyl methacrylate during hand mixing; repeated exposure can lead to contact dermatitis and sensitisation (29,30).

If too much pressure is used during vertebroplasty, or the cement is too liquid when injected, it can leak before it cures (31). A study by Nieuwenhuijse found that around 75 % of vertebroplasties investigated, exhibited some leakage (32). Whilst uncured, cement leakage into blood can cause pulmonary embolism and cardiac perforation. Once cured leaked cement can damage surrounding vertebrae and put pressure on the spinal cord (33).

After mixing, PMMA cements can gradually change in viscosity as the polymer beads swell with monomer (2). Initially viscosity can be low and if the cement is placed too soon it may mix with blood. Conversely, if the viscosity becomes too high before placement, bone penetration and micromechanical bonding may be jeopardized (2).

Cure

As mentioned above, PMMA cements cure via free radical polymerization of Methyl methacrylate monomer, initiated by BP and DMPT. Conversion ratio is the ratio of reacted monomers to the initial level of monomers. The level of BP and DMPT has been reported to have a power law effect on the setting time of PMMA cement (34).

The levels of initiators used can significantly affect the degree of conversion and hence the amount of residual monomer (35). With PMMA cements, induction time, before the onset of cure, is long; typically several minutes (3). Furthermore, final conversion is never 100% (30). It has been reported that monomers can leach out of PMMA cement during the induction time and after cure when less than 100% conversion is achieved (36,37). This can cause problems similar to uncured cement leakage mentioned above. Oxygen inhibits free radical cure. As mentioned above, porosity can reduce mechanical

properties, oxygen trapped in pores can also reduce the level of conversion of PMMA cements (38).

The manufacturers advise that the cure of PMMA materials can be delayed by pre-chilling the components (39,40). The temperature of the materials will affect the kinetics of the polymerization reaction and may affect the level of conversion.

Shrinkage and Heat Generation

There is a volume decrease and heat generation associated with each polymer bond created during composite cement cure. This can cause a rise in temperature of the tissues surrounding the site where the cement material is implanted and tissue necrosis. This necrosis in combination with polymerization shrinkage can result in a loose cement implant. Loads cannot then be passed effectively between the cement and the tissue (21).

MMA is of low molecular weight (MW). This means PMMA cements are subject to high shrinkage (2,41,42) and heat generation (41). Polymerization shrinkage has been measured to be 6 - 7 vol.% for PMMA cements and may result in residual stresses that can cause cracking in cement in TJR procedures and can shorten lifespan of the implant (43,44). Furthermore polymerization shrinkage could damage trabecular bone before loading (45) and be detrimental to the bone-cement interface stability. This could be especially important when implanted in weak osteoporotic bone. Furthermore damage to the bone-cement interface has been postulated as a cause of cement loosening in TJR (21).

Measurement of polymerization shrinkage has been performed via a density bottle method (46) and computer controlled mercury dilatometer method (47).

Mechanical Properties

PMMA cements are far from satisfactory in terms of mechanical properties; the modulus of PMMA is up to an order of magnitude higher than cancellous bone (3,15,48) meaning that cement deflection on loading will be very different from surrounding bone. This could cause damage to weak, low density bone.

PMMA cements are weaker in tension and shear than in compression and exhibit strain rate dependent properties (viscoelasticity) (15). For this reason it is important to know the strain rate and test method used when strength and stiffness values are quoted in the literature. PMMA cements have poor resistance to fatigue and low fracture toughness which can limit their use in applications where cyclical loading bearing is present (15,49).

1.5.3 Composite Cements

A class of cement materials inspired by dental composite materials addresses many of the problems associated with PMMA cements, that are outlined above. Although composite materials do solve some of the problems with PMMA cements, some still remain.

Composition

Dental composites comprise Dimethacrylate monomers (such as Bisphenol A Glycidyl Methacrylate (BisGMA), Urethane Dimethacrylate (UDMA) and Triethylene Glycol Dimethacrylate (TEGDMA)) together with inorganic fillers usually supplied as a premixed paste that is cured by light activated free radical polymerization (50). Light cure, however, is unsuitable for bone cement applications due to the large volume of material and inaccessibility of the implant sites.

Cortoss and Comp06 are pre-mixed, dual paste chemically curing alternatives to PMMA cements that are now commonly used in vertebroplasty. These composite bone

cements are more similar to dental composites than PMMA cements as they contain a mixture of dimethacrylate monomers and silica fillers more commonly found in dental composites. In addition Cortoss contains the calcium containing phase combeite, whilst Comp06 contains Hydroxyapatite.

Bisphenol A is a clear plastic that is commonly used to make drinks bottles and food packaging (51) is present as an impurity in some resins such as BisGMA (52). Hormone mimicking properties have been reported for bisphenol A (53) and have lead to some safety concerns with BisGMA use (52).

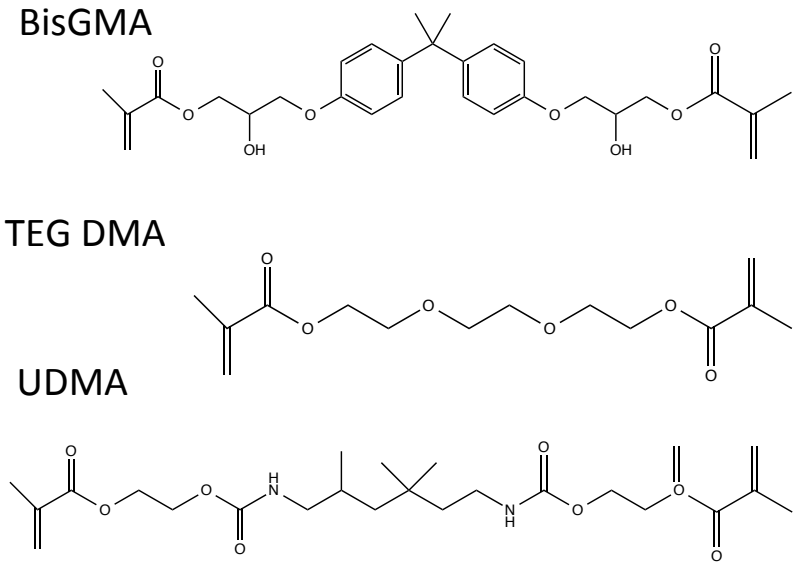

Figure 1-3 Molecular structure of BisGMA TEGDMA and UDMA.

Handling

Dual paste composites such as Cortoss and Comp06 are supplied in double barrelled syringes with automatic mixing tips. This reduces mixing time / variability, surgeon / material contact and potentially patient infection risk. Furthermore, dental composite filler particles, and the filler in composite bone cements, are silica based (54). Unlike the PMMA beads, these do not swell with time. The viscosity of dental composite pastes, and Cortoss, therefore remains stable until methacrylate conversion. Silane coating filler particles decreases the viscosity and improves the handling of Dental composites (55). Cortoss and Comp06 both contain silane coated filler for this reason.

Cure

Dimethacrylate conversion levels in Cortoss, and other dental composites, have been reported to be ~ 50 - 60% (56–59). In principle this is sufficient to bond all monomers into a polymer structure. BisGMA, however, has been reported to exhibit low monomer conversion (60). This could be a problem as some monomer molecules may be free to diffuse into body fluids. A study investigating the effect on conversion of relative amounts of the monomers found in Cortoss (BisGMA, BisEMA and TEGDMA) found that higher levels of BisGMA reduced conversion, whilst TEGDMA increased cure (61).

Shrinkage

Low conversion in combination with high dimethacrylate molecular weight leads to low composite shrinkage (~2 vol.% for dental composites (62)). This compares with ~7 vol.% for PMMA cements (63). As heat generation and shrinkage are proportional; both are related to the number of polymerized methacrylate groups (41). Composites will give less than half the heat generation of PMMA cements. Water sorption in more hydrophilic dental composites can balance out polymerization shrinkage (64) . This could also be the case with composite cements. The large volume of material used, compared to dental applications however, would mean hydration will take considerably

longer than curing time and so any damage to bone caused by shrinkage will be done before it can be counteracted by hydration swelling.

Mechanical Properties

Although flexural strength of composites can be much higher than that of PMMA (65,66) Cortoss has been shown to exhibit lower or comparable strength to PMMA cements (10). A particular problem with Cortoss is the very brittle nature of the material. This brittle behaviour is associated with poor fatigue resistance. Furthermore, a potential problem with BisGMA containing composites, such as Cortoss, used in cancellous bone would be high modulus and brittle fracture (10,58).

1.5.4 Summary of Components and Uses

Although Composite cements are used as an alternative to PMMA cements for some indications, sales figures from Stryker, manufacturers of Simplex P PMMA cement, report 23 million doses[1] of cement have been sold over 45 years since the material was released. Orthovita, manufacturers of Cortoss composite bone cement, reported more modest sales of 7400 units in the three years following its release on the market (67). From this it is clear that whilst composites are viable alternatives to PMMA cements, PMMA is still very much the mainstay of the orthopaedic arthroplasty and vertebroplasty market. Unfortunately there is no available clinical data comparing the longevity of implanted PMMA and Composite cements. The table below summarises the materials and uses described in the previous sections to enable the reader to compare PMMA and composite bone cements and dental composites.

[1] From advertisment in the Journal of Bone and Joint Surgery, Volume 90-A, number 2, February 2008.

[2] Operations were conducted by Vehid Salih, Ensanya AbouNeel and Peter Revell with full

Material	Monomer	Filler	Properties	Uses
PMMA	Monomethacrylate (MMA)	Pre-polymerized PMMA powder + radiopacifier	Hand mixed High shrinkage Incomplete cure Mechanical properties poorly matched to bone Poor fatigue	Vertebroplasty Arthroplasty Bone reconstruction/void filling Used with antibiotics Tumour treatment
Composites	Generally dimethacrylate a mixture of bulk and diluent monomers (dental often monomethacrylate HEMA)	In-organic silane treated glass powder + radiopacifier	Premixed/ injectable Lower shrinkage Good cure Higher strength than PMMA Quasi-brittle and poor fatigue	Vertebroplasty particularly in osteoporotic patients Bone void filler
Dental Composites		In-organic silane treated glass powder	Premixed Low shrinkage Low cure Very high strength Quasi-brittle Poor fatigue	Dental restorations

Table 1-1 Summary of material composition, properties and uses.

1.5.5 Modifications to bone cements

As we have seen in the previous section, there are problems associated with both PMMA and Composite bone cements. In this section, the literature surrounding the modifications that have been made to these materials to address their shortfalls will be reviewed.

Composition

Cortoss and Comp06 already contain calcium-containing phases. Inclusion of Calcium phosphate materials, into dental composites, that participate in secondary reactions (64) or release re-mineralising ions (50) have been shown to improve biocompatibility. The release of remineralizing ions could be useful for the localized treatment of osteoporosis.

Although the usage of antibacterial components in PMMA cements is relatively common, they are still quite a new addition to dental composites. It has been shown that antibacterial agents can be added without affecting mechanical properties (68).

Handling

Pre-mixed and injectable PMMA cements have been developed by Hazenwinkel et al. (34,35,69,70). In these cements the pre-polymerised PMMA filler is pre-dissolved in the monomer phase and so there is no swelling period. These materials were found to have curing and mechanical properties comparable with commercially available PMMA cements.

Cure

Monomer choice has been shown to be an important consideration in conversion levels of composite cements. Long chain, flexible monomers have been shown to achieve higher conversion compared to stiff molecules with the ability to hydrogen bond (71,72). Inclusion of a low molecular weigh monomethacrylate HEMA and the antibacterial agent chlorhexidine has even been shown to increase levels of conversion of a dental composite (73). A range of structurally sophisticated monomers have been introduced into dental composite materials with mixed results regarding effects on cure and mechanical properties due to varying solubility and reactivity of these monomers (50). Sideridou reduced the glass transition temperature of an initial monomer mixture in a light curing composite and found that this resulted in a higher degree of conversion (74).

In the above section, the level of BP was reported to affect the cure of PMMA cements. The rate of polymerization is also dependent on the monomer system used (75). Changing the relative concentrations of monomers (TEGDMA: BisGMA: UDMA) as well as initiators will affect the degree of conversion and time of cure.

The powder to liquid ratio (PLR) of commercial hand mixed PMMA cements is usually kept at a constant 2:1 volume ratio. A study by Lewis investigated changing the PLR of an injectable PMMA cement and found that increasing the PLR increased the rate of polymerization due to an increased amount of BP initiator (76).

Shrinkage

Whilst long chain flexible monomers can improve the degree of conversion, they do not adversely affect polymerization shrinkage (77). Although increasing the degree of conversion should increase shrinkage, the density of double bonds in high molecular weight monomers is lower and so shrinkage will not be increased relative to smaller molecules.

Residual stresses due to polymerization shrinkage have been discussed above as a potential problem for bone cements. It has been shown that curing composites at temperatures over the glass transition temperature (Tg) can result in stress relaxation (78). Choosing a system with a low Tg could remove the problems associated with residual stresses.

Mechanical Properties

As mentioned in the previous section, surface treatment of filler particles can greatly improve the mechanical properties (and handling) of composite materials. The inclusion of silane treated in-organic fillers into PMMA cements has been shown to improve mechanical properties in a similar way to when used in composite bone cements (79). A study into aspect ratio of filler reinforcement has shown that high aspect ratio fillers can also improve mechanical properties but may increase the viscosity (49). Size of fillers is also important; including nano-particles and increased amounts of ZrO_2 radiopacifier increased the mechanical properties of an injectable PMMA bone cement (70).

The addition of fibres to PMMA, dental and bone composites has been investigated. Fibre incorporation into composites can increase strength but the effects of chemistry, concentration and aspect ratio are critical (56,62,80,81). Acrylic resins have been reinforced with fibres made from a range of different materials at varying length scales including nano-scale carbon tubes and micro-scale quartz, polyvinyl alcohol, Kevlar,

calcium phosphate, ceramics like zirconia or silicate glasses (49,56,57,62,80–83). Glass fibres have been preferred for use in dental materials because of their translucency, ease of silane surface treatment and improved flexural strength and fatigue resistance (84).

Monomer choice is also of central importance to tuning of mechanical properties. As discussed in the previous section, dimethacrylate monomers could have lower residual monomer, cross linking monomers have been shown to work well with surface treated glass fibres to improve mechanical properties (85). Puska showed that crosslinking monomers had the ability to bond with silane treated filler better than linear MMA (86). Monomers containing amine groups were added to PMMA cements by May-Pat to increase water sorption and cell attachment and it was found that compressive and bending strength was decreased, but fracture toughness was improved (87).

PMMA cements have been reinforced with βTCP coated in poly(ethylene) glycol resulting in cement with good long term strength – this would be an improvement over Cortoss, which exhibits a strength decline.

1.6 Hypotheses

From the literature conducted above, it is believed that the type of monomer system will affect the handling of the material and will change how effectively the initiator system works, changing the rate and total time taken for the material to polymerize. Calcium phosphate particles can encourage a long term bond between the material and surrounding bone.

In an unpolymerized state, the monomers can be toxic, their size and type will affect how easily they can dissolve water and travel into the body. If initiator chemicals are present in high dosage after polymerization is complete they too can leach out of the material and can cause damage to surrounding tissues and cells.

A good level of conversion will mean more links within the polymer network and so a higher strength.

The heat generated, the percentage decrease in volume due to polymerization shrinkage and the initial and long term toxicity of the product are largely governed by the size and type of the monomers used. As explained earlier, smaller monomers will mean more heat and shrinkage, whilst a high PLR will mean less monomer in a given amount of cement therefore less heat generation.

The polymerized material will absorb water and this can compensate for the polymerization shrinkage.

Good dispersion and bond between the monomer and filler phases will mean a high strength. Using adhesive monomers can allow bonding between the polymer and calcium phosphates found in the material as well as surrounding bone. Also, coating the filler particles with monomer molecules allows a good dispersion of the glass particles in the monomer, and consequently the polymer network.

The secondary calcium phosphate/water reaction and the interpenetrating network that this creates is another mechanism by which the strength is increased.

Fibres can increase mechanical properties if they are well dispersed and have good interfacial bond strength with the polymer phase.

1.7 Project Scope and Aims and Objectives

In the previous section, the modifications that have been made to bone cement materials to improve their performance were summarized. In light of this, this section will summarize the aims of the project. The areas of development in this project (project scope) will be described.

The project aim is to develop bone cement materials that could be used to augment screws in osteoporotic hip fractures and to stabilize vertebral fractures.

From computer modelling and surgeon consultation performed by the sponsoring company Ozics, and information from the above literature review a set of target properties has been drawn up.

Target Properties:

1 The cement must be compatible with delivery via a syringe and mixing tip to avoid surgeon mixing complications.
2 The level of heat and shrinkage of the product should be comparable or less than that of Cortoss in order to be competitive.
3 The formulation curing time should be 1 – 3 minutes to allow manipulation of the implantation site by the surgeon after injection although the material should be fast setting enough to prevent leakage or excessive monomer leaching.
4 The level of monomer conversion should be more than in current products to reduce possible toxicity.
5 The product must be strong enough to transfer the loading between bone and screw in hip, or carry required loads in vertebra. It must also have relatively low stiffness to be compatible with bone movement upon loading and prevent associated bone damage (Ozics deemed that a flexural strength of 50 – 70 MPa is required and that stiffness should be comparable to PMMA cements).

6 Additionally, the cement should not be brittle. Instead it should deform when overloaded to cause pain that will be a signal to the patient that something is wrong rather than the first sign of overloading being catastrophic brittle failure.

Project Objectives:

1 To determine the properties and characteristics of current popular PMMA and composite bone cement materials and a dental composite (chapter 3).
2 To screen possible components for inclusion in cement materials that could fulfil the above target properties (chapter 4).
3 To select candidate components and conduct systematic investigation into their effects on cement properties (chapter 5).
4 To select a monomer and filler system and characterize the in-vitro and in-vivo performance of this prototype formulation (chapter 6) and to investigate the effects of changing the initiator system on shelf life and curing of this material (chapter 7).
5 To determine to what extent the in-vitro and in-vivo response of the selected materials fulfil the target properties and to suggest future research directions and further work (chapter 8) to enable the production of a competitive bone cement product.

2 Materials and Methods

This section summarizes all the materials and the protocols used throughout the project. At the start of each chapter a summary of the materials and methods used is given.

2.1 Materials

2.1.1 Commercial Materials

Name	Supplier	Components		Description
		Monomers	Fillers	
Cortoss	Orthovita	BisGMA BisEMA TEGDMA	Silane treated silica glass, Combeite	Pre-mixed paste in double barrelled syringe (chemical cure following mixing)
Comp06	Ozics	BisGMA BisEMA TEGDMA	Silane treated barium silica glass Hydroxyapatite	Pre-mixed paste in double barreled syringe (chemical cure following mixing)
Palacos R	Heraeus	MMA	PMMA Zirconium dioxide	Monomer liquid and powder supplied separately mixed before delivery (chemical cure following mixing)
Simplex P	Stryker	MMA Poly(styrene)	PMMA Barium sulphate	Monomer liquid and powder supplied separately mixed before delivery (chemical cure following mixing)
Z250	Filtek	UDMA BisEMA,TEGDMA	Zirconia Silica	Premixed syringe - light cure

Table 2-1 Details of commercial materials investigated in this project. Description and component information from manufacturer.

2.1.2 Monomers

Abbreviation	Name	Supplier	Product code	MW
PETA	Pentaerythritol tetraacrylate	Polysciences	01547-100	352
UDMA	Urethane dimethacrylate	Esstech	X850 0000	470
PPGDMA	Poly (propylene glycol)425 dimethacrylate	Polysciences	04380-250	560
DDMA	1-10 decanediol dimethacrylate	Polysciences	02140-25	310
TEGDMA	Tri(ethylene glycol) dimethacrylate	Esstech	X943 7446	228
PPGMMA	Poly(propylene glycol) 300 monomethacrylate	Polysciences	15934-250	370
HEMA	Hydroxyethyl methacrylate	Esstech	X968 7044	130

Table 2-2 Details of Monomers that were used throughout this project. Molecular weight information from manufacturer.

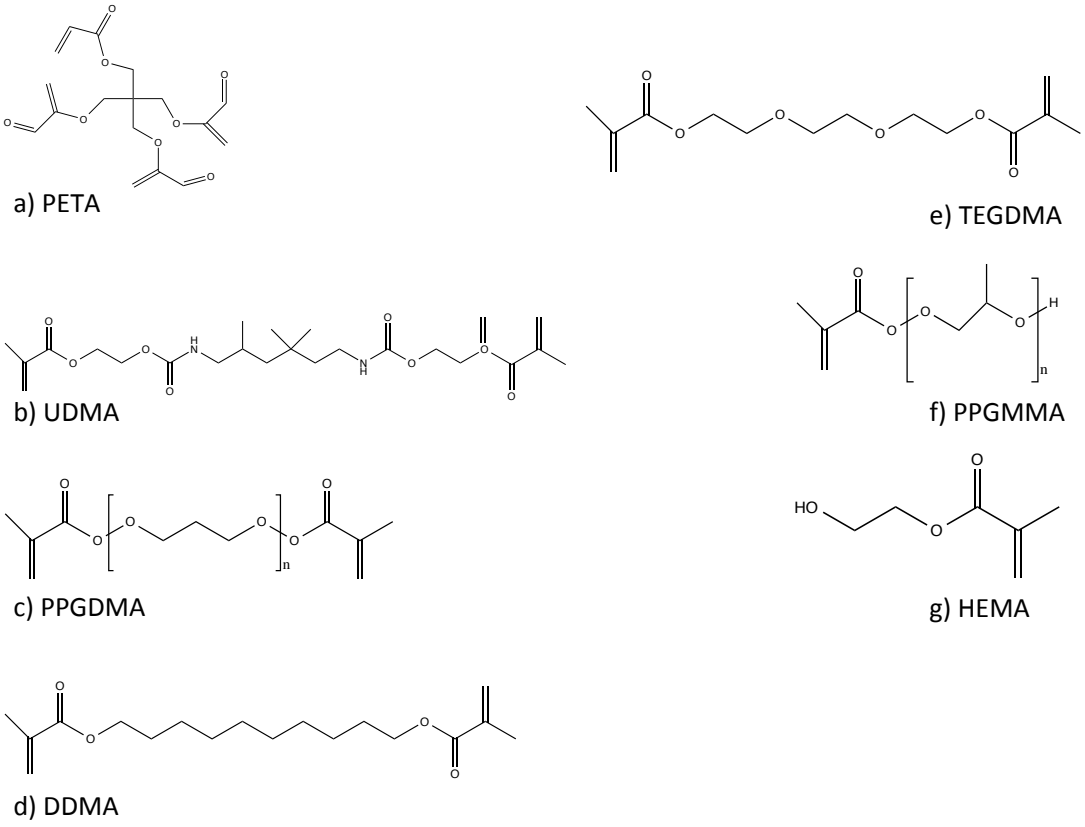

Figure 2-1 Molecular structure of monomers used throughout this project.

2.1.3 Fillers

Shape	Silanated	Abbreviation	Name / manufacturer's code	Size (μm)	Supplier
Particle	NO	G_1	G018-090	3.7	Schott
	YES	G_{1S}	Ultrafine silanated G018-117	1.9	Schott
	YES	G_{2S}	Ultrafine silanated GM27884	2	Schott
	YES	G_{4S}	IF-2025 boro alumino silicate glass	undisclosed	Sci-pharm
	YES	G_{3S}	IF-2019 barium boro alumino silicate glass	undisclosed	Sci-pharm
Fibre	NO	F_A	Chopped para-aramid fibre	undisclosed	Teijin
	YES	F_{GS}	Silane coated borosilicate glass fibre	15x300	MO-SCI

Table 2-3 Details of filler materials used throughout this project. Information from manufacturer.

2.1.4 Initiators, Activators and Inhibitors

	Abbreviation	Name	Supplier	Product code	MW
Initiator	BP	Benzoyl peroxide	Aldrich	228877	242
Activator	DMPT	N, N-Dimethyl -p-toluidine	Aldrich	D189006	135
Inhibitor	BHT	Butylated hydroxytoluene	Fluka	34750	220

Table 2-4 Details of initiator, activator and inhibitor chemicals used throughout this project. Details from manufacturer.

2.2 Methods

A summary of the methods employed in each section can be found at the start of each chapter.

2.2.1 Apparatus Required for Material Preparation

To prevent contact dermatitis associated with monomers, latex gloves were worn for all sample preparation. Hands were washed and gloves changed whenever they came into contact with monomers and after all preparation. A laboratory coat was worn to prevent clothing contamination.

Metal spatulas and glass pipettes were used to handle the fillers and viscous monomers, and diluent monomers respectively.

All weighing was done using a Pioneer analytical balance (Ohaus, UK).

Amber glass bottles were used to contain the monomers and additives during mixing.

Paste mixing was performed by hand using a metal spatula and a rubber mixing-pad (3M ESPE) (Figure 2-2).

Commercial materials and prepared composite pastes were mixed via double barrelled syringes with 2 x 5 cm^3 (Figure 2-3) or 2 x 10cm^3 barrels in conjunction with a delivery gun and screw mixing tips (Sulzer Mixpac, Switzerland, and Orthovita, USA, respectively).

Room condition: temp 23 °C, light on or off as desired, depending on daylight.

Refrigeration: Fridges maintained between 1 – 5 °C with no light.

2.2.2 Commercial Materials Sample Preparation

Commercial materials were prepared for use as described in the following sections.

2.2.2.1 Cortoss and Comp06 Composites

Double barrelled syringes containing Cortoss or Comp06 materials were removed from the fridge 30 minutes prior to use to allow the material to warm up to ambient temperature.

2.2.2.2 PMMA Cements

Equal quantities of the powder and liquid phases of Simplex P PMMA (Stryker) and Palacos R bone cements were mixed on rubber dental mixing pads according to manufacturer's instructions.

2.2.2.3 Z250

Disc specimens of Z250 were sandwiched between sheets of acetate and cured with a blue light-curing unit (L.E. Demetron I, Kerr, USA), for which the power output was 1000 $mWcm^2$. Specimens were exposed to the light source for 60s on each side.

2.2.3 Composite Sample Preparation

2.2.3.1 Monomer Preparation

Monomer mixture (prior to addition of initiators)

First, the desired monomers were mixed together with inhibitor without any initiator/activator. Monomers were weighed into an amber bottle (total amount between 8 and 10 g, mass percentages of components weighed to an accuracy of 0.001g). The order of weighing was from component of smallest amount to largest amount. BHT was pre-dissolved in the diluent monomer of choice at a higher concentration (20x concentrated) to minimise weighing errors.

The amber bottle was capped and the monomer mixture mixed for 15 minutes using a magnetic stirring bar at room temperature at speed setting 2/3. This gave a 'stock monomer mix' that could be stored at 5 °C for up to two months with no effect on the

curing kinetics of the end product. The stirrer bar was removed before storage to prevent any breakdown of the plastic bar by the monomers.

Addition of initiators to monomer mixes

The monomer mixes were at ambient temperature before being combined with initiator/activator and so were either used straight after being prepared or removed from the fridge 30 minutes prior to use. A small amount of the desired monomer mix was weighed into two amber bottles (2-5 g depending on number of specimens to be made).

The desired quantity of initiators/activators were added to the monomer; BP into one bottle and DMPT into the other.

Monomers and initiators were mixed for 30 minutes using magnetic stirring bar at speed 2/3 to ensure complete dissolution of the initiator / activator. Once the monomers were combined with initiator or activator they were mixed with fillers and used on that day to prevent any variability in cure due to monomer instability.

2.2.3.2 Filler Preparation

All fillers were stored at room temperature in airtight containers to ensure that they were kept dry. Care was taken not to introduce moisture into the bulk of the filler materials by decanting small amounts of filler sufficient for two or three day's work at a time.

2.2.3.3 Paste Mixing and Syringe Filling

Depending on the powder to liquid ratio required, an amount of monomer mix (containing initiator) was weighed onto a mixing pad. The required mass of filler(s) was (were) added.

Roughly half the filler was combined with the monomer to make a thin paste. Once a homogenous consistency was achieved, the remaining filler was incorporated. Care

was taken to mix in such a way as to avoid excessive introduction of air to the mixture. The paste was worked with the spatula to remove any visible air bubbles or filler aggregates.

These steps were repeated for the activator containing monomer mix.

Each paste was added to one side of a double barrelled syringe; again care was taken to avoid air bubbles. Stoppers were inserted into each barrel and the syringe was left to stand with the tip pointing upwards to allow the pastes to settle against the stoppers and for air bubbles to escape.

A lid was fastened onto the syringe after a plunger was used to push the pastes to the tip and level the stoppers (Figure 2-4).

Figure 2-2 Filler powder and monomer mix on rubber mixing pad prior to mixing.

Figure 2-3 Double barrelled syringe and screw mixing tip.

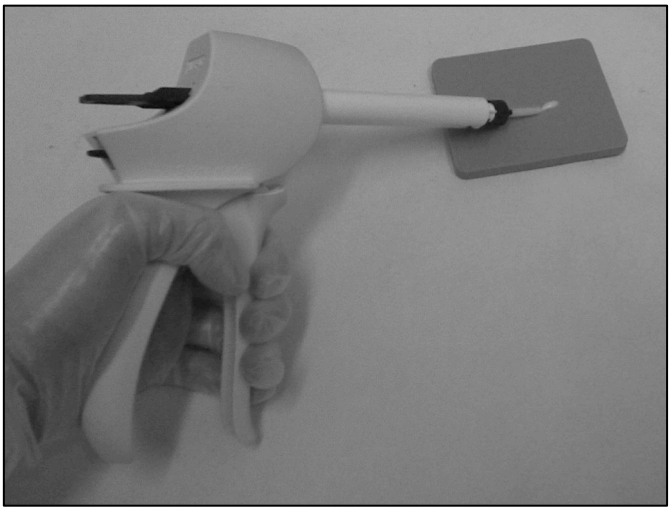

Figure 2-4 Initiator and Activator pastes are combined by being extruded through screw mixing tips via a delivery gun.

2.2.4 Wet Point

The wet point is defined as the minimum mass of monomer added to a filler powder to achieve a cohesive mass, and is given as a percentage of monomer in the resulting paste. 3g of the filler to be tested was weighed onto a rubber mixing pad, small (0.01g)

amounts of monomer were added incrementally to the filler until a barely cohesive paste was achieved. The weight percentage of monomer in the paste was calculated.

2.2.5 Factorial Analysis

Factorial analysis is the main method of analysis that has been used to investigate the materials used. It is a method that allows the effect of more than one variable to be investigated simultaneously.

It is assumed that the reaction process can be expressed in the form of a kinetic expression such as a power law (Equation 2-1). This kinetic expression can be shown to be equivalent to a factorial expression (Equation 2-2) (88). Experimental results, *D*, can be used to determine the effect of each variable on the parameter measured. In effect the rate constants in the kinetic expression are determined from solving factorial equations. In this way it is possible to demonstrate how much the variables under investigation affect properties of interest. Ho and Young (88) performed a two level factorial analysis (simultaneous investigation of two variables; in this report three variables are investigated at one time. For a complete factorial experiment, 8 specimens are then required. The size of a_1, a_2 and a_3 show the size of the effect of each of the three variables (Equation 2-3). Effect of variable 'i' is quantified by a_i; this can be calculated from the ratio of the geometric mean of n specimens (D_n) with variable i at its high and low value respectively. Factorial analysis also enables quantification of interaction effects between the variables. Strong interaction effects, however, complicate understanding of the effects of variables and prevent fitting of simple kinetic expressions. The size of these interactions is given by a_{12}, a_{13}, a_{23} and a_{123}. An intermediate formulation (with intermediate values of each variable) is often tested. If there are no interactions the intermediate formulation will be similar to the average result of the other eight formulations.

$$D = kV_1^{b1}V_2^{b2}V_3^{b3} \Rightarrow \ln(D) = \ln(k) + b_1\ln(V_1) + b_2\ln(V_2) + b_3\ln(V_3)$$ Equation 2-1

$$\ln(D) = \langle \ln(D) \rangle \pm a_1 \pm a_2 \pm a_3 \pm a_{12} \pm a_{13} \pm a_{23} \pm a_{123}$$ Equation 2-2

$$2a_i = \ln\left(\frac{\sqrt[n]{\Pi(D_n)_{\mathrm{var}_i HIGH}}}{\sqrt[n]{\Pi(D_n)_{\mathrm{var}_i LOW}}}\right)$$ Equation 2-3

2.2.6 Fourier Transform Infrared Spectroscopy

Fourier transform infrared spectroscopy (FTIR) can be used to measure the degree of conversion of methacrylates (71,73,88,89). Differential scanning calorimetry (DSC) and Fourier transform Raman spectroscopy (Raman) can also be used (64,78,90–92). These are the most common techniques for finding the degree of conversion.

This section will give some of the reasons why FTIR has been used in this project to record the polymerization reaction and degree of conversion and address some of the technique's limitations compared to Raman and DSC.

With FTIR, there is the opportunity to use a real time monitoring method, that allows not only the degree of conversion to be found but also the rate at which the polymerization reaction progresses. The method of FTIR used in this project is based on that of Young et al. (89) in which the curing of methacrylate systems is monitored in real time producing a curing profile. This is the main reason for choosing FTIR measurement over Raman spectroscopy.

FTIR and Raman spectroscopy are complementary. Peaks that are active in Raman are often weak in FTIR. Peaks selected for polymerization reaction monitoring are central to the success of the technique. The C=C peak (at 1638 cm^{-1} in FTIR), for example, is stronger in Raman than in FTIR. If this peak is used, the FTIR technique can have poor sensitivity to residual monomer levels when conversion is high (88). For this reason, other methacrylate peaks have been used as discussed later in section

2.2.5.2. There can be large variation in FTIR measurements of conversion when using different peaks. It is therefore difficult to compare results with literature when different peaks have been used (71).

With DSC measurements, there is a delay between sample mixing and the start of reaction monitoring due to having to seal the DSC container and place in the instrument. There is less delay between sample mixing and reaction monitoring when using real-time FTIR as, after mixing, the material can be placed on the FTIR crystal in seconds. As a result, very sensitive and accurate measurement of the induction period of materials, especially injectable composites, is possible.

The attenuated total reflectance (ATR) FTIR method used in this project measures the reaction near the surface of the material in contact with the diamond – it cannot easily measure conversion of double bonds in the bulk of materials (93). DSC is better suited to measuring the bulk material reaction as it measures enthalpy changes of an entire volume of material.

2.2.6.1 FTIR Background

The FTIR method was selected as the technique for measuring the polymerization rate and degree of conversion. This section is intended to be a brief explanation of the underlying principles of the technique.

ATR FTIR spectroscopy is a method of vibrational spectroscopy in which the vibrations of molecular bonds after absorbance of incident infrared radiation give information about molecular structure.

Absorbed Infrared radiation causes the bonds between atoms in molecules to vibrate at their resonant frequencies. Different bonds have various strengths/lengths and absorb different wavelengths of radiation. The resonant frequencies correspond to discrete vibrational energy levels (Figure 2-7).

Absorption of infrared radiation causes changes in the electron distribution (dipole moment) of the bond and hence transitions between energy levels (94). The resonant frequencies/vibrational energy levels depend on the size of the atoms and the electron density of the bond. The dipole moment of polar bonds can be more strongly deformed than non-polar bonds and so FTIR can more easily show the asymmetric vibrations of polar groups. For this reason water molecules can be easily detected with FTIR.

FTIR Instrumentation

The purpose of an FTIR instrument is to determine the wavelengths of infrared radiation that are absorbed by a particular material and hence infer the type of bonds that exist between the atoms of the molecule. The intensity of light absorbed at a particular wavelength can be determined by finding the ratio of incident radiation to radiation that has been absorbed/ transmitted (Beer Lambert law).

In FTIR spectroscopy, an IR source is projected, through a sample, onto a detector. An FTIR instrument, therefore, consists of a polychromatic IR radiation source; a sampling method to determine the ratio of intensity of incident to transmitted/absorbed radiation; and an instrument to determine the wavelengths of the incident and transmitted/absorbed radiation.

The sampling method employed in this project to find the intensity of radiation interacting with the sample is attenuated total reflectance (ATR). In this method the material being investigated is placed on a crystal of material with high refractive index (diamond). Radiation from the source has a real component that is totally internally reflected and an imaginary component (at 90° to the real part) that probes the surface of the sample in contact with the crystal (0.5 – 5 μm). At frequencies around where radiation is absorbed, the imaginary component is attenuated, and at other frequencies it is not.

A Michelson interferometer forms part of an FTIR instrument and is used to determine which wavelengths have been absorbed by the material. The interferometer is used conjunction with the Fourier transform to determine the wavelengths of absorbed light from the intensity of the polychromatic radiation after it has interacted with the sample. Figure 2-5 shows the experimental set up of a Michelson interferometer. Light from the sample is split by a beam splitter, which sends half the signal to a moving mirror and half to a fixed mirror. The reflected radiation from the fixed mirror and moving mirror arrive at the detector with a path difference depending on the position of the moving mirror. The interference of the two beams at the detector gives an interferogram of intensity as a function of time. Due to the position of the moving mirror the two beams will only constructively interfere at one point giving an interferogram with a centre burst that quickly dies away at other times. A computer uses the Fourier transform and the Beer Lambert law to convert this interferogram into a plot of Absorbance as a function of wavelength. In an FTIR instrument, all the wavelengths of the source reach the detector simultaneously; a full spectrum can be found in seconds. This makes FTIR spectroscopy suitable for real-time monitoring of polymerization.

FTIR spectra (Figure 2-6) can give qualitative and quantitative information about a material. Whilst the position of the peaks in the spectrum gives information about the chemical groups present, the relative heights of peaks in a spectrum of absorbance vs. wavenumber give quantitative information about the relative amounts of each bond type. This is particularly useful when monitoring polymerization reactions in real time as the relative heights of the peaks corresponding to the methacrylate group infer how many of these groups have polymerized as the reaction progresses.

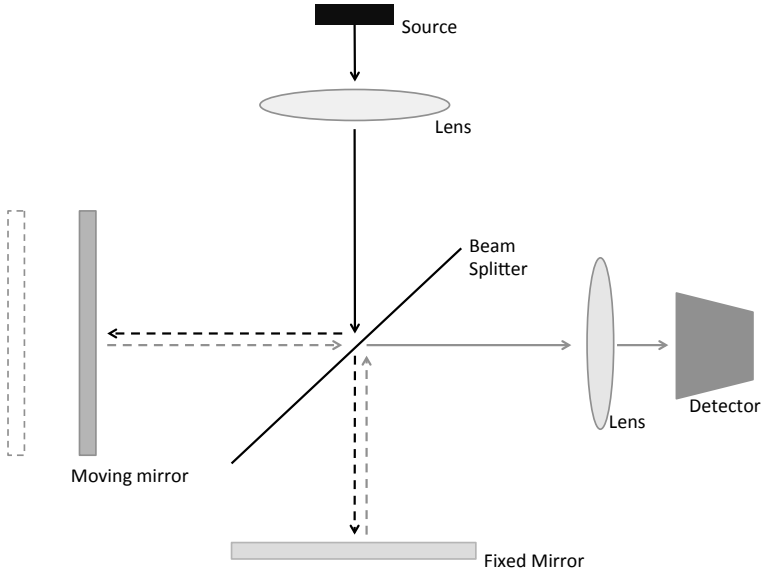

Figure 2-5 Schematic of a Michelson Interferometer. Light from source is split between moving and fixed mirrors, arriving at the detector with a path difference dependent on the position of the moving mirror.

FTIR Resolution

The spatial resolution of the FTIR spectrometer is limited by the size of the crystal. Each spectrum found is the average chemical structure over the whole area of the crystal. In the case of composite cements, the spectrum found will be an average of both the polymer and filler phases.

The wavelength resolution, which is different from the spatial resolution, is defined as the closest division in between discrete wavenumbers that can be detected. To detect two discrete wavenumbers (two distinct lines in the frequency domain), the beam from the sample must be scanned in the time domain for one complete period (from one maximum to the next on the interferogram). The wavelength resolution of an FTIR, therefore, is determined by the distance over which the moving mirror can travel. The resolution is in fact proportional to the reciprocal of the distance the mirror can move. In this project the resolution of the instrument was maintained at 4 cm^{-1}.

2.2.6.2 Cure Profile and Degree of Conversion

Material FTIR spectra, at 25 ºC, were obtained using a series 2000 FTIR spectrometer (Perkin-Elmer, UK) with a temperature controlled golden gate diamond ATR attachment (Specac, UK) and Timebase software. 1 mm thick, 10 mm diameter brass rings, placed around the ATR diamond (maintained at 25 °C), were filled directly with the material to be investigated either from a double barrel syringe (composites) or after 1 minute of mixing (PMMA cements) (n = 4). The top surface of the mixed paste was covered with acetate to prevent surface oxygen inhibiting the polymerization process. Spectra of the lower surface of the specimen were recorded with a resolution of 4 cm^{-1}, every 4 s for 20 minutes from 700 cm^{-1} to 2000 cm^{-1}. Difference spectra were obtained to ensure methacrylate polymerization was the only process causing spectral changes (89). FTIR spectra of each component were obtained and compared with literature to aid peak assignment.

Percentage monomer conversion was estimated using Equation 2-4.

$$Conversion(\%) = \frac{100\left(h_0 - h_t\right)}{h_0} \qquad \text{Equation 2-4}$$

Where h_0 and h_t were taken as peak absorbance at 1320 cm^{-1} above the background level at 1335 cm^{-1} initially and after a time t (Figure 2-6) (73). Final peak height and conversion (C) were calculated by linear extrapolation of data versus inverse time to zero.

If a single reaction is occurring, fractional reaction extent (ξ) can be calculated using Equation 2-5 below (95).

$$\xi = \frac{(A_0 - A_t)}{(A_0 - A_f)}$$ Equation 2-5

Where A_0, A_t and A_f are absorbance above the baseline initially, at time *t,* and finally, at any wavenumber with significant variation. In this project, the absorbance at 1320 cm^{-1} was used. A_0, A_t and A_f were the height of the peak at 1320 cm^{-1} relative to the base at 1335 cm^{-1}. The time to 50% reaction ($t_{0.5}$) was taken as the time at which the reaction extent was 50% of its final level. Reaction extent was plotted against time divided by $t_{0.5}$ to address if methacrylate conversion profiles could be described by a single curve (95).

2.2.6.3 Shrinkage and Heat Generation

Shrinkage and heat generation are both proportional to degree of conversion (96). One mole of polymerizing C=C bonds typically generates 57 kJ of heat (41) and gives volumetric shrinkage of 23 cm^3 (97). The total heat generation and shrinkage due to the composite curing process can therefore be estimated using Equation 2-6 and Equation 2-7.

$$vol(\%) = 23N * 100$$ Equation 2-6

$$Heat(kJ/cc) = 57N$$ Equation 2-7

N is the number of moles of reacted bonds per unit volume in each of the nine cement formulations. This can be estimated using Equation 2-8.

$$N = [M]C\rho_{comp}\sum_i\left(\frac{n_i x_i}{W_i}\right)$$ Equation 2-8

Where [*M*] is the total monomer mass fraction and *C* the final fractional monomer conversion calculated from FTIR. *Σ* indicates a sum over all the monomers in the liquid phase. n_i, W_i and x_i are number of c=c bonds per molecule, molecular weight ($gmol^{-1}$)

and mass fraction of monomer *i* respectively. Assuming the formulation behaves "ideally", and is non-porous, density (ρ_{comp} gcm^{-3}) can be estimated using a simple rule of mixtures (Equation 2-9).

$$1/\rho_{comp} = m/\rho_{monomer} + (1-m)/\rho_{filler} \qquad \text{Equation 2-9}$$

$\rho_{monomer}$ and ρ_{filler} are the densities of the monomer mixture and filler. PMMA cement monomer and filler densities were taken as 0.94 and 1.24 gcm^{-3} respectively, giving an assumed PMMA cement density of 1.08. This assumes that there are no air bubbles in the mixture. The porosity of PMMA bone cements made according to manufacturer's instructions (via hand mixing) has been found to range between 1.08 - 1.2 % (15,23) and so this assumption was taken to be a reasonable one.

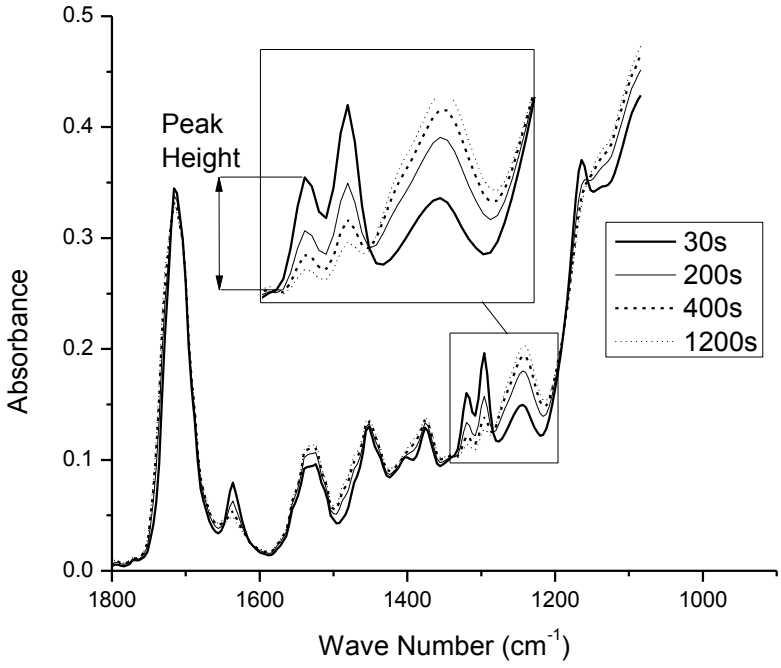

Figure 2-6 FTIR spectra of a curing PFC with time. Inset shows change in absorbance used to determine cure profile. The 1320 cm^{-1} peak used to measure peak height (relative to base at 1335cm^{-1})corresponds to C-H bond in the polymerizing methacrylate group.

2.2.7 Raman Spectroscopy

As already stated the quantum vibrational energy levels in molecules can be used to infer the molecular structure of a substance. Raman spectroscopy is another vibrational spectroscopy method used to determine the quantum energy levels present within a material and hence to determine the molecule bonds present.

In FTIR, the atoms were excited to a higher vibrational energy by certain frequencies of radiation. In Raman spectroscopy, high-energy radiation interacts with the electron cloud of the bonds within a molecule. Photons excite the molecules to virtual energy levels at higher energy than any of their vibrational resonance modes (Figure 2-7). When the molecular bonds relax, they release energy, again in the form of photons. Most of the time the molecules relax to their preferred energy level (for the given temperature) and the photons emitted have the same energy (and hence same frequency) as the photons that were absorbed. These photons are said to be 'elastically' scattered (Rayleigh scattering). Some of the time, however, the molecule relaxes to a higher or lower vibrational energy level, the energy of the photons is not conserved, and so the emitted photons have a different frequency from the incident radiation. These are inelastically, or Raman, scattered photons. Raman scattering can be defined as Stokes or Anti-Stokes scattering (Figure 2-7).

Similar to FTIR spectroscopy, Raman spectra provide both qualitative and quantitative information. The Raman spectrum of a material is a plot of intensity of the scattered radiation as a function of the frequency (Raman) shift. The position of the peaks gives information about the chemical bonding of the molecule whilst the peak intensity is related to the concentration of the bond type. With respect to methacrylate composite materials Raman spectroscopy can be used to give the molecular make-up of a material and also level of methacrylate conversion following the curing reaction as the number of C=C methacrylate bonds decrease.

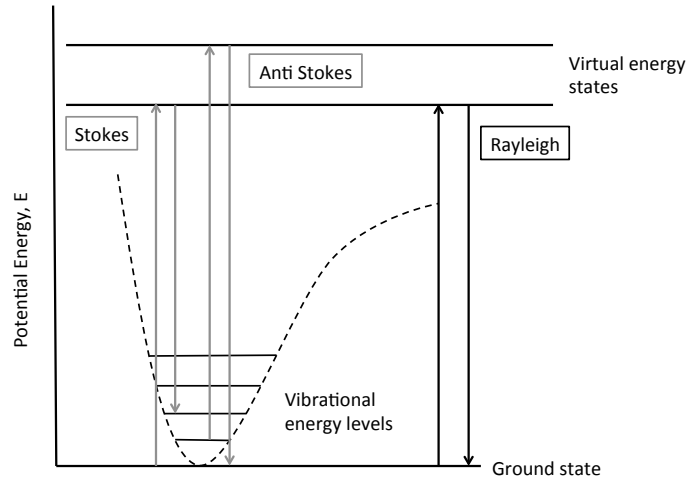

Figure 2-7 Schematic representation of a diatomic molecule. Dashed line represents potential energy, discrete vibrational energy levels are shown. Arrows representative of elastic and inelastic scattering. High-energy laser light excites atoms to a virtual energy level. Emitted photons with a higher/lower energy than the incident photons are inelastically scattered and defined as Stokes/Anti-Stokes scattered respectively.

Raman Instrumentation

A Fourier Transform Raman (Raman) microscope consists of an optical confocal microscope, a laser excitation source (633 nm), and a detector. The sample is first illuminated with visible light, which is focussed on a chosen area. The visible light source is then switched off and the laser source is used to excite the area in focus. Raman scattered photons are then passed through a pin hole aperture to a Michelson interferometer from which the Raman shifted regions are inferred. Rayleigh scattered radiation is prevented from reaching the detector by selective filters. The data from the interferometer give a plot of Raman shift vs. intensity (given as a count of photons).

The optical microscope can be used to focus on a large area, the laser beam can then be moved incrementally giving a spectrum at each increment and generating a map of the chemical structure over the area.

The laser beam focuses only on the surface of the material and so the spectra represent only the surface chemistry of the material. The area to be mapped must be flat so that the laser can remain focused as it scans and clear spectra can be found.

Raman Resolution

In Raman spectroscopy, once again it is the distance travelled by the moving mirror in the Michelson Interferometer that determines the wavelength resolving power of the instrument.

The spatial resolution of the Raman microscope is limited by the optics of the microscope; the slit size and the 'pin hole' aperture size. In most cases this will be around 5 μm, and so features smaller than 1 μm (for example small particles of filler) will not be shown as distinct in a Raman map. In this project, the increment for each spectrum in the mapped areas was 2 μm.

A Lab Ram spectrometer instrument (Horiba Jobin Yvon, France) was used to generate all Raman spectra in this project.

2.2.7.1 Raman Mapping

Biaxial test specimens that had been hydrated for 24 hours prior to biaxial testing were secured on glass slides with adhesive putty and a suitable flat area of 40 μm^2 of the fracture surfaces was illuminated with visible light under 50x magnification. A 633 nm He-Ne laser excited the chosen surface. Raman spectra were generated over the wavenumber range 100-3000 cm^{-1} by averaging two spectra of 20 s acquisition. Wavenumber resolution was maintained at 2 cm^{-1} whilst the confocal hole of 300 μm gave a spatial resolution of around 5 μm as previously mentioned. Spectra were recorded at 4 μm^2 increments over the chosen area. The background was subtracted from all spectra and the area under each was normalized over the wavenumber range.

The component spectra were determined by selecting spectra from either representative areas of the composite or maps of the filler powder or monomer liquid before mixing. Peaks corresponding to particular molecular groups were identified by comparing the component spectra to literature. Each component spectrum was then assigned a colour. Maps were generated by analyzing and colouring each 2 μm area depending on how closely it resembled each of the component spectra.

2.2.8 Biaxial Flexural Testing

In this project biaxial flexural testing has been used to characterize the mechanical properties of formulations. Composite materials are quasi-brittle (as discussed in the Introduction, chapter 1) therefore the compressive strength of composite materials will be higher than the tensile strength. When subject to bending, the bottom edge of a test specimen is in tension. The failure of the specimen is governed therefore by the tensile strength of the material. The tensile strength of a material is defined as the maximum tensile stress in the material at first failure. This is taken to be the critical 'strength' of resin composite materials throughout this project.

There are, however, different experimental setups for determining flexural strength that can lead to variation in the results achieved. This section will explain some of the background of flexural testing, some of the advantages and limitations of biaxial testing compared to other flexural testing methods, and the reasons for selecting the biaxial flexural test protocol that is employed in this thesis.

2.2.8.1 Biaxial Flexural Testing Background

There are many flexural test methods for characterizing maximum tensile stress in a material at failure (and hence the flexural strength of that material). Beam flexural testing (4-point bend) is specified in ISO 5833 for determining the flexural strength of acrylic resin cements. 3 and 4-point bending have been used to determine flexural properties of cement materials (56,57,61,81,84,86,87,98). Biaxial flexural testing has

been used extensively in the determination of mechanical properties of dental materials and bone cements (10,62,64,99–101). The comparison of testing methods has been the subject of research also (99,100,102–105).

In uniaxial testing (such as 3-point and 4-point bending tests) there is a simple stress state (the beam must be long enough to allow this) where the stress varies linearly throughout the thickness of the material with maximum tensile stress on the bottom edge and the stress is uniaxial. In 3-point bend, the maximum stress occurs at one point and in 4-point bend there is a region of uniform tensile stress between the loading points. In biaxial testing the stress state is more complex, and the maximum stress is concentrated on a small volume on the underside of the specimen. The volume over which the maximum stress acts is larger in 4-point than in 3-point bending and both are larger than for biaxial testing. A larger volume subject to maximum stress will mean a more flaws sampled which could result in a more scatter of results (104,106) making 3 and 4-point bending less reproducible than biaxial testing.

Flexural beam testing often requires larger specimens requiring more material at more expense. Rectangular beam specimens can also be difficult to manufacture, increasing the possibility of flaws. One major disadvantage of beam bending flexural tests is the possibility of spurious edge failures due to the likelihood of manufacturing producing flaws at the edges of beam specimens where the maximum shear stress is experienced. Biaxial specimens do not suffer from edge failures in the same way; the disc specimens are easier to make and can be smaller – these are two major advantages of biaxial testing.

In the literature, one of the arguments for using biaxial testing is that for dental materials, biaxial flexure is more representative of occlusal stress state (103). Obviously this project is investigating materials for bone repair. It is envisaged that the bone repair materials will be used in osteoporotic vertebroplasty and femoral neck

screw augmentation. In vertebroplasty the material is mainly be in compression, whilst in screw augmentation the material stress state is more similar to beam bending. As such this argument is not as applicable in this project.

A range of biaxial test method geometries exist; ball-on-ring, ball-on-three-ball, piston-on-ring are a few of these (100). In this project the ball-on-ring biaxial test method is used – care must be taken to ensure the specimens are flat as this method is not as suitable for warped specimens as the similar 'ball-on-three-ball' method.

There are a number of assumptions behind the equation for biaxial strength; the specimen is assumed to be 'thin', that is, the specimen is assumed to be thin enough that it is in a state of plane stress with no through thickness stresses developing. This simplifies the maths considerably and allows an analytical solution for the strength to be found. Generally a 'thin' assumption requires the ratio of the radius to the thickness to exceed 20. This aspect ratio is only four, in this project, so the values of strength found will be an overestimate of the true strength (107). For this reason the values of strength obtained from this method are useful for comparison between different formulations tested in this way with this specimen geometry but cannot be compared with values of flexural strength obtained from different specimen geometry or different test methods like 3-point bend tests.

Although the biaxial method is not perfect in terms of geometry, the benefits of increased reliability and reproducibility, ease of specimen manufacture, ability to use moulds that are cheap and disposable (e.g. circlips at < 5p each) and small specimen size, are thought to be sufficient justification for using biaxial testing over 3-point or 4-point bending.

2.2.8.2 *Poisson's Ratio*

When a material is subjected to bending stresses (as in Biaxial testing), the material will expand and contract out of the plane of loading. Poisson's ratio is a measure of the

in-plane deformation relative to out of plane deformation. The applied load and the measured deflection are used to calculate the strength and the Young's modulus of the material as described in the following sections. Any Poisson's extension or contraction, therefore, has to be taken into account and the Poisson's ratio included in equations. Polymeric materials exhibit what is known as viscoelastic behaviour (108). They have properties that are time dependent (109); their stiffness is dependent on the strain rate (or over what time period the loading is applied). As the stiffness varies with time so does the Poisson's ratio.

Many sources quote Poisson's ratios, for dental composites consisting of polymer and silica phases, ranging from 0.225 - 0.24 (100,102,103,110). In these papers, the test method for determining Poisson's ratio is not mentioned. A dynamic test method (using an ultrasonic test method) can be used, in which ultrasound is used to excite materials at high frequency. This has been reported to result in higher values for material stiffness than static tests and hence lower values of Poisson's ratio (111). It is clear that strain rate is central to the value of Poisson's ratio measured. In a study by Chung the following findings are summarized: In a compressive test with a low strain strain rate of 0.2 mm/min, a low Young's modulus and therefore a high Poisson's ratio (0.4 - 0.44) was found. In a tensile test with a higher strain rate of 0.5 mm/min, a higher Young's Modulus and so a lower Poisson's ratio (0.3 - 0.39) was found. In dynamic testing using ultrasound and hence very high strain rates a higher still Young's modulus, and so lower still Poisson's ratio (0.23 – 0.27) was found (112). Resin-glass composite materials behave differently at different strain rates; the behaviour of the material at ultrasonic frequencies is not the same as at lower strain rates. In the biaxial test method used in this project, the crosshead speed is 1 mm/min and so strain rates are relatively low. It is feasible therefore to use a value for Poisson's ratio more similar to that determined by low strain rate testing. For this reason a Poisson's ratio of 0.3 has been used throughout.

2.2.8.3 Disc Specimen Preparation for Biaxial Testing

Eight brass rings were placed onto two sheets of acetate on a glass block.

Composite Materials (Including Commercial Composite Cements)

A screw mixing tip was fitted to the double barrelled syringe. Using the delivery gun with an even pressure, enough paste to just fill each of the rings (four at a time) was extruded through the mixing tip (Figure 2-4). One disc requires around 0.2 - 0.3 g of paste to fill it (depending on the Powder to Liquid ratio, PLR). The filled rings were covered immediately with another sheet of acetate and topped with another glass block. The weight of the glass block was sufficient to expel excess material from the rings, but occasionally light manual pressure was also required (for example if a high PLR was used).

PMMA Materials

A metal spatula was used to pack the PMMA materials and smooth the surface level with the height of the ring mould. The rings were covered immediately with another sheet of acetate and topped with a glass block. Light manual pressure was applied to expel excess material.

Specimens of all materials were left in the acetate and rings under glass block pressure at least overnight, and for up to 24 hours, to fully cure. The acetate and brass ring moulds were then removed (Figure 2-8).

After de-moulding, the surface and edge of each disc was checked to make sure it was flat and smooth.

2.2.8.4 Hydration

Discs that were to be tested in their hydrated state were added, individually, to sterilin tubes containing 20 ml distilled/deionized water and stored at 37 °C for 24 hours, or longer, prior to testing.

2.2.8.5 Flexural Testing

Central deflections during the testing should not exceed half of the thickness in order for maximum stress and modulus equations to be valid (107). Eight discs were tested to determine biaxial mechanical properties.

The biaxial flexural strength (BFS), elastic modulus and fracture behaviour of the composite formulations was found using a 'ball-on-ring' biaxial testing method. In this method, a hydrated disk specimen was placed on a knife edge ring support (radius 4mm) and then loaded by a spherical tip in an Instron 4505 Universal Testing Machine (Instron, USA) (Figure 2-9). The load and central deflection of the disk were recorded and plotted on a load vs. deflection graph (Figure 2-10) from which the maximum load at fracture and the pre-fracture slope were determined to find the biaxial flexural strength and elastic modulus respectively.

Strength

BFS, can be determined via Equation 2-10:

$$BFS = \frac{L_{\max}}{t^2}\left[(1+\upsilon)\left(0.485\ln\left(\frac{a}{t}\right)+0.52\right)+0.48\right] \qquad \text{Equation 2-10}$$

Where *BFS* is biaxial flexural strength (MPa)*,* L_{max} is maximum load (N), *a* is support radius (mm) and *t* is average thickness of specimen (mm).

Modulus

The elastic modulus of a disk specimen was found from the slope of the load deflection plot from a biaxial test for a range of different support situations by Higgs et al. (Equation 2-11) (113) The deflection of the centre of the disk specimen during testing is related to the applied load by Equation 2-12. β_c is a variable related to the number of equally spaced supports and is determined by solving Equation 2-13. Assuming a ring support is equivalent to an infinite number of equally spaced supports; as m tends to infinity and *βc* tends to a value of 0.5024. Substituting this *βc* value into Equation 2-12 and differentiating with respect to ω gives an expression for the rate of change of load

with deflection, in terms of the Young's modulus, *E*, which is equivalent to the gradient of the load/deflection plot from a biaxial test (Equation 2-11).

$$\frac{\partial L}{\partial \omega} = \frac{Et^3}{0.5024a^2}$$ Equation 2-11

Where *E* is Young's (elastic) modulus (GPa) and $\delta L/\delta\omega$ is the slope of the load deflection plot.

$$\omega_{\max} = \beta_c \frac{L_{\max} a^2}{Et^3}$$ Equation 2-12

Where ω_{max} is central deflection and β_c is related to *m*, the number of equally spaced supports.

$$\beta_c = -0.064 - \frac{2.2}{m^3} + \left(0.57 + \frac{3.25}{m^3}\right)\left(1 - \upsilon^2\right) + h^3\left[-0.38 + \frac{11.05}{m^3} + \left(0.52 - \frac{7.85}{m^3}\right)\left(1 - \upsilon^2\right)\right]$$ Equation 2-13

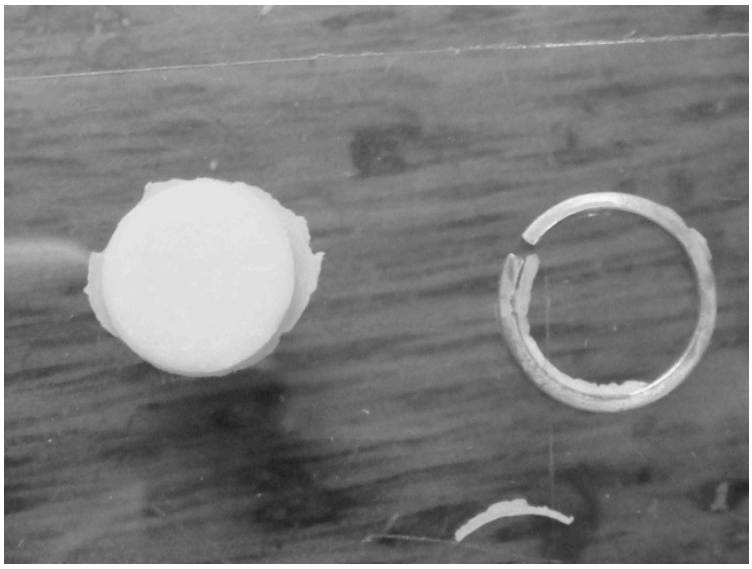

Figure 2-8 Biaxial disc specimen after being removed from bass ring mould, before edges have been smoothed by removing excess material.

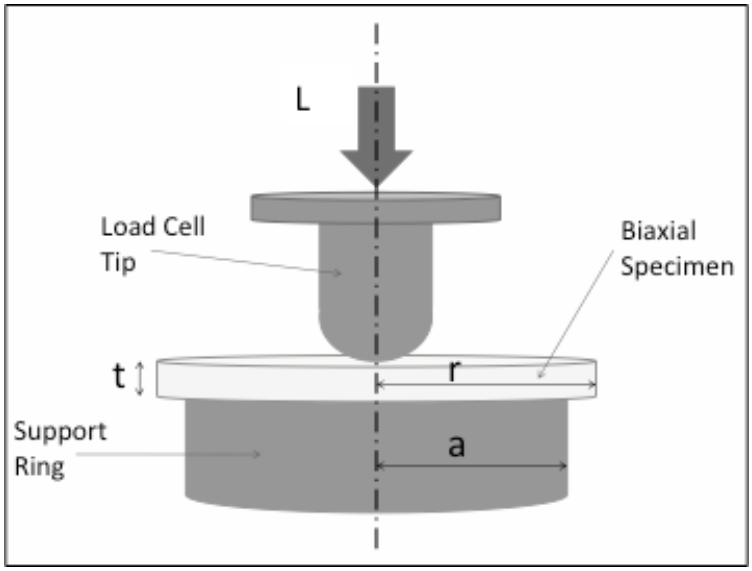

Figure 2-9 Schematic of biaxial test. Disc specimen is placed on a 'knife edge' circular support. The load cell tip (ball bearing) is lowered onto the specimen at 1 mm/min and the corresponding load vs. displacement is recorded. A maximum of central deflection of 0.5t (0.5 mm) is permited.

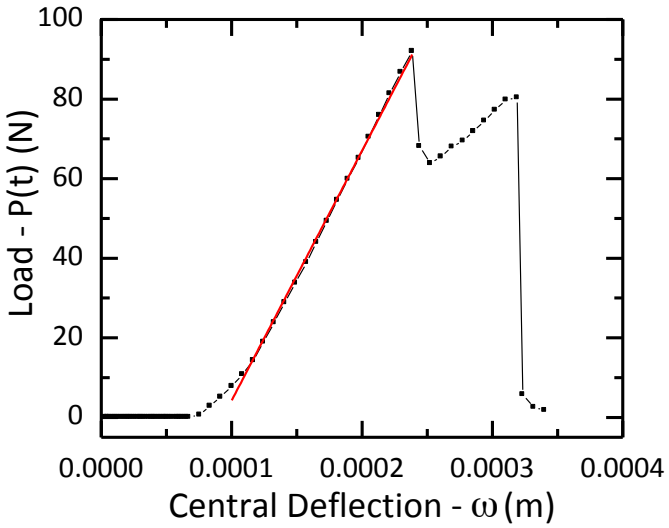

Figure 2-10 This is the load vs. central deflection plot generated by the computer connected to the load cell. The flat region (ω < 0.075 mm) is before the load cell makes contact with the disc specimen. The slope of the plot for 0.075 < ω < 0.24 mm depends on the stiffness of the material. At 0.24 mm the specimen fractures. The load at this point determines the BFS of the material.

2.2.9 Bound Analysis

It is possible to predict the envelope within which the modulus of a composite will lie based on the moduli of the components and the structure of the composite. The simplest models for predicting composite bounds are the Voight and Reuss models. A Voight composite is one in which the phases are in parallel and as such are deformed by the same amount (iso-strain), the applied stress is shared between phase one and phase two proportionally according to their relative stiffnesses. The uniform strain condition leads to a linear equation for the composite stiffness (114)

$$E_{Voight} = \sum_n E_n f_n \qquad \text{Equation 2-14}$$

In a Reuss composite the phases are in series, and hence under the same stress, the deformation is shared proportionally according to the stiffness of each phase (114)

$$E_{\mathrm{Re}uss} = \sum_n \frac{f_n}{E_n} \qquad \text{Equation 2-15}$$

Voight and Reuss composites are described as the upper and lower rule of mixtures bounds for composites. Generally Voight and Reuss models provide the envelope within which the actual composite modulus will be found.

The composite formulations in this study are examples of particulate reinforced composite materials. The Hashin Shtrikman lower bound model (115) can be used to predict the modulus of a particulate composite consisting of stiff particles in a continuous compliant phase (Equation 2-16). Conversely the Upper bound predicts the stiffness of a composite of compliant particles in a stiff continuous phase (Equation 2-17). The Hashin-Shtrikman bounds are derived from a concentric spheres model in which it is assumed that particles are spherical and do not interact with one another (116).

$$E_{HS,Lower} = \frac{9K_L G_L}{3K_L + G_L}$$ Equation 2-16

$$E_{HS,Upper} = \frac{9K_U G_U}{3K_U + G_U}$$ Equation 2-17

Where E is young's modulus or stiffness, K is bulk modulus (Equation 2-18) and G is shear modulus (Equation 2-19) (all GPa).

$$K_{L/U} = K_{m/f} + \frac{f_{f/m}}{\frac{1}{K_{f/m} - K_{m/f}} + \frac{3f_{m/f}}{3K_{m/f} + 4G_{m/f}}}$$ Equation 2-18

$$G_{L/U} = G_{m/f} + \frac{f_{f/m}}{\frac{1}{G_{f/m} - G_{m/f}} + \frac{6\left(K_{m/f} + 2G_{m/f}\right)f_{m/f}}{5G_{m/f}\left(3K_{m/f} + 4G_{m/f}\right)}}$$ Equation 2-19

Where *f* is the volume fraction of a phase. In the Voight-Reuss models, the subscripts '*1*' and '*2*' refer to the individual phases. In the Hashin-Shtrikman model the subscripts '*m*' and '*f*' refer to the polymer and filler phases respectively, whilst '*L*' and '*U*' denote upper and lower bounds. The Young's moduli of UDMA and PPGDMA unfilled polymer resins were taken to be 2 GPa (114) and 0.03 GPa (117) respectively. The modulus of the glass filler was taken to be 72 GPa (118).

The stiffnesses of the PFCs were predicted using the Voight-Reuss and Hashin-Shtrikman models. In the Voight-Reuss case the PFCs were treated as three phase composites; phases one and two being the UDMA and PPGDMA respectively, and phase three the glass. HEMA was assumed to have negligible effect on the mechanical properties because of its very small volume fraction.

The Hashin-Shtrikman model here is for a two phase composite. The organic phase of the PFC materials was a co-polymer of PPGDMA, UDMA and HEMA. Again the effects of HEMA were ignored. It was assumed that the polymer phase was a co-polymer of

UDMA and PPGDMA that fulfilled an iso-stress condition due to polymer crosslinking; both polymers were assumed to be subject to the same stress and share deformation according to their relative stiffnesses as in a Reuss composite. The Reuss-stiffness of the polymer phase was found and this was used as E_m in the Hashin-Shtrikman bound analysis. The filler phase was modeled as a spherical particulate filler in the Hashin-Shtrikman analysis.

2.2.10 Scanning Electron Microscopy and Energy Dispersive X-ray Analysis

All scanning electron microscopy (SEM) images were captured using JSM-5410LV Scanning Microscope (Jeol, USA) and INCA software. Energy dispersive x-ray (EDX) analysis was performed using an Inca X-Sight 6650 detector (Oxford Instruments, UK).

Biaxial specimens were left in their sterilin tubes, with the lid placed on loosely, to thoroughly air dry for at least 7days prior to imaging with SEM or EDX elemental analysis.

2.2.10.1 Imaging

Biaxial Specimens Fracture Surfaces

Biaxial specimens that were to be imaged were mounted onto stubs with fast setting epoxy adhesive with the fracture surface positioned parallel to the stub base.

Filler Materials and PMMA Powders

A thin layer of filler material was mounted onto stubs using adhesive carbon tabs. The mounted specimens were then sputter coated (gold and palladium coating). The accelerating voltage for the scanning electron beam was set at 10 kV.

2.2.10.2 EDX Elemental Analysis

Specimens were mounted as described above in section 2.2.10.1.

Adhesive conductive carbon tape was used to connect mounted specimens of Cortoss, Comp06, and Z250 to their stubs. These specimens and the filler particles were then elementally analyzed without any further coating. The PMMA cements were carbon coated and elementally analyzed. The accelerating voltage for the scanning electron beam was set at 25 kV

2.2.11 Accelerated Ageing

Essentially the Arrhenius equation gives a relationship between the rate of the reaction in question and temperature (Equation 2-20). It was assumed that the spontaneous polymerization of composite bone cement formulations will have an Arrhenius type temperature dependence.

$$k = A\exp\left(\frac{E_a}{RT}\right) \qquad \text{Equation 2-20}$$

Where k is a rate constant, A is the frequency factor (the total number of free radicals generated per second, not all will result in propagation of the polymer chain (polymerization)), E_a is Activation energy, R is the universal gas constant and T is temperature in Kelvin.

The formulations consist of two pastes containing Benzoyl Peroxide (BP) and Dimethyl-para-toluidiene (DMPT) respectively. The rate of spontaneous polymerization of each of these pastes (the shelf life) of the formulation can be related to their storage temperature. In the case of the BP paste the rate of spontaneous polymerization will be controlled by the rate of decomposition of BP. Varying levels of BP/inhibitor and inhibitor will alter the level of spontaneous polymerization at various temperatures and hence follow a different Arrhenius relationship (different frequency factor and possibly activation energy).

The decomposition of the BP or the monomer into free radicals was assumed to be the rate limiting step in the spontaneous polymerization. It was therefore assumed that the rate constant would be directly proportional to the reciprocal of the time taken to polymerize (Equation 2-21). Time to polymerization was defined as the time at which at least one milimetre of polymerized material was seen around the edge of the specimen.

$$k \propto \frac{1}{t_s} \qquad \text{Equation 2-21}$$

Where t_s is polymerization time.

Formulations (uncured) were placed in incubators (maintained at 60 °C, 45 °C, and 37 °C) and monitored every 30 minutes during office hours over two days. When a material showed signs of beginning to cure, it was monitored every ten minutes until the time of set was reached and recorded. The time of set (t_s) was defined as the time taken for 1 mm of cured material to be observed at the edge of the specimen. Three specimens of each formulation were placed in the incubators at 6 hour intervals. In this way it was hoped that if the time of set fell overnight then it could be observed in one of the other specimens placed at a later start time. The natural logarithm of the cure times was plotted against the reciprocal of the corresponding incubator temperature. The Arrhenius equation is given below (Equation 2-22). The Arrhenius coefficients were found from a linear fit of the data plotted according to Equation 2-23.

$$\frac{1}{t_s} = A\exp\left(\frac{E_a}{RT}\right) \qquad \text{Equation 2-22}$$

Taking logs of the Arrhenius equation gives the following straight line equation:

$$\ln\left(\frac{1}{t_s}\right) = \ln(A) + \frac{E_a}{RT}$$ Equation 2-23

From the established Arrhenius relationships for varying levels of BP, Inhibitor and DMPT it is possible to predict the time at which spontaneous polymerization will occur for a given storage temperature and hence what the shelf life of the formulation will be at different temperatures.

The natural log of the reciprocal of the polymerization time can be plotted against the inverse of the temperature in degrees Kelvin for each temperature. This gives three points from which a line of best fit can be found. The gradient of this line gives the activation energy (E_a) and the y-axis intercept gives the Frequency factor (A) for the system.

2.2.12 In-vivo

In many respects the lower femoral implantation procedure is an excellent model for the response of trabecular bone to an implant material. The trabecular bone region of the lower femur is similar in structure to that found within human vertebrae.

Holes were made in the lateral cortex of distal femoral condyles (both right and left sides) of male New Zealand rabbits[2]. The animals, weighed between 2.3 kg and 2.5 kg. A hole of 2 mm diameter was drilled to a depth of 3 mm; this hole was then reamed to a diameter of 4 mm. The bleeding was stemmed with a swab before the materials were implanted.

The allocation of materials to holes was random and the composition of all materials can be found in Table 2-5. There were four replicates of each material and time of implant (n=4). 8 implant sites were filled with low viscosity composite cement and 8

[2] Operations were conducted by Vehid Salih, Ensanya AbouNeel and Peter Revell with full ethical approval.

with commercially available high viscosity PMMA cement, Palacos R (Heraeus PLC, UK).

2.2.12.1 Sterile Cement Manufacture

All cement manufacture/portioning was undertaken in a fume hood sterilized with 70% ethanol.

Palacos R

Portions (0.4 g) of Palacos powder were weighed into sterile jars (sterilized with U.V. radiation for 20 mins). These jars remained sealed at room temperature until opening in the operating theatre where the powder was combined with 200 µl of room temperature Palacos liquid. When the cement had reached the 'dough' consistency recommended by the manufacturer it was implanted by hand into the implant site.

Composite material

The filler was sterilized by UV light for 20 minutes prior to mixing. The monomer was not sterilized as it was hypothesized that it was sufficiently toxic to prevent bacterial growth. The components of the composite cement were combined in the sterile fume hood and then added to a sterile double barrelled syringe (sterilized by immersion in 70 % ethanol for one hour and then air dried in sterile fume hood for 12 hours). The composite cement was prepared on the day prior to implantation and stored at 4 °C until use. The composite cement was injected into the implant site from the double -barrelled syringe using a mixing gun via a sterile mixing tip (sterilized by immersion in 70 % ethanol for one hour and then air dried in sterile fume hood for 12 hours).

2.2.12.2 Post Implantation Care and Euthanasia of Animals

The animals were allowed to move freely in individual cages during the implant time. At one or four weeks the animals were euthanized by barbiturate injection.

2.2.12.3 Specimen Removal

The distal end of the femur was removed and fixed in a 5 % formalin solution. Notes were made on the explanted sites detailing whether the material was visible and how well the wound had healed relative to other sites. Any abnormalities or infections were noted.

2.2.12.4 X-Ray Microtomography Analysis

X-ray microtomography (micro CT) images of the fixed samples were found using the following instrument settings: 50 kV, 800 mA, (power of 40 W) with an exposure time of 5 s through 0.75 mm aluminium. The minimum transmission was 4.3 %. The samples were rotated around the axis of the femur, with images being taken every degree for 360° of rotation. The images were averages over 4 frames per rotation step. These images were reconstructed to give cross sectional images through the thickness of the sample in either the coronal, sagittal, or transverse planes. Micro CT images were used to determine the radiopacity of the implanted materials relative to the surrounding bone. The tissue/material interface was also examined for evidence of bone contact and material interdigitation and distribution. This will give insights into the biocompatibility/effect of curing exotherm, and the effect of cement viscosity.

After micro CT images were obtained, the samples were embedded in Technovit resin and prepared as cut and ground sections (20 μm thick) using an Exakt system (Heraeus PLC, UK). Sections containing the implant site were made as transverse sections and stained with Toluidine blue methods and Goldner's Trichrome stains. In addition, samples of spleen, heart and lung tissue were taken at the time of explant and analyzed for any abnormalities. Samples (approx. 5 x 5 x 5 mm) were taken from

each of the organs at the time of death. Routine techniques for sampling were used (e.g. left ventricle of heart, lower lobe of lung, cross section in middle of spleen, cross section of kidney including pelvis, left lobe of liver). Microscopy screening, by experienced histopathologist, checked the features of each organ for normality and evidence of pathological changes[3].

2.2.12.5 Histological Analysis

The histological sections were examined to determine the biological response to the implant materials (including cellular evidence of inflammatory response and fibrous tissue formation), bone contact and material interdigitation and distribution.

Name	Liquid	Powder	Powder: Liquid (by weight)
Palacos	MMA	PMMA powder, BaSO4	2:1
Composite cement (prototype PFC from chapter 6)	PPGDMA, UDMA, HEMA (10:9:1)	Silica glass powder (G_{4S}), Silica glass fibres (F_{GS}) (3:1)	3:1

Table 2-5 Materials used in in vivo work.

[3] All histological work was undertaken by Tom McInnes

3 Commercial Comparisons

3.1 Abstract

The aim of this chapter was to characterize commercially available PMMA and composite bone cements in order to provide benchmark properties for a successful bone repair material.

Raman mapping and SEM and EDX analysis together provided detailed information on the chemistry and microstructure of the materials investigated. The reaction extent vs. normalized time, from FTIR analysis, was plotted for each material and the conversion, induction time and time to 50% reaction were found. Finally biaxial testing was used to find the flexural strength and stiffness along with the fracture behaviour. The curing profiles, levels of conversion, shrinkage and mechanical and fracture properties were found and compared to the chemistry and phase composition of each material to suggest what materials would be useful in a bone repair material. In conclusion, high molecular weight bifunctional monomers that can chemically bond to fillers will increase the curing and strength of the materials, however the powder to liquid ratio must be balanced to maintain a sufficiently low modulus.

3.2 Introduction

In the introduction (chapter 1) the different types of bone repair material were introduced. In this chapter, two PMMA and two composite bone cements will be investigated along with one dental composite material.

3.3 Aims and Objectives

This chapter aims to characterize and compare the chemical composition, microstructure, curing and mechanical properties of commercially available bone cements and a dental composite. Characterizing each material will provide benchmark

properties for development of new bone cement materials. Comparison with literature will highlight areas in which improvements can be made.

The Raman spectra of each material and available component spectra will be found and spectral peaks associated with the characteristic chemical groups for each material.

The microstructure of cured materials will be investigated and compared to the advertised composition of each material. It is hoped that a novel microstructure characterization method, using Raman mapping, can be established and used with SEM and EDX, to give information about the chemistry of materials at the macroscopic scale including:

- Size, chemistry, surface structure and dispersion of filler particles
- Chemistry of polymer phase
- Interaction between polymer and filler phases e.g. bonding between polymer and filler.

The shape of curing profile and level of cure are to be established, and the inhibition time (t_i) and time to 50% cure ($t_{0.5}$) are to be quantified using FTIR.

Polymerization shrinkage will be calculated from degree of conversion and actual or estimated material composition. Comparison of shrinkage values obtained via calculation, and values from literature, will allow the shrinkage calculation method to be validated.

In terms of mechanical properties, the biaxial flexural strength and Young's modulus, as well as the fracture behaviour, for each material will be determined.

Possible links between the microstructure, curing and mechanical properties will be discussed, including possible failure mechanisms, and candidate materials will be proposed for incorporation in new bone repair materials.

3.4 Hypotheses

It is envisaged that spectra obtained by Raman mapping will be sufficiently variable across an area to enable determination of size, shape and dispersion of the inorganic and polymer filler components within the polymer matrix phases. Chemical variations determined on the micron scale obtained by combining Raman spectral maps and SEM images might provide greater insight into how different phases interact.

It is hypothesized that there will be a link between the level of cure and the mechanical strength of the materials as is reported in the introduction (chapter 1) of this thesis. It is thought that degree of conversion of composite materials should be lower than for PMMA materials as the former are dimethacrylate and will have fewer unbound monomer chains at lower levels of conversion. The calculated shrinkage of dental composite materials is reported in literature to be lower than for composite bone cements and PMMA cements. It is thought that the calculation method for polymerization shrinkage should give results that reflect this.

Literature suggests that dental composite and composite bone cement materials with high filler contents and long chain dimethacrylate monomers will have higher flexural strengths and Young's moduli than PMMA cements. Whilst most of the values of strength in literature are found via 3-point bending experiments, this thesis employs biaxial testing for the reasons outlined in the material and methods chapter. It is thought that the biaxial testing will give strength results consistently higher than those found from 3-point bend tests. It is not known how the Young's modulus results will compare to those found from 3-point bend tests.

Areas in which currently available bone cements fall short of biological requirements have been discussed in the introduction of this chapter. Comparison of the chemistry, composition and curing and mechanical properties of these five commercial materials

could highlight which components are responsible for certain material attributes and therefore determine possible avenues of development for a new bone cement material.

3.5 Materials and Methods

In this chapter, the following four commercial bone cements and one dental composite were investigated and compared:

Simplex™ P	Stryker®, UK	PMMA Bone cements
Palacos R®	Heraeus, UK	
Cortoss™	Orthovita, USA	Composite Bone cements
Comp06™	Ozics, Switzerland	
Filtek™ Z250	3M™ ESPE ™, UK Ireland	Dental Composite

Table 3-1 Commercial materials to be investigated with manufacturer and description.

The composition of each material was ascertained from collating information from the manufacturer's information and literature. The fracture surfaces of each material were examined with SEM and Raman spectroscopy was used to make spectral maps of these surfaces.

The curing profiles and degree of conversion were determined via FTIR (n=4) using changes in intensity of those spectral peaks identified as being involved in free radical polymerization (see chapter 2; Materials and Methods). Polymerization shrinkage was calculated from degree of conversion and formulation composition. The flexural strength and stiffness of the commercial materials was found by biaxial testing of disc specimens (n=8). The fracture behaviour was also observed during biaxial testing.

3.6 Results

3.6.1 Material Composition, Chemistry and Microstructure

3.6.1.1 Product Descriptions

Simplex P and Palacos R

Simplex P and Palacos R are chemically curing PMMA bone cements that are supplied as separately packaged powder and liquid components that are mixed in the OR prior to implantation. The powder contains polymer beads, radiopacifier and BP. The liquid component contains MMA monomer, DMPT and inhibitor. On mixing the polymer beads swell and dissolve in the monomer and the initiator system initiates free radical polymerization.

Cortoss and Comp06

Cortoss and Comp06 are two paste, chemically curing, composite bone cement systems. The monomers and fillers are pre-mixed and supplied in a double barrelled syringe. These pastes have low enough viscosity to be easily syringeable and so are deemed to have excellent handling properties compared to the PMMA cements above. One paste contains BP and the other DMPT. On mixing through a screw mixing tip, these components initiate free radical polymerization.

Z250

Z250 is a restorative dental composite material. It is supplied as a single packable pre-mixed paste containing monomer and filler phases as well as photoinitiators. The paste can be polymerized by exposure to intense blue light.

The composition of the commercial materials from manufacturer's information or literature is summarized in Table 3-2. The quantities of the components are given where this information was available.

Product Name	Monomers	Fillers	Initiators & Inhibitors	Filler content (vol.%)
Simplex P	MMA	MMA-Styrene copolymer, PMMA, $BaSO_4$	1.7 - 2.3 wt.% BP, 2.5 vol.% DMPT, 77 ppm HQ	62
Palacos[+]	MMA chlorophyll	PMMA-methacrylic acid copolymer ZrO_2 chlorophyll	0.75 % BP**, 1.0 wt.% DMPT, 64 ppm HQ	62
Cortoss[††]	BisGMA, BisEMA, TEGDMA	glass ceramic, combeite, (3-methylacryloxy-propyltrimethoxy silane)	BP* DHEPT* BHT*	41[~]
Comp06	BisGMA, BisEMA, TEGDMA	Barium boroaluminosilicate glass fumed silica fillers, Hydroxyapatite powder (3-methylacryloxy-propyltrimethoxy silane)	2.0 wt.% BP 2.5 wt.% DMPT 1.0 wt.% BHT	46[§]
Z250	BisGMA, UDMA, BisEMA,	Zirconia/Silica (3-methylacryloxy-propyltrimethoxy silane)	amine*, CQ[†], BHT*	30

Table 3-2 Summary of properties of commercial products. All information from manufacturers usage instructions unless otherwise stated. [+](2) [§]Communication with Ozics *type and quantity information is unavailable, **(40) [†](119)[††](10) [~](59)

3.6.1.2 SEM Images and Raman Mapping

Simplex P

A SEM image of simplex powder is provided in Figure 3-1 below. Raman analysis compared with Simplex manufacturers information and known Raman spectra of PMMA (120), polystyrene (121) and barium sulphate (122,123) from literature confirmed that the round beads (up to 30 μm in size) are MMA-Styrene copolymer. The smaller beadlets (around 1 μm in size) contain both PMMA and barium sulphate –

although it was not possible to distinguish between these in EDX analysis of the filler alone.

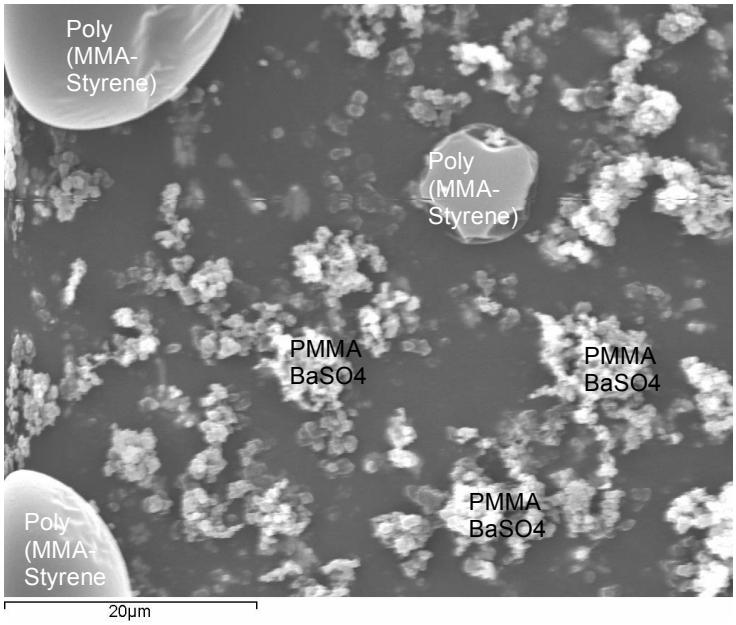

Figure 3-1 SEM image of Simplex P filler powder. Large smooth particles are MMA-styrene co-polymer, smaller flaked particles are either PMMA / barium sulphate.

Figure 3-2 is an SEM image of the fracture surface of a Simplex P biaxial specimen in which pores ranging from 15 – 100 µm are observed. A high magnification SEM image of an area of the fracture surface (Figure 3-3), shows polymer network interspersed with small beadlets and a 25 µm region of polymer containing no beadlets – this indicates either that the pre-polymerized MMA-styrene beads has not dissolved in the MMA liquid prior to polymerization or that this is a region in which the small flaked beadlets have been pulled out of the polymer matrix.

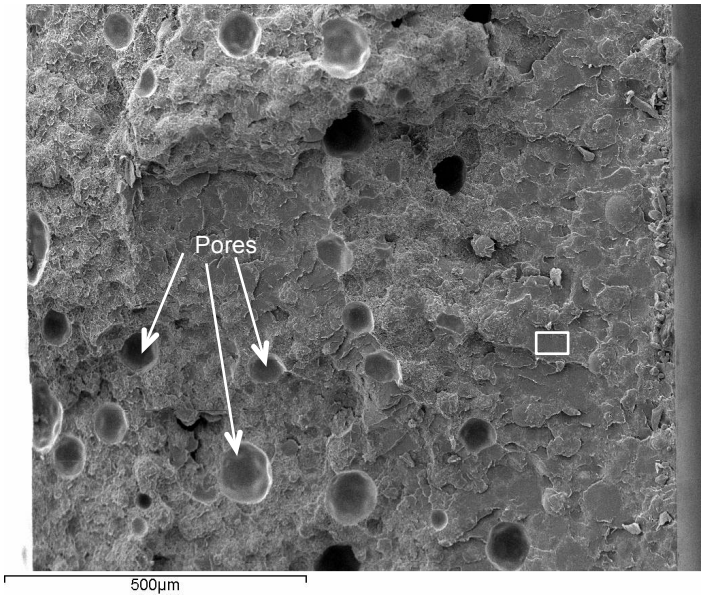

Figure 3-2 SEM image of a fracture surface of a Simplex P biaxial specimen. Can clearly see pores (smooth holes) in material up to 100µms in size. Boxed area shown in Figure 3-3.

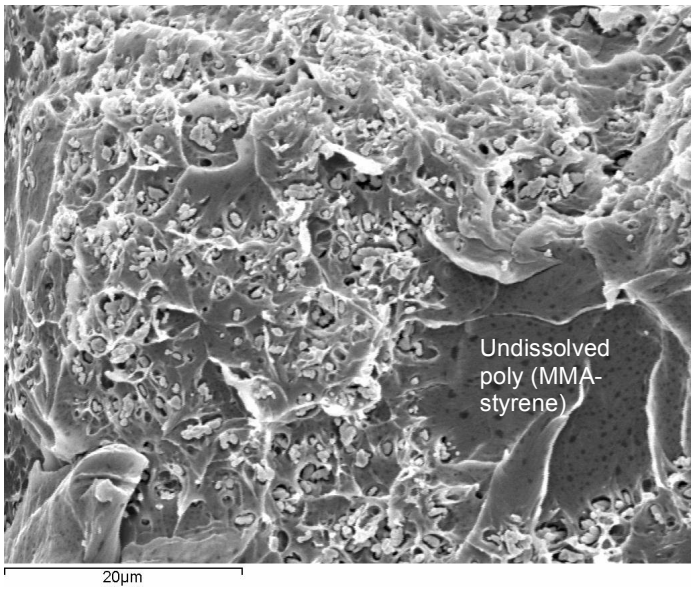

Figure 3-3 Boxed area from figure 2 here shown at higher magnification. Region with no flaked particles thought to be either undissolved MMA-Styrene co-polymer bead or a region where flaked beadlets have been pulled out of matrix during fracture.

The spectra of the phases of Simplex P used to construct the Raman map are shown in Figure 3-4. The MMA-styrene co-polymer spectrum is characterized by peaks at 606, 1002 and 1457 cm^{-1} due to the styrene aromatic ring (121). Peaks at 812 cm^{-1} and 1731 cm^{-1} correspond to C-O-C and C=O vibrations respectively of PMMA (124). The

MMA spectrum has a peak at 1731 cm^{-1} as would be expected, corresponding to methacrylate C=O. The 1620 cm^{-1} peak corresponds to the C=C of the methacrylate group. Subtracting a PMMA spectrum from the combined PMMA-barium sulphate spectrum isolated the barium sulphate spectrum, as it was not possible to find areas of pure $BaSO_4$ with the Raman technique. The barium sulphate spectrum was confirmed by comparison with a spectrum found by Degen and Newman (122).

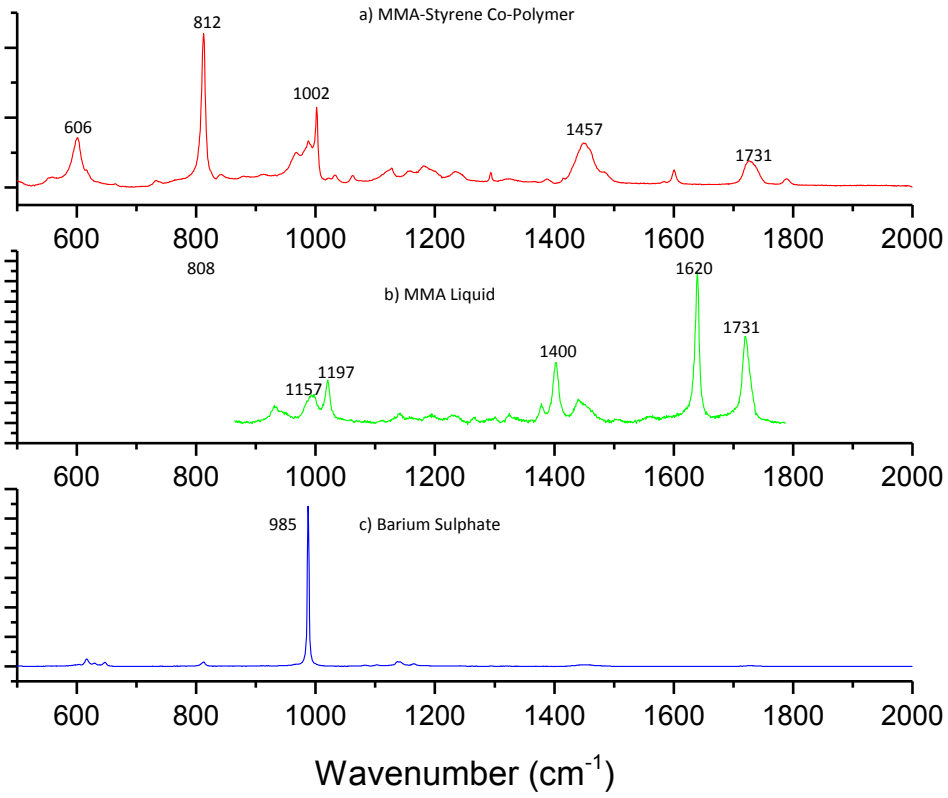

Figure 3-4 Raman spectra of components of Simplex P. RED: MMA-Styrene copolymer, GREEN MMA liquid, BLUE: barium sulphate.

In the Raman map of Simplex P (Figure 3-5) the blue map represents areas with a barium sulphate spectrum. The green map indicates areas in which a MMA liquid spectrum was detected. The red map indicates regions that have a spectrum corresponding to the MMA-styrene polymer beads. These three coloured maps when overlaid give the fourth map in the series in Figure 3-5. In the overlaid map, pink

represents regions in which MMA-styrene co-polymer and barium sulphate spectra are co-incident, whilst yellow denotes areas of C=C presence in the polymer phase.

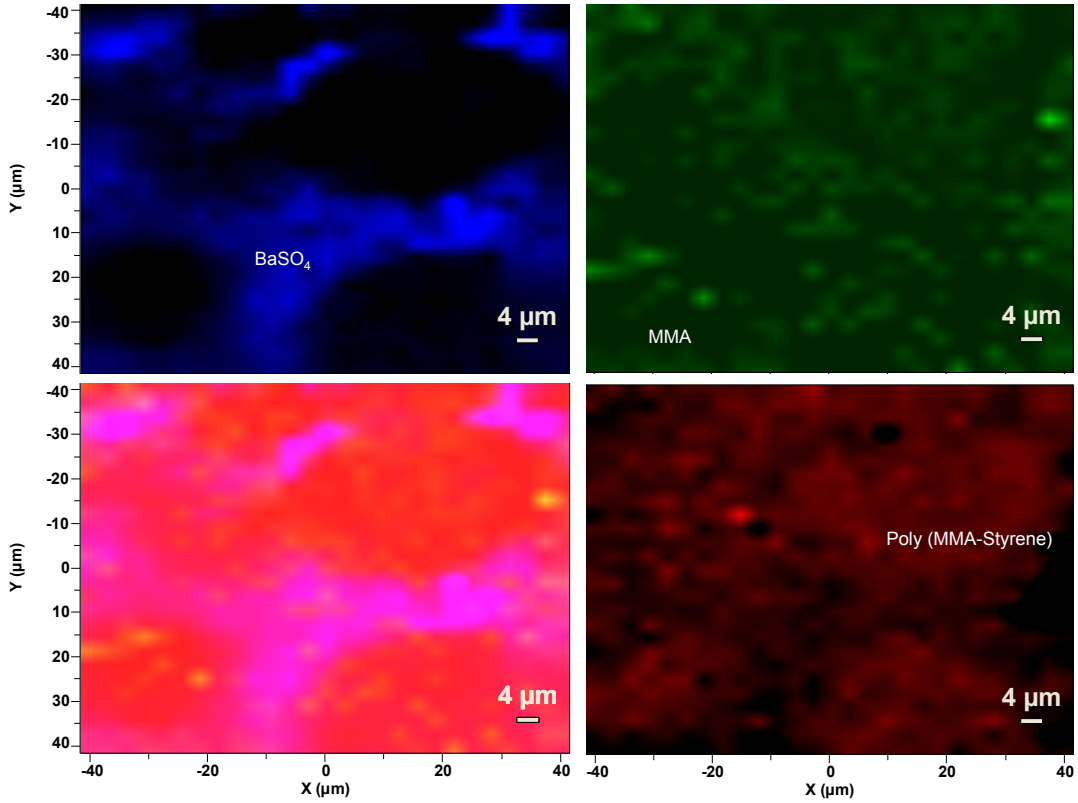

Figure 3-5 Raman maps of a region of the fracture surface of a Simplex P biaxial specimen. The blue map, 1, indicates regions where the spectrum for barium sulphate is present. The Green map, 2, indicates areas where the MMA monomer spectrum is detected. The red map, 3, shows where the spectrum of the MMA-styrene co-polymer was detected. Map 4 is the other three component maps superimposed.

Palacos R

The SEM image of the Palacos powder prior to mixing with the monomer liquid (Figure 3-6) shows polymer beads (PMMA-methacrylic acid) that are 15 – 30 µm in diameter and mainly smooth, and bubbly particle agglomerates. The bubbly particle agglomerates were found to contain Zirconium by EDX and so are thought to be radiopacifier ZrO_2.

Figure 3-7 shows a large scale SEM image of the fracture surface of Palacos, it has fewer voids than the Simplex. An image at higher magnification (Figure 3-8) shows the

polymer network interspersed with ZrO_2 particle agglomerates. The polymer network looks to have pulled away from the ZrO_2 particles during fracture. The polymer is smooth and there are no areas resembling the polymer beads from the powder.

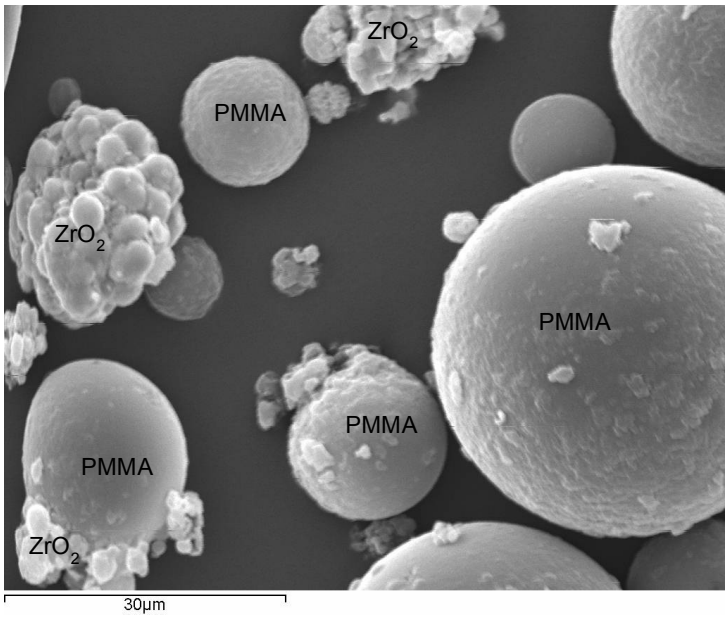

Figure 3-6 SEM image of Palacos filler powder. Large smooth particles are PMMA-methacrylic acid, bubbly particle agglomerates are Zirconium dioxide confirmed by EDX.

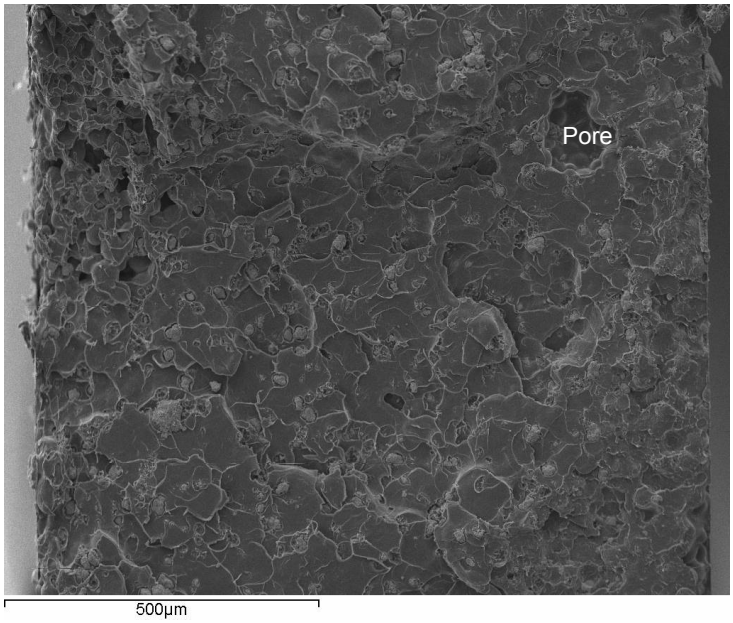

Figure 3-7 SEM image of fracture surface of Palacos Biaxial specimen showing the entire thickness of the sample. One large pore is visible in this area.

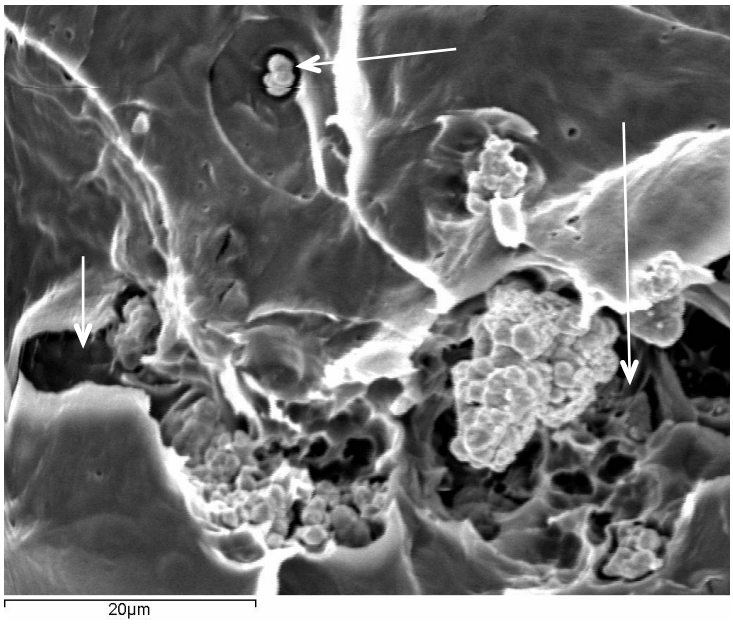

Figure 3-8 SEM image of Palacos fracture surface at higher magnification. ZrO_2 particles have space around them where polymer has pulled away during fracture (arrows). Polymer appears smooth – no visible polymer particles still in tact.

The spectra for each component used to make the Raman map of Palacos and the peak wavenumbers are in Figure 3-9. The Polymer phase is characterized by the 816 cm^{-1} peak corresponding to C-O-C chemical group, with the 1736 cm^{-1} peak due to C=O stretching (120,124). The methyl methacrylate monomer phase again is differentiated from the polymer by it's prominent C=C peak. The ZrO_2 finger print region comes below 750 cm^{-1} and is consistent with monoclinic zirconium dioxide (125).

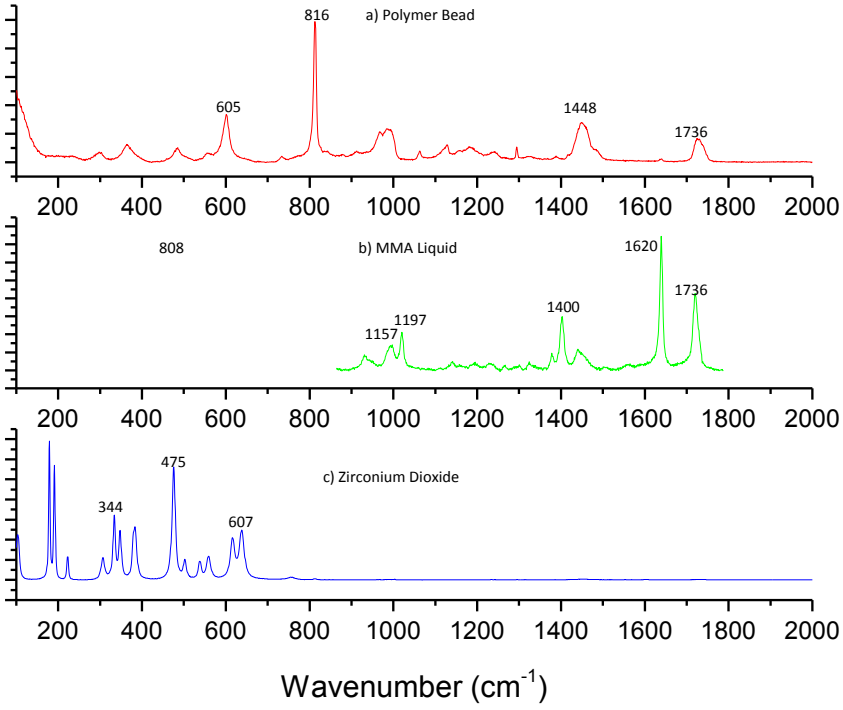

Figure 3-9 Raman spectra of components of Palacos R. RED: PMMA bead from filler, GREEN MMA liquid, BLUE: Zirconium Dioxide.

The Raman map of Palacos is shown in Figure 3-10. The red areas are where the polymer bead spectrum was detected. The green areas indicate regions where the spectrum is most similar to MMA liquid. The blue areas indicate the ZrO_2 particle agglomerates with a size of around 25 μm. All three phases are distinct and separate

as was thought from the EDX analysis. As with the Simplex P map, the green region denotes unpolymerized monomer.

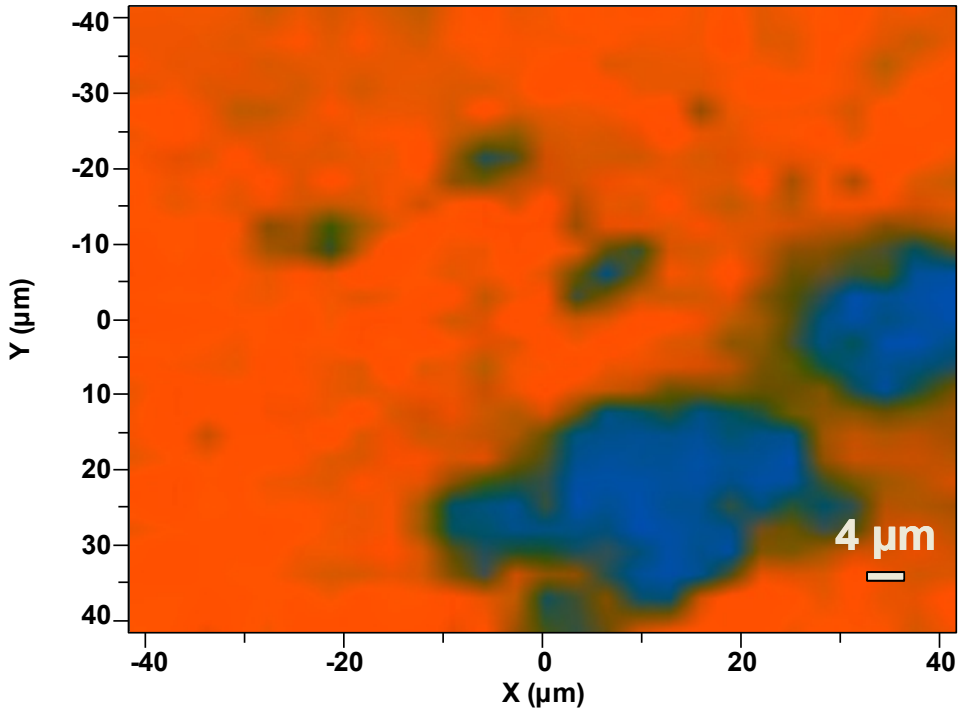

Figure 3-10 The overlaid Raman map of a region of the fracture surface of a Palacos biaxial specimen. Blue indicates regions where the spectrum for Zirconium Dioxide is present. Green indicates areas where the MMA monomer spectrum is detected. Red shows where the spectrum of the PMMA polymer beads was detected. The three phases in Palacos are distinct and so only the overlaid map is displayed.

Cortoss

Figure 3-11 and Figure 3-12 show the fracture surface of Cortoss. The higher magnification SEM image (Figure 3-12) indicates that the fracture surface of Cortoss consists of large angular particles (20x5 µm) interspersed in a mixture of smaller rough particles and polymer. The fracture surface shows some large angular particles protruding with other angular shaped 'holes' (of the same size as the large angular particles). Other round holes were present (50 µm) although are not shown in Figure 3-12 – these are air bubbles from the mixing and sample injection processes.

Using EDX it was found that both the large angular particles and the small rough particles contain calcium and silicon. The large angular particles contain sodium,

calcium, silicon and oxygen so may be combeite ($Na_2Ca_2Si_3O_9$) although Si: Ca = 2.5 was higher than expected. This could be a consequence of surrounding particles with high Si content. The smaller particles contain oxygen, barium, calcium and silicon (Si: Ca = 5) and so likely to be a barium containing glass.

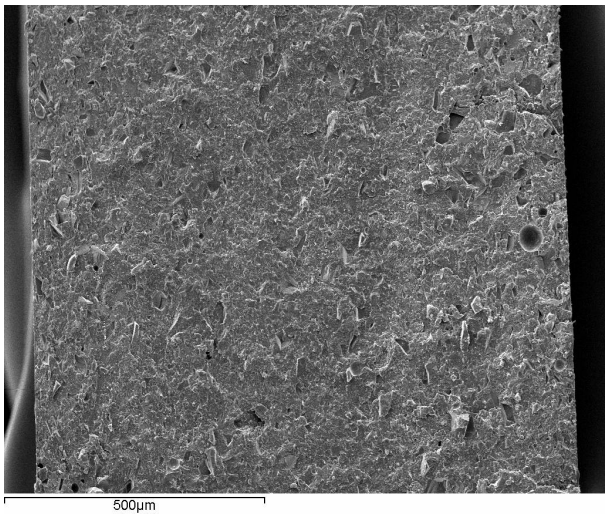

Figure 3-11 SEM image of cross section of Cortoss biaxial fracture surface.

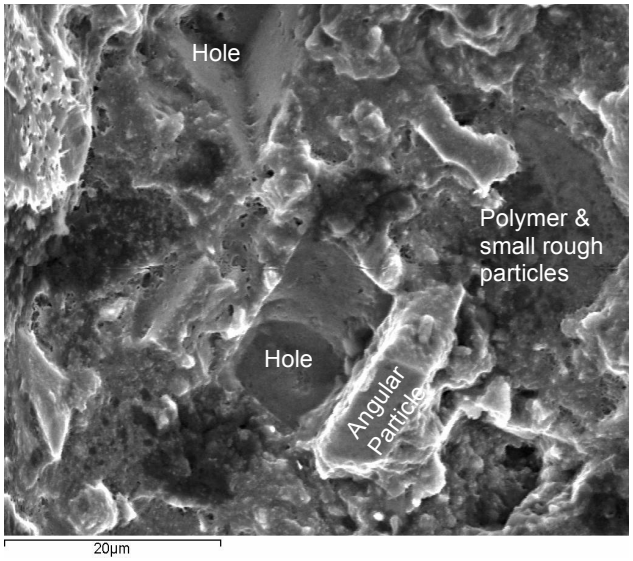

Figure 3-12 SEM image of the fracture surface of Cortoss. Large angular particles were interspersed in, what looks like, a mixture of Polymer and smaller rough particles. Holes the same shape and size as the large angular particles also evident.

The spectra used to construct the Raman map of the Cortoss fracture surface are shown in Figure 3-13. The glass phase is characterized by strong peaks at 1371 cm^{-1}

and 1400 cm^{-1}. The polymer phase is characterized by a peak at 1612 cm^{-1}, which represents the aromatic carbon ring in both the BisGMA and BisEMA; the C-O-C group in these monomers is also responsible for the 1115 cm^{-1} peak. There is also a double peak at 1400 cm^{-1} and 1455 cm^{-1}, which represents the aliphatic C-H vibrations for TEGDMA, BisGMA and BisEMA. There is a slight 1640 cm^{-1} peak which represents C=C in unpolymerized methacrylate groups. The third phase was assumed to correspond to Combeite. It is characterized by a single strong broad peak at 984 cm^{-1}. Although the Raman spectrum of combeite could not be confirmed by comparison with literature.

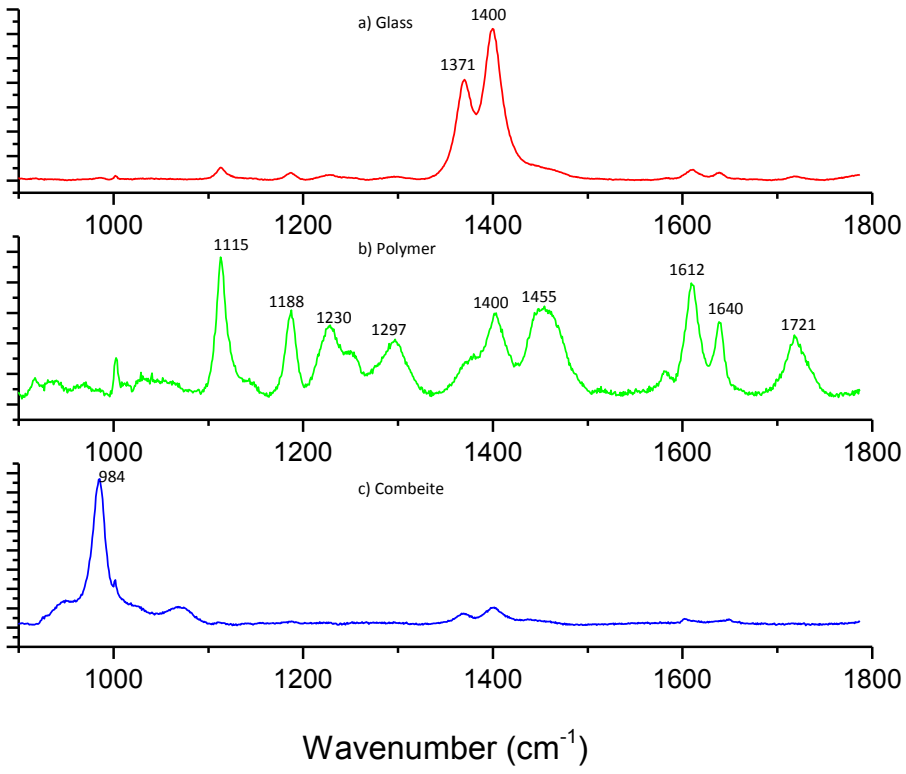

Figure 3-13 Raman spectra of components of Cortoss. RED: glass filler, GREEN BisGMA, BisEMA TEGDMA polymer, BLUE: Combeite phase.

Polymer spectra from the Raman map (Figure 3-14) were comparable at all points indicating no phase separation of the different monomers at the micron scale. Raman mapping indicates that there are distinct glass particles of the order of 5 μm but in addition areas consistent with flocs of submicron glass particles. Larger regions with

combeite spectrum were detected particularly in the top left corner of the Raman map. The size was consistent with the larger particles seen in EDX and tentatively assigned as combeite. The glass, polymer and combeite are generally well separated

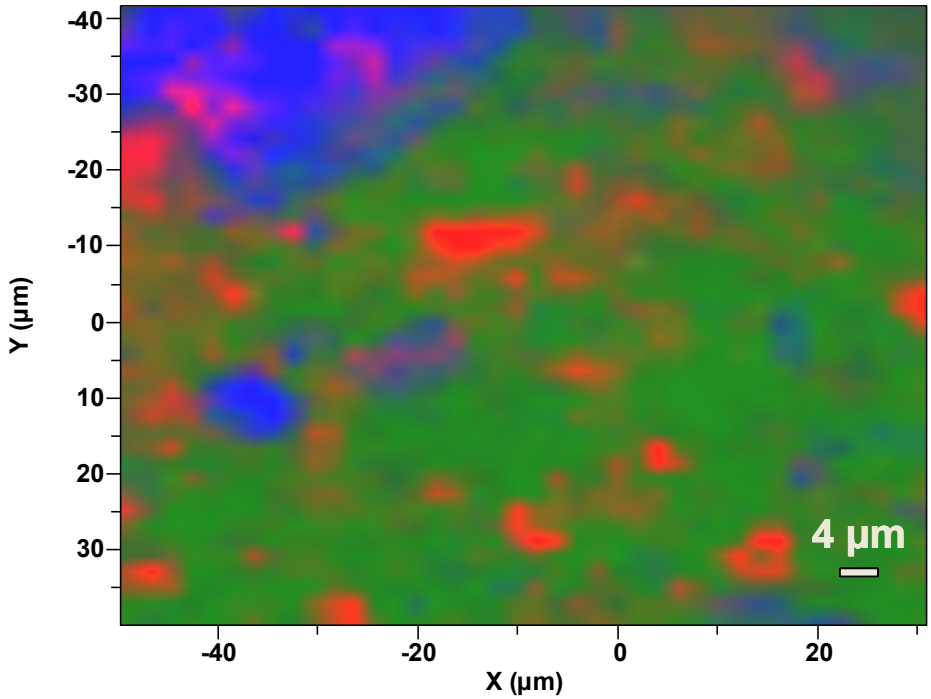

Figure 3-14 Raman maps of a region of the fracture surface of a Cortoss biaxial specimen. This map superimposes where the spectra of each phase is detected. The green corresponds to polymer, the red to glass and the blue to combeite-type areas respectively. The phases are mainly separate apart from some association between the glass and combeite in the top left hand corner indicated by a pink colour. The size of the glass particles can be estimated. The top left corner shows some pink (coincident glass and combeite spectra) this is thought to be due to small glass particles on top of a larger combeite particle.

Comp06

The Glass phase of Comp06 was available and could be imaged separately (Figure 3-15). This glass has a range of particle sizes with large angular crystals around 15 µm in size and smaller flocs of crystals from 0.5 – 5 µm in size. EDX analysis of this glass powder showed that it contains Al, Si, S and Ba (oxygen excluded) (molar ratios approximately: Al, 6Si, 0.3S, Ba).

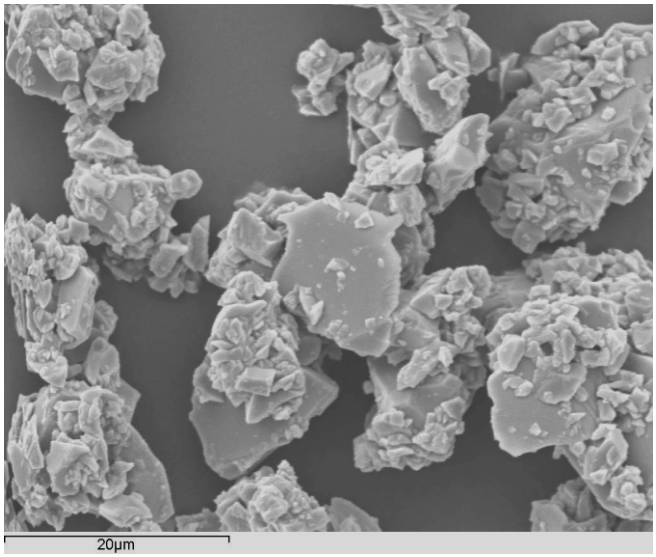

Figure 3-15 SEM image of glass phase of Comp06. Particle size ranges from 0.5-15 µm.

Round holes (20 µm) that are present in the SEM image of the fracture surface of Comp06 (Figure 3-16) are assumed to be air bubbles from the mixing and sample injection processes. The high magnification SEM fracture surface image of Comp06 (Figure 3-17) shows some large angular particles protruding with other angular shaped 'pull out holes' (similar to Cortoss). Using EDX, these large particles were found to contain aluminium, silicon and a small amount of barium consistent with the glass. The hydroxyapatite phase (formula $Ca_{10}(PO_4)_6(OH)_2$) was difficult to detect by EDX.

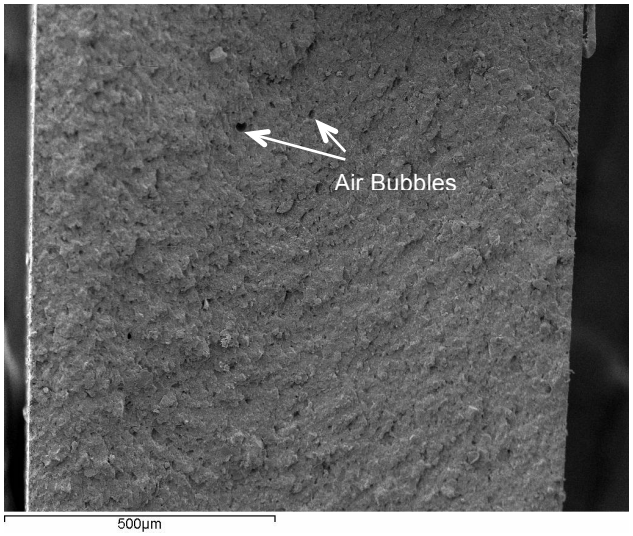

Figure 3-16 SEM image of cross section of Comp06 biaxial fracture specimen. Air bubbles shown with arrows.

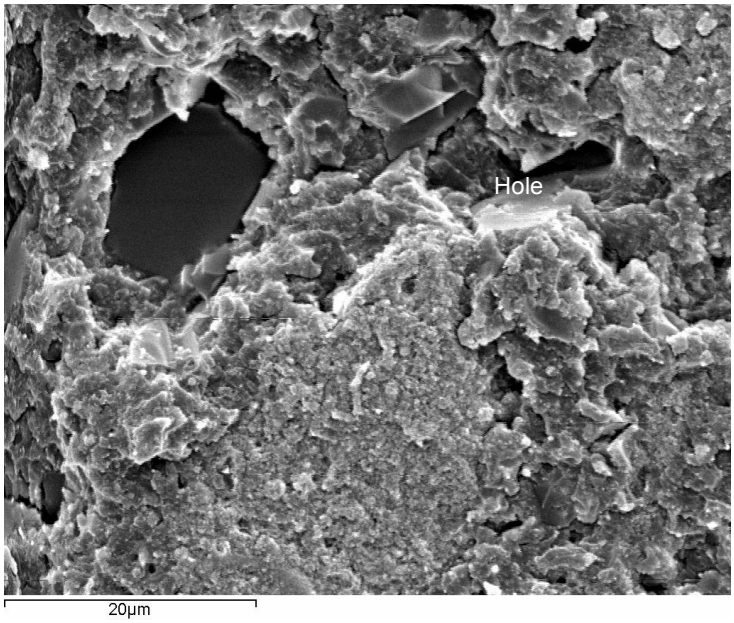

Figure 3-17 SEM image of fracture surface of Comp06 biaxial specimen. 'Pull-out' hole visible and labelled.

The spectra of each of the phases used to construct a Raman map of Comp06 is given in Figure 3-18. The polymer phase contains BisGMA and BisEMA similar to Cortoss and so is characterized once again by the aromatic peak at 1609 cm^{-1}. There is also a 1410 cm^{-1} polymer peak which represents the aliphatic C-H vibrations and slight 1640 cm^{-1} peak which represents C=C in unpolymerized methacrylate groups. The calcium phosphate phase is characterized by a strong peak at 960 cm^{-1} (P-O symmetrical stretching in PO_4) (126). This is comparable with the Raman spectra for hydroxyapatite. The glass phase is characterized by a strong double peak near 1400 cm^{-1}.

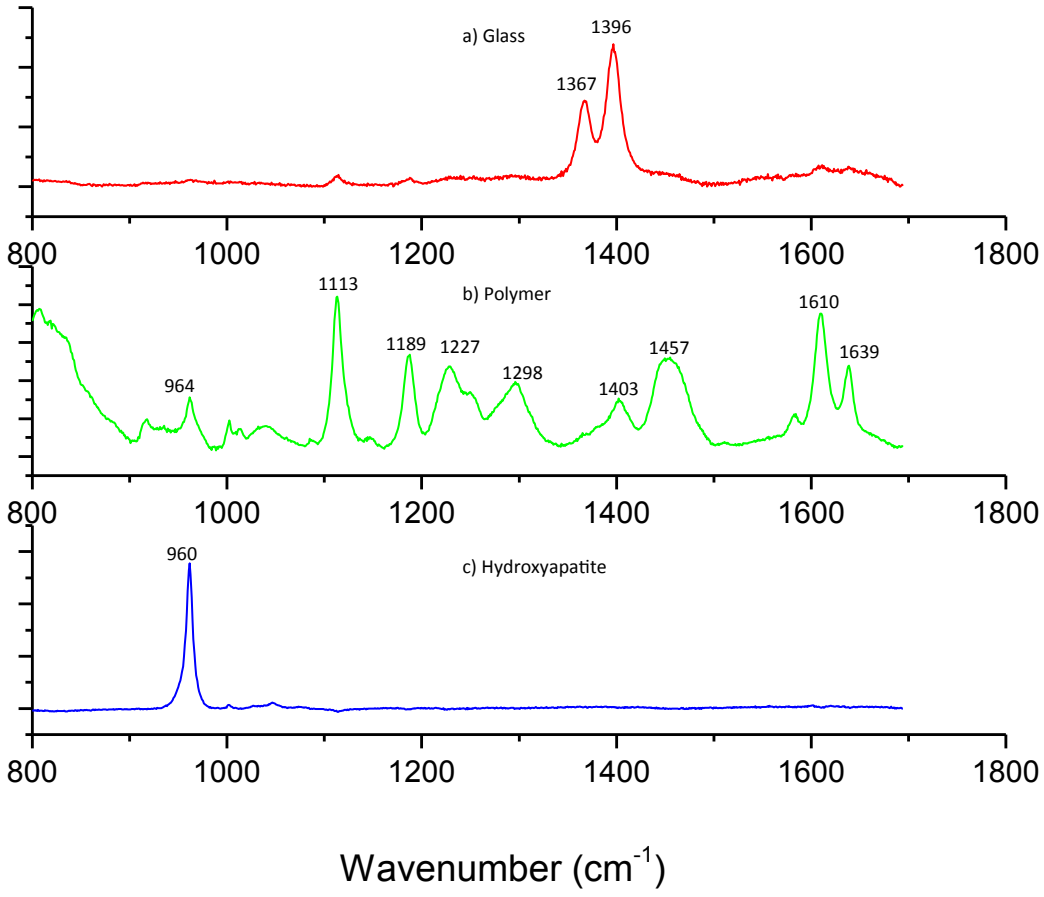

Figure 3-18 Raman spectra of phases used to construct Raman map of Comp06. a) Glass spectrum shown in Red plot. b) Polymer spectrum shown in green plot. c) Hydroxyapatite phase shown in blue.

Figure 3-19 shows the Raman map of the fracture surface of Comp06 with red representing glass, green representing polymer, and blue representing hydroxyapatite. Monomer spectra were comparable at all points indicating no phase separation of the different monomers at the micron scale. In the relatively small area examined primarily only smaller (3-5 μm) glass and hydroxyapatite particles were observed. The glass and Calcium Phosphate phases are separate with no association of the two in the region examined.

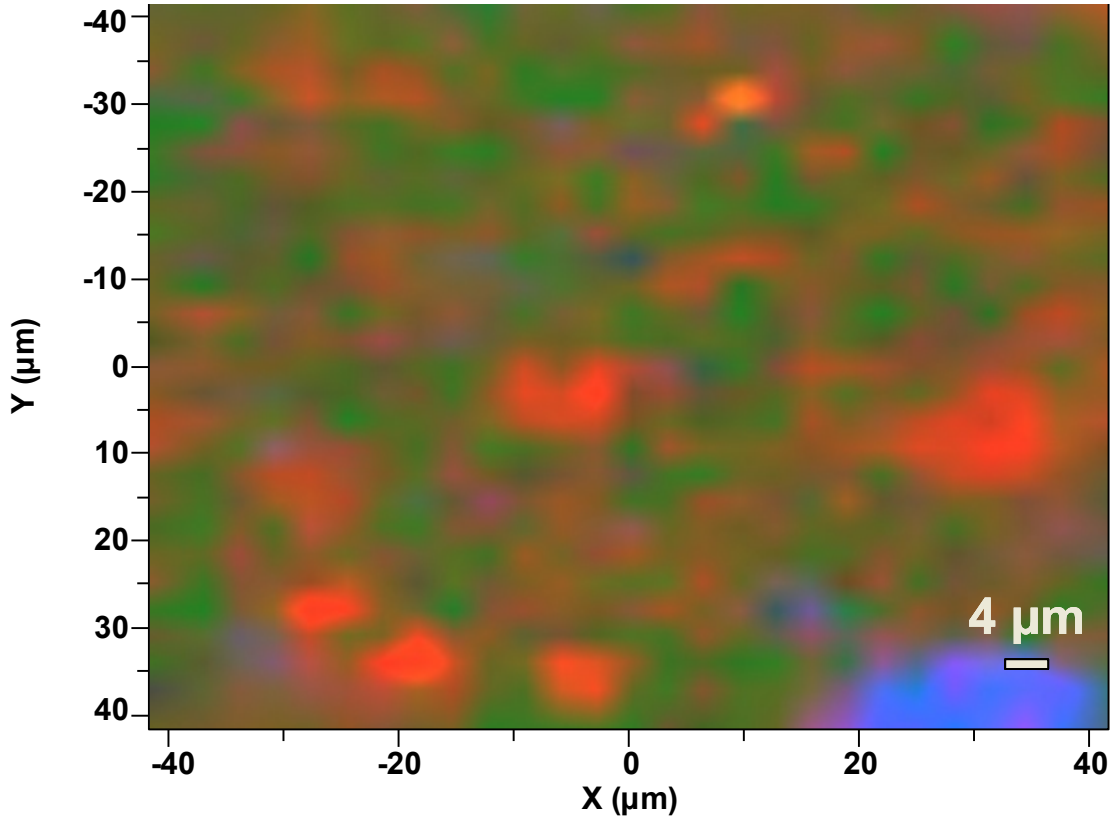

Figure 3-19 Raman map of fracture surface of Comp06. Red regions correspond to glass spectrum. Green areas are polymer. Blue areas denote Hydroxyapatite.

Z250

The grain structure of the Z250 (Figure 3-20, high magnification in Figure 3-21) is very different from the PMMA cements and the composite bone cements. It is difficult to distinguish on the SEM image between the reinforcement glass filler and the polymer network. The glass particles are not distinct and the size cannot be determined from either of the SEM images. EDX of the fracture surface confirmed that the filler phase contained only Si, O and Zr with no calcium. The fracture surface is uneven but it is not clear whether the cracks that lead to failure have propagated through the filler particles or at the interface between the filler and the polymer network.

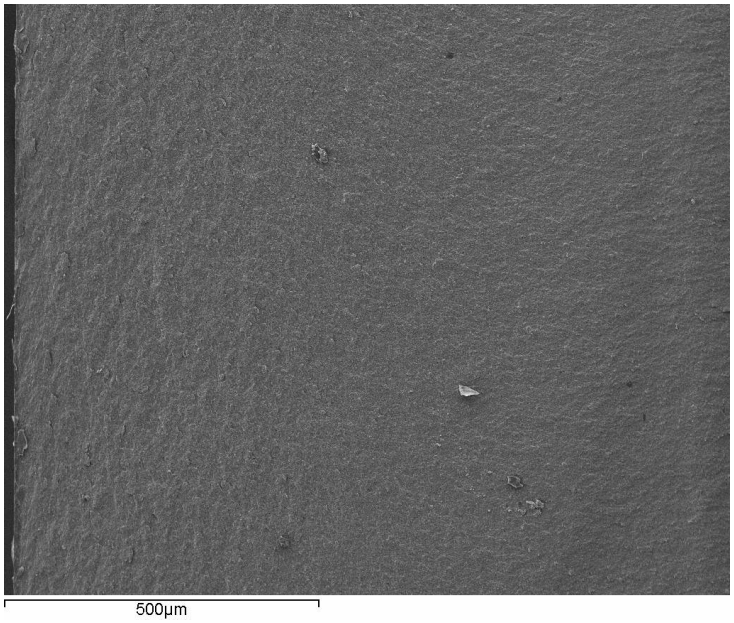

Figure 3-20 SEM image of cross section of biaxial fracture specimen of Z250. Very low porosity.

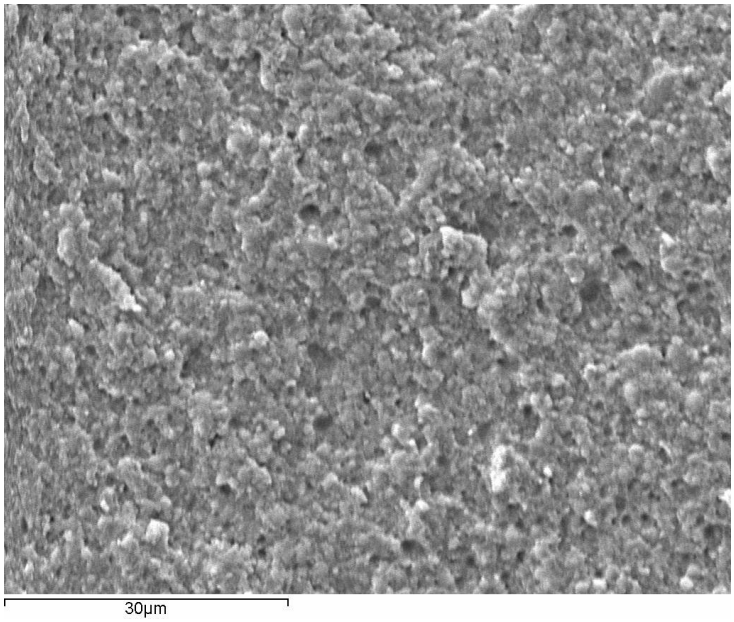

Figure 3-21 High magnification SEM image of fracture surface of Z250. Filler particles and monomer are indistinguishable at this scale.

The spectra of each of the phases is given Figure 3-22. The polymer phase is characterized by a peak at 1607 cm^{-1}, which represents the aromatic carbon ring in both the BisGMA and BisEMA. There are also peaks at 1400 – 1450 cm^{-1} in the

polymer spectrum representing the aliphatic C-H vibrations and slight 1638 cm^{-1} peak which represents C=C in unpolymerized methacrylate groups.

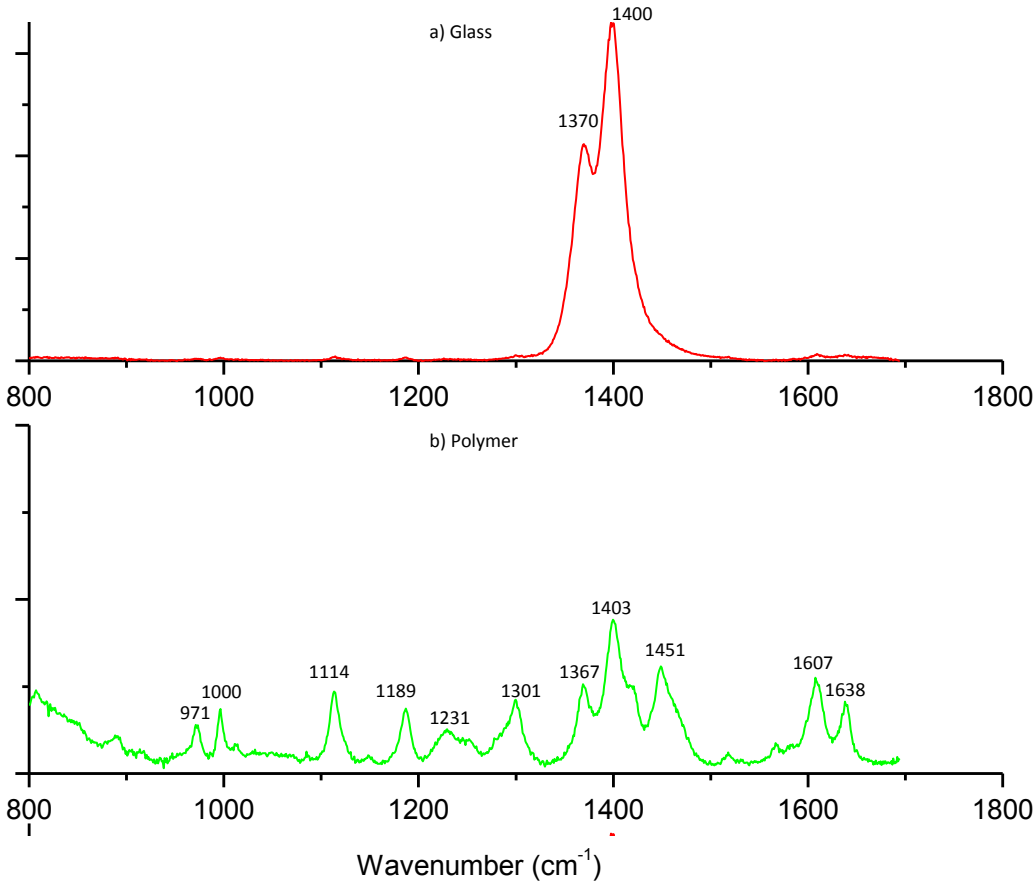

Figure 3-22 Raman spectra of phases used to construct Raman map of Z250. a) Glass spectrum shown in Red plot. b) Polymer spectrum shown in green plot.

The Raman map of the fracture surface (Figure 3-23) shows regions with the polymer spectrum in green and regions of glass in red. The regions of red indicate that the size of the filler in Z250 is around 2 – 4 μm. The particles appear, on the whole, well dispersed but with some regions of flocculation of smaller particles (submicron).

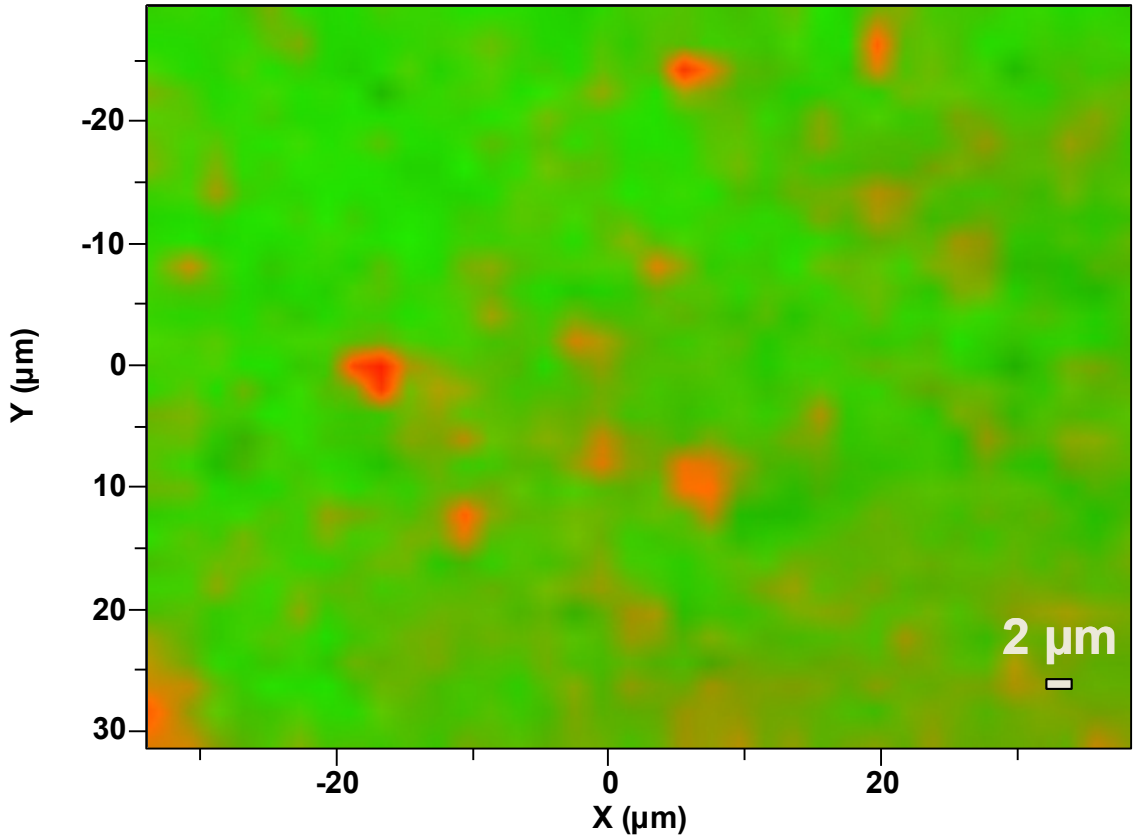

Figure 3-23 Raman map of Z250. Glass particles are around 2 µm in size and shown in red. Polymer phase is shown in green.

3.6.2 Conversion, Cure times and Shrinkage

Table 3-3 gives the cure times and conversion of all materials. Palacos has a shorter inhibition time and faster cure than Simplex with a higher level of conversion. Conversely Cortoss bone cement has the shortest inhibition time before the start of polymerization. All materials have much higher double bond conversion than Z250 whilst Palacos and Simplex P cements have higher conversion than Cortoss and Comp06. Comp06 has a similar conversion level to Cortoss whilst having a longer inhibition time and working time.

Product Name	Conversion (%)	t_{inh} (s)	$t_{0.5}$ (s)	Shrinkage (vol.%)
Simplex P	76 ± 1	276 ± 29	406 ± 28	6.2 ± 0.1
Palacos R	86 ± 2	170 ± 16	281 ± 19	6.9 ± 0.2
Cortoss	64 ± 4	130 ± 29	232 ± 21	3.8 ± 0.1
Comp06	64 ± 0	171 ± 17	416 ± 15	3.7 ± 0.1
Z250	49 ± 1	light cure		1.8 ± 0.1

Table 3-3 Cure times, levels of conversion and calculated shrinkage values for all materials.

Figure 3-24 gives the normalized cure profiles of all the materials. All the materials have a similar shape to these plots, however, they are not totally overlapping.

The sharpness of the plots varies between the materials. Z250 has the steepest profile with the start and end of polymerization being the most abrupt – this is as expected as it is the only light curing material.

The shape of the PMMA cement profiles is overlapping in the range $0.5 < t/t_{0.5} < 1$. At earlier times, however, the Palacos displays a region in which the level of monomer appears to increase (corresponding to a negative value for reaction extent). This behaviour is consistent with swelling and dissolution of the polymer beads; as the beads swell/dissolve the material makes better contact with the crystal and so the level of monomer looks to increase slightly before polymerization begins. The Simplex P

does not exhibit swelling or dissolution behaviour. After $t/t_{0.5} > 1$, the Palacos and Simplex profiles no longer overlap, the Palacos has more complete conversion.

The Cortoss and Comp06 profiles overlap until $t/t_{0.5} > 1.5$. After this time, the rate of polymerization of the Cortoss is faster than the Comp06 leading to a slightly more angular shape. The rate of polymerization of Cortoss and Comp06 is slower (with a more gradual curve) in the latter stages of polymerization compared to the PMMA cements and Z250.

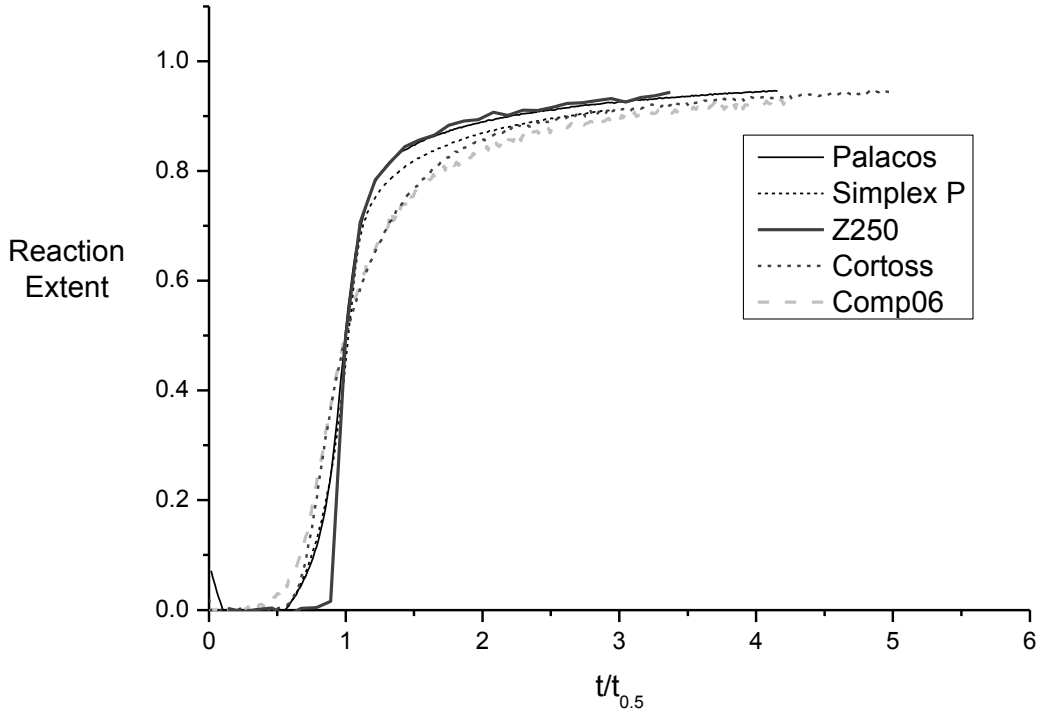

Figure 3-24 Cure profiles of PMMA, Z250[4], Cortoss, Comp06.

[4] Z250 exposed to light source at $t/t_{0.5} = 0.6$

3.6.3 Strength, Modulus and Fracture Behaviour

Palacos and Simplex P have mean strengths of a 145 MPa and 126 MPa respectively (Figure 3-25). These strengths are not statistically different. The elastic moduli of Palacos and Simplex P cements are both 1.6 GPa (Figure 3-26). Z250 has a much higher BFS and modulus than both the PMMA cements (Figure 3-25 and Figure 3-26). Cortoss and Comp06 have comparable BFS to both PMMA cements but have higher modulus. Both the BFS and E of Cortoss and Comp06 are lower than for Z250 (Figure 3-25 and Figure 3-26).

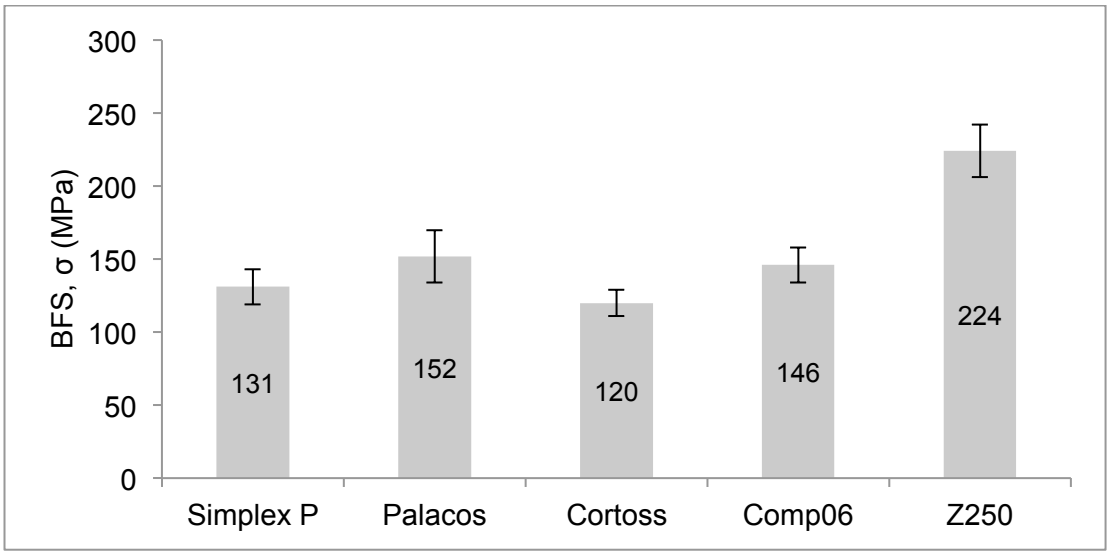

Figure 3-25 Strength of PMMA, Z250, Cortoss, and Comp06 BFS of composite bone cements and PMMA cements are similar. Z250 has a significantly higher BFS than all other materials.

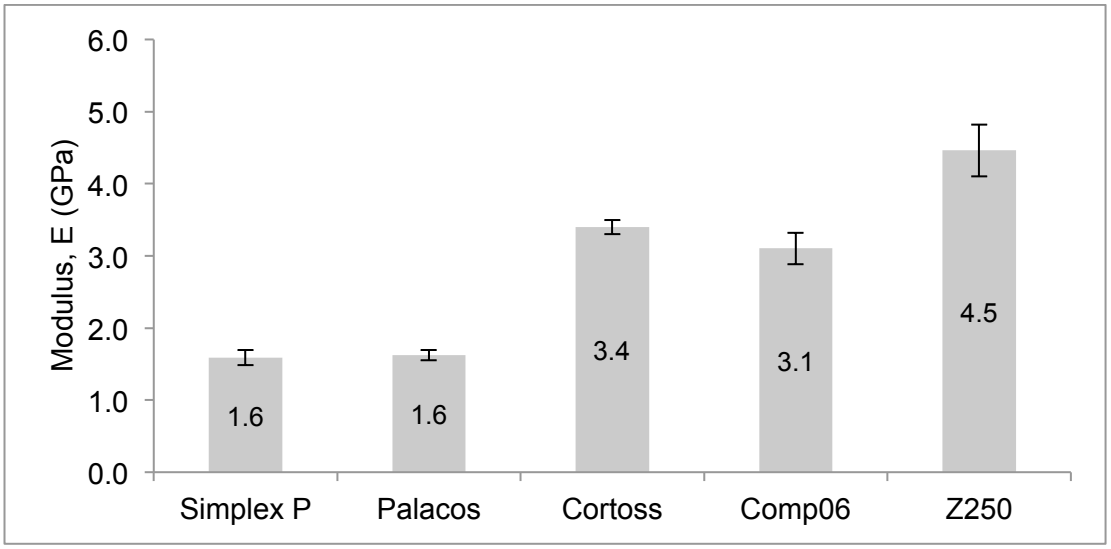

Figure 3-26 Moduli of PMMA, Z250, Cortoss, and Comp06. Moduli of PMMA cements are lower than composite bone cements. Z250 has a significantly higher modulus than all other materials.

Figure 3-27 shows the load/deflection plots for all the materials. The PMMA cements have a 'ductile' type of behaviour compared to the Z250, Cortoss and Comp06 which all exhibit brittle fracture. The number of 'break points' in the graph is indicative of how many pieces the sample fractured into; one or two indicates a break into 3 pieces, whilst 3 indicates a break into quarters.

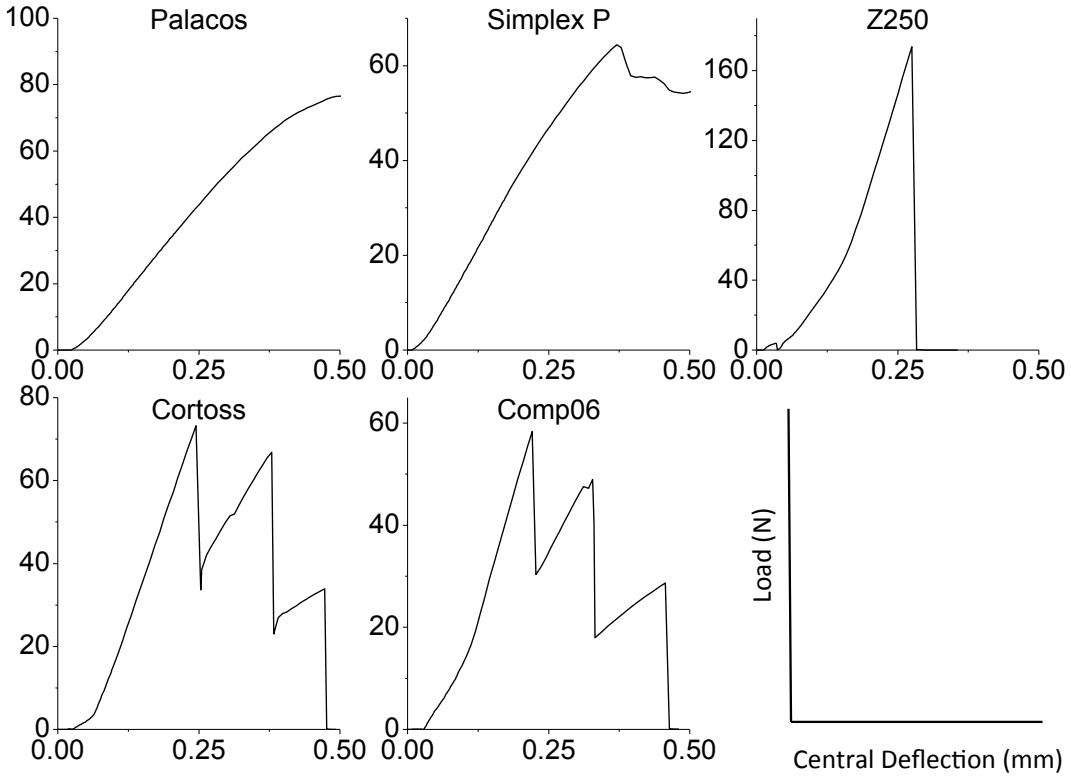

Figure 3-27 Typical load / deflection graphs for each material during biaxial testing. PMMA cements have a quasi-ductile fracture shape whilst the composites display a quasi-brittle fracture pattern with no ductile regions at the loading rate of the biaxial tests.

3.7 Discussion

3.7.1 Microstructure and Chemistry from SEM, EDX and Raman

The MMA-styrene copolymer spectrum has many of the same groups as PMMA. In the 'red' Raman map of Simplex P (Figure 3-5), it is therefore difficult to distinguish the poly (MMA-Styrene) beads from the PMMA flaked beadlets. The dark regions in the blue map, however, could better show where un-dissolved poly(MMA-styrene) beads are. Another way to locate areas of poly(MMA-styrene) would be to isolate the styrene spectra and use this to represent the co-polymer phase. In the overlaid map, points at which a barium sulphate spectrum and a poly(MMA-styrene) spectrum were detected were coincident and appeared pink. It is thought that these regions are due to the PMMA beadlets; it is possible, therefore, that barium sulphate coats the flaked PMMA beadlets. A mixture of components in the flaked beadlets would explain why barium was detected in them by EDX analysis. This could, however, simply be because the barium sulphate particles are small and the resolution of the Raman and EDX is not good enough to distinguish between them and PMMA. Bright green/yellow spots show where incomplete polymerization has occurred – C=C double bonds. These regions occur mainly around the outside of the undissolved poly(MMA-Styrene) beads. MMA has a similar spectrum to PMMA and so the entire map appears slightly green.

The Raman map of Palacos Figure 3-10 shows that the radiopacifier and polymer phases are distinct; the spectra representing each phase described the structure of the material well. This is because the ZrO_2 particles in Palacos were large enough for the resolution of the Raman map to accurately detect them.

The Raman maps of Simplex P and Palacos R have approximately 165 μm^2 and 90 μm^2 unreacted methacrylate in a 1600 μm^2 area; Raman therefore predicts 10 % and 6 % residual monomer respectively. FTIR cure analysis estimate 24 % and 14 % residual monomer for Simplex P and Palacos R respectively. Raman mapping is

therefore not considered an effective tool for estimating the degree of conversion. Usually when Raman is used to calculate the degree of conversion, the average spectrum over a mapped area is compared before and after cure (64). This method is obviously only useful for dual pastes or light cure composites.

Silicate glass spectra in literature mainly identify a peak at around 1000 cm^{-1}, however, this peak could not be detected in glass contained in Comp06; only a double peak at 1350 cm^{-1} and 1400 cm^{-1} was detected in Raman analysis of the glass alone. For this reason, areas with spectra similar to this in the other composite materials (Cortoss and Z250) were assumed to be glass despite not matching glass spectra from literature.

The EDX method was unable to detect phosphorous in Comp06 and therefore the presence of hydroxyapatite could not be confirmed using EDX. Heavy elements, such as barium used as a radiopacifier, scatter x-rays more than lighter ones; it is thought that these heavy elements swamp the x-ray detector preventing the detection of phosphorous in all but very few areas. From the Raman analysis, the volume fraction of silica glass relative to hydroxyapatite in the composite was high; silicon from adjacent glass molecules was thought to be masking the detection of hydroxyapatite also. The hydroxyapatite phase was, however, detected by Raman spectroscopy of the Comp06 fracture surface. In the Raman map of Cortoss and Comp06 the areas of combeite and hydroxyapatite were of similar size and so it is thought that these two composites contain similar amounts of these compounds, however, this would need to be confirmed by mapping of more areas. In EDX analysis, small rough particles were identified in Comp06 that contained aluminium: silicon: sulphur: barium in molar ratios of approximately 1: 6: 0.3: 1. The mass of sulphur detected was very low and so it was assumed that it was contamination on the sample from handling. X-Ray fluorescence (XRF) analysis found that the glass in comp06 contained the elements Al: Si: Ba in the molar ratio 1:8:1. EDX examines only the surface (top few microns) of a sample,

whereas in XRF[5], the sample is ground, the bulk properties can be better determined (127). It is thought that the different penetration depths of each technique could account for differences in results.

The microstructure and texture of Cortoss can be seen to be coarser than for comp06 and Z250 from the SEM images (Figure 3-12, Figure 3-17 and Figure 3-21). In Comp06 the microstructure (via SEM and Raman mapping) had a finer texture than Cortoss. Flocculation would be expected with submicron particles due to surface energy penalties associated with the large surface area of small particles encouraging agglomeration.

3.7.2 Cure Profiles, Conversion and Shrinkage

Palacos has a shorter inhibition time than Simplex P despite having a swelling period associated with polymer dissolution in the liquid monomer. It is thought that the dissolution of Palacos polymer prior to cure, seen in the cure profile and suggested by SEM and Raman mapping, allows a faster subsequent curing reaction than Simplex P. In Simplex P the MMA-styrene copolymer particles appear not to dissolve in the MMA monomer. This is consistent with the curing profile showing no 'swelling' region. The regions with no barium are where the MMA-styrene copolymer beads are – suggesting that they may not have dissolved. It is thought that the solubility of pure PMMA in Palacos has higher solubility than the poly(MMA-Styrene) in Simplex P.

The PMMA cements have a higher degree of conversion than the composite bone cements and Z250, however, from Table 1 it can be seen that the composite bone cements and Z250 contain cross linking monomers whereas the PMMA cements contain only mono-methacrylates and so the conversion is not a clear indicator of which material has lower residual monomer. More discussion of this can be found in chapter 5.

[5] XRF analysis performed by Dr Wendy Xia.

Polymerization shrinkage was calculated from degree of conversion and material composition. As discussed in the materials and methods chapter (chapter 2), polymerization shrinkage and heat generation are proportional to the monomer volume fraction and average molecular weight per methacrylate group. Cortoss contains 41 vol.% filler. Simplex P monomer fraction is 38 vol.%. Using rule of mixtures to find material density will slightly overestimate shrinkage, as it does not take into account any volume due to voids.

The low molecular weight of the Simplex P monomer is therefore the primary reason for its higher shrinkage. Simplex P has been measured to have polymerization shrinkage of between 5 and 7 % (2,42) and Kuehn theorized that PMMA cements will shrink by 7 % on curing (41). These values are comparable than the 6.9 % calculated in the present study despite assuming no voids. In the quoted studies, large volumes of material could have increased polymerization temperatures, enabling higher conversion[6] and hence shrinkage. Therefore, despite non-zero porosity, shrinkage measured is similar to calculated value. Z250 was calculated to have a 1.8 % decrease in volume following polymerization. This figure compares well with reported values for dental composites (around 2 % (62)). This is in part due to the high molecular weight monomers and high filler content that these materials consist of, and partly due to the low conversion of the bifunctional monomers (55 – 75 % conversion, (128)). Cortoss contains similar monomers to Z250 but exhibits around 65 % conversion and so the shrinkage of this material was calculated to be higher than dental materials.

The exact amounts of the monomers in Cortoss, Comp06 and Z250 were not divulged by the manufacturer, the shrinkage results were calculated assuming equal quantities of each monomer, and so it does not make sense to compare the literature values to calculated values to validate the calculation method. The values of shrinkage from literature correspond well to those values calculated for the PMMA cements in which

[6] Discussion of polymerization temperature and subsequent conversion in Chapter 5.

the composition is known. For this reason the calculation method is thought to be a reasonable way to predict polymerization shrinkage.

The SEM image of Palacos (Figure 3-8) shows gaps between polymer and ZrO_2. There is no chemical bonding between the radiopacifier particles and the polymer material. It is thought that the gaps between the ZrO_2 and the polymer could have been enlarged due to polymerization shrinkage of the polymer phase. There are similar levels of shrinkage predicted in Simplex but smaller gaps appear around the PMMA-barium phase because the size of the beadlets is smaller than that of the ZrO_2 particles in Palacos. There is no evidence of shrinkage in the composite materials.

3.7.3 Strength, Modulus and Fracture Behaviour

Biaxial flexural strength (BFS) and Young's modulus (E) of both Simplex P and Cortoss have been found by Boyd et al (10). Cortoss was found to have BFS of around 100 MPa with a modulus of 1.7 GPa, whilst Simplex P was found to have BFS of 150 MPa and Modulus of around 1.1 GPa. Boyd et al. used the ball-on-three-ball arrangement for biaxial testing. It is thought that the different values obtained from this study are due to the different test method employed. As discussed in the introduction and materials and methods chapters (chapter 1 and chapter 2) the strength results obtained from the same test methods and materials in different laboratories give widely varying results. Further, different test methods (for example 3-point bend vs. biaxial methods, and different biaxial methods) can result in different values for strength and modulus and so it is thought that there is little point in comparing BFS and modulus results from literature to those in this project. Rather the strength and modulus values serve as a comparison between other materials in this study.

Palacos contains only monofunctional MMA and has low stiffness relative to strength. This may be because the polymer beads dissolve in the monomer prior to cure and there are fewer voids at the filler/polymer interface compared to polymer/glass

composites. Also unpolymerized monomer acts as plasticizer in both the PMMA cements, reducing the modulus.

In amorphous polymers such as PMMA, strength is increased by raising molecular weight and chain entanglements. With PMMA a long period of dissolution prior to cure may reduce interfacial weakness at the bead / monomer interface. Preventing flocculation of the radiopacifying components (e.g. barium sulphate) could also improve strength. In composites, silane treatment enables a chemical bond between filler and polymer.

The fracture surface of Z250 has a fine but rough texture. Karacaer et al. reported a rough texture of reinforcement post fracture as indicative of a good interfacial bond (129). The high strength of Z250 and rough texture are therefore indicative of a good interfacial bond between the filler and polymer phases.

The grain size of the materials is also indicative of the strength in the composite materials. The smaller filler size in Z250 corresponds to the highest strength although as discussed this is assuming a similar level of bond strength between filler and polymer in the different materials.

The modulus of the material is linked the modulus and volume fraction each of the phases (114). The PMMA cements have low modulus polymer filler and so have low modulus overall. The composite cements have more flexible long chain monomers and lower filler volume fraction than Z250 and hence a lower modulus.

Fewer air bubbles were seen in Cortoss and Comp06 than the PMMA cements. The most air bubbles were seen in simplex P and the least in Z250. It is thought that this is due to the mixing techniques, with the premixed composite materials exhibiting lower porosity. Hand mixing of PMMA cements is thought to be a major source of porosity and variability in porosity. The level of porosity has been shown to correlate with the modulus (28) and this is demonstrated in this project; the lowest modulus materials

being the PMMA cements with highest porosity, and the highest stiffness pairing with the lowest porosity is Z250. Intermediate porosity and stiffness were exhibited by Cortoss and Comp06.

The texture of the fracture surface in the SEM images of Simplex and Palacos (Figure 3-3 and Figure 3-8) would indicate that the polymer network stretched and failed in tension. This is consistent with the ductile shape of the load/displacement curve. There are some holes in Figure 3-8 which are evidence that the ZrO_2 particles have 'pulled out' rather than fracturing indicating that the interface is weak between these two phases reducing strength as discussed above.

The fracture behaviour of the composite materials is quasi-brittle, with no plastic deformation. The Cortoss and Comp06 fracture surfaces (Figure 3-12 and Figure 3-17) show some large angular particles protruding with other angular shaped 'holes' (of the same size as the large angular particles). This behaviour is suggests that the interface between the polymer phase and this angular phase is weaker than the strength of the particles; the particles 'pull out' rather than breaking, debonding such as this can encourage crack initiation as reported by Basaran et al. (79). Brittle cracking around the filler reinforcement is consistent with the brittle fracture shape of the load/deflection plot for these materials.

3.8 Conclusions

SEM and Raman mapping proved to be useful in characterizing the microstructure and chemistry of the commercial PMMA and composite bone cements and the light curing dental composite. EDX gave variable results and was not sensitive to small amounts of compounds containing low atomic mass elements (like hydroxyapatite in Comp06).

Polymerization shrinkage was calculated from level of conversion and material composition. This method for predicting polymerization shrinkage gave similar values to other shrinkage measurement methods, but did not take into account porosity.

The microstructure of the materials along with the curing and mechanical characterization implied the failure mechanisms of the materials. The introduction chapter suggested that current PMMA bone cements had levels of residual monomer and polymerization shrinkage that were too high. Conversely, composite bone cements were too stiff and without sufficient strength for load bearing applications. Curing results suggest that the high molecular weight, and flexible dimethacrylate monomer BisEMA used in Cortoss and Comp06 results in higher conversion than less flexible monomers used in Z250. This monomer choice and a high filler content resulted in lower shrinkage than the lower molecular weight monomethacrylates used in the PMMA cements. From the Biaxial test data and SEM images it is clear that the bond between the polymer and filler and the grain size of the materials is central to the strength whilst a low modulus can be achieved by using high volume fractions of low modulus components. The PMMA cements had ductile fracture whereas the composite materials were inherently brittle. High molecular weight flexible dimethacrylate monomers should be used in conjunction with high filler content to give materials with high conversion with low shrinkage. Fillers that bond to the polymer phase will help increase strength. The level of filler will need to be optimized to maintain low shrinkage and low modulus.

4 Component Screening

4.1 Abstract

The aim of this chapter was to select monomers and fillers that, when incorporated in a composite, show the potential to improve on the properties of current commercial PMMA and composite bone cement materials.

The effect of various fillers and monomers on the handling, cure, calculated shrinkage and mechanical properties of their composites were investigated and compared.

It was found that the filler G_{4S}, which is currently used in Comp06, made composites with the lowest viscosity enabling the highest filler content, which resulted in high strength and could result in lower polymerization shrinkage.

PPGDMA also resulted in composites with good handling properties and high conversion. High molecular weight and crosslinking ability meant composites with lower shrinkage and comparable strength and modulus to Cortoss and Comp06 were possible.

Glass fibres prevented brittle fracture when incorporated in composites at high weight percentages, but did compromise handling.

In conclusion, composites made with silane treated glass G_{4S} and glass fibres F_{GS} and PPGDMA combined with UDMA and HEMA have the potential to outperform current bone cement materials and a systematic study of the effects on composite properties of these components should be conducted.

4.2 Introduction

In the previous chapter, composite bone cements, Cortoss and Comp06, were found to have excellent handling properties. It is thought that a successful alternative composite material should also be deliverable via a syringe and mixing tip.

The shrinkage of PMMA materials was found to be high with composite materials having lower values. High molecular weight monomers and high filler contents are responsible for lowering shrinkage.

PMMA materials did not achieve 100 % conversion and so will have residual monomer. The conversion of BisGMA composites was found to the around 65 % and this combined with the health concerns surrounding BisGMA (discussed in the introduction, chapter 1) mean that UDMA is thought to be a better base monomer for composite bone cements. In addition, UDMA composites have been shown to have superior mechanical properties to BisGMA composites (130). TEGDMA is the most common diluent monomer used in bone and dental composites, although poly(propylene glycol) methacrylates have been reported by some as having enabling high conversions and crosslinking due to molecular flexibility (131–133). In the studies by Abou Neel and Zhao, PPGDMA is copolymerized with polylactide to produce a degradable polymer. In this project PPGDMA is used as a pure polymer and is not degradable.

The merits of silane treated glass fillers were discussed in the introduction (chapter 1) and the previous chapter (chapter 3). Silane treatment is thought to be essential for a good bond between filler and polymer in a composite material thereby enabling high strength.

Also reported in the Introduction (chapter 1) were the wide ranging effects of fibre incorporation on composite mechanical properties. Silane treated glass fibres do have the potential to increase the strength of composites and improve the fatigue resistance by modifying the fracture behaviour.

4.3 Aims and Objectives

The aim of this chapter is to select monomer and filler systems, from the candidate materials, that have the potential to solve some of the problems of PMMA and composite bone cements identified in the previous chapters.

The selection will be based on the handling, curing characteristics, calculated shrinkage and mechanical properties of composites made with each of the candidate components. The success of each composition will be determined by comparison with other candidate composites and commercial materials.

The effect of surface treatment and size and shape of filler particle on the handling and mechanical composite properties was to be determined along with the effect of filler composition on composite radiopacity. The effect of the monomer system on the composite handling, curing and mechanical properties was investigated.

4.4 Hypotheses

In terms of filler incorporation, based on the information gleaned from the literature review (chapter 1) and the results of the previous chapter, it is thought that silane coated glasses will lower composite viscosity enabling high filler content and result in higher BFS/Modulus.

It is thought that fillers containing barium will make more radiopaque composites than those containing low atomic weight elements.

It is envisaged that incorporation of silane treated fibres will change fracture patterns and could increase composite strength.

The hypothesized function of the monomers investigated in this chapter is described in Table 4-1.

	Abbreviation	Name	MW	Function	
High Cross Linking	PETA	Pentyaerythritol tetraacrylate	352	Four polymerizable groups - high cross linking.	Very high Cross linking for high strength but low elasticity
High molecular weight	UDMA	Urethane Dimethacrylate	470	High molecular weight, Low functional group density.	Cross linking for strength and high molecular weight for low Shrinkage/heat generation
Standard diluent	TEGDMA	Tri(ethylene glycol) Dimethacrylate	228	Double methacrylate, low viscosity	Used by many as a diluent (as discussed in introduction, chapter 1)
Flexible diluents	PPGDMA	Poly(propylene glycol)425 dimethacrylate	560	Long chain, flexible, cross linking, low viscosity	Flexible chain between functional groups, to improve conversion and lower viscosity to improve handling
	DDMA	1-10 decanediol dimethacrylate	310		
	PPGMMA	Poly(propylene glycol)300 monomethacrylate	370	Long chain, flexible, low viscosity	
High Conversion	HEMA	Hydroxyethyl methacrylate	130	Single methacrylate, Low viscosity.	Single methacrylate polymerizes residual double bonds to improve conversion. Low viscosity to improve handling

Table 4-1 Summary of function of various diluent and bulk monomers. Molecular weight of monomers listed along with a summary of intended function.

In addition, PPGMMA and PPGDMA were thought to be more hydrophobic than Poly (ethylene glycol) methacrylate (PEGMMA) or Poly (ethylene glycol) dimethacrylate (PEGDMA) preventing excessive water sorption therefore increasing strength.

4.5 Materials and Methods

A selection of monomer and filler materials (candidate materials), selected based on the performance of commercial materials tested in chapter 3 and experimental formulations reported in literature, were investigated via SEM and EDX and then incorporated into composite formulations. These formulations were characterized in terms of composition, handling, cure (times and level of conversion), shrinkage and mechanical properties.

Firstly, five particulate glass fillers (G_1, G_{1S}, G_{2S}, G_{3S} and G_{4S}), a glass fibre filler (F_{GS}), and an aramid fibre filler (F_A), were imaged and their particle size estimated via SEM. Their elemental composition was found with EDX. The experimental particle size and composition were compared to information from the manufacturer.

Handling vs mechanical properties

The wet point of each glass was found. As explained in chapter 2 (materials and methods) the wet point is the amount of monomer that must be added to filler to make a cohesive mass, and is given as a percentage of monomer in the resulting paste. Composites were made from each of the particulate glasses, G_1, G_{1S}, G_{2S}, G_{3S} and G_{4S}, (composition as in table 4-2) were then biaxially tested. The first task was to ascertain whether the wet point correlated to particle size, handling or strength/modulus and then determine the effect of silane treatment on composite properties.

Radiopacity

Composites containing silanated glasses, G_{1S}, G_{2S}, G_{3S} and G_{4S}, were used to fill 2 mm holes drilled in rabbit tibbial bone and their radiopacity compared using microCT.

Effect of fibre incorporation

The effect of fibre incorporation on handling and mechanical properties was tested by comparing composites made with G_{1S} glass and either 10 wt.% or 50 wt.% F_{GS} fibres (table 4-2).

Effect of HEMA

The effect of incorporating the diluent monomer HEMA was investigated by finding the handling, curing characteristics (normalized cure profile and curing times) and biaxially testing composites containing HEMA against those without (table 4-2). All composites PLR 4:1 with G_{4S} glass filler.

Variation of diluent monomers

The effect of various diluent monomers (PETA, PPGMMA, PPGDMA, DDMA, TEGDMA) on the handling, cure, calculated shrinkage and mechanical properties of composites (table 4-2) was assessed.

Polymerization shrinkage was calculated from degree of conversion and material composition.

Full details of all methods can be found in Materials and Methods (chapter 2).

Handling vs mechanical properties and radiopacity			
Monomer (wt.%)	PLR	Fillers	
75 % UDMA 25 % TEGDMA 5 % HEMA	3:1 (G_1, G_{1S}, G_{2S}) 4:1 (G_{3S} and G_{4S})	containing one of G_1, G_{1S}, G_{2S}, G_{3S} or G_{4S}	
Fibre incorporation			
Monomer (wt.%)	PLR	Fibres (wt.% of filler)	Fillers
65 % UDMA 22.5 % TEGDMA 12.5 % HEMA	3:1	10 % or 50 %	G_{1S} and F_{GS}
Effect of HEMA			
Monomer (wt.%)	PLR	Fillers	
64 % UDMA 21 % TEGDMA 14 % HEMA OR 64 % UDMA 35 % TEGDMA	4:1	G_{4S}	
Variation of diluent monomers			
Monomers (wt.%)	PLR	Filler	
30 % diluent monomer 65 % UDMA 5 % HEMA	4:1	G_{4S}	

Table 4-2 Chapter 4 composite compositions. Throughout this thesis, monomer quantities are given as percentages of total monomer. Filler content is either given as PLR or weight percentage of total composite mass. For example a composite quoted as having 75 wt.% UDMA, will have a monomer system that contains 75 wt.% UDMA. Unless otherwise stated all composites in this chapter contain 0.5 wt.% BP / DMPT with 70ppm BHT where these quantities are percentage of total monomer mass. Fibre quantities are given as percentage of filler mass.

4.6 Results

4.6.1 Filler Screening

4.6.1.1 Characterization of Fillers

Five glass filler particles and two fibre fillers were investigated via SEM and EDX. The elemental composition from manufacturer's information and from EDX is displayed in Table 4-3. The elemental composition was determined by taking EDX spectra at a minimum of three different sites. If the spectra obtained at the three sites were substantially different then more spectra were obtained until the most common elements could be determined. There are some elements that were not detected and some discrepancy as to the relative amounts of the compounds present in the fillers was observed. For example, phosphorous was not detected in glasses G_1 or G_{1S} whilst boron was absent from EDX analysis of G_{2S} G_{3S} and G_{4S}. Nitrogen was not detected in the aramid fibres. Calcium, aluminium and magnesium were detected in the glass fibres (F_{GS}) in addition to silicon and oxygen, as expected, but once again boron was not detected. Sodium was found in the EDX spectra of G_{3S} in addition to those elements expected. This indicates some of the limitations in using EDX for elemental analysis.

The particle sizes quoted by the manufacturers were either given as a d50 size or as a size range. The quoted particle sizes can be compared to the SEM images of the filler materials (Figure 4-1 and Figure 4-2); it was found that the sizes were in good agreement. Some of the glass fibres are longer than the 300 µm quoted by the manufacturer but they were observed to make up less than 10 % of total. The aspect ratio of the aramid fibres can be seen to be similar to the glass fibres for the majority of fibres but some in the SEM image are approaching 1 mm in length these were observed to make up between 1 – 2 % of total.

Name	Manufacturers Information		Information from EDX[7]
	Size (μm)	Manufacturer Composition	Elemental composition (molar ratio)
G_1	3.7*	SiO_2, SrO, Al_2O_3, F, ZnO, P_2O_5, Na_2O	18F, 3Sr, 7Si, 6Al, Zn, 2Na
G_{1S}	2*	SiO_2, SrO, Al_2O_3, F, ZnO, P_2O_5, Na_2O	16F, 3Sr, 8Si, 6Al, Zn, 2Na
G_{2S}	2*	SiO_2, BaO, B_2O_3, Al_2O_3	9Si, Ba, 2Al
G_{3S}	10 – 40	SiO_2, B_2O_3, Al_2O_3	24Si, 2Na, 1Al
G_{4S}	12 – 40	SiO_2, BaO, B_2O_3, Al_2O_3	6Si, Ba, Al
F_A	N/A	$[-NH-C_6H_4-NH-CO-C_6H_4-CO-]_n$	3C, O
F_{GS}	15 x 300	SiO_2, B_2O_3	7Si, 2Ca, 2Al, Mg

Table 4-3: Seven types of glass particle, subscript 's' denotes silane treatment. *d50 size quoted, otherwise particle size range given. Manufacturer composition given in order of largest first.

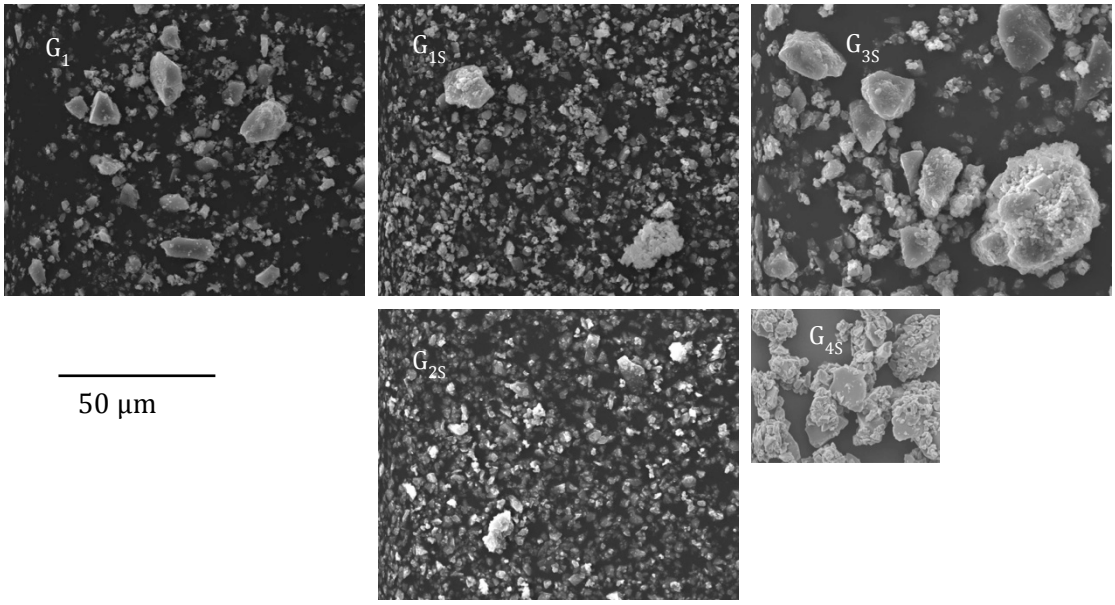

Figure 4-1 SEM images of glass particles.

[7] EDX and SEM analysis of filler materials performed by Dr Nicky Mordan

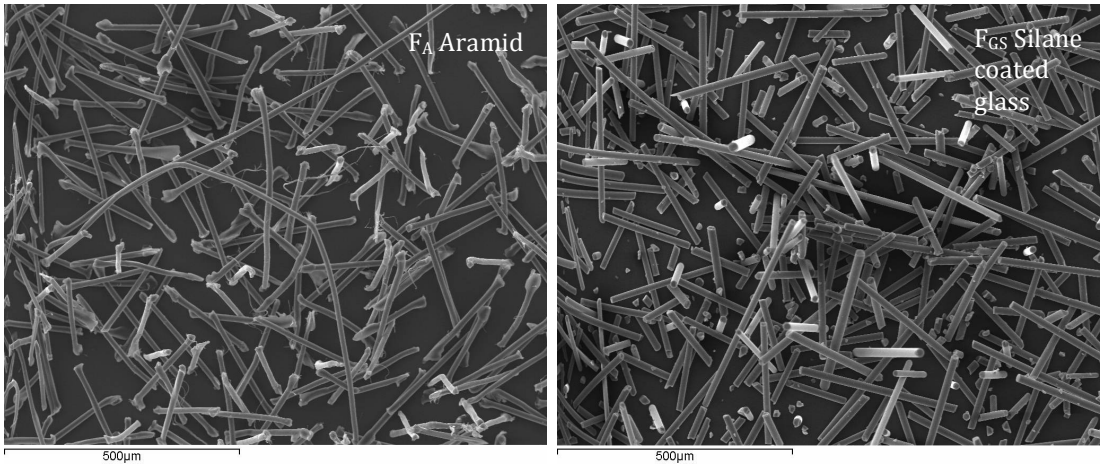

Figure 4-2 SEM images of aramid (F_A) and glass (F_{GS}) fibres.

4.6.1.2 Comparison of Particulate Fillers

The wet point of the available particulate fillers was determined (Figure 4-3). In the case of the non-silane treated glass, this cohesive mass was very stiff and packable. For the silane treated glasses, at the wet point, the paste was also stiff and packable but only a small amount more monomer was necessary to turn the material into a flowable paste. Glass G_{4S} had a lower percentage of monomer at the wet point than all the other glasses. Both G_{3S} and G_{4S} were flowable/syringeable with 80 wt.% filler (PLR 4:1) and so biaxial specimens were made with this level of filler. Glasses G_{1S} and G_{2S} were only syringeable at slightly lower filler contents (75 wt.% - 78 wt.%) and so biaxial specimens were made with 75 wt.% filler.

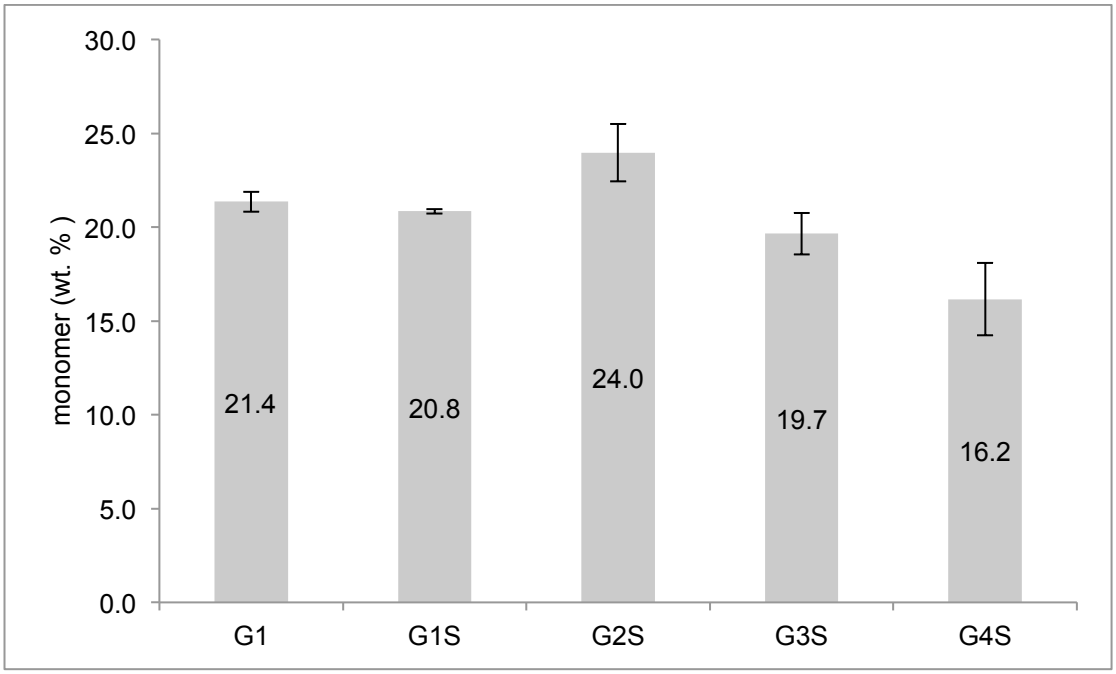

Figure 4-3: Wet Point of glass filler materials. Values are percentage of filler in a filler/monomer paste. Monomer mixture is 70 wt.% UDMA; 25 wt.% TEGDMA; 5 wt.% HEMA. n=2, error bars are range of results.

Figure 4-4 and Figure 4-5 show that the strengths and stiffnesses of the silanated glass composites were significantly higher than the strength and stiffness of the non-silane treated glass composites. The formulation containing G_{4S} had the highest strength and was significantly stronger than the G_{2S} composite. The strength of the non-silane treated glass composite was poor, and so glass G_1 was discounted from further testing.

The stiffnesses of the silane treated glass composites were all significantly higher than that of the non-silane treated glass composite.

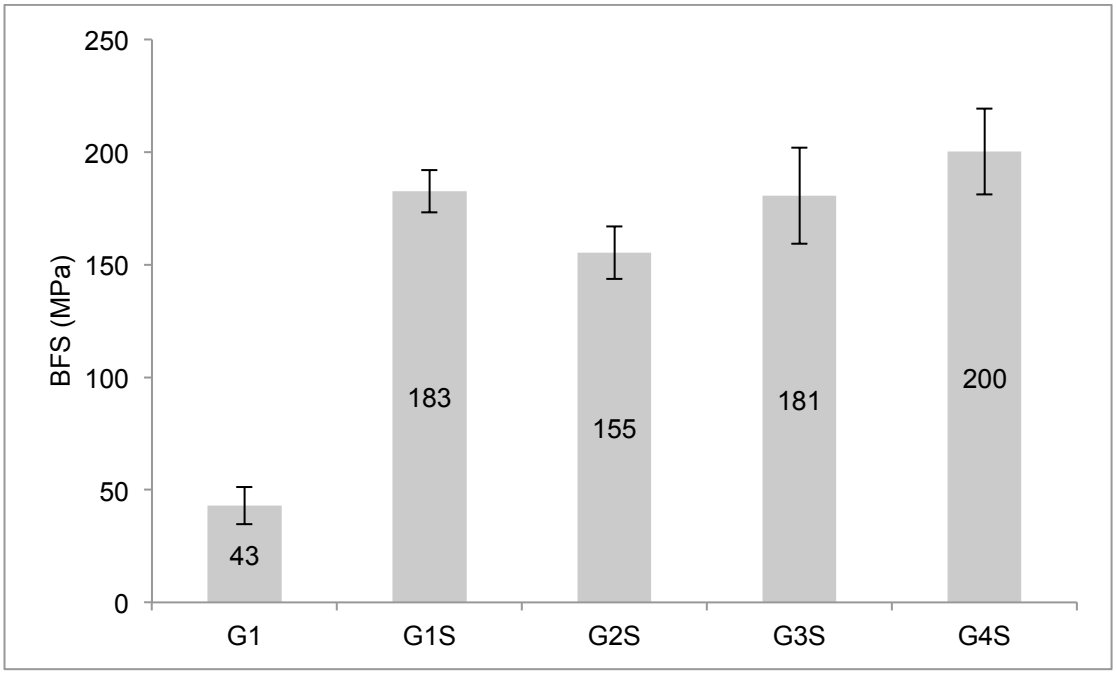

Figure 4-4 Biaxial Flexural Strength of composites made with unsilanated glass and silane treated glasses. Silane treated glasses have significantly higher strength, n=8, error bars are 95% confidence interval.

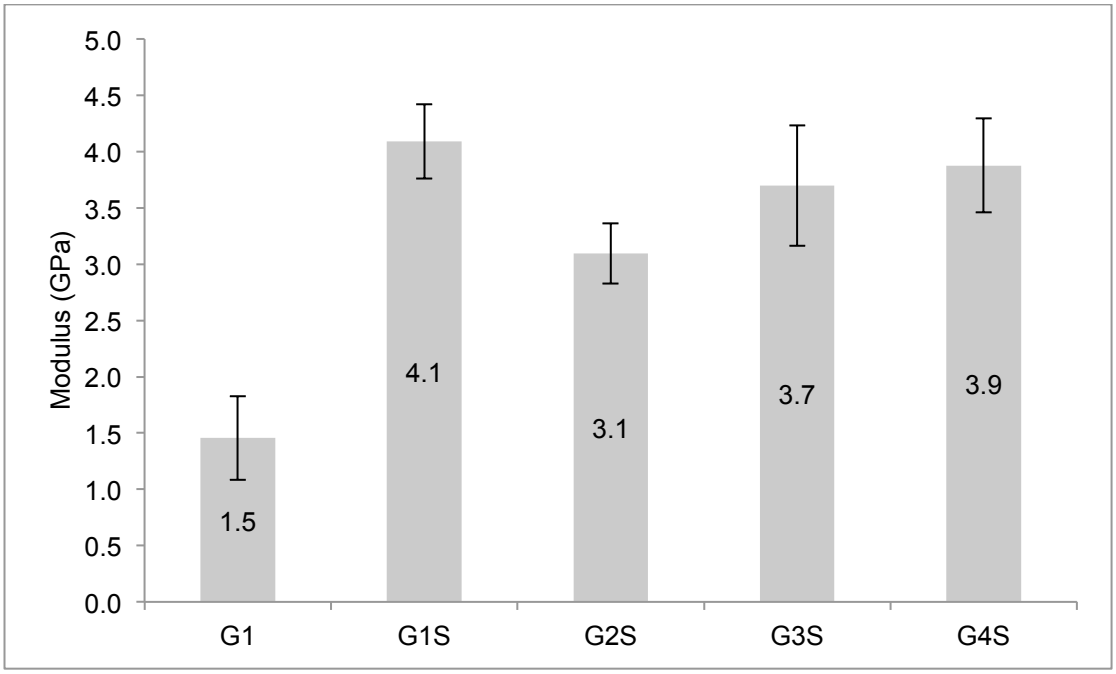

Figure 4-5 Elastic moduli of composites made with unsilanated glass and silane treated glasses. The composites made with silane treated glasses are significantly stiffer than the unsilanted glass composite. n=8, error bars are 95% confidence interval.

The radiopacity of silanated glass composites can be seen in Figure 4-6. The same composition as in biaxial testing was used. The visibility of all the glasses is good apart from G_{3S} whichG_{3S}, which is not as radiopaque as the others as expected from the glass compositions.

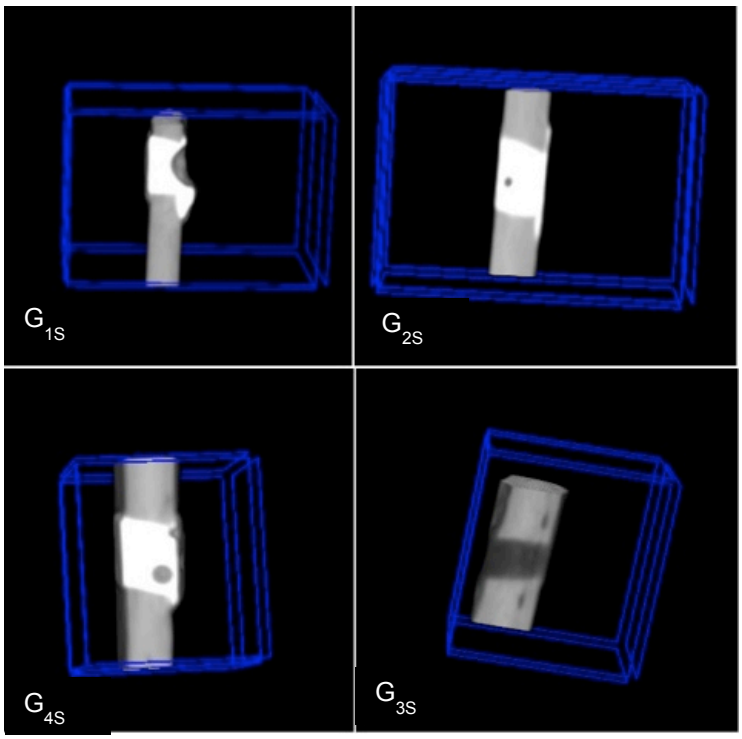

Figure 4-6 MicroCT images demonstrating radiopacity of Silane treated glass composites relative to Rabbit tibial bone.

4.6.1.3 Fibre Incorporation

Table 4-4 shows the filler and fibre content of the fibre composites that were biaxially tested. Substitution of some of the particulate filler with fibres in all compositions reduced flowability, although the effect was minor in the glass fibre composites. Aramid fibre composites had very poor handling when combined with G_{1S} glass and so G_{4S} glass was used instead. The compositions with higher percentages of both glass and aramid fibres were less cohesive than their low fibre counterparts. All compositions, however, (aside from 5 wt.% aramid fibre composite) were syringeable.

In addition to the poorer handling, the strength and stiffness of the aramid fibre composites was lower than the glass fibre composites due to the lack of chemical bonding between the fibre and monomer network (Table 4-4).

The 50 wt.% glass fibre composites and the 5 wt.% aramid fibre composites exhibited less brittle fracture behaviour than the low percentage fibre composites (Figure 4-7).

Composite	Filler :Filler: Fibre (by mass)	BFS (MPa)	E (GPa)
G_{1S} + F_{GS}	90:10	165 ± 14	3.9 ± 0.5
	50:50	178 ± 11	4.7 ± 0.5
G_{4S} + F_{A}	99:1	134 ± 9	3.2 ± 0.4
	95:5	116 ± 9	2.9 ± 0.4

Table 4-4 BFS of fibre composites with varying filler / fibre type and content. Altering the fibre content does not significantly affect the strength, although the silane treated fibre composite have significantly higher BFS. n=8, errors are 95% confidence interval.

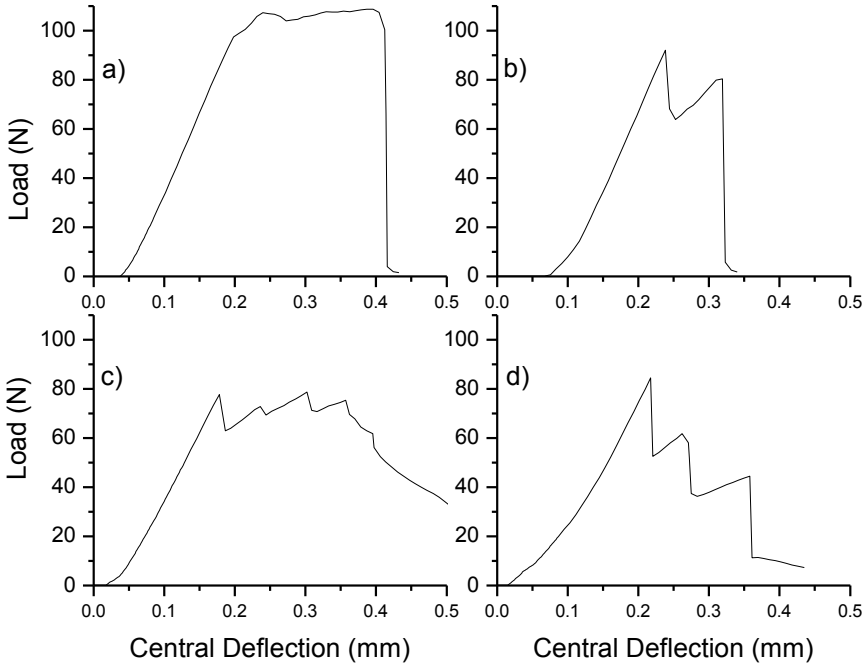

Figure 4-7 Fracture behaviour of fibre composites. a) G_{1S} + 50 wt.% F_{GS}. b) G_{1S} + 10 wt.% F_{GS} c) G_{4S} + 5 wt.% F_A d) G_{4S} + 1 wt.% F_A. High fibre composites (a and c) exhibit more ductile fracture behaviour. Maximum Load carried by aramid fibre composites is lower than for glass fibre composites as Kevlar fibres are not silane treated. There is therefore poor bonding between fibres and filler/polymer phases.

4.6.2 Monomer Screening

4.6.2.1 Effect of HEMA

The addition of HEMA made the composites less viscous and less 'oily' in appearance.

The curing profiles of the composites with HEMA had a more abrupt end to curing than those without; for t > t0.5 the curve of the curing profile for the HEMA composite was sharper (Figure 4-8). Furthermore, HEMA delayed $t_{0.5}$ significantly but had lesser effect on inhibition time (Table 4-5).

The conversion of the materials containing HEMA was slightly higher than those without (Table 4-5).

Addition of HEMA further increased biaxial strength and stiffness.

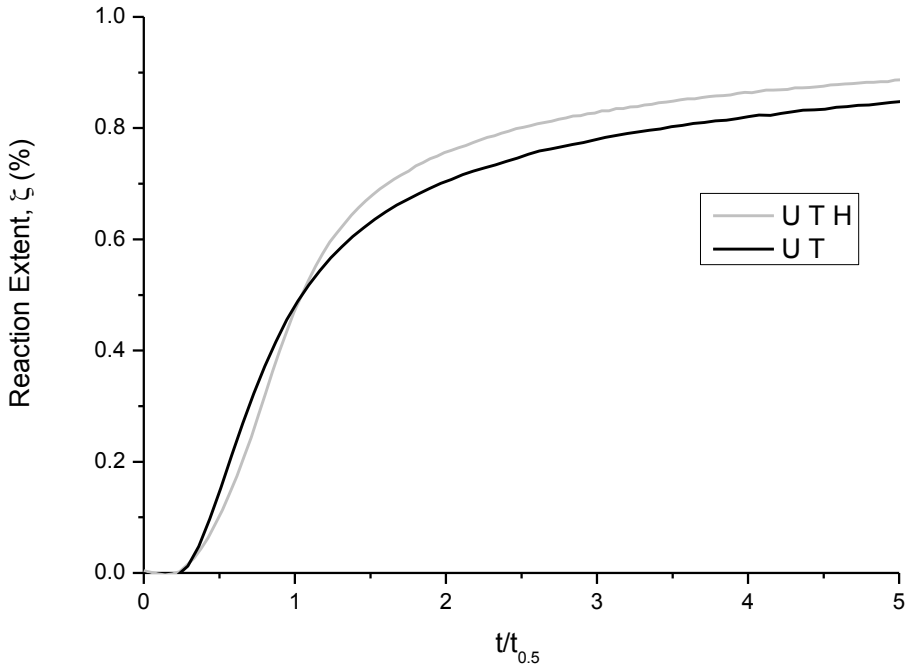

Figure 4-8 Normalized cure profiles of composites with and without HEMA. Cure is sharper for the HEMA containing composite.

Monomers	Conversion (%)	t_{inh} (s)	$t_{0.5}$ (s)	BFS (MPa)	Modulus (GPa)
UDMA TEGDMA	69 ± 2	16 ± 5.3	55 ± 9.3	125 ± 9	3.3 ± 0.3
UDMA TEGDMA HEMA	74 ± 2	19 ± 5	85 ± 8	152 ± 10	3.9 ± 0.2

Table 4-5 Conversion, Cure times, BFS and Modulus for composites with and without HEMA. Composites both contain UDMA, TEGDMA and G_{4S} filler

4.6.2.2 Variation of Diluent Monomers

There were no significant differences in the handling of the composites made with the different diluent monomers; all composites were syringeable.

From the normalized cure profiles (Figure 4-9) it can be seen that rate of cure in the latter half of the curing reaction (after $t_{0.5}$) correlates with the effective molecular weight of the composite monomer phase for all but the PPGDMA composite. With higher effective molecular weight, cure is faster after $t_{0.5}$.

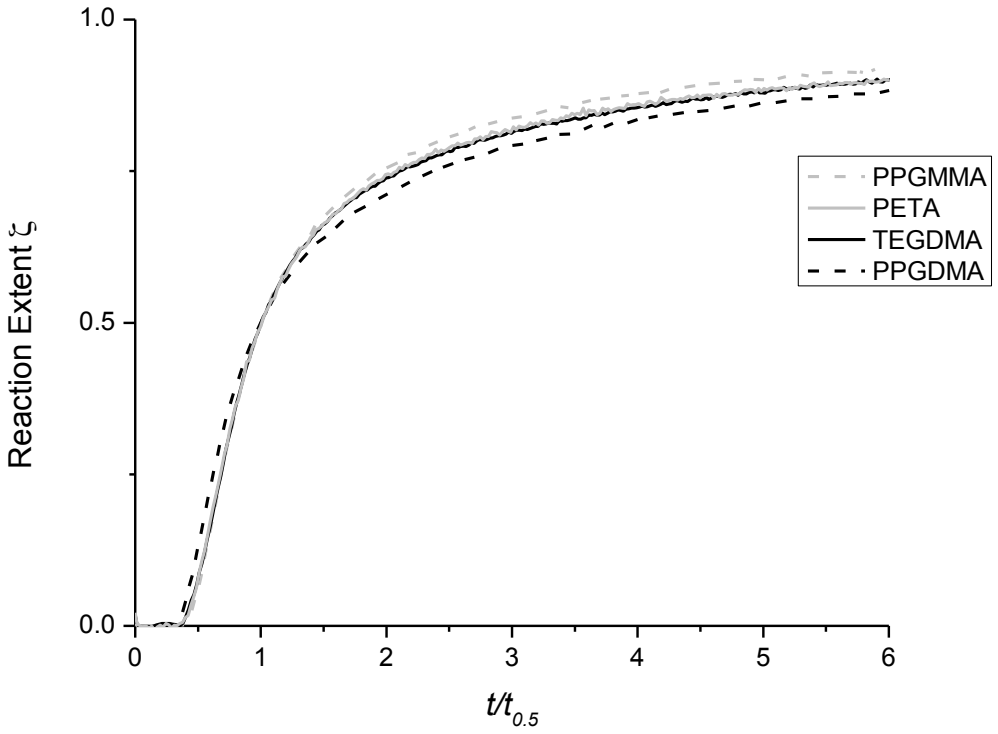

Figure 4-9 Normalized cure profiles for composites containing different diluent monomers. Materials in legend listed in the order of fastest cure after $t_{0.5}$.

Table 4-6 summarizes the conversion and cure times in which TEGDMA has been replaced with different diluent monomers. PPGMMA had the highest level of conversion, followed by PPGDMA, TEGDMA and PETA, whilst DDMA composites did not cure satisfactorily, and so no cure times were determined nor biaxial testing performed for this material.

Monomer	Conversion (%)	$t_{0.5}$ (s)	t_i	Molecular Weight per methacrylate group	Calculated Shrinkage (vol.%)
PPGMMA	80 ± 1	211 ± 18	0.42 ± 0.01	270	3.6 ± 0.1
TEGDMA	70 ± 1	164 ± 7	0.40 ± 0.02	193	4.5 ± 0.1
PPGDMA	76 ± 1	198 ± 12	0.35 ± 0.02	243	3.6 ± 0.1
DDMA	16 ± 2	Poor Cure - no biaxial testing, no measurement of cure times.			
PETA	65 ± 4	175 ± 12	0.41 ± 0.04	212	3.5 ± 0.2

Table 4-6 Summary of level of conversion for each composite containing a different diluent monomer alongside 65% UDMA and 5% HEMA. Effective molecular weight is average molecular weight per methacrylate group in composite monomer system. n=4, errors are standard deviation.

The strengths (Figure 4-10) and stiffnesses (Figure 4-11) of the materials made with varying diluent monomers do not correlate with either the effective molecular weight or conversion of the monomer phase. The material made with PPGMMA has the lowest BFS with the material with TEGDMA having the highest. The PPGMMA composite also has the lowest stiffness with the TEGDMA and PETA composites having the highest Young's modulus.

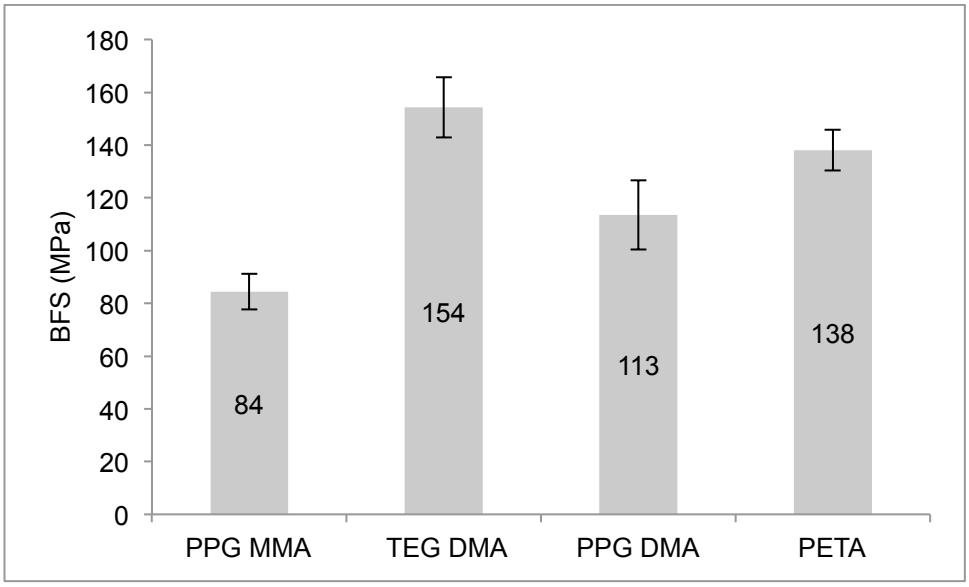

Figure 4-10 BFS of materials containing different diluent monomers. . n=8, error bars are 95% CI.

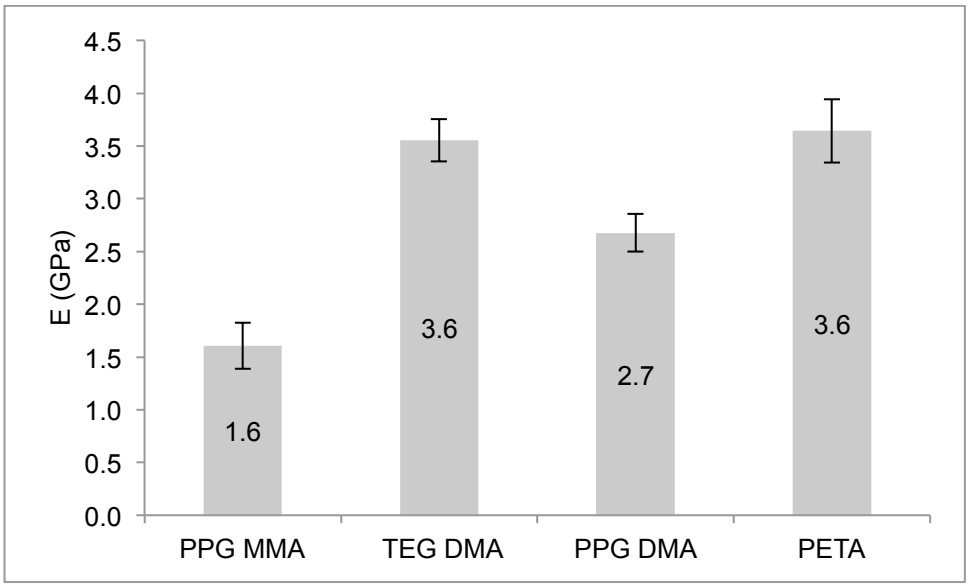

Figure 4-11 Young's Modulus of materials containing different diluent monomers. n=8, error bars are 95% CI.

4.7 Discussion

4.7.1 Filler Screening

As was seen in chapter 3, EDX analysis is not sensitive to lower mass elements. In particular EDX spectra failed to identify the presence of phosphorous and boron in the glass fillers and nitrogen in the aramid fibres. As discussed previously, in the case of glass materials, it is thought that this is due to the EDX detector becoming swamped by heavier elements such as barium and strontium. Oxygen was detected despite being present at the same levels as nitrogen.

The wet points of the glasses correlated with the mechanical properties of their composites. The lower the amount of monomer required to make a cohesive paste, the higher the BFS and stiffness of the composite. Silane treatment lowered the viscosity of the composites significantly at monomer contents just past the wet point. Composites made with glasses G_{3S} and G_{4S} were syringeable at higher filler content than those formulaltions containing G_{1S} and G_{2S} – they therefore enable lower shrinkage composites. The strengths of the silane treated glass composites (Figure 4-4) were comparable to Z250 (224MPa) and were significantly higher than both the PMMA cements (152MPa for Palacos, 131MPa for Simplex P) and Cortoss and Comp06 (120MPa and 146MPa respectively). The silane treated glass composites (Figure 4-5) were significantly stiffer than the PMMA cements (1.6GPa for Palacos and Simplex P), and similar in modulus to Comp06, Cortoss and Z250 (3.1GPa, 3.4GPa and 4.1GPa respectively). A high strength with a low stiffness is desirable in bone repair applications. All materials failed in a brittle manner. Glass G_{4S} is the same glass that is used in the commercial composite Comp06. The UDMA, TEGDMA, HEMA monomer system together with silanated glass facilitates higher PLR whilst maintaining syringeability compared to BisGMA composites such as Cortoss and Comp06.

There was a strong correlation between modulus and strength in the glasses tested. The ratio of BFS to modulus for each glass was G_1: 2.9 %, G_{1S}: 4.5 %, G_{2S}: 5 %, G_{3S}: 4.9 %, G_{4S}: 5.1 %. The value of 2.9 %, for the non-silane treated glass, is particularly low. This could be due to higher air incorporation / porosity, compared to the silane glasses, reducing the modulus. Porosity is expected to reduce both strength and modulus (as discussed in the introduction) but it would seem to have more effect on the stiffness.

4.7.1.1 Fibre Incorporation

The aramid fibres are less dense than the glass fibres (ρ_{aramid} = 1.44 ρ_{glass} = 3) and are not silane treated. This made it impossible to add as high a weight percentage of aramid fibres as glass fibres. The lack of fibre silane treatment is one of the reasons for poorer handling of the aramid fibre composites compared to the glass fibre composite.

Following first failure of the composite, there was a pseudo-plastic region in the load deflection graphs of all of the high fibre composites in which there was fibre bridging of the cracks. In the case of the 5 wt.% aramid fibre composite, this fibre bridging was not as sustained as for the glass fibre composites. It is thought that this is due to a lack of chemical bonding between the fibre and polymer or filler phases as the aramid fibres were not silane treated.

4.7.2 Monomer Screening

4.7.2.1 Effect of HEMA

HEMA is more hydrophilic than TEG DMA and so it was thought that the water sorption of a HEMA containing composite could be higher than one where HEMA is replaced by TEGDMA. In addition to this, conversion was increased by adding HEMA. Higher conversion will result in higher polymerization shrinkage but if the water sorption is higher the polymerization shrinkage could be more effectively compensated for. The

conversion level of the HEMA composite was significantly higher than the BisGMA containing commercial composites Cortoss and Comp06.

HEMA does not cross link; it is thought that the end of cure is more abrupt because the HEMA containing composite does not cross link to the same extent as the non-HEMA composite, although this does not adversely affect the strength.

4.7.2.2 Variation of Diluent Monomers

The late polymerization rate was shown to be faster for higher molecular weight monomers for all but the PPGDMA composite. Conversion after 50% is thought to be mainly due to crosslinking; the reaction kinetics and polymerisation mechanisms are discussed in more depth in chapter 5. The higher molecular weight molecules, if they are not flexible, will not be able to crosslink as easily as low molecular weight or flexible chains and hence the crosslinking phase could be short – there is a more involved discussion of the polymerization reaction kinetics in the next chapter (chapter 5).

The shrinkage of the diluent monomer composites was similar to those calculated for Cortoss and Comp06 in the previous chapter. The different diluent monomers all have different hydrophobicity and so will encourage different amounts of swelling due to water sorption. This is something that should be investigated along with empirical measurements of shrinkage.

Despite the composite made with PPGMMA having the highest conversion, it had the lowest BFS and Modulus. This is because the monomethacrylate could not cross link resulting in lower strength and modulus. Monomethacrylates have also been shown to have poorer interaction with silane treated fillers due to lack of cross linking as was discussed in the introduction. This poor interfacial bond will also lower strength and stiffness. The composite containing PPGDMA has a reasonable strength and low modulus compared to the commercial bone cements (Cortoss, Comp06, PMMA) mentioned in the previous chapter. It also had higher conversion and lower predicted

shrinkage compared to the more typical TEGDMA composite. PPGDMA has not been used in a commercial material before.

4.8 Conclusions

Silane treated glasses enable better handling, and higher PLR. Higher PLR and chemical bonding between filler and polymer enables high flexural strength and modulus.

Glasses containing heavy elements such as barium give better radiopacity than glasses that do not contain such heavy elements.

Glass G_{4S} was deemed to have performed the best out of all the glasses tested based on handling, strength and modulus values for its composites.

Glass and Aramid fibres both changed the fracture pattern of composites, but the silane treated glass fibres, F_{GS}, were thought to enable better fibre bridging without compromising on strength.

A small quantity of HEMA increased the conversion and mechanical properties of composites and improved handling by lowering monomer viscosity.

PPGDMA was considered the best diluent monomer based on cure rate, conversion (free monomer remaining) and modulus; but with a small compromise on strength. It is thought that PPGDMA could be a good candidate material for incorporation in commercially competitive bone cement materials.

PPGDMA, G_{4S} glass and F_{GS} fibres will be the subject of a systematic study in the next chapter.

5 Systematic Variation of Key Components

5.1 Abstract

The aim of this chapter was to investigate the effects of systematically varying the levels of PPGDMA, filler G_{4S} and F_{GS} fibres on composite properties.

A novel dimethacrylate monomer, PPGDMA, was used with UDMA, HEMA and silica glass particles and fibres to create a set of PPGDMA fibre composite (PFC) dual paste chemically curing materials that were compatible with delivery via a double barrelled syringe and mixing tip.

The degree of conversion and curing kinetics of the PFCs, Cortoss and Simplex P were found using FTIR whilst the mechanical properties (including flexural strength and Young's modulus) were obtained via biaxial flexural testing. The curing kinetics were investigated and an equation derived to describe the curing profiles of the PFCs / bone cements in terms of their time to half reaction and inhibition time. The curing profile equations were compared to kinetic theory for free radical polymerization and used to infer possible reaction mechanisms for the PPGDMA system. The curing profiles and equations and mechanical properties of the PFCs and Cortoss and Simplex P bone cements were compared. It was found that PFC materials had more complete conversion, and faster cure than Cortoss and Simplex P meaning possibly lower residual monomer and less chance of monomer leakage during implantation. The flexural strength of some of the PFC materials was comparable to Cortoss and Simplex P but with reduced modulus, more accurately matching the properties of trabecular bone and being less likely to damage weak osteoporotic bone. Incorporating fibres into the PFC materials prevented brittle fracture seen in Cortoss and mimicking the fracture behaviour of Simplex P. It is thought that a material with intermediate levels of PPGDMA, G_{4S} glass filler and F_{GS} fibres could be a viable alternative to existing bone cements.

5.2 Introduction

In the introduction to this thesis (chapter 1) some of the shortcomings of current bone cement materials were highlighted. Namely the poor cure and high shrinkage of PMMA cements, and high stiffness and brittle fracture of composite materials.

In the previous chapter a monomer (UDMA, PPGDMA and HEMA) and filler system (silane coupled barium silica glass, G_{4S}, and silica glass fibres, F_{GS}), that were shown to have the potential to combat these shortcomings, were selected for further testing.

The systematic study of these selected components is the subject of this chapter.

5.3 Aims and Objectives

The aim of this chapter is to systematically vary the levels of selected monomers, and fillers to ascertain their effect on the cure, conversion, and mechanical properties of dual paste, chemical cure bone cement formulations. Establishing effects of components over a practical range will enable the relative quantities of monomers and fillers to be balanced to produce a material that may have the potential to combat the inadequacies of current bone repair materials.

5.4 Hypotheses

As discussed in the previous chapter and the introduction to this chapter, PPGDMA is a long chain flexible monomer. It is intended that the range of PPGDMA investigated in this chapter, will produce composite formulations with reduced stiffness yet a high degree of methacrylate conversion and good flexural strength compared to BisGMA containing composites.

Further, it is thought that altering the level of PPGDMA will result in curing times and rates that vary significantly, providing insight into the possible reaction mechanisms for this monomer system.

PPGDMA is low viscosity. It is hoped that this will allow a high level of silane coupled filler to be incorporated and enable good interaction between filler and monomer phases resulting in materials that are compatible with syringe and mixing tip delivery and have high flexural strength. Finally, addition of silane coupled glass fibres is hoped to produce materials with a non-brittle fracture pattern with their inclusion having no detrimental effect on flexural strength.

5.5 Materials and Methods

First, a three variable factorial design experiment was performed to investigate the effects of level of PPGDMA monomer, IF2019 glass filler and GL0271F fibres on the cure rate, conversion level, BFS and Young's modulus. In this chapter formulations are referred to as PPGDMA Fibre Composites (PFCs).

Poly(propylene) Glycol 425 Dimethacrylate (PPGDMA) was combined with UDMA in weight ratio 3:1, 1:1 or 1:3. UDMA and PPGDMA contained approximately 150 and 100 ppm monomethyl ether hydroquinone (MEHQ) inhibitor respectively. In addition, UDMA and PPGDMA were supplemented with 70 and 170 ppm butylated hydroxy toluene (BHT). 7 wt.% HEMA was then added. 0.5 wt.% benzoyl peroxide (BP) or 0.5 wt.% dimethyl paratoluidine (DMPT) were included to make initiator, or activator, liquids respectively.

1, 5 or 25 wt.% silane coupled silica glass fibres (F_{GS}) were mixed with silane coupled radiopaque silica glass filler (G_{4S}). The resultant powders (60, 75 or 80 wt.%) were hand mixed with the liquids to make separate initiator, and activator, pastes as per the method of paste manufacture detailed in chapter 2.

Nine different formulations were investigated with three variables (PPGDMA, powder (P) or Fibre (F) content) using a two level factorial design (detailed in chapter 2) with one intermediate formulation (Table 5-1).

5.6 Results

5.6.1 Physical, Chemical and Mechanical Properties of PFC Formulations.

5.6.1.1 Mixing and Handling

For all PFCs, initial viscosity was sufficiently low to enable use of the commercial syringe and automatic mixing tips. It took between 2 and 4 seconds for the pastes to flow through the mixing tips. The pressure on the gun required was higher for formulations with greater powder content and lower PPGDMA due to their greater viscosity. Whilst the syringe was in continuous use the paste did not set in the tip. Material, however, left within the tip set between one and seven minutes.

It is most useful to compare the handling and mixing characteristics of the PFC materials to the commercial materials Cortoss and Comp06, that were introduced in Chapter 3, because these materials are dual paste, chemical cure, composite bone cements containing similar components and delivered in the same way as the PFCs. The bore of the PFCs mixing tips were the same as were used for Comp06 and smaller than those used for Cortoss. The pressure required to extrude PFC 7 and 8 was similar to that required for Cortoss and Comp06 and was lower than for PFC 3 and 4. The viscosity of the PFCs containing high filler content and low level of PPGDMA (PFC 3 and 4) were similar to Cortoss paste, whilst the Comp06 paste was more fluid and similar to PFC 7 and 8.

5.6.2 FTIR Data

5.6.2.1 Final Conversion and Curing Profiles

Conversion and curing times of the PFC formulations can be found in Table 5-1.

	PPGDMA (wt.% of monomer)	UDMA (wt.% of monomer)	HEMA (wt.% of monomer)	Powder (wt.% of composite)	Fibre (wt.% of powder)	Conversion (%)	$t_{0.5}$ (s)	Shrinkage (%)
PFC1	23	70	7	60	1	69 ±3	114 ±15	4.8 ±0.2
PFC2					25	71 ±1	98 ±4	4.9 ±0.1
PFC3				80	1	70 ±1	214 ±44	3.0 ±0.0
PFC4					25	73 ±1	233 ±15	3.2 ±0.1
PFC9	46.5	46.5		75	5	82 ±4	163 ±5	4.0 ±0.2
PFC5	70	23		60	1	96 ±3	284 ±12	5.9 ±0.1
PFC6					25	97 ±5	240 ±15	6.0 ±0.3
PFC7				80	1	95 ±4	401 ±79	3.7 ±0.2
PFC8					25	92 ±4	337 ±17	3.6 ±0.1

Table 5-1 Formulation compositions: Methacrylates (PPGDMA, UDMA and HEMA), powder and fibre contents are given as weight percentages of total monomer, composite or powder respectively. FTIR analysis performed at 25 °C. Results shown: Shrinkage, $t_{0.5}$, conversion, BFS and Modulus. Errors are 95 % confidence intervals. For Shrinkage, $t_{0.5}$ and Conversion n=4. For BFS and Modulus n=8.

FTIR spectra of curing PFCs were as expected for polymerizing composite bone cements (Figure 5-1). Difference spectra were also all characteristic of methacrylate polymerization (Figure 5-2). The largest changes in absorbance were observed at 1265, 1300 and 1320 cm^{-1} due to a change in methacrylate C-O stretching vibration with polymerization. Absorbance changes were also

noted at 1730, 1700 and 1640 cm^{-1} due to methacrylate C=O vibrational shifts and C=C loss respectively.

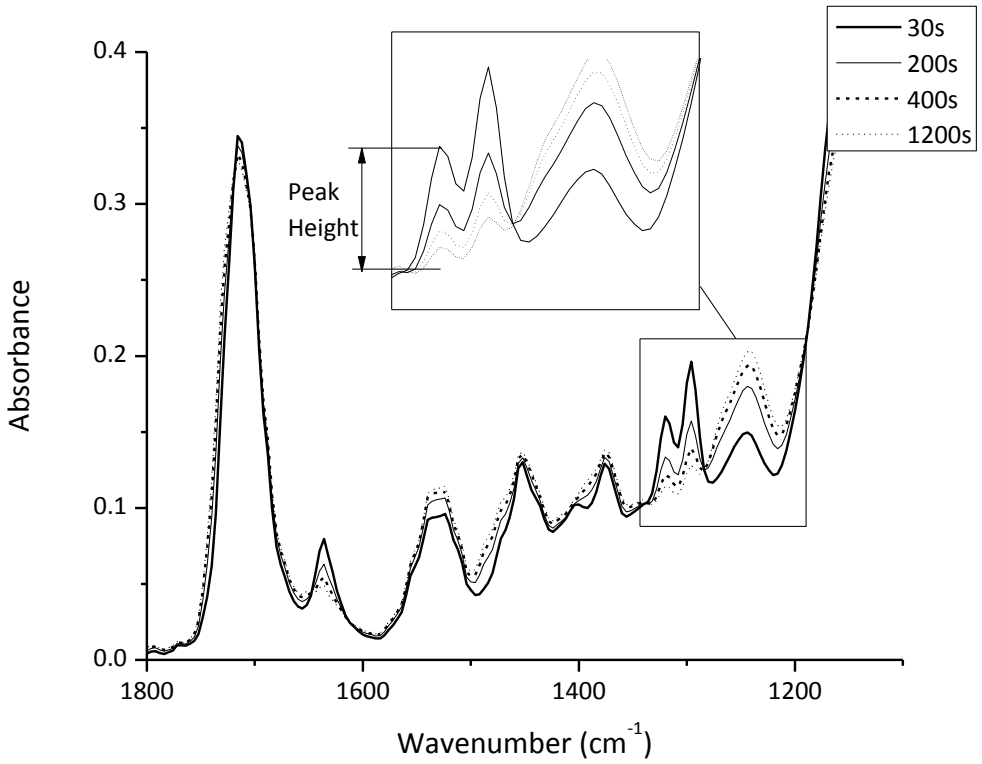

Figure 5-1 FTIR spectra of a curing PFC 9 with time. Inset shows change in absorbance used to determine cure profile. The 1320 cm^{-1} peak used to measure peak height corresponds to C-O bond in the polymerizing methacrylate group. Only peaks corresponding to Methacrylate group are changing – indicating only one reaction (polymerization) proceeding.

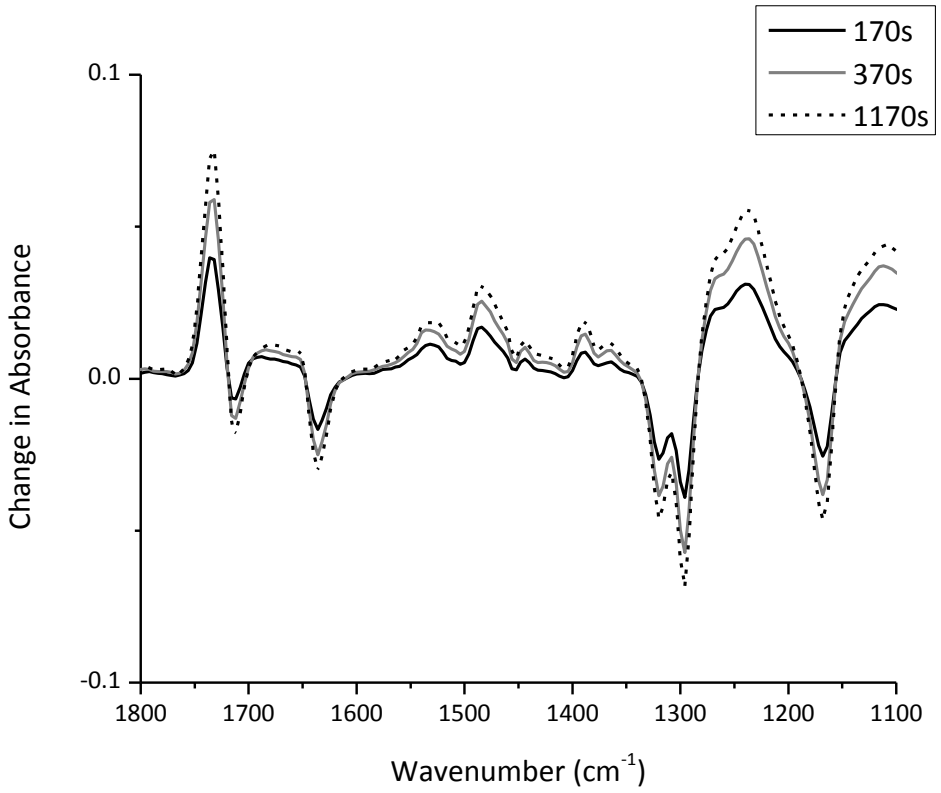

Figure 5-2 Difference spectra of PFC 9 – showing wavenumbers where maximum changes in absorbance take place.

All PFC conversion profiles demonstrated an inhibition period followed by rapid reaction (Figure 5-3). Extrapolated final conversions and $t_{0.5}$ are provided in Table 5-1. By $4t_{0.5}$, reaction extent was over 80% for all samples (Figure 5-3). Below $t/t_{0.5} = t_i$ = (0.35 +/-0.04), reaction extent was negligible for all PFC. Conversely, in the range $0.35 < t/t_{0.5} < 1$, a constant gradient $d\zeta/d(t/t_{0.5}) = 0.5/(1-t_i)$ = (0.77±0.03) was observed. In this range reaction extent is therefore given by the equation of a straight line

$$\zeta = \frac{1}{2(1-t_i)}[t/t_{0.5} - t_i] \qquad \text{Equation 5-1}$$

The reaction rate slowed for $t/t_{0.5}$>1.1.

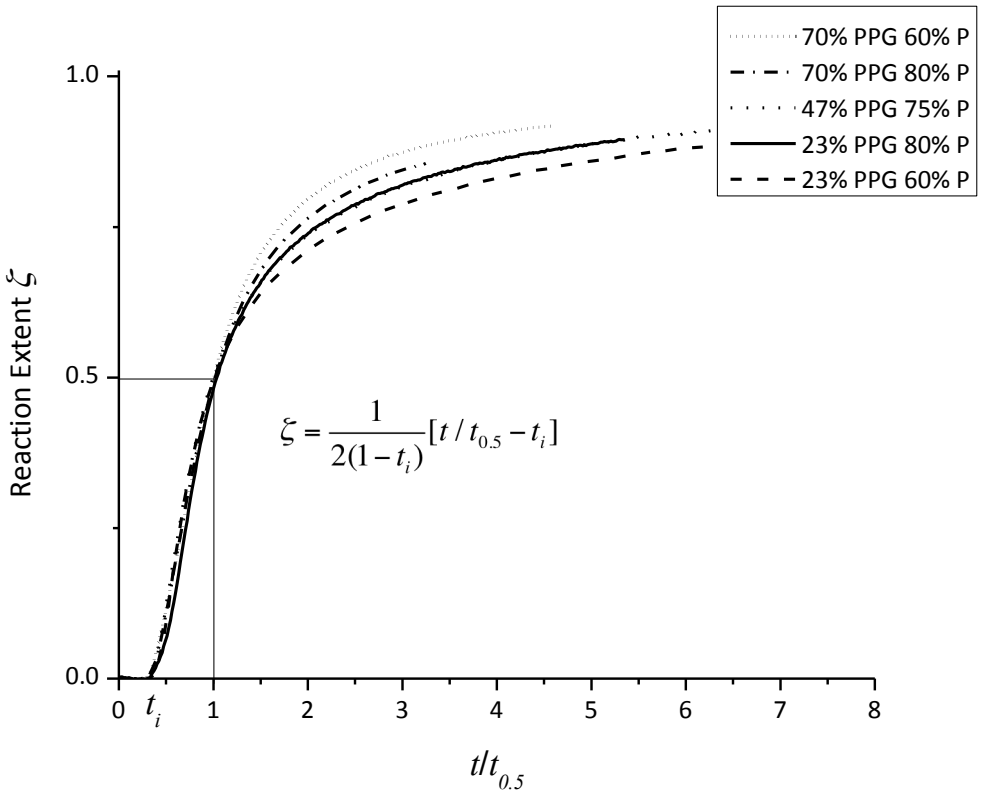

Figure 5-3 Reaction extent, ς, (see equation 1) versus normalized time, $t/t_{0.5}$. Within experimental error, this plot for all formulations, overlaps with ς <50%. Beyond this point reaction extent versus $t/t_{0.5}$ tends to 1 more rapidly if PPGDMA level is high. The legend provides formulation composition in order of reaction extent at $t/t_{0.5}$=3.

PPGDMA content was the only variable to affect PFC final conversion (Figure 5-4). It increased on average from 69 to 97% with increasing PPGDMA level from 23 to 70 wt.% of the monomer. Conversion of the intermediate PFC (82 %) was close to the average result (Table 5-1).

Increased PPGDMA and powder content both significantly raised PFC $t_{0.5}$ (Figure 5-4). With 60 % powder, average $t_{0.5}$ was 106 and 262 s with 23 and 70 % PPGDMA respectively. With 80 % powder, these increased to 224 and 369 s. The intermediate formulation $t_{0.5}$ (163 s) was close to the average of those with 60% powder. This is consistent with a linear increase in $t_{0.5}$ with raising PPGDMA but an abrupt change when powder content exceeds 75 %.

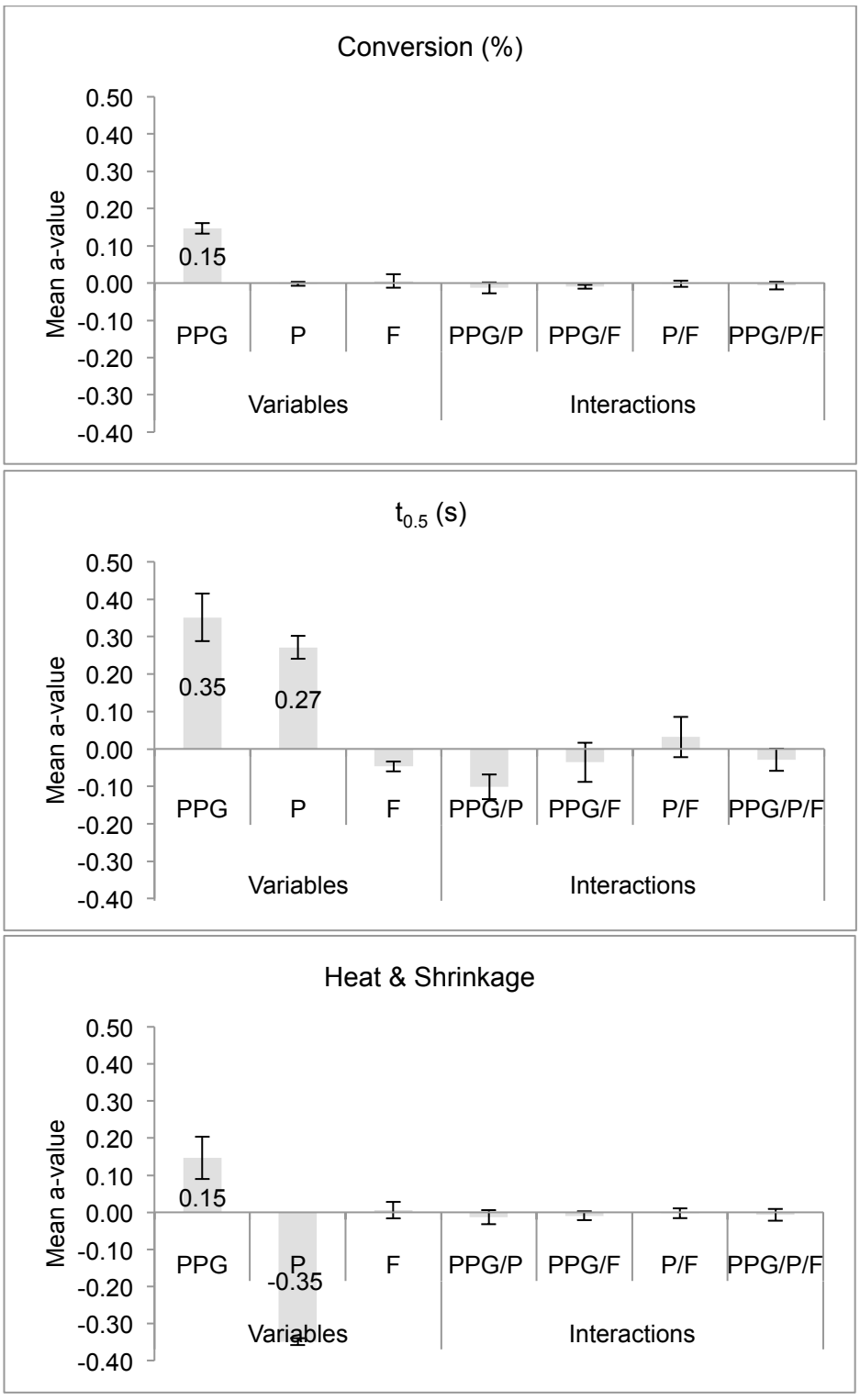

Figure 5-4 Quantification of effects of variables (PPGDMA, powder (P) or fibre (F) content) and variable interactions on final monomer conversion, time to 50 % reaction extent ($t_{0.5}$) and shrinkage/heat generation. Error bars are 95% confidence interval (n=4). Those crossing zero indicate no significant effect of fibre content or variable interactions.

5.6.2.2 Shrinkage and Heat generation

The calculated shrinkage values varied between 2.9 and 6.3 %. Heat generation (in $kJcm^{-3}$ of cement) equals shrinkage divided by 40.4. Factorial analysis indicates PFC shrinkage (and therefore also heat generation) was reduced most by raising powder content (Figure 5-4). Increasing PPGDMA also resulted in slightly higher shrinkage as effects of greater monomer conversion outweighed higher average monomer molecular weight. Cortoss shrinkage was calculated to be 3.7 % and comparable with the average value of all PFCs. Simplex P PMMA had the highest calculated shrinkage of 6.2 % due to the low monomer molecular weight.

5.6.3 Biaxial Testing

5.6.3.1 Strength and Modulus

PFC biaxial flexural strength and modulus are summarized in Table 5-2. BFS ranged between 37 and 158 MPa with moduli varying between 0.3 to 2.9 GPa.

	PPGDMA	UDMA	HEMA	BFS (MPa)	E (GPa)
	(wt.% of monomer)				
PFC1	23	70	7	158 ±19	1.8 ±0.1
PFC2				138 ±12	2.0 ±0.2
PFC3				116 ±13	2.7 ±0.3
PFC4				117 ±11	2.9 ±0.3
PFC9	46.5	46.5		91 ±7	1.2 ±0.1
PFC5	70	23		37 ±4	1.6 ±0.1
PFC6				40 ±4	0.3 ±0.0
PFC7				64 ±8	0.4 ±0.0
PFC8				61 ±3	1.2 ±0.1

Table 5-2 PFC Biaxial Flexural strength and Young's modulus. Average over n specimens and errors are 95% confidence interval. (n=8).

The factorial analysis revealed that BFS was affected most by PPGDMA level (Figure 5-5). In Figure 5-6 the BFS and Modulus values have been averaged over fibre content (e.g. average of PFC 1 and 2). Raising powder content increased strength at high PPGDMA level but had the opposite effect at low PPGDMA. This gives a strong factorial interaction term (Figure 5-5). The intermediate formulation (PFC 9) had strength comparable with the average PFC result.

PFC stiffness was reduced most by increasing PPGDMA and also declined on reducing powder content (Figure 5-5). The intermediate PFC modulus (2.0 GPa) was comparable with the PFC average.

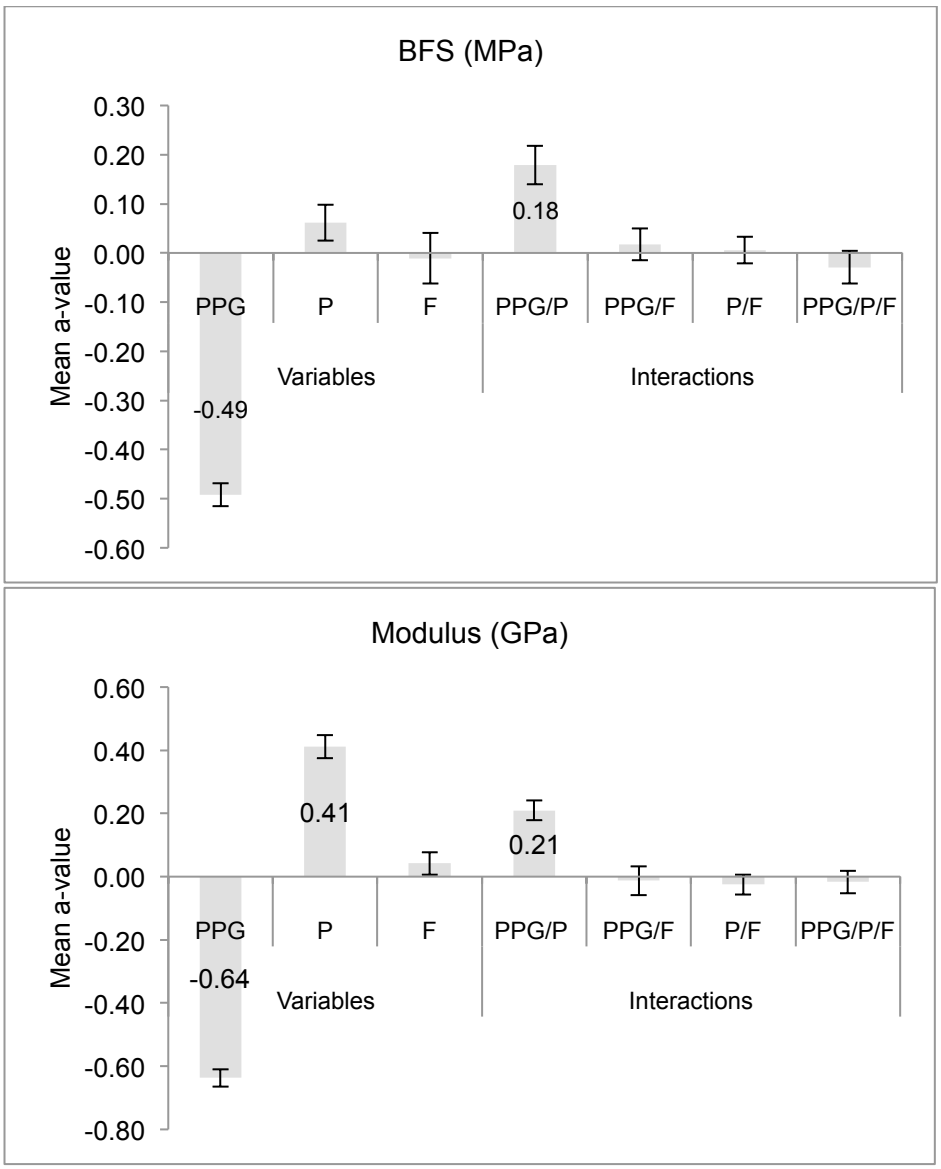

Figure 5-5 Factorial analysis giving effect of variables on BFS and Young's Modulus. PPGDMA has the greatest effect on both properties. Effects of powder are complex but smaller. The effect of Fibre content (F) is not experimentally significant as 95% confidence interval error bars cross zero.

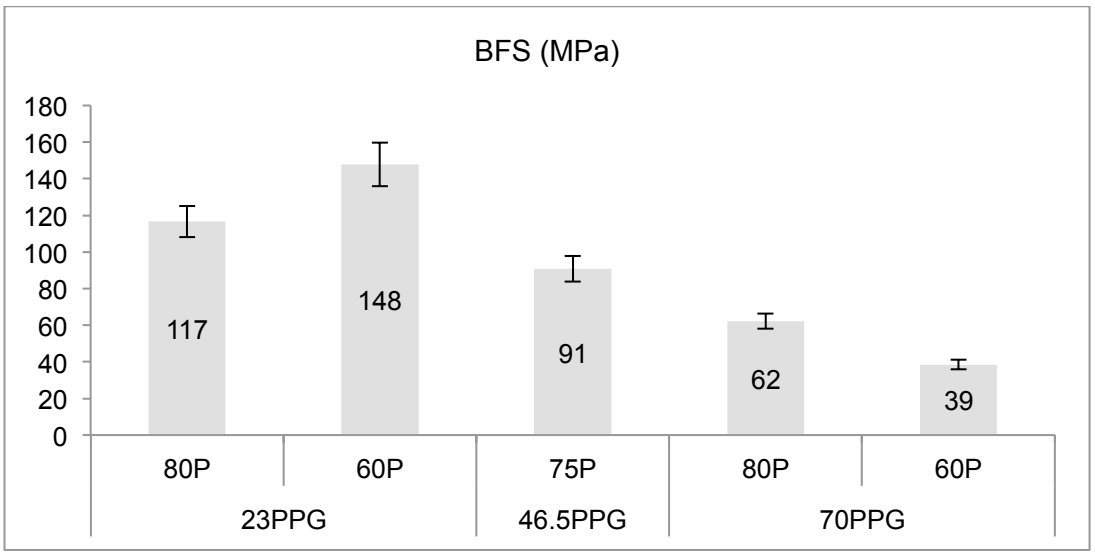

Figure 5-6 Average BFS as a function of PPGDMA percentage in monomer and total powder percentage (P). This demonstrates that reducing PPGDMA monomer level increases strength. With high PPGDMA raising powder content increases strength. At low PPGDMA higher powder reduces strength. Error bars are 95 % CI (n=16 for all 23 % PPGDMA and 70 % PPGDMA specimens, averaged over eight specimens at high fibre content and eight specimens at low fibre content as F did not significantly affect BFS results; for example the 80P/23PPG bar refers to an average over PFCs 3 and 4, the 60P/23PPG bar refers to an average over PFCs 1 and 2, whilst the 80P/70PPG bar refers to an average over PFCs 7 and 8 and the 60P/70PPG bar is an average of 5 and 6. For 46.5 % PPGDMA, 75 % P n=8; the 75P 46.5PPG bar is the mean value for PFC 9).

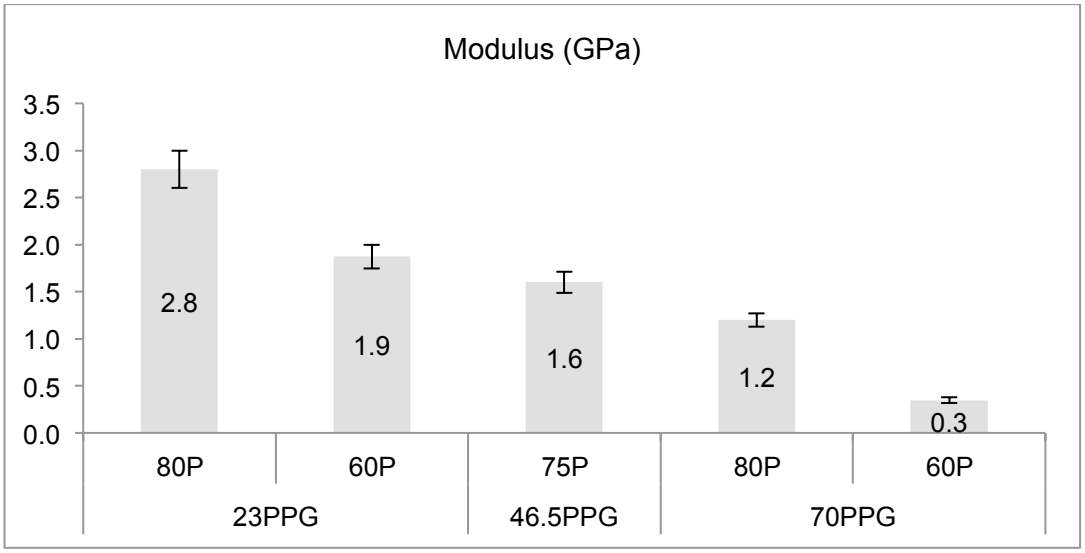

Figure 5-7 Average modulus as a function of PPGDMA and P wt.%. This indicates that raising the former but reducing the later both decrease Modulus. Error bars are 95 % CI (n=16 for all 23 % PPGDMA and 70 % PPGDMA specimens, averaged over eight specimens at high fibre content

and eight specimens at low fibre content as F did not significantly affect BFS results. For 46.5 % PPGDMA, 75 % P n=8).

Figure 5-8 compares the measured stiffness values of the PFC materials to the values predicted by the Voight-Reuss and Hashin-Strikman models. The measured values lie in between the values predicted by the iso-stress and iso-strain models, as is typical for all composite materials. The Hashin-Strikman upper bound, which predicts the stiffness of a composite consisting of compliant particles in a stiff matrix, overestimated the stiffness of the PFC materials as expected; given that the composites are glass reinforced polymers.

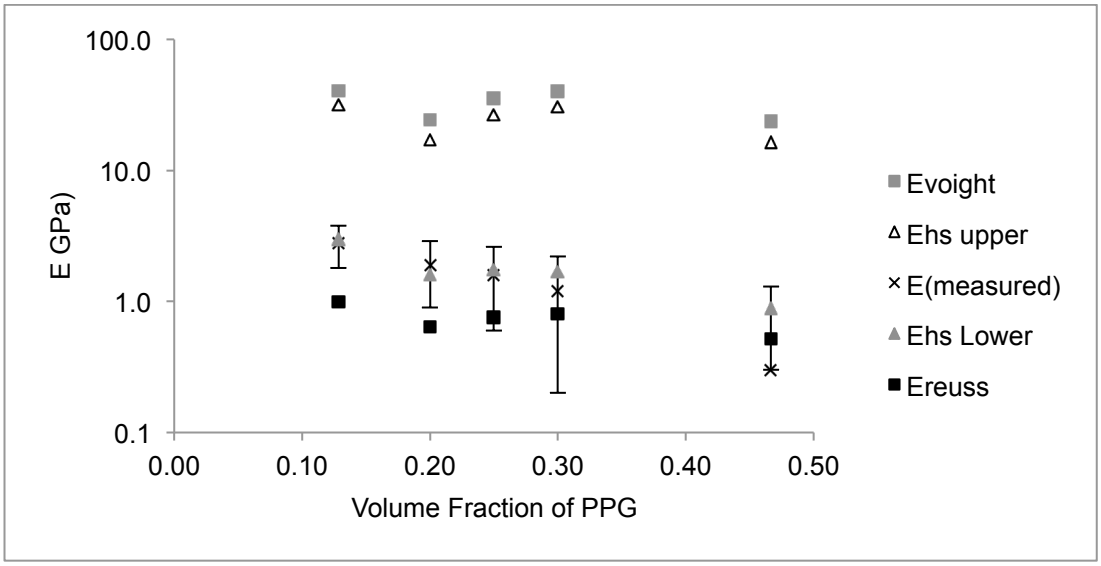

Figure 5-8 Comparison of PFC modulus values and predicted values using Voight-Reuss and Hashin-Shtrikman composite models. PFC modulus values ($E_{measured}$) lie within the Voight-Reuss Upper and Lower bounds as expected, and correspond closely to those modulus values predicted with the Hashin-Shtrikman Lower bound.

5.6.4 Fracture Behavior

Low fibre content samples all had brittle failure (Figure 5-9). Raising fibre content had no significant effect on stress at first yield but increased deflection at final failure. The increase in load observed for 23 % PPG / 80 % P in Figure 5-9 is due to a larger sample thickness only.

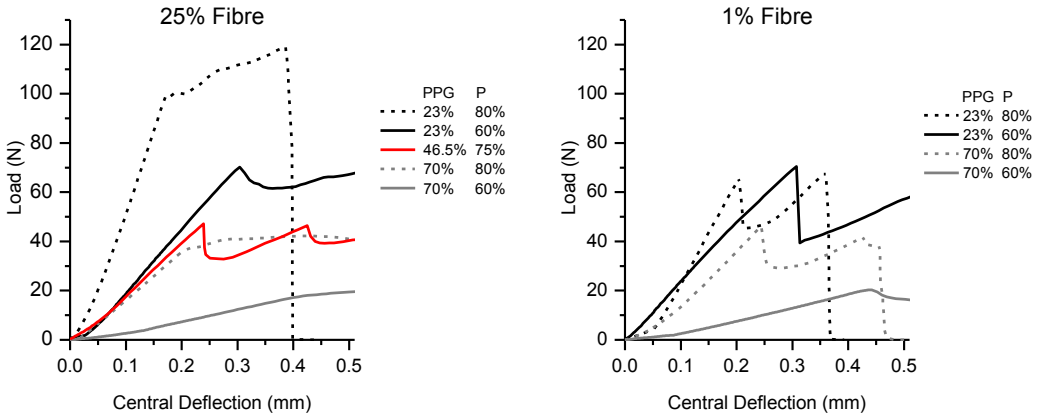

Figure 5-9 Example fracture patterns for formulations containing 1 % or 25 % fibres, the red line represeents the intermediate formulation, PFC, with 5 % fibres. At high fibre content brittle fracture is avoided, and the fracture behavior more comparable with Simplex P (see Figure 3-27) is exhibited.

5.7 Discussion

The above study has compared nine systematically varying PFCs that have suitable rheological characteristics for use as dual pastes in double barrelled syringes with automatic mixing tips. The composites are similar to those used in commercial bone void filler Cortoss apart from replacement of 1) BisGMA base monomer with more flexible, higher curing UDMA, 2) TEGDMA with a high molecular weight PPGDMA diluent 3) some of the silica particles with fibres and 4) removal of Combeite phase. Property comparisons have been made with commercial PMMA bone cement and Cortoss composite to assess feasibility of using PFCs for bone repair.

5.7.1 Mixing and Handling

Only qualitative assessment has been made of the handling and mixing characteristics of PFCs. This is useful to establish how easy and practical they were to use in comparison to Cortoss and Comp06 materials.

The PFC pastes are pre-mixed and do not contain polymer filler particles and so there was no wait for swelling and no change in viscosity required before implantation as when mixing PMMA cements. The easy and rapid PFC mixing would save the surgeon time and facilitate a fast set. The syringe units would need to be supplied sterile. Application via the mixing tip end directly into the implant site would avoid contact with other operating theatre surfaces and thereby reduce bacterial contamination risk. Furthermore, with syringe delivery multiple applications of different volumes many minutes apart are possible. Low levels of material left to set within the tip would seal the barrels after use preserving the remaining cement in a sterile, stable and unmixed state. The sealed tip can subsequently be replaced with a new sterile tip as and when more material is required. The use of a smaller bore mixing tip than Cortoss could enable more precise application. In comparison, Simplex P and Palacos took one minute to mix by hand and 10 minutes to set at room temperature. For

small volumes, one minute of mixing was sufficient to allow the PMMA cements to achieve 'dough' consistency associated with polymer swelling.

The glass particles and fibres used in the above study are silane treated. This aids filler dispersion, reduces paste viscosity and enables greater filler content as was seen in chapter 4. The filler used also combines a range of particle sizes to raise theoretical maximum packing density (134). The maximum PFC filler content was set a couple of per cent lower than would be used to make a stiff paste dental composite to enable syringe use. This was 11 wt.% higher than Cortoss powder content.

5.7.2 FTIR Data

5.7.2.1 *Final Conversion and Curing Profiles*

Methacrylate peak assignment has been performed by many authors (71,89,120,135,136). As mentioned in chapter 3, the exact location and intensity of the FTIR peak is dependent on the environment that the chemical group is in.

Difference Spectra

Difference spectra are much less variable for different compositions. FTIR spectra show peaks for all components including glass filler whereas in difference spectra, only peaks that change significantly during curing will be apparent.

Young et al. (89) found difference spectra for curing RMGIC's containing UMDA, TEGDMA and HEMA. Peaks due to absorbance changes for C-O, C=O, C=C, and C-H of the methacrylate group were identified at similar wavenumbers to peaks in the difference spectra for a PFC (Table 5-3).

Absorbance changes for C-H bend, N-H deformation and C-O-C asymmetric stretch were also observed in RMGIC's (89) and in the PFCs in this study (Table 5-3).

Changes in absorbance during polymerization, lead to changing peaks on the difference spectra. At some wavelengths this is due directly to polymerization of the methacrylate group. For example, as the material polymerizes, the number of C=C bonds decreases and there is a reduction in intensity of the C=C peak at 1637 cm^{-1}. At other wavenumbers, however, peak changes are indirectly associated to polymerization. An example of this would be changes in the carbonyl peaks. In the PFCs there are two peaks associated with C=O as the carbonyl group is part of the urethane linkage in UDMA and in the methacrylate groups of all the monomers. The NH groups of UDMA can hydrogen bond. It is reported that hydrogen bonds can interact with the carbonyl of the urethane linkage in UDMA and lead to changes in absorbance at 1699 cm^{-1} whereas the peak for C=O of the methacrylate group at 1720 cm^{-1} is unaffected by hydrogen bonding (71). When unpolymerized, the C=O of the methacrylate group is conjugated with the C=C, during polymerization this conjugation is lost and so the intensity and position of the 1720 cm^{-1} C=O peak reduces (71).

Increasing peak wavenumber (cm^{-1})	Decreasing peak wavenumber (cm^{-1})	Chemical Group	Reported Position
1733	1711	C=O stretch	1730, 1700 **1720
	1638	C=C stretch	1635 **
1530		N-H deformation	1525 **
1480		C-H scissor	1484
1440			1452
1386		C-H bend	1386
1364			
	1320	C-O stretch	1320
	1300		1300
1265			1268
1238		N-H deformation, C-O stretch	1240, 1245 **
	1167		1167 **
1114		C-O-C asymmetric stretch	1120 **

Table 5-3 relative positions of FTIR peaks changing in absorbance during polymerization of PFCs and composites reported in literature. **(89)

Polymerization kinetics of dental composites with the above initiators have previously been studied using differential scanning calorimetry (DSC) (137). The conversion of Cortoss has also been studied using DSC (59). The use of syringes combined with ATR FTIR, however, enables chemical changes to be monitored at much earlier times – from immediately after mixing. The degree of conversion from DSC for Cortoss was found to be significantly higher than the value found from FTIR in this study (59). In FTIR, it has been reported that there is the potential for microgaps to open up (due to polymerization shrinkage)

between the crystal and the material (138), changing the area in contact with the crystal which could lead to errors in measuring conversion. PFC spectra, however, overlap well at wavenumbers that are unchanging in the curing reaction and so it is uncertain whether there were any microgaps during cure. It is uncertain therefore, whether debonding due to shrinkage could account for errors in the FTIR measurement of degree of conversion and could account for differences in values between these two techniques.

The reaction mechanisms for an inhibited methacrylate free radical addition polymerization were given in the Introduction chapter. An equation for the rate of initiation can be given by the assumed initation mechanism, in which the rate depends on the concentrations of the initator system components and the rate constant of initiation. The rate of initiation is then (137)

$$R_i = 2fk_d[A][B] \qquad \text{Equation 5-2}$$

Where R_i is the rate of initiation, *f* is the initiator efficiency (that is how many collisions between radicals and monomer molecules result in successful polymerization) and [*A*] and [*B*] are the amine and BP concentrations in the monomer. Similar expressions for rate of propagation (R_p), rate of inhibition (R_z) and rate of termination (R_t) can be derived from the propagation, inhibition and termination reaction equations:

$$R_p = k_p[M_n^{\bullet}][M] \qquad \text{Equation 5-3}$$

$$R_z = k_z[M_n^{\bullet}][Z] \qquad \text{Equation 5-4}$$

$$R_t = 2k_t[M_n^{\bullet}]^2 \qquad \text{Equation 5-5}$$

Where [M] is the concentration of monomer molecules and $[M_n^{\bullet}]$ is the concentration of monomer and polymer free radicals.

Using the stationary state approximation the rate of change of monomer and polymer free radicals [$M_n^{\bullet}$] is (16)

$$-\frac{d[M_n^{\bullet}]}{dt} = R_t + R_z - R_i = 0 \qquad \text{Equation 5-6}$$

Substituting for R_t and R_z

$$-\frac{d[M_n^{\bullet}]}{dt} = \underbrace{2k_t[M_n^{\bullet}]^2}_{A} + \underbrace{k_z[M_n^{\bullet}][Z]}_{B} - \underbrace{R_i}_{C} = 0 \qquad \text{Equation 5-7}$$

Early Time Inhibition

From Inhibition reaction

$$-\frac{d[Z]}{dt} = k_z[Z][M_n^{\bullet}] \qquad \text{Equation 5-8}$$

At early times, with strong inhibition, bimolecular termination (term A, Equation 5-7) may be neglected. Equation 5-7 and Equation 5-8 can then be combined and simplified to give the rate of change of inhibitor concentration (16)

$$-\frac{d[Z]}{dt} = k_z[Z]\frac{R_i}{k_z[Z]} = R_i \qquad \text{Equation 5-9}$$

Assuming initiator concentrations are sufficiently high for R_i to remain constant, integration of Equation 5-9 gives

$$[Z] = [Z_0] - R_i t \qquad \text{Equation 5-10}$$

$[Z_0]$ is the initial inhibitor concentration.

Rearranging Equation 5-7 (neglecting term a) gives [$M_n^{\bullet}$] in terms of R_i and [Z]

$$[M_n^{\bullet}] = \frac{Ri}{k_z[Z]}$$ Equation 5-11

constructing an equation for the propagation step of polymerization (Equation 5-3) and substituting for $[M_n^{\bullet}]$ from Equation 5-11, the rate of change of monomer concentration

$$-\frac{d[M]}{dt} = R_p = k_p[M_n^{\bullet}][M] = k_p \frac{R_i}{k_z[Z]}[M]$$ Equation 5-12

Now substituting for [Z] (from Equation 5-10) into Equation 5-12

$$-\frac{d[M]}{dt} = \frac{k_p[M]R_i}{k_z\left(\underbrace{[Z_0] - R_i t}_{A}\right)}$$ Equation 5-13

Equation 5-13 is only valid when $t < [Z]/R_i$.

This predicts an inhibition period given by

$$t_i t_{0.5} = \frac{[Z_0]}{R_i} = \frac{[Z_0]}{2fk_d[A][B]}$$ Equation 5-14

In the above PFC formulations, amine and initiator concentrations are constant. Furthermore, added inhibitor levels vary only slightly with composition. The inihibition time is directly proportional to the $t_{0.5}$ time and can be found from multiplying the $t_{0.5}$ times by 0.35 (as explained earlier in this chapter). The doubling of inhibition time with raising PPGDMA content may therefore be a consequence of *f* being larger for UDMA than PPGDMA (from Equation 5-14). Varying oxygen solubility / reaction inhibition in the different monomers, however, may also play a role. The increased inhibition time with the highest powder content may be due to greater oxygen incorporation due to filler not being completely “wet” by the monomer. Alternatively, the glass surface may enhance inhibition. The longer inhibition time of Cortoss is due to a combination

of all these factors, although because exact initiator concentrations are not known, it is difficult to comment further than this.

Simplex P contains double the concentrations of BP and DMPT and less inhibitor. Greater inhibition time for Simplex P may therefore be a consequence of *f* being smaller. Additionally, early reaction may be prevented and t_i enhanced because BP must dissolve / diffuse, from the surface of the filler phase, into the monomer phase before any reaction can occur.

Early Monomer Conversion Rate

The steady state assumption also implies that $R_i = R_t$ and so

$$R_t = R_i = 2k_t[M_n^{\bullet}]^2 \qquad \text{Equation 5-15}$$

hence it is possible to express the concentration of monomer and polymer radicals in terms of R_i and k_t

$$[M_n^{\bullet}] = \sqrt{\frac{R_i}{2k_t}} \qquad \text{Equation 5-16}$$

Once most of the inhibitor has been consumed, substituting from Equation 5-16 gives the rate of change of monomer concentration [M] (from Equation 5-3) as

$$-\frac{d[M]}{dt} = k_p[M_n^{\bullet}][M] = k_p[M]\sqrt{\frac{R_i}{2k_t}} \qquad \text{Equation 5-17}$$

Comparing Equation 5-14 and Equation 2-17 indicates that increasing R_i will decrease the inhibition time and increase monomer reaction rate, but to a lesser extent. Decreasing the concentration of a weak inhibitor, or retarder, could similarly affect both properties. A strong inhibitor, however, should only affect the inhibition time as it will be used up during the inhibition period.

Immediately subsequent to the inhibition period the polymer concentration, [*P*], will be negligible. Furthermore, the total number of polymer molecules formed is

much smaller than initial monomer molecules. Moreover, larger polymer molecules are slower diffusing. The propagation step should therefore dominate over crosslinking until most of the monomer has formed into linear chains with pendant unreacted methacrylate groups. From Equation 5-1 the experimental intermediate PFC reaction extent then gives monomer loss rate as

$$\zeta = -\frac{d[M]}{dt} = \frac{0.77\phi C}{t_{0.5}} \qquad \text{Equation 5-18}$$

f is the average number of methacrylate groups per monomer and C final conversion.

C and $t_{0.5}$ increase on average by factors of 1.3 and 1.9 on raising PPGDMA in the PFC. From Equation 5-18, rate of monomer reaction therefore decreases by a factor of 1.5. This would be expected from Equation 5-17 if R_i doubles on reducing PPGDMA as the inhibition times suggested. This would indicate k_p, k_t and [*M*] may be comparable for UDMA and PPGDMA. This is reasonable given their chemical and size similarities. Raising powder content may decrease intermediate reaction rate because oxygen continues to inhibit the reaction after other inhibitors have been consumed. Equation 5-17 also predicts conversion rate should decline with monomer consumption. This effect may, however, be counteracted by continuing consumption of inhibitors or the "gel effect" (otherwise known as autoacceleration in which reaction rate increases sharply due to large molecular size limiting diffusion and therefore termination as described in the introduction, Chapter 1) (139). More viscous monomers such as BisGMA have a more pronounced autoacceleration phase (due to the gel effect) and this is why the reaction rate is steeper for Cortoss than the PFCs.

The higher concentrations of initiators and low inhibitor levels in Simplex P would enable rapid reaction once the BP has dissolved. Fast reaction, however, may lower mechanical properties due to reduction in polymer molecular weight.

Furthermore, it may cause greater temperature rise due to reduced time for heat dissipation.

Crosslinking and Final Conversion

After 50 % conversion, the reaction rates for PFC with low PPGDMA began to decline (Figure 5-3). For PFC with high PPGDMA, reaction rate remained high until a reaction extent of 0.7. Most free monomer is likely to have been consumed at approaching 50% conversion and further methacrylate conversion is subsequently due to crosslinking. Vitrification may explain the sharper decline in reaction rate, after a reaction extent of 0.5, of Cortoss than the PFCs (comparing Figure 3-24 with Figure 5-3). As monomers are consumed Tg increases (74). Polymerization generally ceases when material Tg is 20 to 40 ^{o}C above surrounding temperature (140). Although Morgan suggests that polymerization ceases when material Tg is equal to temperature of system because of vitrification (91) Polymers with lower Tg will therefore have higher maximum possible degree of conversion at a given temperature of reaction (91). Polymers of UDMA and TEGDMA have Tg of 68 ^{o}C and 65 ^{o}C respectively whilst BisGMA has a Tg of 130-140 ºC (141). The maximum conversion of UDMA / TEG DMA composites and Cortoss is, therefore, around 70% as polymerization is limited by Tg of polymer system and polymerization temperature (74). The greater chain flexibility and lower Tg of PPGDMA (~ -22 ^{o}C), however, enables increased conversion (132). PMMA has a higher Tg (107 ^{o}C) (132) preventing conversion reaching 100% at 25^{o}C.

Crosslinking and / or increase in polymer molecular weight also increases Tg (74) but to a lesser extent than initial polymerization. When conversion begins to slow, the PFCs are likely close to a glass state. They may then continue to crosslink for some time with only minor further increase in Tg. If Tg does not increase significantly then polymerization may continue for a longer time. At this time both crosslinking and termination steps are likely to be slow and diffusion

controlled and so rate of polymerization in this phase is slow. The PMMA conversion ceases more abruptly than observed with the PFC. This would be consistent with Simplex P having no crosslinking capability.

Incomplete conversion leaves a percentage of toxic free monomer, which might also reduce mechanical properties as discussed in chapter 3. In the body, however, use of larger volumes of cement will lead to high temperature rises increasing the surrounding temperature of the cement. Although this may cause tissue necrosis it will enable greater conversion.

All the PFCs had lower calculated shrinkage than Simplex P and Palacos PMMA. As discussed in the materials and methods chapter (chapter 2); polymerization shrinkage and heat generation are proportional to the monomer volume fraction and average molecular weight per methacrylate group. PFCs with 80 and 60 wt.% glass filler contain 42 and 66 vol.% monomer respectively, whilst Cortoss contains 41 vol.% filler. Simplex P monomer fraction is 38 vol.%.

Cortoss calculated shrinkage is comparable to PFC 7 and 8, yet achieves this with lower conversion carrying more risk of leaching monomers post cure.

Dental composites typically have volumetric shrinkage of around 2% (62) which is comparable with the values calculated above for the high filler content PFCs. This is possible because the high molecular weight of the new formulation diluent compensates for the greater conversion with UDMA than BisGMA.

5.7.3 Biaxial Testing

5.7.3.1 Strength and Modulus

In flexural strength studies the sample is under compression in the top surface and tension in the lower surface. The latter generally has the most influence on flexural strength. With crystalline materials, maximum theoretical tensile strength is proportional to modulus but this is reduced by flaws that initiate crack

propagation (139). Crosslinking prevents crack propagation. In composite materials the interface between phases is often the point of greatest weakness / cause of failure. In PMMA cements, including non-organic fillers, polymer/filler interface is a weakness as filler particles can act as crack initiation sites (5).

Composite strength is raised through improved filler dispersion/impregnation (wetting). This reduces voids, which may act as crack initiation sites at particle surfaces. Moreover, it could enhance physical micromechanical interlocking between the particles and matrix. Chemical bonds between filler and matrix can further increase mechanical properties by enabling better stress transfer between phases (62,80,81). In PFCs and Cortoss, silane treatment increases filler hydrophobicity and thereby monomer wetting. The silane methacrylate group also enables chemical bonding between the monomer and filler during polymerization (84). PMMA bead dissolution prior to cure may have the same effect.

With high levels of PPGDMA, increasing filler content raised strength. In this case the monomer is very fluid which may enable good particle wetting. After cure, load may then be more effectively transferred to stronger filler particles. With low PPGDMA, strength declined with raising powder content. This may be due to the polymer phase being stronger than the glass. Alternatively, the more viscous monomer may less effectively wet the filler particles. Particle agglomerates may then form particularly at high powder content. Agglomerates reduce strength by introducing flaws (81). They may also trap oxygen locally reducing chemical and physical bonding between the filler and organic phase (142).

Modulus

Increasing the powder content results in an increase in modulus of PFCs, independent of the level of PPGDMA.

It is clear that modulus of the PFC materials depends on the stiffnesses of the constituent phases as the measured values lie within the envelope of the Voight-Reuss models. Increasing the powder content results in an increase in modulus of all PFCs, due to higher volume of high modulus filler. There is good agreement between the measured PFC stiffness values and those predicted by the Hashin-Strikman lower bound. The deformation and hence the stiffness of the polymer can be thought of as being totally governed by the more compliant PPGDMA phase, implying that the structure of the polymer phase corresponds to the 'springs in parallel' iso-strain composite model; The flexible propylene backbone of the PPGDMA creates regions of the polymer that attract a large proportion of the overall deformation. The stiffness of the polymer is governed by how much the polymer chains can deform in between crosslinks. The crosslinking increases the amount of recoverable strain.

When PPGDMA is high and filler is low, good stress transfer between filler and polymer ensures increasing volume of the higher modulus phase increases the composite modulus. When the PPGDMA is low and the filler is low, the filler is still fully wetted, and this same dependency of the stiffness on the respective phase stiffnesses and volume fractions applies.

The low Tg of PPGDMA gives a more flexible, lower stiffness, polymer/composite material than PFCs with high UDMA content. Likewise BisGMA/BisEMA/TEGDMA polymer in Cortoss is stiffer than that found in PFCs with high PPGDMA content and so the modulus of Cortoss is similar to PFC 3 and 4.

In this study modulus and strength of PFCs are linked; the higher the strength of formulations PFC 1 - 4 corresponds to a higher modulus. With PFCs 5 - 8 both the strength and the modulus are reduced. As mentioned above, the deformation of the PFCs and hence the modulus is governed by the deformation of the polymer. When the polymer phase contains high levels of PPGDMA, the

polymer will attract large deformations. Incorporation of any particulate reinforcement will result in a small number of voids and imperfections although the silane treatment may provide a strong interfacial bond, it will never be perfect. These large polymer deformations will result in cracking, initiated at these imperfections at the filler/matrix interface, at lower loads than for a higher modulus material with lower deflections. The crosslinking does, however, prevent polymer chain disentanglement and so it is likely that the failure of the PFC materials will be due to cracking at the polymer/filler interface.

Crosslinking (due to bi-functional monomers) in the PFC materials increase their extension at failure.

For traditional engineering materials, e.g. titanium, strength is usually of the order of 2% of Young's modulus (143). Composite bone cements, such as Cortoss and Comp06 have strength of around 4 – 5 % of the modulus. For Simplex P and Palacos cements this value is higher, strength is around 8 – 9 % of stiffness. For PFCs with high PPGDMA, the extension at failure is larger still and the strength can reach up to 12 % of the stiffness. Reducing the modulus relative to the strength is particularly important in applications such as vertebroplasty and screw augmentation when stabilizing osteoporotic hip fractures. More flexible cement materials may prevent damage to adjacent vertebrae, as over stiffening of cement treated vertebrae can be a major cause of adjacent vertebral fracture (144–146). Treatment with Simplex P cement has been shown to lower the stiffness of the vertebral body obviating a stress-riser effect in adjacent vertebrae and so a similar stiffness to PMMA cement would seem desirable (19). Additionally cement augmentation could make screw fixation of hip fractures more suitable for osteoporotic bone. The flexible cement material could prevent screw pull out and damage to surrounding weak bone by enhancing the stress transfer between bone and screw. For screw-free hip fracture fixation, however, a stiffer material would be more suitable. PFCs in this

study have moduli that more closely match that of trabecular bone (< 3 GPa, (143)) compared to Cortoss.

Effect of Fibre Reinforcement on BFS and Young's Modulus

As discussed in the introduction (chapter 1) the effects of fibre incorporation reported in literature are varied but most authors explain the importance of having a good interfacial bond between fibres and polymer matrix for the reinforcement to enhance the mechanical properties. Examining the effect of fibre reinforcement in this study it is clear that the fibres did not affect either the strength or stiffness of the PFCs. It is possible for fibre incorporation to have no effect if the negative effect (increased crack initiation) is balanced out by the reinforcing effects (strong interfacial bond with chosen monomer system, length sufficient for fibre bridging, and decreased crack propagation).

5.7.3.2 Fracture Behaviour

Brittle fracture of the PFC with low fibre content was typical of that observed with conventional dental composites and Cortoss (99). With high fibre content cracks that opened in the material at first failure were bridged (see Figure 5-9). The load was carried, with increasing deflection up until the fibres failed. The behavior seen with Simplex was comparable with PFCs with high fibre content.

5.8 Conclusions

PPGDMA can be used as a diluent to produce dual paste PFC bone cement with rheological characteristics suitable for use in a commercial double barrelled syringe with a smaller bore mixing tip than Cortoss. PFC reaction rate decreased with raising PPGDMA level and was inversely proportional to the inhibition time. Use of the syringe gave a short mixing time enabling use of pastes with a short inhibition time and fast subsequent cure. Potentially problematic BisGMA and TEG DMA can be replaced by UDMA and PPGDMA monomers resulting in lower shrinkage and better conversion which could mean PFCs exhibit better biocompatibility than Cortoss.

The Lower the PLR and fibre content, the less viscous the material but this had to be balanced with the effects of reducing strength and heat generation and shrinkage associated with a higher proportion of monomer. All formulations were compatible with delivery via a syringe and mixing tip.

Increasing PPGDMA reduced modulus but also strength. Furthermore, formulations with low PPGDMA had strength and modulus comparable to Simplex P PMMA but much faster cure, lower calculated shrinkage / heat generation and potentially lower residual monomer. PFCs could therefore be a PMMA alternative. The strengths of PFCs were similar to Cortoss but those with high levels of PPGDMA had lower modulus, which better matches that of bone. Finally high fibre content PFC had fracture profiles similar to Simplex P, whilst low fibre content formulations exhibited brittle fracture similar to Cortoss. Incorporation of fibres could overcome the problem of brittle fracture of Cortoss.

Based on the results of this chapter, a formulation with intermediate values of PPGDMA and PLR, with a high level of fibres was made as a prototype product. The curing and mechanical properties of this prototype product, along with further in-vivo investigations, are presented in the next chapter.

6 Prototype PFC In-vitro Characterization and In-vivo Implantation

6.1 Abstract

The aim of this chapter was to characterize the in-vitro and in-vivo performance of a single PFC formulation to evaluate its viability as an alternative to existing bone cement materials.

The levels of PPGDMA, powder (P) and fibre (F) were set in an attempt to produce a PFC material with optimal properties compared to those measured in chapter 5. The curing and mechanical properties of this optimized formulation (referred to as Prototype formulation) were obtained as described in chapter 2. The biaxial flexural strength and the elastic modulus of the material were comparable to current bone repair materials. Particularly considering the long term BFS, the PFC material performed better than Cortoss and fracture behaviour of this formulation was non-brittle unlike Cortoss. The levels of PPGDMA and PLR have been balanced to obtain these mechanical properties whilst enabling good conversion and favourable cure kinetics. From these results the PFC prototype was shown to be an improvement in several areas compared to existing bone repair materials.

The Prototype formulation and a high viscosity PMMA cement were implanted in lapine models and the in-vivo responses were investigated and compared. The sterile manufacture and implantation procedures are as per chapter 2. The implant sites were examined after one week and four weeks in-vivo.

Micro CT analysis showed that the injectable PPGDMA cement was more radiopaque than the PMMA cement. Bleeding at the implant site was thought to prevent interdigitation of both types of cement into the surrounding bone.

Preliminary investigation suggested that the in-vivo response of the prototype PFC was excellent; histological examination showed no instances of infection or inflammation due to the implanted material. Some PMMA implantation sites showed infection and inflammatory response. From this, the PFC prototype was shown to be a viable alternative to PMMA cements in-vivo.

6.2 Introduction

In chapter 5 systematic investigation of PFC materials was carried out to ascertain the effect of varying the levels of PPGDMA, glass filler G_{4S} and glass fibre F_{GS} on the properties of so called PFC composites. It was thought that intermediate values of these components could produce a PFC that was a viable alternative to PMMA and composite bone cements.

For PFC materials to be regarded as viable they must have favourable handling, curing and mechanical properties and an improved biological tissue response when implanted compared to existing materials.

The handling, curing and mechanical assessment that has been used throughout this project was deemed to be an acceptable way of measuring in-vitro performance, and, as mentioned in the materials and methods (chapter 2) a lapine model is thought to be an excellent way to assess in-vivo performance.

6.3 Aims and Objectives

The aim of this chapter was to characterize the in-vitro and in-vivo performance of a single PFC formulation to evaluate its viability as an alternative to Cortoss composite bone void filler and Palacos R PMMA bone cement for osteoporotic vertebroplasty and fracture fixation applications.

The levels of PPGDMA, powder (P) and fibre (F) were set in an attempt to produce a PFC material with optimised properties compared to those measured in chapter 5. The PFC formulation (‘prototype’) contained intermediate levels of monomer, filler and fibre

compared to the formulations investigated in chapter 5. That is, the levels of the components for the 'prototype' formulation were chosen to try and produce a material with an acceptable strength/stiffness compared to exisiting bone cement materials whilst having comparable or lower shrinkage and heat generation and higher conversion. The prototype composition was set with 0.5 wt.% BP and 0.5 wt.% DMPT. The cure was controlled with 70 ppm BHT (as in previous chapters, initiator quantities given as weight percentages of monomer phase).

The objectives of the in-vitro testing were to determine the following for the prototype PFC:

1. The handling and mixing. Evaluated by eye.
2. The shape of the curing profile (FTIR)
3. The cure times and degree of conversion (FTIR)
4. Polymerization shrinkage (calculated from FTIR and composition)
5. Biaxial flexural strength and Young's modulus (Biaxial testing)
6. Fracture behaviour (Biaxial testing).

Quantitative assessments of parameters 2-4, and qualitative analysis of parameters 1 and 5, were used to compare the prototype PFC to the PMMA cements, composite bone cements and the dental composite characterized in chapter 3.

The objectives of the preliminary in-vivo implantation experiment were as follows:

1. Confirm material could be sterilized and injected and set in vivo
2. Assess the suitability of the material viscosity
3. Assess the ability of the material to wet and bond bone in presence of blood
4. Compare the radiopacity of PFC to trabecular and cortical bone
5. Ensure no toxic reaction by examining organs after extraction
6. Assess bone integration via microCT and histology

7. Qualitative assessment of bone formation via appearance of bone and cellular presence in histological sections.

The in-vivo response of the prototype PFC formulation was compared to Palacos R PMMA cement.

6.4 Hypotheses

It was thought that choosing intermediate values of monomer, filler and fibre, based on the results of chapter 5, would produce a formulation with curing and mechanical properties that were comparable or better than existing bone cements.

Nearly equal quantities of PPGDMA and UDMA (with a small amount of HEMA) combined with a high level of silanated filler were envisaged to produce a material with handling properties that enabled easy delivery and precise application via a double barrelled syringe and mixing tip.

The monomer and initiator levels were chosen to enable a rapid, reliable and complete cure compared to existing bone repair materials.

The inclusion of a high level of the diluent PPGDMA was intended to reduce the modulus of the PFC material to better match the stiffness of trabecular bone whilst maintaining strength values comparable with Cortoss, Comp06 and PMMA cements.

The handling, cure, chemical composition and mechanical properties of the prototype were intended to allow host tissue to maintain normal metabolic function and have a close interface when implanted in-vivo, without any inflammatory response or fibrous encapsulation.

6.5 Materials and Methods

Materials

In the prototype PFC the monomer phase contained 50 wt.% PPGDMA, 45 wt.% UDMA, 5 wt.% HEMA. The filler phase consisted of 75 wt.% G_{4S} glass and 25 wt.% F_{GS} glass fibres. The composite was 80 wt.% filler; 4:1 PLR. Please see Materials and methods (chapter 2), for details of material sources.

Methods

The PFC paste was manufactured as per the protocol in chapter 2. The handling of the material was assessed by eye. The cure profile, cure times (normalized inhibition time and $t_{0.5}$) and degree of conversion were determined via FTIR analysis. Mechanical properties including fracture behaviour, biaxial flexural strength and Young's modulus were found through biaxial testing of disc specimens.

The PFC material components were sterilized and mixed in a sterile environment prior to in-vivo implantation. The PFC and Palacos R implants were removed, when the animals were killed, after one and four weeks and the sites examined by microCT. Histological sections were made and stained with either Goldner's trichrome or Toluidine blue stains.

For full details of methods please refer to Materials and methods (chapter 2).

6.6 Results

6.6.1 Prototype Formulation Characterization

Table 6-1 shows a summary of the properties of the prototype formulation including Conversion, $t_{0.5}$, Shrinkage, BFS and Stiffness compared to the commercial materials tested in chapter 3 and PFC 9 from chapter 5. Figure 6-1 shows the normalized cure profile for the prototype PFC. With PMMA cements, the inhibition period (Table 6-1) was longer but subsequent polymerization reaction sharper than the prototype formulation. Furthermore, there was no 'swelling period' with the prototype PFC materials due to the insoluble silica filler (small changes seen in FTIR spectra of Simplex P in the first few minutes were attributed to swelling where dissolution of polymer into the monomer phase reduced the double bond density in the solution prior to the onset of polymerization).

The Prototype PFC normalized cure profile is shown in Figure 6-1 superimposed on those of composite bone cements, PMMA cements, Z250 dental composite and PFC9. The prototype PFC profile has the same shape as the other PFC's, and, at later times it is most similar to PFC 9. The inhibition time of the prototype PFC is shorter than for the all the commercial bone cements aside from Cortoss. The normalized inhibition time (t_i) for the prototype is less than for Cortoss.

The BFS of the Prototype formulation was of the same order of magnitude as all the commercial PMMA and composite bone cements and similar to PFC9. The stiffness was between that of the commercial PMMA and composite cements and higher than PFC9 due to increased filler content. The biaxial specimen fracture surfaces can be seen in Figure 6-4. The rough texture is indicative of a good interfacial bond between the particulate and the polymer (147). The filler fibres are protruding – this shows that the fibres are 'pulling out'.

The BFS of Cortoss decreased by 39 % after four weeks, and 58 % after 20 weeks, whilst the stiffness decreased by 27 % and 43 % respectively (Figure 6-2). The prototype formulation exhibited first a BFS decrease of 18 % after four weeks, but the strength after 20 weeks was found to be unchanged from the original value. The stiffness of the Prototype formulation was unchanged after four weeks, but increased by 13 % after 20 weeks.

Load versus deflection of the Prototype formulation (Figure 6-3), however, was similar to the PMMA cements. It did not exhibit brittle fracture behaviour unlike Z250, Cortoss or Comp06. The non-brittle fracture behaviour was maintained after both four and 20 weeks hydration at 37 °C (data not shown).

Name	Conversion (%)	t_{inh} (s)	$t_{0.5}$ (s)	Shrinkage (vol.%)	BFS (MPa)	Modulus (GPa)
Simplex P	76 ± 1	276 ± 29	406 ± 28	6.2 ± 0.1	131 ± 12	1.6 ± 0.1
Palacos R	86 ± 2	170 ± 16	281 ± 19	6.9 ± 0.2	152 ± 18	1.6 ± 0.1
Cortoss	64 ± 4	130 ± 29	232 ± 21	3.8 ± 0.1	120 ± 9	3.4 ± 0.1
Comp06	64 ± 0	171 ± 17	416 ± 15	3.7 ± 0.1	146 ± 12	3.1 ± 0.2
Z250	49 ± 1	light cure		1.8 ± 0.1	224 ± 18	4.5 ± 0.4
PFC 9	82 ± 4	52 ± 5	163 ± 5	4.0 ± 0.2	87 ± 7	2 ± 0.1
Prototype PFC	80 ± 1	64 ± 5	207 ± 4	3.2 ± 0.0	93 ± 3	2.2 ± 0.1

Table 6-1 Summary of properties of prototype formulation, containing 50%PPGDMA, 45% UDMA, 5% HEMA; 80% Filler (3:1 Particle: Fibre), compared to commercial materials and PFC 9. Errors are 95% CI, n=4 for conversion, cure times and shrinkage. n=8 for BFS and Modulus.

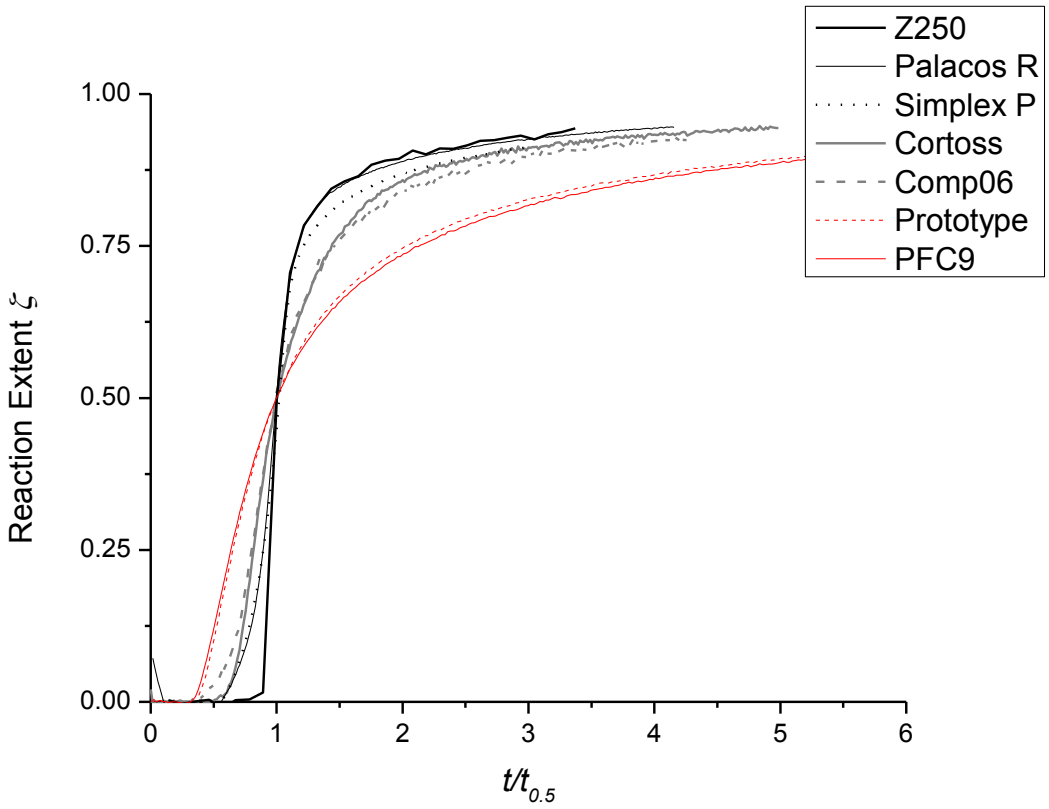

Figure 6-1 Normalized cure profile of prototype formulation (50%PPGDMA, 45% UDMA, 5% HEMA; 80%P (3:1 Particles: Fibres) marked in red. This largely overlaps other PFC's.

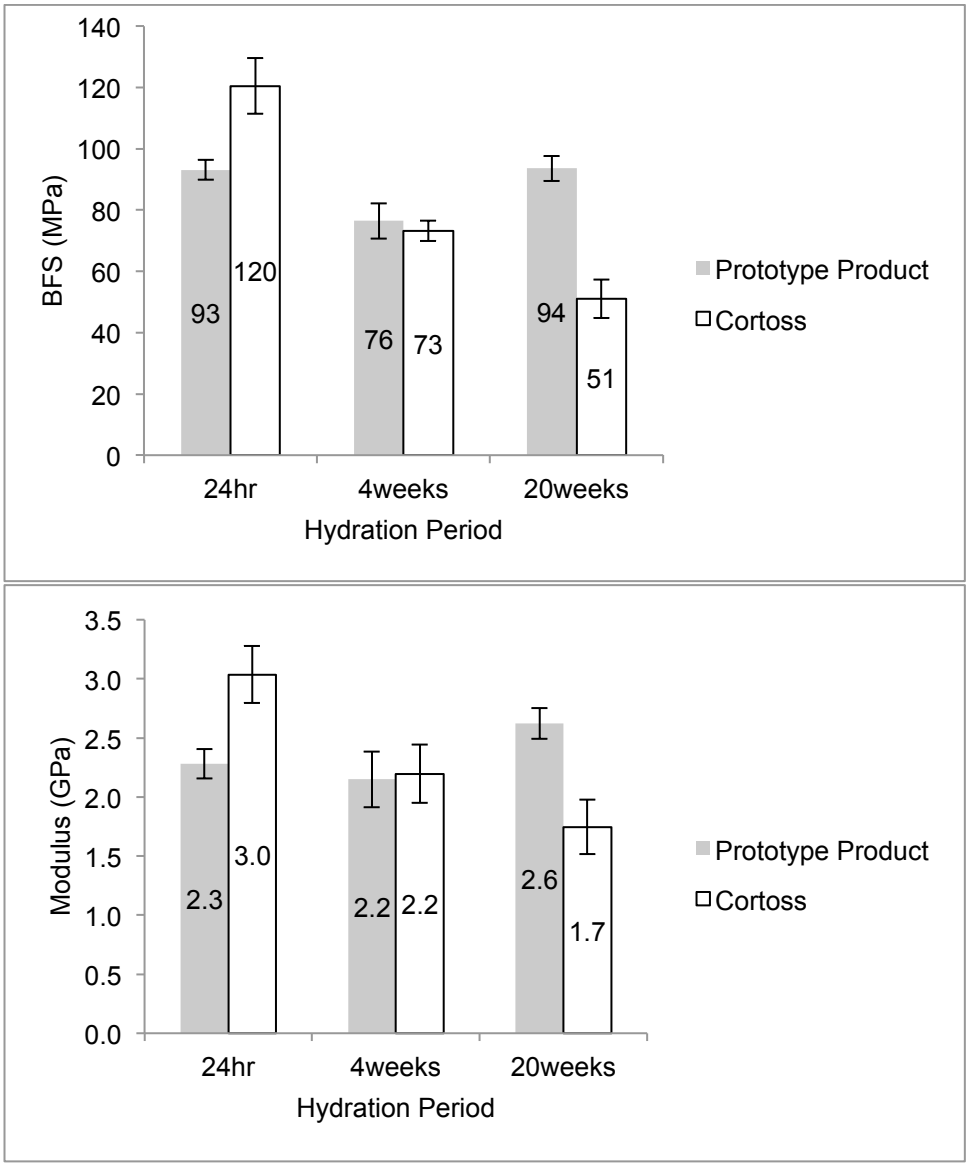

Figure 6-2 Effects of hydration period on biaxial flexural strength and elastic modulus. Cortoss showed a significant decline in BFS after 4 weeks storage in water at 37 °C. The elastic modulus of Cortoss also dropped after 4 weeks and 20 weeks hydration. The BFS of the prototype product is shown to decrease after 4 weeks hydration. BFS of PFC after 20 weeks, however, is not significantly different to its 24-hour hydration value. There is an increase in stiffness for the PFC over 20 weeks hydration.

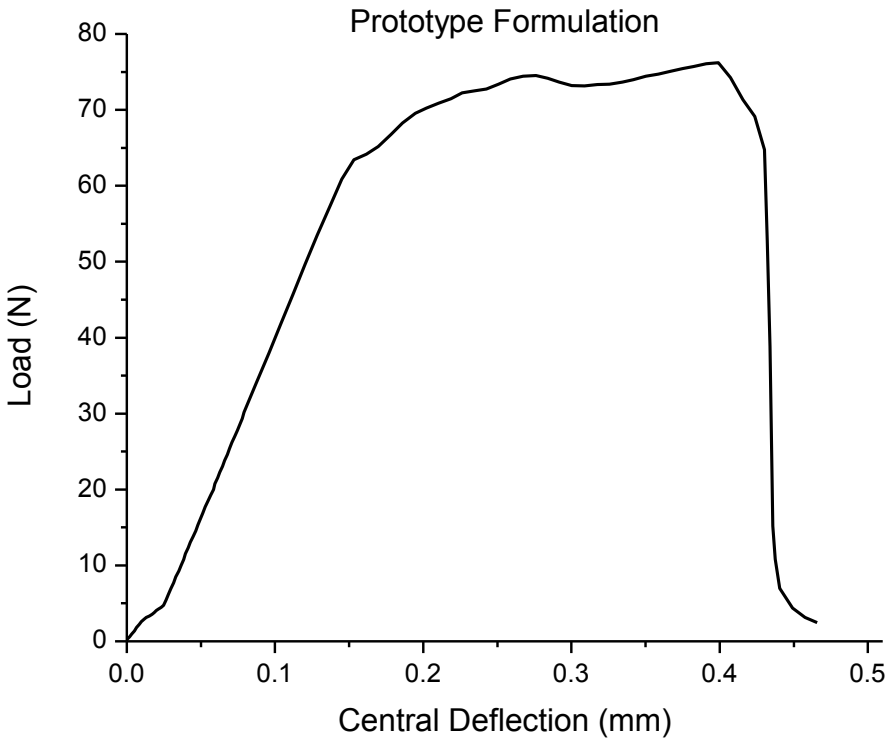

Figure 6-3 Load vs. Deflection plot for Prototype formulation. 3:1 ratio of particles to fibres in filler phase prevents brittle fracture through fibre bridging as with high fibre content PFC's.

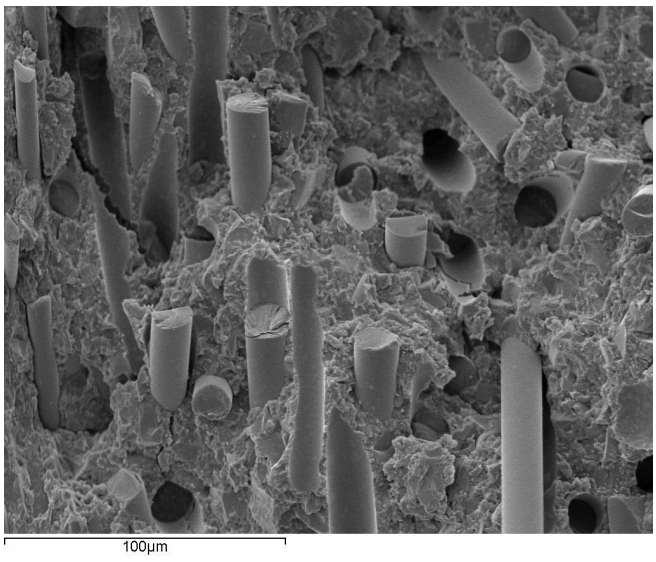

Figure 6-4 Prototype PFC biaxial specimen fracture surface. Reinforcing fibre fillers can be seen protruding from the surface where the interfacial bond has failed and the fibre has 'pulled out'

6.6.2 In-vivo Implantation of Prototype PFC

6.6.2.1 Surgical Procedure and Outcomes

The PFC cement had a markedly lower viscosity than Palacos, with the former being a flowable paste and the latter being a putty-like dough. Bleeding occurred at the implant site. This could displace the liquid PFC before cure. The PFC, however, did not mix with the blood. The PMMA was not displaced by bleeding during implantation as the dough could be packed into the implant defect.

The PFC cement was pre-mixed meaning that there should be no alteration of monomer/powder ratio due to clinician mixing. The PMMA was not pre-mixed and so there was scope for accidental change in monomer/powder ratio although to the best knowledge of the experimenters no such alteration occurred.

The PFC was probed 45 s after injection into the site and was found to be hard. PMMA was found to be set, by probing, 90 s after application (packing into defect).

Explant notes can be found in Table 6-2 Inspection of the one-week specimens after removal revealed no infections for either material, although one of the PFC defect sites was empty and the material found encapsulated in surrounding soft tissue. There were three infections observed for the four-week PMMA filled defects. One of the four-week PFC sites was again found empty with the material encapsulated in surrounding soft tissue.

Implant duration	Animal Number	Material	Notes
One Week	665R	Palacos	V
	666R		N Material totally encapsulated out of wound. No inflammation
	667R		N
	671L		N
	668R	PFC	N
	669 L		V
	670 L		V
	671R		N
Four Weeks	655R	Palacos	V
	656R		V Abscess, lots of cystic fluid, large amount of material outside of defect.
	657R		V Sterile infection in synovial capsule condular ridge worn
	661L		N Abscess
	658R	PFC	V
	659R		N
	660L		N Material totally encapsulated out of wound. No inflammation
	661R		N

Table 6-2 extraction notes for implanted materials after one and four weeks. N: material not visible in defect. V: Material visible in defect.

6.6.2.2 Micro CT

The Micro CT images of the PFC implants after one-week show empty defects in two out of four implant sites (Figure 6-5). This was as expected from the visual inspection during extraction. The microCT images of 669L and 670L in the transverse plane show that the PFC material does not fill the defect well, the outline of the defect is visible with a gap between it and the implanted material. Despite incomplete filling of the defect, good contact can be seen at some points.

The micro CT images of the Palacos implants after one week showed that there were three empty defects out of the four implant sites Figure 6-6. The microCT image of implant site 665R shows the top edge of the implant having close contact with the host bone.

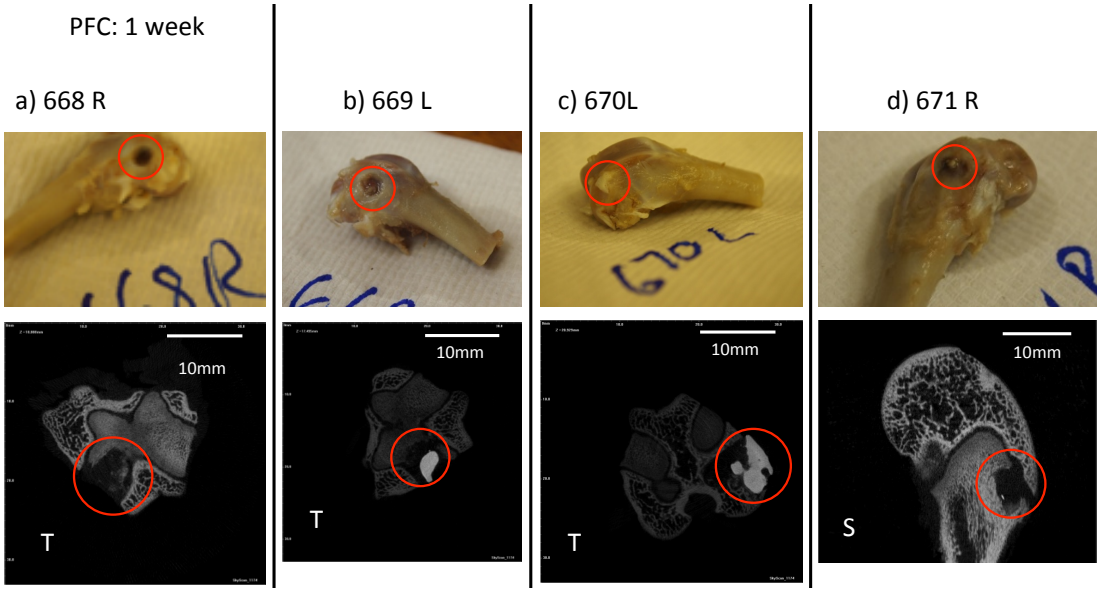

Figure 6-5 PPGDMA Micro CT images after one week in vivo. Material visible in 669L and 670L. Defect visible in 668R and 671R. Defect sites marked with red circles. Images marked with T and S are in the transverse and sagittal planes respectively.

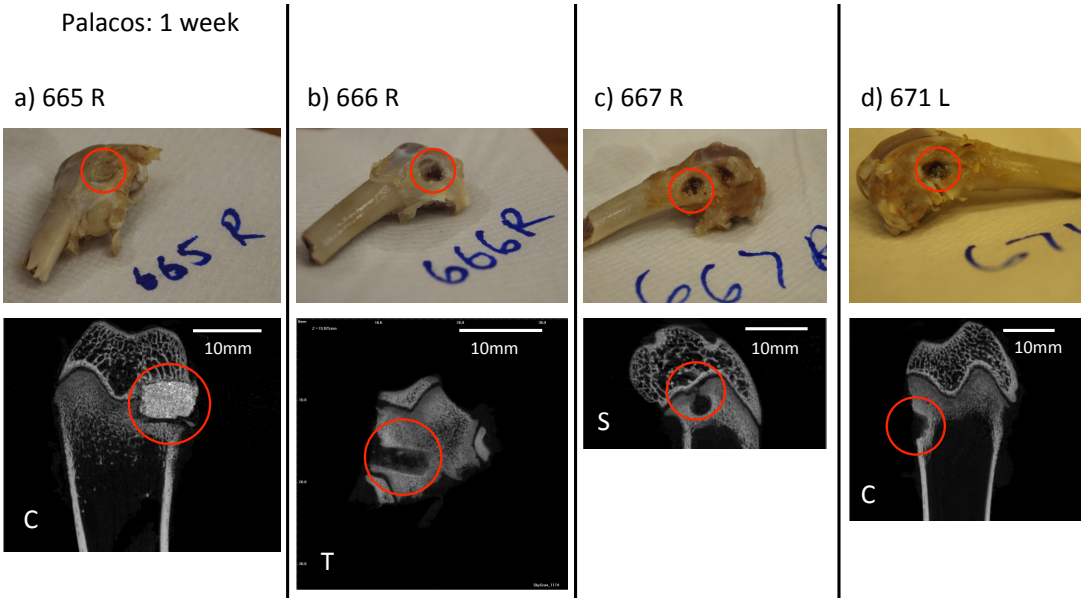

Figure 6-6 Palacos Micro CT images after one-week in-vivo. Material visible only in 665R. Defect visible in all other specimens. Defect sites marked with red circles. Images marked with T, S and C are in the transverse, sagittal and coronal planes respectively.

Micro CT images of the implants after four weeks in-vivo showed three empty defects where PFC was implanted (Figure 6-7) and one empty defect where PMMA was implanted (Figure 6-8)

One of the four week PFC implants, 658R, has voids within the material. Two of the voids measure less than 1 mm. The large void at the bottom of the implant site measures around 3 mm. Aside from around the large void, the material appears to be in close contact with the host bone.

The PMMA implanted into sites 655R and 657R is well packed into these defects with good contact at the interfaces seen in the microCT images. The PMMA material is not fully packed into the 656R site, the outline of the defect can be seen above and to the right of the plug of PMMA material with a gap in between. There is also excess material visible outside of this defect.

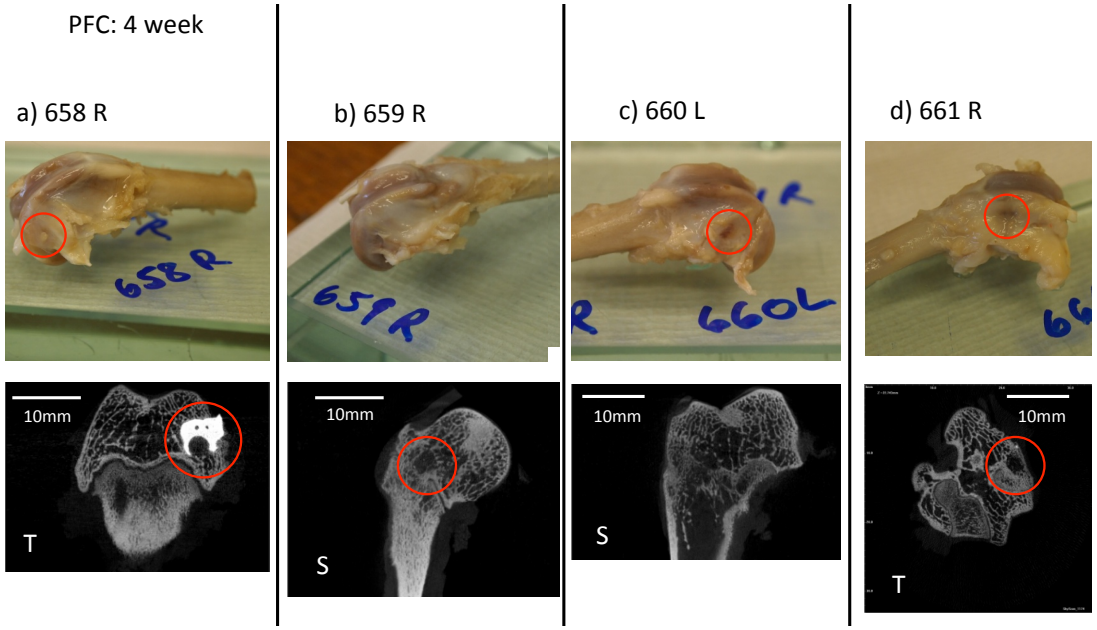

Figure 6-7 PPGDMA Micro CT images after four weeks in-vivo. Material only visible in 658R defect visible in 659R and 661R. Defect sites marked with red circles. Neither material nor defect visible in 660L. Images marked with T and S are in the transverse and sagittal planes respectively.

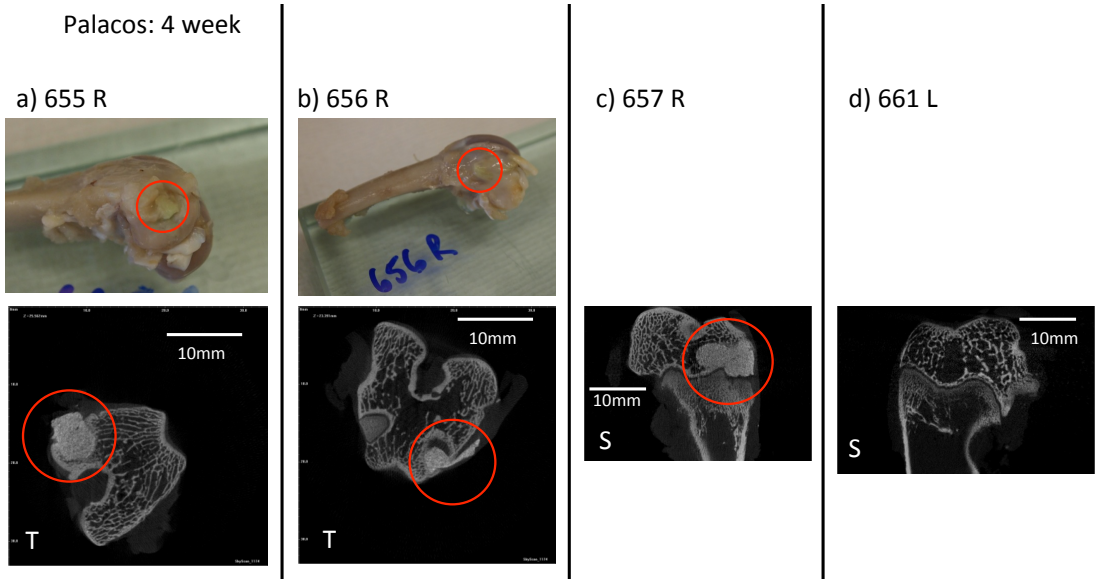

Figure 6-8 Palacos Micro CT images after four weeks in-vivo. No explant image available for 657R or 661L. Defect sites marked with red circles. Images marked with T and S are in the transverse and sagittal planes respectively.

Whether or not there is fibrous encapsulation of the implants cannot be seen on the micro CT images.

The PFC cement was more radiopaque than the PMMA (for example site 658R, Figure 6-7, versus 655R, Figure 6-8). The PMMA cement had a radiopacity more similar to cortical bone.

6.6.2.3 Histology

Histological evaluation of the heart, lung, kidney, liver and spleen samples showed normal healthy organs for all animals, despite the recorded infections and displaced materials.

All images of histological sections are in the transverse plane. Sections were stained with Toluidine blue or Goldner's trichrome stains. When stained with toluidine blue, and viewed with polarized light, lamellae that are orientated in one direction, appear blue, whereas those at 90° to this appear yellow. Mature bone is highly organized with parallel aligned collagen bundles, whereas immature bone has more randomly orientated collagen bundles. When sections are viewed under polarized light, with this stain, the degree of organization of the tissue can be a sign as to whether the bone is mature or immature. Cartilaginous fibrous tissue is shown as wavy pink regions with toluidine stain. When using Goldner's trichrome stain, mineralized / mature and unmineralized / immature bone are coloured as green and red/gold respectively. Cartilage and fibrous tissue shows as purple.

PFC After One Week In-vivo

Figure 6-9 andFigure 6-10 show sections of two of the implant sites treated with PFC after 1 week. Figure 6-9 shows a section of implant site 670L stained with toluidine blue viewed with polarized light. The blue and yellow regions indicate normal bone remodelling behaviour. There are no giant cells (multinucleated macrophages) and no other indications of an inflammatory response or thermal necrosis. There is no

evidence of new bone growth near to the implant. The gap between the implanted material and the bone tissue is due to slide processing due to the shape and appearance of the gap. It is thought, therefore, that whilst in-vivo the bone was in good contact with the implant at this point.

Figure 6-10 is a section of implant site 668R stained with Toluidine Blue. MicroCT investigation of this site showed that the defect site was empty; the histological section, however, shows that there are fingers of bone within the defect region. It is clear that the morphology of the bone is different on the left of the defect (denser with smaller holes (osteocyte lacunae) which are further apart, compared with new bone (depicted by arrows) where there is much less of a lamellar (layered) pattern and the lacunae are large and closer together.

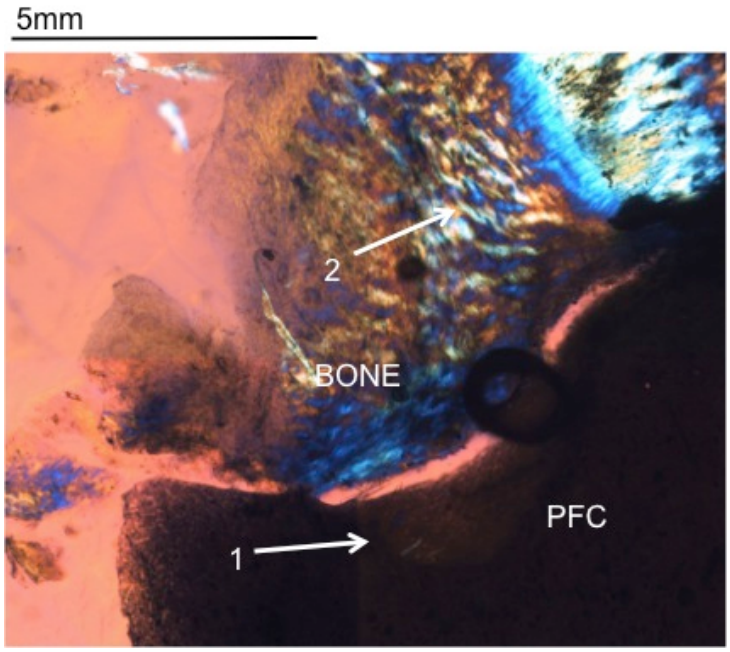

Figure 6-9 670L PFC after one week with toluidine blue stain. Very thick section makes it difficult to see cellular detail in bone tissue however, a combination of blue and yellow bone surrounding the implant is evidence of normal metabolic remodelling activity. Slide processing caused gap between bone and material – but evidence of good apposition between material and bone prior to this. No inflammatory response.

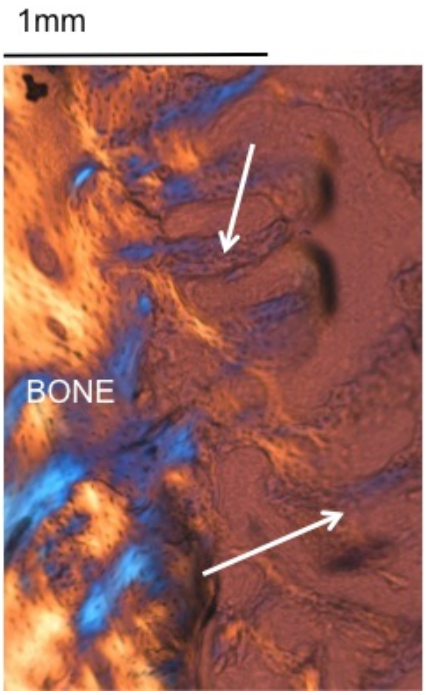

Figure 6-10 668R PFC after one-week in-vivo. Section showing empty defect site and surrounding tissue – material dislodged in-vivo. Blue/Yellow coloured 'fingers' (two such fingers shown by arrows).

Palacos After One Week In-vivo

Figure 6-11 and Figure 6-12 show sections of Palacos implant sites after one-week in-vivo. In Figure 6-11 there is no evidence of material or tissue in the defect site. This is in agreement with the MicroCT image for this site. In both Figure 6-11 and Figure 6-12 the surrounding bone tissue cell distribution and tissue colouring is indicative of normal bone remodelling in healthy tissue and there is no evidence of inflammatory response or thermal necrosis.

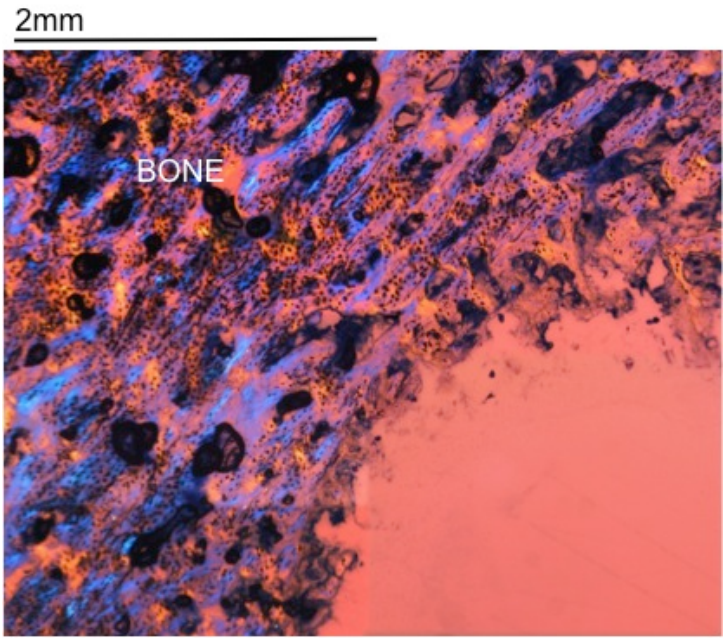

Figure 6-11 666R Palacos one-week in-vivo with toluidine stain. Section showing empty defect site and surrounding bone tissue. No tissue visible inside defect. Bone colouring and cell density around defect indicate no inflammatory response.

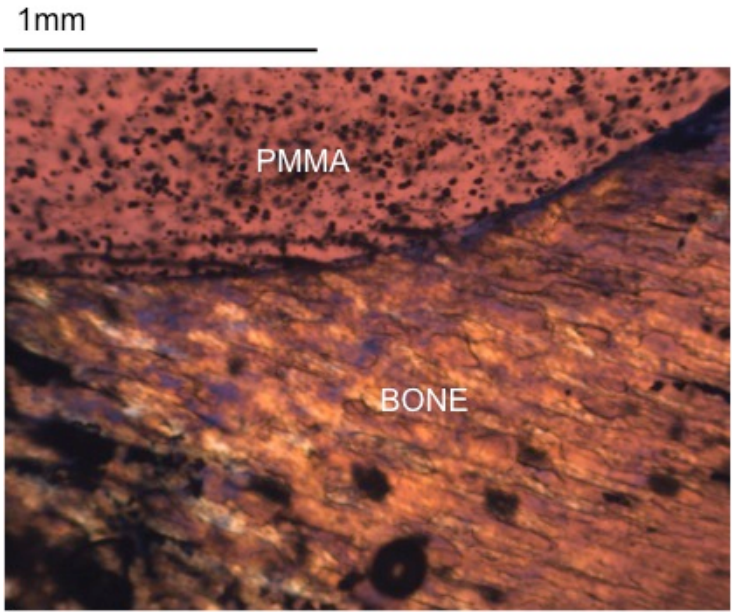

Figure 6-12 665R Palacos after one-week in-vivo with toluidine blue stain. The slide is too thick to see cellular detail in bone tissue but interface between bone and PMMA shows good apposition, with blue/yellow bone tissue indicative of normal bone metabolic behaviour.

PFC After Four Weeks In-vivo

The histological images for PFC implants after four weeks in-vivo Figure 6-13 to Figure 6-16 show close contact between the implant material and the surrounding normal viable bone. There appears to be new bone growth up to the implant in Figure 6-17 indicated by a higher density of lacunae and less organized tissue structure. There is no evidence of any inflammatory response and the colouring and texture of bone further from the implants is indicative of normal remodelling behaviour and shows no thermal damage.

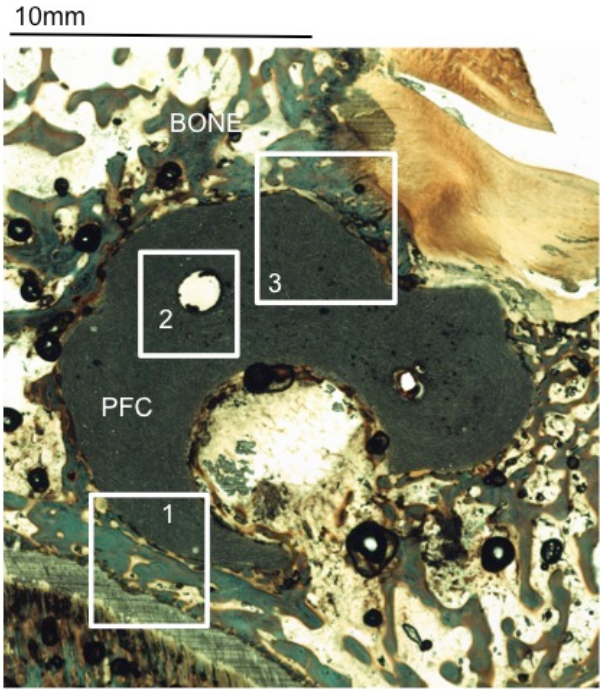

Figure 6-13 658R PFC after four weeks. Goldner's Trichrome stain. See Figures 6-13, 6-14 and 6-15 for details of regions of interest in boxes 1, 2 and 3.

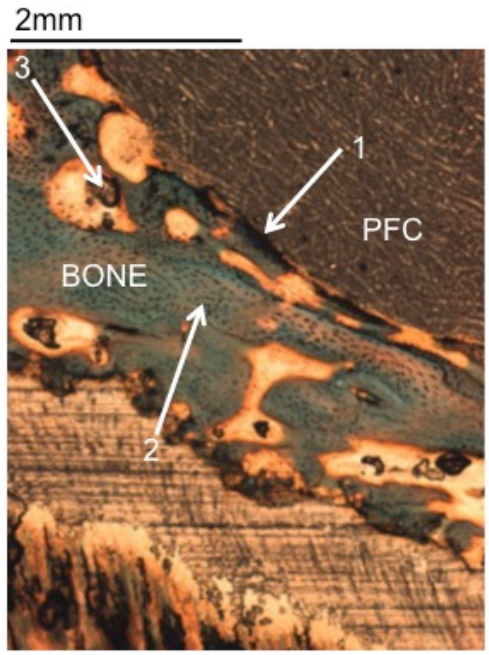

Figure 6-14 658R box 1: Good contact between host bone and material: Arrow 1: presence of blue coloured lamellar bone close to material. Arrow 2: Dots are lacunae containing osteocytes. Arrow 3: bubble in resin.

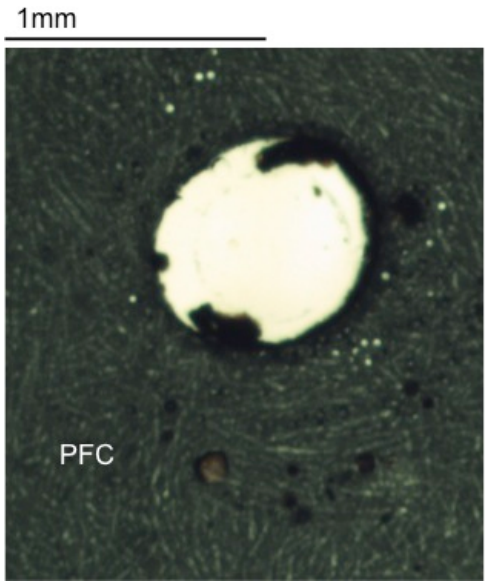

Figure 6-15 658R box 2: Air bubble in material. Can clearly see fibres in material too – aspect ratio well defined

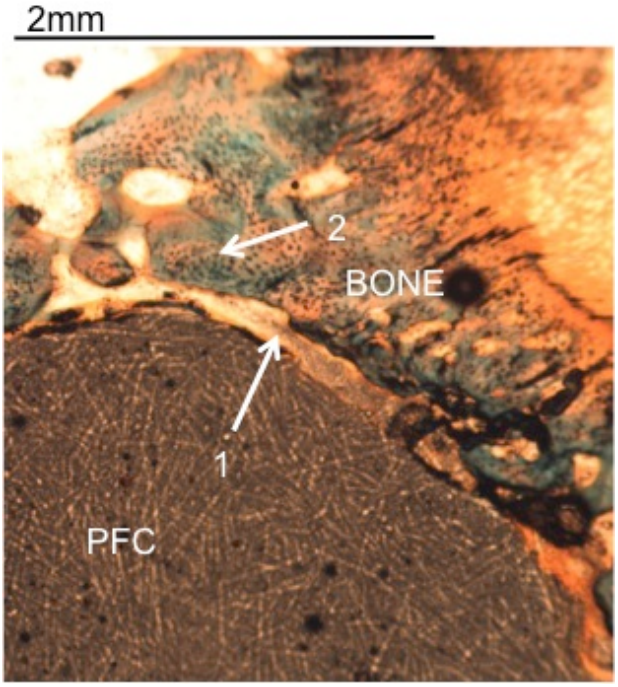

Figure 6-16 658R box 3: Gap here thought to be due to slide processing as other regions show good contact between lamellar bone and composite. Arrow depicts region of blue and yellow indicative of normal viable bone.

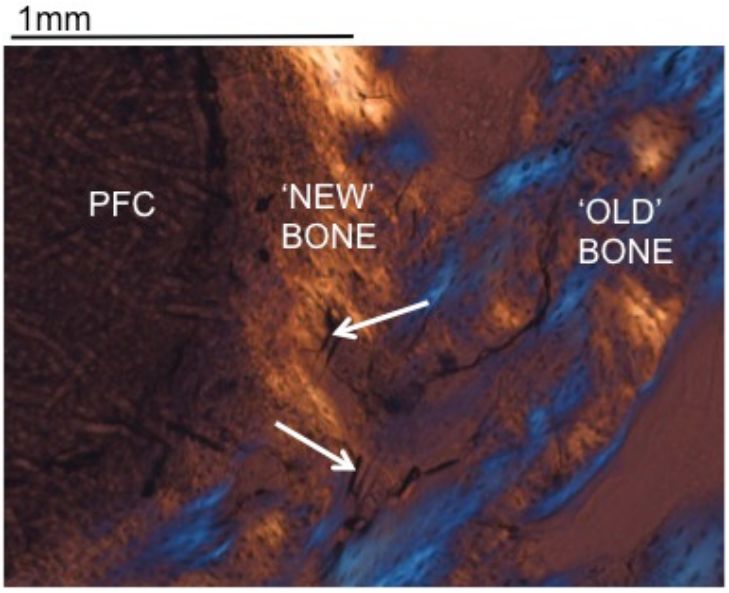

Figure 6-17 658R PFC after four weeks. Toluidine Blue stain. Interface between material and bone is yellow in colour indicating deposition of new woven bone next to implant. Density of lacunae in blue and yellow 'old bone' further away from material indicative of normal bone metabolic activity. No inflammatory response. Fibres 'in' bone (depicted by arrows).

Palacos After Four Weeks In-vivo

The histological sections for PMMA implanted for four weeks (Figure 6-18 to Figure 6-21) also show good apposition of surrounding tissue to the material surface. However there is no evidence of new bone formation unlike the PFC sections. Similar to the PFC implant sections, there is no cellular inflammatory response and no giant cells are present around the implants and again there is no evidence of thermal necrosis.

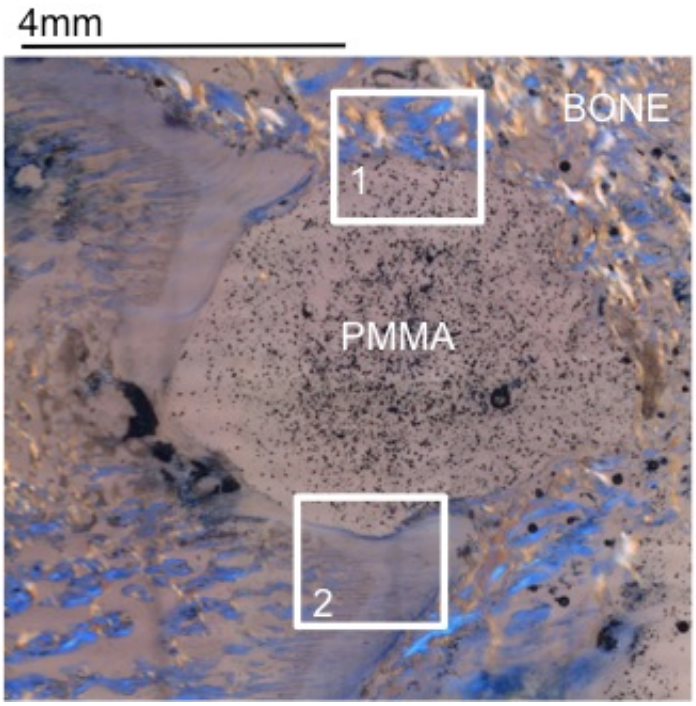

Figure 6-18 656R Palacos after four weeks with Toluidine blue stain. Good bone apposition next to material, no inflammatory response.

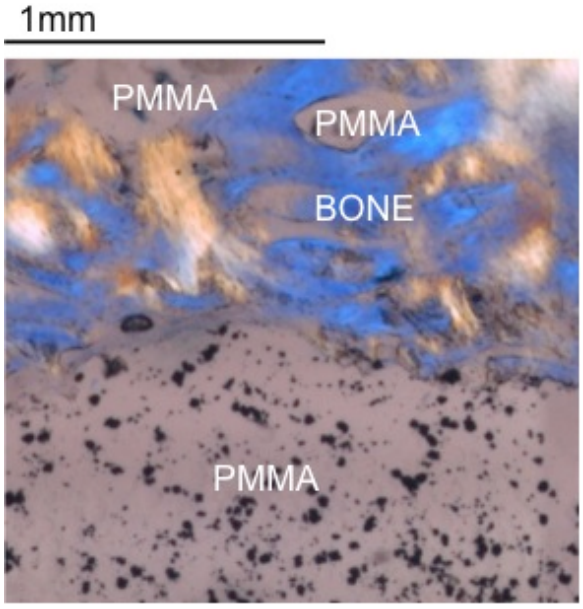

Figure 6-19 656R Box 1 intimate contact between Palacos material and Bone. Blue and yellow bone regions indicative of normal bone metabolic activity. Normal osteocyte abundance with no evidence of inflammatory response.

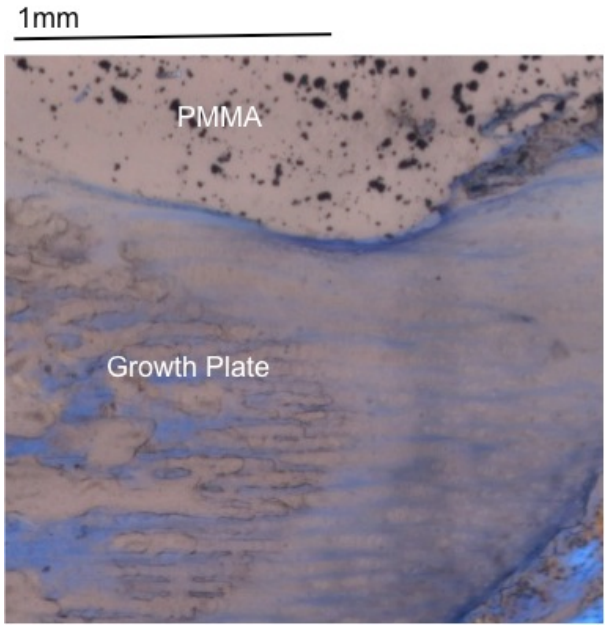

Figure 6-20 656R Box 2 PMMA cement with adjacent cartilaginous tissue of growth plate. Once again, issue shows no signs of inflammatory response to PMMA cement.

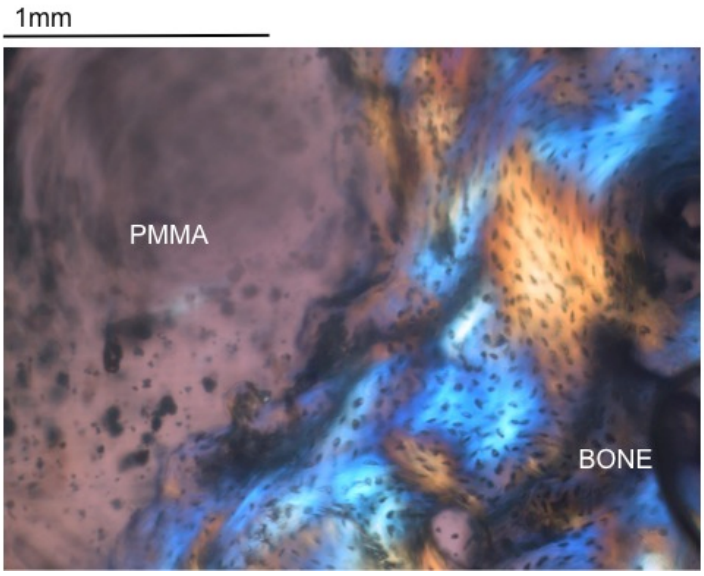

Figure 6-21 656R deeper section, Palacos after 4 weeks with toluidine blue stain; As with Figure 6-18, shows good apposition between bone and Palacos material with no inflammatory response. No new bone formation, but blue/yellow pattern and osteocyte distribution indicative of normal bone metabolic activity. This slide is too thick, and so some regions are out of focus.

6.7 Discussion

6.7.1 Prototype Formulation Characterization

The conversion of the prototype Formulation is not significantly different to PFC 9 as the levels of the three monomers are very similar; in the prototype PFC, compared to PFC9, 1.5 wt.% of UDMA and 2 wt.% of HEMA are replaced by PPGDMA, the filler level is increased by 5% and the proportion of fibres is increased. Palacos conversion is slightly higher, whilst that of Simplex P, Z250, Cortoss and Comp06 (Table 6-1) is significantly lower than the PFC.

The time to 50% reaction for the prototype formulation is significantly shorter than those times measured for all the commercial materials, excluding the light cured Z250 (Table 6-1).

The calculated shrinkage for the prototype formulation (Table 6-1) was lower than for PFC9 and the commercial composite bone cements due to the high filler content.

The conversion and time to cure have profound implications on the amount of residual monomer that the patient is exposed to both during the implantation procedure before cure and afterwards. The benefits of a high level of conversion have been discussed previously (chapter 3 chapter 5) and so it is very encouraging that this prototype exhibits such favourable curing characteristics, compared to PMMA cements, Cortoss and Comp06 (Chapter 3), when considering it for bone repair applications.

The shrinkage of the material during cure can affect the interdigitation of the cement into the surrounding host bone as discussed in the introduction (chapter 1) and chapter 3. The prototype PFC combines the effects of high molecular weight monomers, with high conversion, and high filler content leading to a lower calculated shrinkage than that calculated for PMMA and Cortoss (chapter 3) and lower than PMMA shrinkage values from literature. Indeed the prototype formulation shrinkage is approaching the value quoted for dental composites. The low shrinkage value calculated for the

prototype PFC compared to the other commercial materials, combined with fluid rheological properties, suggests that the PFC could create a mechanically sound interface with host bone. An excellent interface is necessary for the longevity of the implant.

The benefits of a shorter induction time, prior to the onset of cure, and time taken for the material to cure were discussed with an orthopaedic surgeon[8]. Low viscosity cement materials that are slow curing carry a risk of migrating into the patient's circulation and, in the case of vertebroplasty, putting pressure on the spinal cord (31,32). For this reason high viscosity Palacos is recommended for vertebroplasty. Cement infiltration of surrounding bone, however, could be compromised when using packable cement. Manipulation of the injection site is done prior to injection. Swift cure of cement subsequent to injection is beneficial to the surgeon as it facilitates fast fixing of the fracture site with minimal opportunity for the material to migrate. A flowable material will still be fluid enough to intermingle with surrounding bone, and create a mechanically sound bone/material interface at low injection pressures.

The strength of the Cortoss declined when stored for extended periods in water at 37 °C. This strength decline after 4 weeks was the same magnitude as that observed by Boyd et al. (10). Boyd suggested that the reason for this strength decrease is related to BisGMA encouraging water sorption, which plasticizes the cement. It is also thought that the strength decline could be in part due to the dissolution of the combeite phase (Combeite degrades, releasing sodium and calcium ions and soluble silica, (148) as this is also a problem reported with MCPM/bTCP containing composites (64).

The strength decline, after 4 weeks, observed for the prototype product is smaller than for Cortoss. The prototype product contains UDMA and PPGDMA, both without hydroxyl groups. The prototype product does, however, contain a small quantity of

[8] The curing time of orthopaedic cements was discussed with Auvo Kaikonnen, in September 2010, during the 2010 European Society for Biomaterials conference in Tampere, Finland.

HEMA, which does contain hydroxyl groups that will encourage water sorption and therefore lead to plasticizing of the material and ultimate strength loss. The level of HEMA is small and therefore the plasticizing effect is smaller than for BisGMA containing Cortoss.

Silane coupling provides a chemical bond between the filler and the polymer phases in methacrylate composites that can prevent hydrolytic degradation of the filler phase preventing strength decline when stored in wet conditions (149). Both the prototype PFC and Cortoss contain silane coupled glass filler. In Cortoss, however, the combeite phase is not silane coupled and so it is thought that the lack of interfacial bonding between the polymer and combeite is also responsible for hydrolytic degradation and subsequent poor long term strength of this material. It is hypothesized water sorption has a more detrimental effect on the polymer phase than the filler phase when the filler is silane coupled (147). It is difficult to quantify the efficacy of silane treatment other than by indirect methods such as strength of composites and handling of material prior to cure. The fracture surface in Figure 6-4 could be considered as evidence of a good interfacial silane bond between the particulate filler and polymer whereas the fibre pull out could be indicative of less effective silane coupling of the fibre filler.

The strength of the prototype product, however, returns to its 24-hour value after 20 weeks hydration with an associated stiffening. This contradicts what is expected if water sorption is plasticizing the material. In materials that contain MCPM and bTCP it has been hypothesized that a ‘self healing’ mechanism reverses decreases in strength associated with water sorption by reaction of the MCPM and bTCP to form a brushite phase (64). It is thought that the FGS fibres (which contained calcium Table 4-3) could react with other components in the PFC material, but that this reaction would be insufficient to produce a self-healing mechanism in the bulk of the material that results in greater stiffness and flexural strength. Ferracane et al. have some data suggesting an increase in flexural strength of dental composites after ageing in water. This

apparent increase was attributed to large variability in flexural strength results because the test method used (three point bend) is sensitive to surface condition of specimen (150). A large variability in results due to sensitivity of test method to specimen surface condition is thought to be a much more likely cause for the observed increase in BFS and stiffness between 4 and 20 weeks of the PFC material. The error expected for a mechanical test of this kind is around 10 %; the error observed in the 20 week tests is quite low, meaning that a change from 76 MPa to 93 MPa appears significant. It is thought that surface condition of the specimens after 20weeks and only a small sample size is responsible for a smaller than expected error. The observed increase in BFS from 4 weeks to 20 weeks is thought therefore to be insignificant. It is thought that there is probably a small decrease in BFS over the storage period and a larger number of specimens at each time period are therefore required to give a better estimate of this. Furthermore, the observed increase in stiffness of the PFC material is thought to be insignificant for the same reason.

The decline in BFS of the PFC material was less than for Cortoss after 4weeks, which is encouraging. Boyd et al. (10) showed that PMMA cements did not have a decline in strength following extended periods of hydration; the PFC cement performs better than Cortoss in terms of long term strength and modulus and comparably to PMMA cements in terms of mechanical properties after 24hours. Despite the changes in BFS and Modulus, the fracture behaviour of the PFC material remained unaltered for all the storage periods. A decrease in strength is expected; usually decreases in fracture toughness/ strength are attributed to water plasticizing the polymer and polymer hydrolysis (150).

As discussed in chapter 5, the strength, for current composite bone cements (Cortoss and Comp06), was around 4 – 5 % of the stiffness. For the prototype PFC, the strength is also around 4 % of the stiffness. The flexural strength of the PFC is above the required 50 MPa and the modulus is above the 1.8 GPa required by BS 5833. The

compressive strength required by both ASTM 451F and BS 5833 is 70 MPa. Although this has not been determined for the prototype PFC, it must be considered in further development of the material.

6.7.2 In-vivo Implantation of Prototype PFC

6.7.2.1 Surgical Procedure

The animals used received implants in both hind legs. First and foremost this was to maximize the number of implantation sites, whilst reducing the number of animals required in line with animal testing ethical framework 'the 3 R's' (Replacement, Refinement, Reduction (151)). Secondly, bones need to be loaded to heal effectively (152), implantation in both hind legs prevented the animals from 'favouring' the implanted limb and affecting the host healing response. Finally, allocation of implant materials was random.

The PMMA was not pre-mixed and so there was scope for accidental change in monomer/powder ratio, due to spillage and evaporation, and therefore change in properties. In this respect the PPGDMA cement was more reliable as there was no possibility for changing the composition due to hand mixing. Some pre-mixed cements phase separate during storage. The PFC materials were stored in the syringes for 24 hours before implantation; no phase separation was noted in this time. Phase separation after longer periods of storage is something to be considered in development of PFCs for bone repair.

Three cases of infection were observed following excision of PMMA material. This is much higher than the rate of infection recorded for human vertebroplasty (153). The higher infection rate is attributed to a less clean operating environment than is used with human procedures and hand mixing of the PMMA material in the open environment of the operating room.

The PFC material cured faster than at the lower in-vitro temperatures, setting solid within 45 seconds of injection. It has been reported that thermal necrosis occurs in a rabbit model when tissue temperatures are above 50 °C for more than one minute (154). This is at odds with findings for humans, however, where nociceptive nerve endings are reported to be ablated at 42 – 45 °C. Furthermore, the amount of material injected in rabbits is considerably lower than into humans so temperature rise will be much reduced. The rabbit femur model is therefore not expected to be good at predicting the thermal response of human trabecular bone to cement placement.

In this study, neither Palacos nor PFC mixed with blood preventing which might cause decreases in cement mechanical properties associated with blood entrapment (155).

The fact that many of the defect sites were found to be empty when recovered is considered to be a major problem with the surgical procedure. Bleeding has been reported to reduce the strength of the material/bone interface significantly (156). It is therefore thought that bleeding prevented the material from infiltrating the trabecular bone surrounding the implant sites. Without good mechanical interaction, the implants came loose. The PMMA cement had a lower incidence of displacement; the higher viscosity material could be packed into the defect halting bleeding more effectively than the PFC cement, enabling a mechanically superior interface. If more effective methods of stopping bleeding had been used the lower viscosity PFC material may not have been at a disadvantage. In human vertebroplasty, there is not as much bleeding as the cement is injected into an existing fracture, rather than a defect that has been freshly made. Displacement of implanted material due to bleeding in vertebroplasty is, therefore, not envisaged to be a significant problem. In joint replacements, cement material is implanted when there is active bleeding (157). In this procedure bone/cement interface can be improved by lavage and pressure on the curing cement (158). The latter, however, is incompatible with low viscosity materials.

6.7.2.2 Micro CT

The Micro CT instrument manufacturer recommends a minimum of 15% transmission to get a good/clear reconstructed image, but because of the thickness of specimens, the minimum transmission in this study was 4.3 %. This means that the image contrast is not as strong as desired.

The large and small voids in the four-week PFC implanted material (658R) are thought to be due to air bubbles in the pre-mixed material that were not removed by mixing. Small voids such as those measuring less than 1mm have been reported in human vertebral augmentation (159) and are thought to be air bubbles introduced from the injection syringe.

The PFC was more radiopaque than PMMA and so could be considered as better for surgeons. The silica glass component of the PFC cement, however, contains barium. Barium sulphate, also an additive in some PMMA cements, has been associated with causing bone resorbtion, as discussed in the introduction (chapter 1). Further to this, Togawa et al reported that macrophages surrounding PMMA implants in humans contained particles of barium sulphate (159). Barium sulphate can also affect the mechanical properties of PMMA cement. The opacifying component found in Palacos, ZrO_2, has fewer adverse effects on mechanical properties compared to $BaSO_4$ (3).

6.7.2.3 Histology

In a histologic evaluation of human vertebroplasty, Togawa et al has reported cement in venous tissues (159). Neither the PFC cement nor Palacos, however, exhibited problems with cement leakage/migration into venous tissue or organs. The serious complications associated with this cement migration were, therefore, avoided.

Regions of blue and yellow bone with normal lacunae density and size next to the implant in histological sections were taken as evidence of bone remodelling and normal

metabolic activities. Cartilaginous fibrous tissue at the material/bone interface would suggest fibrous encapsulation.

In general the histological sections in this study have been used to give a qualitative sense of the host response to the implant materials. A good response was deemed one where there was a good snug interface between the host bone and the implanted material; poor apposition would be evidence of fibrous encapsulation and a poor response. As well as the physical look of the implant/material interface, the lacunae concentration at the interface was compared to bone further from the implant. If the cell concentration at the interface were higher than surrounding tissue it would suggest immature bone. The presence of macrophages or other multinucleated giant cells would suggest an inflammatory response. For both PFC and PMMA cements after one-week in-vivo, there was one implant site where the material had stayed in place and was sectioned effectively. Intimate contact between material and healthy host bone was seen, implying a good early response to both materials.

It is not known at what point the implants came loose from the empty defect sites 668R and 666R (shown in Figure 6-10 and Figure 6-11 respectively). It is difficult, therefore, to get a fair idea of the biological response of the host to the implant as the duration of implantation is not known. In Figure 6-10 (668R; PFC after 1week) the structure and lacunae size/concentration of the bone ‘fingers’ within the defect indicates that they both consist of woven bone. Piattelli et al. observed that it took up to 9 weeks for mineralized bone to be found in PTFE membrane lined 8mm defects in rabbit tibia metaphyses (160). One week is therefore not considered sufficient time for mature bone to form in a defect. It is thought that the PFC material did not fully fill the defect and became dislodged during the implantation procedure or shortly afterwards allowing formation of new, immature tissue in the defect. In site 666R the totally empty defect in Figure 10 implies that either immature tissue or the material that was in the defect was

removed during slide processing or that the PMMA material was dislodged just prior to extraction, or during extraction. This is another negative of the implant procedure.

In Figure 6-15 the large void is thought to be an air bubble due to delivery method rather than a void created by bleeding, as there is no evidence of blood cells within the void.

In Figure 6-17 the fibres 'in' bone surrounding implant could be migration of fibres due to bioactivity, but are more likely to be due to processing of slides.

No thermal necrosis was evident in the histological images for either material at either implant duration. Erbe et al. and Verlaan et al. found that thermal necrosis was not a problem in rabbit and goat models respectively (161,162). It is postulated that it is blood flow in-vivo that helps to dissipate heat on cure and prevent the high temperatures that are reported in-vitro (163).

Togawa et al, also found that foreign body giant cells and mononuclear macrophages were identified in the thin membrane surrounding implanted PMMA (159). In the present study, however no cellular inflammatory response was seen. Despite the lack of evidence for a cellular response it is thought that foreign body reaction could be more important than thermal necrosis (sheep model) (164).

Neither the PFC cement nor the PMMA cement exhibit any fibrous encapsulation of the implant. Conversely, Togawa et al. have shown that for PMMA cement, there was no direct bone apposition to the cement; there was instead a thin fibrous membrane separating tissue from PMMA (159). Revell et al. also report fibrous encapsulation of PMMA cements after 6 weeks implantation (36).

Erbe showed Endosteal/periosteal bone surrounding both PMMA and a composite containing bioactive glass filler (Cortoss) after four weeks in-vivo (161). More bone contact, however, was seen with Cortoss. Cortoss showed apposition of new bone in

Rabbits at 24 weeks. This is similar to the response to the PPGDMA cement at four weeks, which shows new bone growth up to the implant and possible integration of fibres with bone tissue. This could be due to the bioactive nature of glass, but could also be due to histology processing.

Revell et al. report that some quantitative assessment of histological sections can be made; a percentage of viable bone in contact with implanted bone cement can be found by examining the perimeter of implanted cement in a section (36). However, this will only give a useful estimate of biocompatibility when a number of implant sites can be examined. In the present study this was not possible as too many implants came loose.

6.8 Conclusions

The handling and mixing of the prototype PFC were suitable for syringe and mixing tip delivery, however, the viscosity was too low for an in-vivo situation in which bleeding was not completely stemmed. The PFC materials were found to cure faster at 37 °C than at room temperature.

The shape of the curing profile of the prototype PFC formulation was most similar to PFC9, with a more gradual cure than Cortoss, Comp06 and PMMA materials. The polymerization shrinkage was calculated to be lower than for the commercial composite and PMMA bone cements despite the level of conversion being higher. The BFS of the PFC prototype was comparable to commercial materials but the stiffness was lower than for Cortoss and Comp06 – the benefits of lower stiffness are discussed in chapter 5. The long term strength and stiffness of the PFC material is variable, although initial results indicate that the PFC material does not decline in strength after ageing in water as much as Cortoss. Addition of fibres enabled a non-brittle fracture pattern as demonstrated in chapters 4 and 5.

In-vivo implantation of the PFC material confirmed that the material could be sterilized, injected and cured in-vivo. There were no recorded infections for PFC implant sites. As mentioned above, the viscosity of material did cause some problems and the material did not bond to bone in the presence of blood. There were regions in which good apposition between PFC and bone was observed – it is thought that bleeding was more successfully stemmed in these areas. Furthermore the close contact of host bone to the implanted PFC, normal metabolic activity of surrounding bone tissue and regions of osteoid growth adjacent to PFC are all evidence that the material induced a biological response superior to PMMA cement. The PFC was found to be more radiopaque than Palacos R PMMA cement and cortical bone. Despite evidence in the literature to the contrary (mentioned in chapter 1) barium present in glass did not appear to cause a negative bone response.

PFC is an implant material with good biocompatibility and radiopacity that may be suitable for use in humans for fixation of osteoporotic fractures via percutaneous vertebroplasty.

7 Effects of Initiator and Inhibitor System Concentrations on Curing and Shelf Life of Prototype PFC.

7.1 Abstract

In the previous chapter an in-vivo and in-vitro characterization of a prototype PFC formulation was performed. Although this formulation performed well when cured immediately after mixing or after 24 hours refrigerated storage, it is necessary to have an appreciation of how long the material can be stored for before spontaneously polymerizing and what the effects of changing the levels of initiators are on the curing.

The aim of this chapter was to perform a factorial design (using the Prototype PFC monomer and filler systems) to investigate the effects on the curing times and degree of conversion of DMPT, BP and BHT levels. Accelerated ageing of 1 and 2 % BP PFC pastes was performed to predict the shelf life of these pastes at room temperature and 4 °C.

Increasing BP will significantly increase the conversion of PFC formulations when low amounts of BHT are present. The level of DMPT had the largest effect on the lead in time/time to 50% of the three variables investigated. This suggests that the effect on cure time and rate of lower BP and higher BHT can be balanced by addition of DMPT. The effects of initiators and inhibitors are highly specific to the monomer system used.

Decreasing the level of BP relative to BHT increases the shelf life of PFC formulations. BP will be consumed during the shelf life period and so it is clinically relevant that the PFC pastes still have high levels of conversion even at very low levels of BP (0.125 %).

7.2 Introduction

In chapter 5 it was found that increasing the level of diluent monomer (PPG) slowed down the rate of polymerization and resulted in higher levels of conversion. Cure times and rates were compared with kinetic theory and an equation was derived that implies a linear relationship between cure time and inhibitor, monomer and initiator concentrations.

In the previous chapter the monomer and filler systems were chosen to create a prototype PFC formulation that was characterized in terms of strength, modulus, cure and in-vivo response – the initiator system was kept constant throughout.

Many authors report how the initiator system can affect material properties. In this chapter the cure times and levels of conversion will be examined. Previous work at the Eastman has suggested that doubling the level of BP and DMPT will decrease the time to half reaction by factors of 1.2 and 2 respectively for UDMA/TEGDMA/HEMA composites (165). Hasenwinkel et al. have reported a power law relationship (exponent of -0.5) between BP and DMPT concentration and setting time when used to initiate a two solution PMMA cement (34).

Inhibitors are substances that neutralize the action of polymer and initiator free radicals and therefore slow down or stop the polymerization reaction depending on how efficient the action of the inhibitor is (16). An amount of initiator to overcome the level of inhibitor is required for polymerization to begin / reach a desired level. In this study Butylated Hydroxytoluene is the inhibitor being investigated. It is a common inhibitor for use in methacrylate based composites and PMMA bone cements (both Cortoss and Comp06 contain BHT). A study by Rosentritt suggests that BHT will have a linear effect on the inhibition time and reaction rate in TEG DMA/BisGMA composites when used with a light cure initiator system (138).

The in-vitro and in-vivo characterization of the prototype PFC formulation that formed the subject of the last chapter focused on the immediate curing profile following a 24 hour storage period between mixing and implantation. Ensuring a reproducible cure after a period of storage as well as favourable cured cement properties is central to developing a viable bone repair product.

The BP paste of each formulation will spontaneously cure over time and it has been shown that this spontaneous cure follows Arrhenius type temperature dependence (16,166). Once the Arrhenius equation is determined the effect of temperature on the spontaneous cure will be known and the shelf life of the material for a range of storage temperatures can be predicted.

7.3 Aims and Objectives

This chapter aims to investigate the effects of changing the initiator system on the curing profile of the prototype. The relative levels of initiator Benzoyl Peroxide (BP), acceleratoractivator Dimethyl Para-toluidine (DMPT) and inhibitor Butylated Hydroxytoluene (BHT) were to be altered to establish their effects on the following:

- The shape of curing profile and level of cure.
- Quantification of inhibition time (t_{inh}) and time to 50% cure ($t_{0.5}$).
- Comparison of kinetic theory equations from Chapter 5 with experimental conversion and cure profile results.
- Determination of inhibition mechanism of BHT

It is also the aim of this chapter to make preliminary investigations into how the level of BP affects the time that PFC materials can be stored before spontaneously curing (shelf life) and discuss areas in which greater depth of investigation is still required for development of this prototype PFC.

7.4 Hypotheses

Previous work at the Eastman (discussed in the introduction to this chapter) has suggested that doubling the concentration of both BP and DMPT decreases the time to 50% reaction of UDMA/TEGDMA/HEMA composites by factors of 1.2 and 2 respectively. It is thought, therefore, that increasing the level of BP and DMPT, whilst keeping the monomer levels constant, will reduce the inhibition time and the time to 50 % whilst increasing the level of BHT will increase the inhibition time and $t_{0.5}$.

In terms of the shelf life, an Arrhenius type equation is assumed. It is thought that increasing the level of BP/DMPT will reduce the shelf life whilst increasing the level of BHT will increase the shelf life.

7.5 Materials and Methods

A three variable factorial design experiment was performed varying the initiator system of the prototype formulation, from the previous chapter (Table 7-1). The nine initiator factorial design (IFD) formulations listed below were investigated to establish the effect of level of initiator, BP; activator, DMPT; and inhibitor, BHT on conversion and cure time/rate.

Specimen ID	VAR 1 DMPT (wt.%)	VAR 2 BP (wt.%)	VAR 3 BP/BHT	BHT (ppm)
IFD1	0.25	0.125	17.5	71
IFD2			70	18
IFD3		0.5	17.5	286
IFD4			70	71
IFD5	1	0.125	17.5	71
IFD6			70	18
IFD7		0.5	17.5	286
IFD8			70	71
IFD9	0.25	0.75	35	71

Table 7-1 Variable 1 (VAR 1) is level of DMPT, variable 2 (VAR 2) is level of BP and variable 3 (VAR 3) is ratio of mass of BP to mass of BHT. BP and DMPT given as wt.% of total monomer mass. BHT in ppm of monomer mass.

The variables were chosen to allow the effects of large changes in BP, DMPT and BHT to be observed. In preliminary studies, using a factorial design with low and high levels of BHT fixed (either 18 or 294 ppm) then a formulation containing 0.125 % BP and 0.25 % DMPT and 294 ppm BHT did not polymerize sufficiently. Conversely a formulation containing 0.5% BP, 1.0% DMPT and 18ppm BHT set within the mixing tip of the double barrelled syringe. Changing BP and DMPT by a factor of four and BHT by a factor of 16 will result in composites with curing levels and times that are practical for measurement whilst also allowing the effects over large ranges of initiator, activator and inhibitor to be observed.

The formulation contained equal quantities of PPGDMA and UDMA (both at 47.5 wt.% of total monomer mass) and a small amount of HEMA (5 wt.% of total monomer mass) combined with silanated barium silica glass (G_{4S}) and glass fibres (F_{GS}) at a total PLR of 4:1 (glass content 75 wt.% of total filler mass, fibres at 25 wt.% of total filler mass).

Formulations were manufactured and the level of conversion and normalized cure profiles were found for each formulation as per the methods detailed in chapter 2.

The stability of the material with time (shelf life) can be tested by doing accelerated ageing tests as detailed in ASTM F1980 (167). This protocol was modified as explained in chapter 2; the Arrhenius dependence of the PFC material was determined by placing formulations containing either 1 or 2 % BP (with 140 ppm BHT) in incubators maintained at 60 °C, 45 °C and 37 °C and monitored periodically to see at what time point they begin to cure.

7.6 Results

7.6.1 Effect of Initiators

The normalized cure profiles for the 9 IFD formulations are shown in Figure 7-1. From inspection of this figure it can be seen that the normalized inhibition times, t_i, are longer for those formulations containing low levels of DMPT (IFDs 1-4). The subsequent reaction is sharper for these IFDs and for $t_i < t/t_{0.5} < 1$ the reaction rates are steeper. The intermediate formulation (IFD9) is similar in shape to IFDs 1-4.

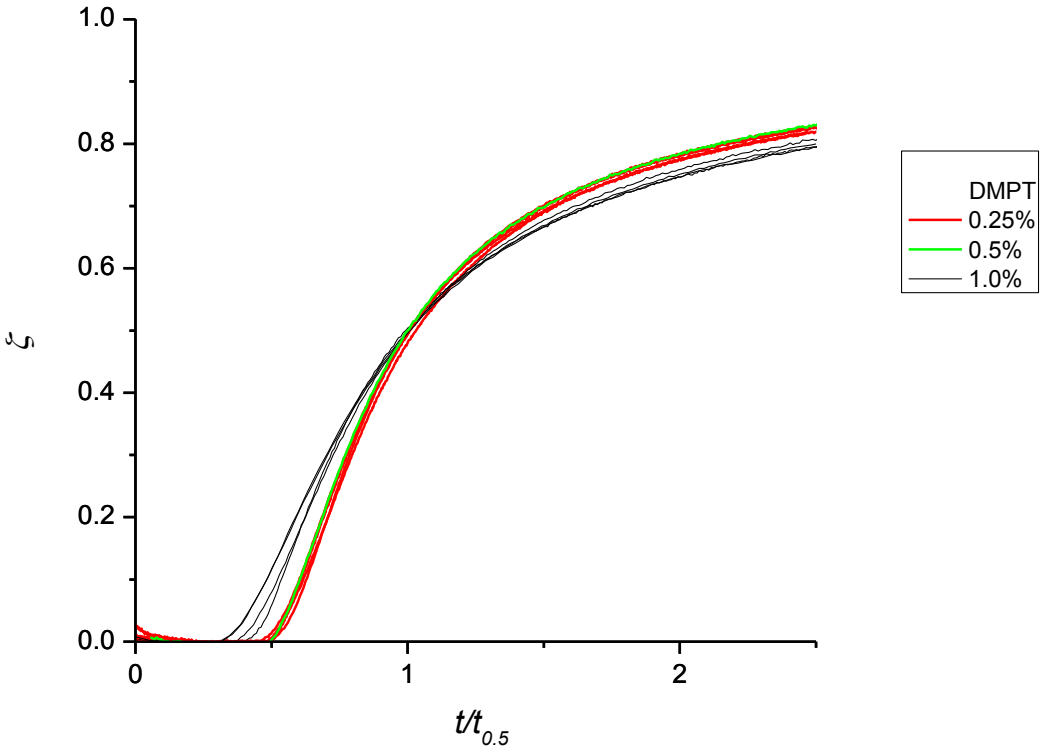

Figure 7-1 Normalized cure profiles of BHT factorial design formulations. DMPT has major greatest effect on normalized inhibition time and cure profile. IFDs1-4; red, IFD'sIFDs 5-8; black, IFD9; green trace.

The factorial analysis a-values of the conversion, $t_{0.5}$ and t_i results are shown in Figure 7-2. The level of DMPT is the major factor that affects the time to 50 % reaction extent, with BP and BP/BHT having smaller yet still significant effects.

There are small interaction effects on $t_{0.5}$ between the levels of DMPT and BP and the level of DMPT and the BP to BHT ratio however, these interactions, however, are small in comparison to the size of the effects of DMPT, BP and BP/BHT and so it is difficult to tell if they are significant or not. The a-values for normalized inhibition time and conversion are small in comparison to experimental errors and so it is difficult to interpret the effects of the variables on these properties from factorial analysis; further analysis is required and outlined next.

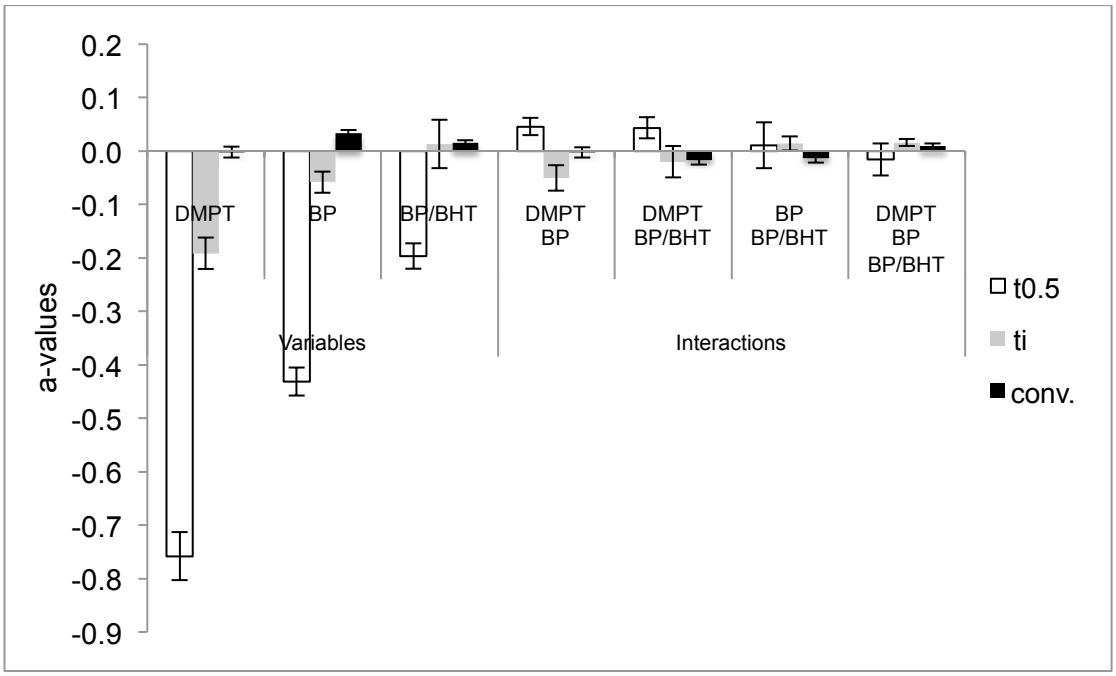

Figure 7-2 Factorial analysis giving effect of variables on time to 50% reaction extent, $t_{0.5}$; normalized inhibition time, t_i; and conversion. The level of DMPT has the largest effect on the time to 50% reaction, followed by BP and then the ratio of BP to BHT. The effect of interactions are considered experimentally insignificant as they are comparatively small or the 95% confidence interval error bars cross zero. DMPT also has an effect on t_i. The effects of the other variables/interactions on t_i and the effect of all variables on conversion are relatively small and so the above factorial analysis method is not useful for interpreting how the initiator system affects these properties.

To ascertain the effects of each variable on the levels of conversion the formulation composition with absolute level of BHT and final conversion is tabulated (Table 7-2). Increasing the level of BP results in an increase in conversion, although this increase is only significant when the level of BP relative toto BHT is high.

Specimen ID	DMPT (wt. %)	BP (wt.%)	BP/BHT	BHT (ppm)	Conversion (%)
IFD1	0.25	0.125	17.5	71	76 ± 4
IFD2			70	18	85 ± 2
IFD3		0.5	17.5	286	85 ± 1
IFD4			70	71	87 ± 1
IFD5	1.0	0.125	17.5	71	79 ± 2
IFD6			70	18	80 ± 1
IFD7		0.5	17.5	286	86 ± 1
IFD8			70	71	85 ± 2
IFD9	0.25	0.75	35	71	78 ± 4

Table 7-2 IFD formulation composition including absolute level of BHT. Formulation degree of conversion.

To investigate effects of the variables and interactions on $t_{0.5}$ and t_i these data have been plotted against the IFD composition in Figure 7-3 and Figure 7-4 below. IFDs 1-4 have smaller $t_{0.5}$ and t_i than IFDs 5-8. Both IFDs 1-4 and 5-8 show a reduction in $t_{0.5}$ as BP and BP/BHT increase.

From Figure 7-3 the ratio of $t_{0.5}$ values on comparing IDF samples 1/2,3/4,5/6 and 7/8 were 1.5, 1.7, 1.3 and 1.4 respectively. The change in BHT from IFD2 to IFD1, IFD4 to IFD3, IFD6 to IFD5 and IFD8 to IFD7 is a factor of four in each case. Thus a four-fold increase in BHT increases $t_{0.5}$, on average, by a factor of 1.5. Though as reaction rate increases (increase DMPT and BP), increasing BHT has less effect. This suggests that the inhibitor has only a minor effect on $t_{0.5}$ largely at low initiator concentrations.

Comparing analysis from Figure 7-3 to factorial analysis results (Figure 7-2) for $t_{0.5}$ suggests that the interaction terms with DMPT are insignificant as the trends in behaviour for IFDs 1-4 are the same as for IFD'sIFDs 5-8.

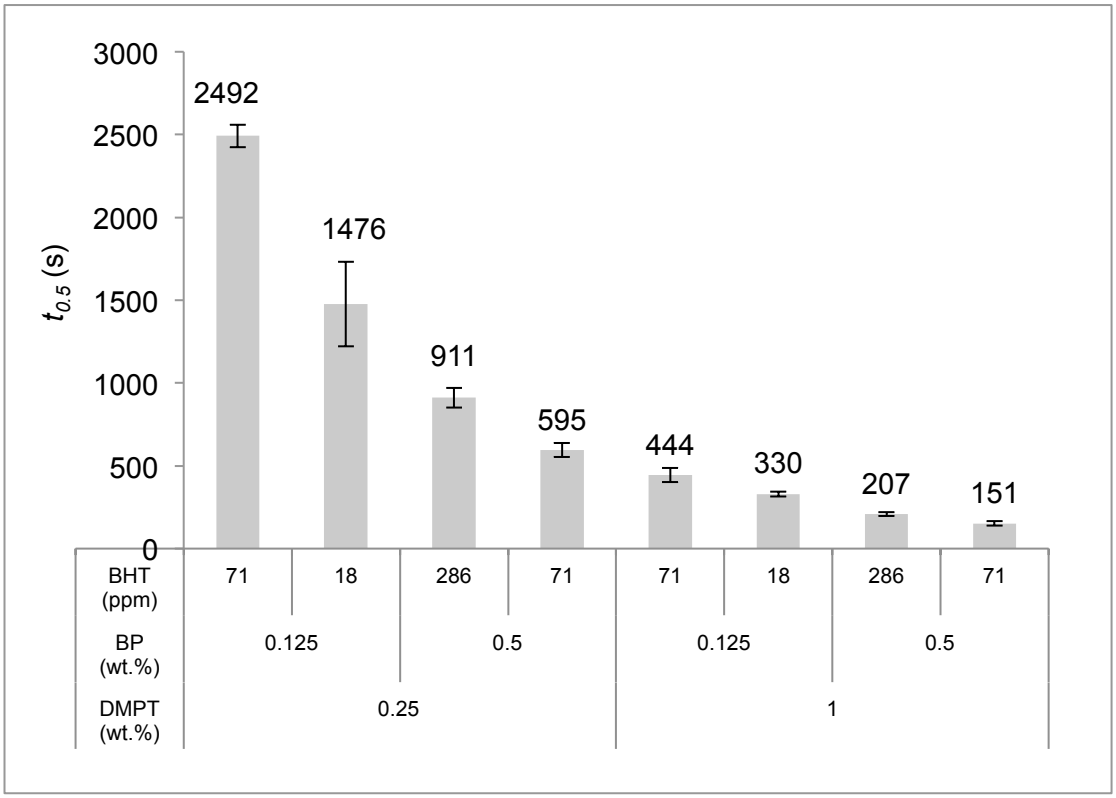

Figure 7-3 Time to 50% reaction vs. IFD formulation composition. Levels of DMPT and BP shown as wt.% of total monomer mass, BHT given as ppm (again of total monomer mass).

t_i is around 0.5 for all samples with DMPT of 0.25 wt.% and tends to 0.3 with high DMPT (Figure 7-4). This reflects the increased $t_{0.5}$ for low DMPT compared to high DMPT. With low DMPT t_i is also slightly lower with higher BHT. As well as increasing time for half reaction, high BHT therefore increases inhibition period but to a slightly lesser extent.

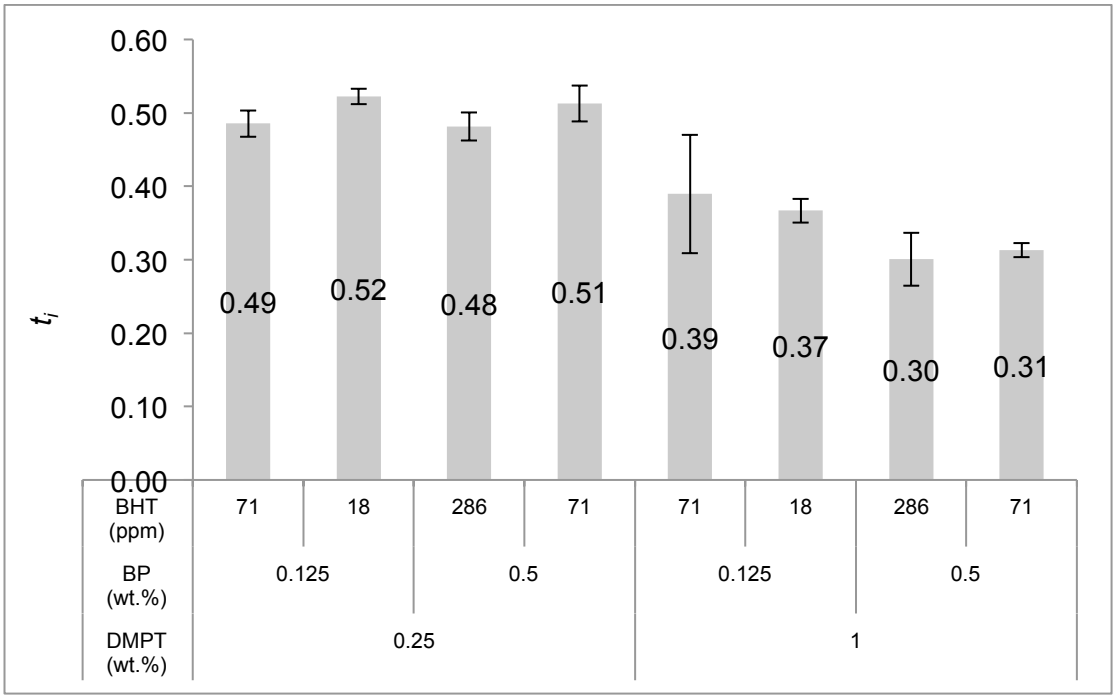

Figure 7-4 Normalized inhibition time, ti, vs. IFD formulation composition. Levels of DMPT and BP shown as wt.% of total monomer mass, BHT given as ppm (again of total monomer mass).

The results for IFD9 (conversion = 78±4 %, $t_{0.5}$ = 496±17 s and t_i = 0.48±0.02) are not similar to the average of the other specimens. Instead IFD9 lies in between IFD4 and IFD5.

7.6.2 Accelerated Ageing Studies

The time of set for 1 % BP paste and 2 % BP paste (each with 140ppm BHT) range from just over 1.5 hours (2% BP at 60 °C) to nearly 28 hours (1 % BP at 37 °C) (Table 7-3) below. The times to set are plotted in Figure 7-5; the activation energy (Ea) and frequency factor (A) can be found from the line of best fit of the plotted cure times. The activation energy for the two formulations is similar whereas the frequency factor of the 2% BP formulation is 24 times higher than that for the 1% BP formulation (Table 7-3).

The predicted shelf lives of the two formulations, at 23 °C, range from 4.1 to 5.7 hours for the 2% and 1% BP pastes respectively. At 4 °C these predicted setting times increase to just under 57 days and just over 65 days (Table 7-3).

BP (wt.%)	BHT (ppm)	Temperature (°C)	t_s (min)	Ea (kJ mol^{-1})	A (min^{-1})	predicted shelf life (min)	
						@23 °C	@4 °C
1	140	37	1670	87	3.2E+11	137	1564
		45	700				
		60	160				
2		37	1280	94	7.9E+12	98	1367
		45	335				
		60	95				

Table 7-3 The setting times of the two formulations, with activation energies and frequency factors from the plotted data. Predicted shelf lives of each formulation – 1 % BP paste has smaller frequency factor and hence an increased predicted shelf life at both 23 °C and 4 °C compared to 2 % BP paste.

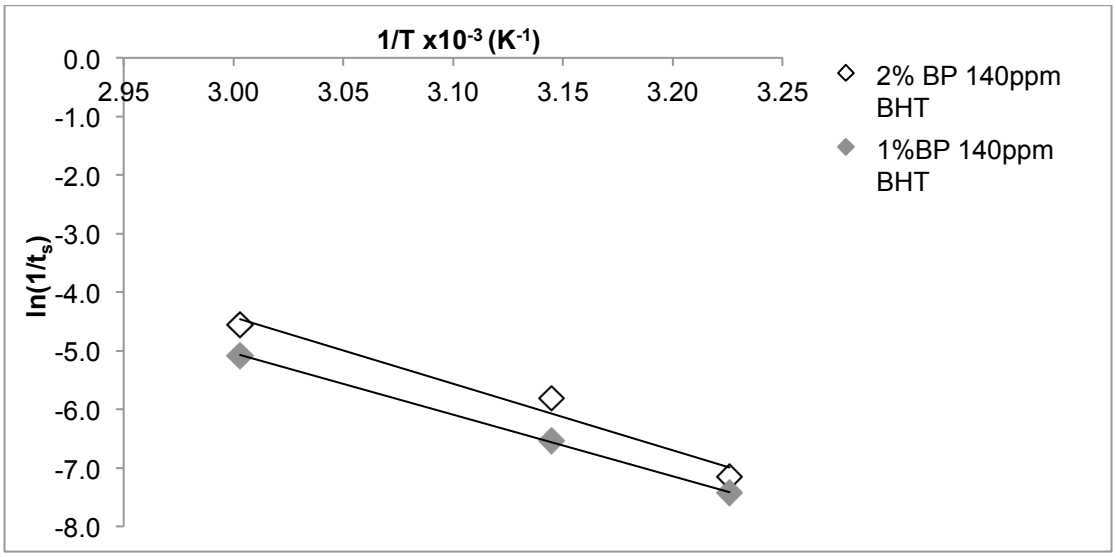

Figure 7-5 Plot of ln(1/ts) (y-axis) vs. 1/T (x-axis). The Activation energy (E_a) and frequency factor (A) for the 2 formulations can be found from the gradient and the intercept, respectively, of the line of best fit of the cure time vs. Temperature plot.

7.7 Discussion

7.7.1 Effect of Initiators

An increase in level of DMPT will result in a decrease in $t_{0.5}$. This is due to the decreased inhibition time, and also a faster reaction. It is thought that DMPT could acts to stabilize the free radicals that BP produces. Increasing the level of DMPT would therefore ill result in more stable free radicals reducing the time taken to 'use up' the BHT inhibitor prior to polymerization and increasing the reaction rate whilst polymerization has begun.

The factorial analysis results provided useful insight into the size of effects of variables on measured material parameters in previous chapters. In this chapter, however, the factorial analysis is difficult to interpret the effect of the BP, BP/BHT or the interactions on t_i as the a-values are very small.

An increase in BP means an increase in conversion. A low level of BP, interestingly, does still result in a level of conversion that is similar to Cortoss, Comp06, Simplex P and Palacos bone cements (Table 7-2). This is important as it suggests that if the level of BP is depleted (by up to 75 %) following storage then the formulation will still cure satisfactorily. A study by Hasenwinkel et al showed that level of DMPT had a significant effect on conversion/residual monomer of a two solution injectable MMA bone cement but that BP did not have a significant affect over the ranges investigated (35). The range of DMPT was similar to that used in this chapter, however the range of BP was higher, the lowest amount being coincident with the high amount used in this chapter. The level of inhibitor used by Hansenwinkel is not known and methyl methacrylate was used rather than the dimethacrylate monomer system used here. As seen in chapter 5, the monomers have a significant effect on conversion and curing times and this, in part, will explain the discrepancy between Hasenwinkel's study and this one. It is clear that the effects of DMPT and BP are dependent on the level used, with both

Hasenwinkel's study and this chapter showing different behavior for different levels of these chemicals. Furthermore, the type and level of inhibitor relative to the amount of BP is shown here to affect the action of the initiator and its effect on conversion. The difference in findings between Hasenwinkel's study and this one can therefore be attributed to the differences in levels of initiators and level and type of inhibitors.

Increasing the level of BP also decreases $t_{0.5}$ as Equation 7-1 below would suggest.

$$t_i t_{0.5} = \frac{[Z_0]}{R_i} = \frac{[Z_0]}{2fk_d[A][B]} \qquad \text{Equation 7-1}$$

If concentration of DMPT ([*A*]) and BP ([*B*]) and monomer system are constant, then *f* (initiator efficiency) should be constant for a given formulation in which initiator and monomer/filler systems are kept constant. It is clear that the effect of changing initiator levels is highly dependent on what monomer system is being used; chapter 5 and Rosentritt and Hasenwinkel have all shown different effects of increasing levels of BP and DMPT on cure time (34,138).

Equation 7-1 implies that changing the concentration of inhibitor should have a linear effect on the inhibition time but this was not the case; changing BHT by a factor of 4 changed the inhibition time, on average, by a factor of only 1.4. This discrepancy can be attributed to the level of inhibitor already present in the monomer when received from the manufacturer. The PPG from the manufacturer contains 100ppm BHT and 100ppm MEHQ, the UDMA contains between 100 and 200ppm MEHQ and the HEMA contains between 40 and 60ppm MEHQ. This means that when changing the amount of BHT from 18 – 71ppm, the actual factor change in total inhibitor amount could range from 1.25 to 1.3, whilst increasing BHT from 71 -– 286 ppm will result in a factor change of between 1.3 and 2.0. From this it is clear to see a more linear agreement in changing inhibitor amount to changing inhibition time. Obviously the experimental error

of this experiment reflects the unknown quantity of inhibitor in the monomer when received from the manufacturer as well as errors in measurement of the added BHT.

It is important to discuss here whether the manufacturer added inhibitor should be removed from the monomers prior to use. The aim of this project ultimately is to enable the production of a commercial composite bone cement. It was felt that it would be more useful to determine the effects of initiators and inhibitors over practical ranges on monomers in the state that they were received from the manufacturer to better simulate how a potential product would be manufactured.

There are interaction effects between the BP and DMPT; the BHT has a different effect at low levels of BP/DMPT compared to at high levels. Polymerization rate constants cannot, therefore, be determined from this factorial design experiment. For this reason overall trends in behaviour are thought to be more important and interesting than finding quantitative effects of the initiator system.

It has been shown that BHT has a linear effect on inhibition time when in high enough ratio with Camphorquinone light activated initiator [Rosentritt/Palin, 2010]. Similarly, Cook et al. found that BHT increased inhibition time effectively at low reaction rates only making it a good stabilizer (168).

Hasenwinkel et al. have reported how the level of BP and DMPT and inhibitors affect the mechanical properties of PMMA bone cements (34). It would be necessary to check the BFS and modulus and fracture behavior of the IFD formulations to fully understand the effects of altering the initiator system.

7.7.2 Accelerated Ageing Studies

Only one repeat for each formulation was performed; this was only designed to be a very preliminary study into the shelf lives for the materials at ranges of BP and BHT that have been used in previous chapters. The discussion that follows compares the Arrhenius coefficients found from this study to those in literature. In order to find the

statistical relevance of these results it is necessary to perform more repeats. Furthermore only two levels of BP have been investigated – to design a bone repair material with an adequate shelf life, an understanding of the effects of storing the DMPT paste and both BP and DMPT pastes with higher levels of inhibitor is required.

Increasing the level of BP is thought to increase the concentration of free radicals, increasing the number of molecular collisions that are successful and hence decreasing the time to set. It is expected that changing the level of BP should therefore only affect the frequency factor and the activation energy should be unaffected. The activation energy for the two formulations was similar, whilst the frequency factor differed by a factor of 24. This seems to fit with expected behavior although, as mentioned above, the 95% confidence interval cannot be found as only one repeat was performed. In a previous study by Shim et al. the activation energy for methyl methacrylate with BP were 129 $kJmol^{-1}$ whilst the frequency factor was found to be between 2.1 and 3.8 x 10^{18} (166). The activation energy for thermal decomposition of BP is quoted as being 124 $kJmol^{-1}$ by Odian (16). Both the activation energy and the frequency factor are dependent on how the BP interacts with the monomer system and so it is expected that they should be very different from the values found in this study. Furthermore neither Shim nor Odian have an inhibitor present; the efficiency of the BP and hence the kinetics of spontaneous polymerization will be affected by the presence of BHT.

The time to cure was predicted at 25 °C (room temperature) and 4 °C (refrigerated). It is envisaged that the level of BHT will have to be increased substantially to achieve similar shelf life values at 4 °C to Comp06 and Cortoss. From the BP/DMPT/BHT factorial design, it was seen that BHT is a more effective inhibitor when at large concentrations in comparison to BP. Furthermore it is thought that levels of BP will be consumed during the shelf life period and so it is clinically relevant that the PFC pastes still have high levels of conversion even at very low levels of BP (0.125 %).

7.8 Conclusions

The factorial analysis shows that the level of BP affects the conversion of the formulations when low amounts of BHT are present; increasing BP will significantly increase the conversion when a large quantity of BP relative to BHT is present. For the ranges of initiator that have been tested the BP level can be depleted by around 75 % and the formulation will still cure to a satisfactory level. There are interactions between all three variables with respect to conversion and so it is not possible to evaluate kinetic equation coefficients.

Neither the level of BP nor the level of DMPT, have a linear effect on the cure rate/time; the results of this factorial analysis contradict the previous work at the Eastman. The level of DMPT has the largest effect on the lead in time/time to 50% of the three variables investigated. This suggests that the effect on cure time and rate of lower BP and higher BHT can be balanced by addition of DMPT.

BHT has a more significant inhibiting action when the level of BP used is low.

It is clear that the effects of initiators and inhibitors are highly specific to the monomer system used. It is therefore necessary to determine the behavior of the initiator system over a suitable range to ensure reliable cure.

Decreasing the level of BP relative to BHT has been shown to increase the time to set (via spontaneous polymerization) and hence the shelf life of the BP paste of a PFC formulation. It is thought that changing the level of BP affects the frequency factor only, although more repeats are required to ascertain statistical relevance. Similar shelf life experiments should be performed for the DMPT paste and both pastes for a range of BHT levels.

8 Conclusions and Further Work.

This chapter summarises the main conclusions of each chapter of this project followed by a description of the further work necessary to further develop the prototype PFC formulation together with some preliminary data in some of these areas.

8.1 Conclusions

As mentioned in the introduction to this thesis, the ultimate goal of this project was to develop a composite material that is a viable alternative to PMMA and composite cements for bone repair – particularly in osteoporotic vertebral and femoral neck fracture fixation applications. The previous chapters have dealt with selection and tuning of components resulting in the production of a prototype PFC formulation that was then characterized in-vitro and implanted in-vivo to assess its curing and mechanical properties and its biological response. The initiator system of the prototype PFC was then investigated to establish its effects on the curing and shelf life of the material.

Inspection of the literature surrounding bone cements, in the introduction chapter, suggested that current PMMA bone cements had levels of residual monomer and polymerisation shrinkage that were too high. Conversely, composite bone cements were too stiff and without sufficient strength for load bearing applications.

In chapter 3, two composite bone cements, two PMMA bone cements and a dental composite material were investigated and characterized in terms of their chemistry/ microstructure, curing, shrinkage and mechanical properties. A novel Raman technique for characterizing the chemistry and structure of fracture surfaces together with SEM and EDX methods, visual inspection, FTIR cure analysis and biaxial mechanical testing enabled a comparison of the materials in terms of the properties that were deemed to be critical to bone cement success; namely, handling, residual monomer, curing time, strength, stiffness and fracture behaviour. The Raman mapping technique in particular

could be very useful for characterizing materials recovered from in-vivo to compare the chemistry of materials prepared in the operating room with subsequent contact to body tissues to those prepared in the laboratory and tested in vitro. The results of chapter 3 confirmed the reported problems with the materials investigated and the analysis methods used suggested that high molecular weight and flexible monomers combined with a silane treated filler would result in a material with high conversion and low shrinkage, good interfacial bond strengths enabling high strength, but with relatively high modulus.

In chapter 4, a selection of fillers and monomers were screened to ascertain their effect on composite properties. The silane treated glass (G_{4S}) enabled the best handling, PLR and composite strength compared to the other particulate fillers, whilst inclusion of barium proved to make the glass highly radiopaque. Silane treated glass fibres (F_{GS}), included at high levels, were found to prevent brittle fracture. Including HEMA increased conversion and strength of composites whilst incorporation of PPGDMA improved conversion and lowered composite modulus but did slightly reduce strength.

PPGDMA, G_{4S} glass and F_{GS} fibres were selected as the subject of a systematic study in chapter 5.

Within the range investigated, composites containing PPGDMA, G_{4S} filler and F_{GS} fibres were found to be syringeable and capable of achieving flexural strength comparable to current cement materials whilst having a lower modulus than Cortoss and Comp06. Potentially problematic BisGMA and TEGDMA can be replaced by UDMA and PPGDMA. The latter has not been used before in composites for bone repair but results in lower shrinkage and better conversion which could mean PFCs exhibit better biocompatibility than Cortoss. The effects of each variable on the curing kinetics were investigated. PFC curing profiles were compared to classical polymerisation reaction kinetics, and equations characterising each stage of the

reaction process were established. As PPGDMA has not been used before, this investigation was thought to give crucial insight into the potential of UDMA and PPGDMA to replace TEGDMA and BisGMA. The levels of filler and PPGDMA monomer had to be balanced to ensure good filler wetting for strength whilst maintaining low shrinkage. Incorporation of fibres could overcome the problem of brittle fracture of Cortoss.

A formulation with intermediate values of PPGDMA and PLR, with a high level of fibres was made as a prototype PFC formulation. The curing and mechanical properties of this prototype product, along with further in-vivo investigations, were presented in chapter six. Although easily syringeable, the viscosity of the prototype PFC formulation was too low for an in-vivo situation in which bleeding was not completely stemmed. The PFC materials were found to cure faster at 37 °C than at room temperature. The levels of PPGDMA and filler selected were found to produce a material with mechanical and fracture properties that compared favourably with current cement materials; strength was comparable whilst modulus was reduced compared to composite bone cements and brittle fracture was prevented. PFC is an implant material with good biocompatibility and radiopacity that may be suitable for use in humans for fixation of osteoporotic fractures via percutaneous vertebroplasty.

The monomer and filler systems of PFC materials were investigated but the initiator system was not optimized. In chapter 7, the effect of varying initiator and activator levels, of the prototype PFC formulaaltion, on the composite curing properties was investigated. It is clear from comparison of the results of this chapter and literature that the effects of initiators and inhibitors is highly specific to the monomer system used. It is therefore necessary to determine the behaviour of the initiator system over a suitable range to ensure reliable cure.

The relative levels of initiator and inhibitor are central to controlling spontaneous polymerization and hence the shelf life of the BP paste of a PFC formulation. It is thought that changing the level of BP affects the frequency factor only, although more repeats are required to ascertain statistical relevance.

In summary it is felt that the investigations described and discussed in this thesis show that the prototype PFC formulation could be an excellent alternative to PMMA and composite cements for osteoporotic vertebral fracture fixation and hip fracture screw augmentation. It is hoped that the Raman mapping of commercial materials and the investigations around the curing kinetics of the PPGDMA containing composites add something new to the extensive literature surrounding materials for bone repair.

8.2 Further Work

Whilst the handling, cure, flexural strength and modulus and fracture behaviour of PFC materials and commercial PMMA and composite bone cements have been characterized, there are some areas that could be investigated to further characterize these materials to better understand the effects of material composition on performance. This section will introduce these topics.

In the introduction chapter, porosity was discussed as having a major effect on the curing and mechanical properties of PMMA and composite bone cements (25,146) and vacuum mixing was shown to control the number and size of voids in PMMA materials (23,26). The porosity of PFCs and commercial materials was not measured in this project but an idea of the porosity was ascertained from inspection of the SEM images of the fracture surfaces of PFCs. It is hypothesised that evacuation of a PFC material could be used as part of a novel sterilisation technique. Some very preliminary studies into the feasibility of this technique have been conducted; PFC materials were mixed with chloroform and then evacuated to remove the chloroform. It is hoped that the chloroform could render the pastes sterile and evacuation would reduce porosity of the material. It is thought that evacuation was sufficient to remove the chloroform, as it was not detected in FTIR curing analysis and syringe delivery was unaffected, but did not affect the porosity, as it was found that neither the strength or modulus of PFC materials nor the curing were affected.

Generally composite bone cements are sterilized via aseptic mixing of monomers and conventional methods of sterilising filler materials. Chapter 6 showed that monomer toxicity and UV sterilisation of fillers was sufficient to prevent infection in a lapine implantation procedure. However, for human applications a more rigorous sterilisation procedure is required by ISO 5833 and ASTM F451. The ability of the chloroform-evacuation technique to sterilise the paste was not investigated. This is an essential next step in development of PFC materials for clinical use.

Polymerization shrinkage was calculated in this project but was not measured. Shrinkage has been found via a density bottle method by Buruiana (46) and computer controlled mercury dilatometer method by Skrtic (47). Measurement of shrinkage by one of these methods should be performed to fully evaluate the shrinkage calculation method.

In the chapter 7, very preliminary data was found regarding the shelf life of the BP containing paste of PFC materials. As mentioned in the conclusions section above, more repeats are required to assess the statistical relevance of the findings whilst similar shelf life experiments should be performed for the DMPT paste and both pastes for a range of BHT levels. Sideridou et al. found the Arrhenius coefficients of experimental bone cement formulations via DSC (169). Comparison with this technique is suggested as a method of evaluating the trends found via the varying incubator storage method of this project.

As the literature review demonstrated poor fatigue life is one of the major shortfalls of current bone repair materials. The addition of fibres has been shown to improve the fatigue response. In this project fibre addition was shown to prevent brittle fracture of PFC materials. The fatigue behaviour and fracture toughness of PFCs should be evaluated to give a complete picture of the effects of fibre addition. Methods for characterizing fatigue and fracture toughness are set out in ISO16402 and ISO13586 respectively. In ISO13586 the method for quantifying fracture toughness involves calculating the KIC for mode 1 crack opening under plane strain. Hasenwinkel et al. used a similar single edge notched test from ASTM E399-83 to evaluate KIC (also under plane strain), as a measure of the fracture toughness of PMMA materials (35). In ISO 16402 two methods of determining the fatigue response of materials are described. The first looks at a range of stress methods (defining standard S-N curves) the second looks only at low stress levels, and it is thought because the stresses on bone cements in vivo are mainly low levels stresses (particularly in the case of elderly

osteporotic patients) that the second method is critical for evaluating the fatigue of bone cement materials.

Water sorbtion & solubility

The water sorption and solubility of bone cements post cure would be interesting to investigate as bone cement materials must perform in a hydrated environment and water sorption could give give valuable information about possible degradation/wear mechanisms. The water sorption would be found by measuring mass and volume changes; ISO4049 provides tests for dental materials for these things, to date there is no equivalent standard for orthopaedic materials.

Viscosity

The viscosity of PMMA changes throughout mixing due to swelling of polymer beads in the MMA liquid. Composites containing non-organic fillers, however, exhibit constant viscosity until onset of cure. Rheology of composites was qualified by whether the material was syringeable. This property could be quantified by determining how it can flow through capilliary tubes or by using cone and plate viscometer prior to cure. This aparatus would enable both oscilliatory and continuous shear to be measured. It is suggested that continuous shear would be more relevant due to the continuous way in which the materials are sheared when used with a double barreled syringe and mixing tip. Also as mentioned in the introduction chapter, ISO5833 stipulates that viscosity should not change by more than 10% on storing, stability of viscosity, therefore, is also important. Qualitative handling properties are important too and surgeon feedback on how easy new materials are to work with is central to ensuring their success as products. Some of feedback has been determined following the in-vivo testing of the prototype PFC although implant site and volume were not the same as human arthroplasty/vertebroplasty.

Creep

All polymers exhibit viscoelastic behaviour, particularly this is important as in-vivo, strain rates experienced by the materials will vary significantly. Loading is often flexural and so as with strength, flexural stresses are common and hence tensile creep behaviour is therefore of particular interest for bone cement materials. ASTM D2990 has details of measuring both the compressive and tensile modulus of creep. The loading conditions in-vivo should be examined so that the predominant mode of stress on a material is determined so that meaningful data can be gleaned from creep tests of different sorts.

Impact

Impact strength testing is covered by ISO179/180. It is thought that bone cement materials should perform in a similar way to host bone in impact tests so that should traumatic overloading occur, the material will not act as a 'weak link'.

Biocompatibility

The possible levels of leachable agents from bone cement materials have been inferred, in this project, from degree of conversion data and molecular size. Leachable agents e.g. monomers could be measured by High Performance Liquid Chromatography (HPLC) analysis of fluid in which bone cements have been immersed during cure to simulate in-vivo curing conditions. This would give some idea of the species leached during and following cure.

8.3 Final Remarks

In conclusion, the author feels that this thesis has been a successful start to the development of an injectable composite bone repair material that would be well suited to fixation of osteoporotic bone in vertebroplasty and screw augmentation of hip fracture fixation procedures. The effects of incorporating a range of fillers and monomers on composite properties has been established and compared with literature. In particular this project has given insight into the effects on cure and mechanical composite properties of the novel diluent monomer PPGDMA. PPGDMA has the potential to produce materials that have superior properties to current materials.

9 Bibliography

1. Pryor LS, Gage E, Langevin C-J, Herrera F, Breithaupt AD, Gordon CR, et al. Review of Bone Substitutes. Craniomaxillofacial Trauma Reconstr. 2009 Oct;2(3):151–60.

2. Encyclopedia of biomaterials and biomedical engineering. 2nd ed. New York ; London: Informa Healthcare USA; 2008. 4 p.

3. Jaeblon T. Polymethylmethacrylate: properties and contemporary uses in orthopaedics. J Am Acad Orthop Surg. 2010 May;18(5):297–305.

4. Lewis G. Viscoelastic properties of injectable bone cements for orthopaedic applications: State-of-the-art review. J Biomed Mater Res Part B-Appl Biomater. 2011 Jul;98B(1):171–91.

5. Puska M, J. A, Vallittu P. Polymer Composites for Bone Reconstruction. In: Tesinova P, editor. Advances in Composite Materials - Analysis of Natural and Man-Made Materials [Internet]. InTech; 2011 [cited 2013 Jul 22]. Available from: http://www.intechopen.com/books/advances-in-composite-materials-analysis-of-natural-and-man-made-materials/polymer-composites-for-bone-reconstruction

6. Cancer Facts & Figures 2013. Am Cancer Soc Atlanta Ga. 2013;(500813).

7. Giannoudis PV, Dinopoulos H, Tsiridis E. Bone substitutes: an update. Injury. 2005 Nov;36 Suppl 3.

8. Van Staa TP, Dennison EM, Leufkens HGM, Cooper C. Epidemiology of fractures in England and Wales. Bone. 2001 Dec;29(6):517–22.

9. P. H, U. B. Bone substitutes in vertebroplasty. Eur Spine J. 2001 Oct 1;10:S205–S213.

10. Boyd D, Towler MR, Wren A, Clarkin OM. Comparison of an experimental bone cement with surgical Simplex® P, Spineplex® and Cortoss®. J Mater Sci Mater Med. 2008 Jan;19(4):1745–52.

11. Verlaan J-J, Cumhur Oner F, Dhert WJA. Anterior spinal column augmentation with injectable bone cements. Biomaterials. 2006 Jan;27(3):290–301.

12. Lewis G. Injectable bone cements for use in vertebroplasty and kyphoplasty: State-of-the-art review. J Biomed Mater Res B Appl Biomater. 2006;76B(2):456–68.

13. Stankewich CJ, Swiontkowski MF, Tencer AF, Yetkinler DN, Poser RD. Augmentation of femoral neck fracture fixation with an injectable calcium-phosphate bone mineral cement. J Orthop Res Off Publ Orthop Res Soc. 1996 Sep;14(5):786–93.

14. Mattsson P, Larsson S. Stability of internally fixed femoral neck fractures augmented with resorbable cement. A prospective randomized study using radiostereometry. Scand J Surg SJS Off Organ Finn Surg Soc Scand Surg Soc. 2003;92(3):215–9.

15. Saha S, Pal S. Mechanical properties of bone cement: A review. J Biomed Mater Res. 1984;18(4):435–62.

16. Odian G. Principles of Polymerization. 4th ed. Wiley-Interscience; 2004.

17. Odian G. Principles of Polymerization. 4th ed. Wiley-Interscience; 2004.

18. Lewis G. Alternative acrylic bone cement formulations for cemented arthroplasties: Present status, key issues, and future prospects. J Biomed Mater Res B Appl Biomater. 2008;84B(2):301–19.

19. Provenzano MJ, Murphy KPJ, Riley LH. Bone Cements: Review of Their Physiochemical and Biochemical Properties in Percutaneous Vertebroplasty. Am J Neuroradiol. 2004;25(7):1286 –1290.

20. Nomura Y, Teshima W, Kawahara T, Tanaka N, Ishibashi H, Okazaki M, et al. Genotoxicity of dental resin polymerization initiators in vitro. J Mater Sci Mater Med. 2006 Jan;17(1):29–32.

21. Lewis G. Properties of acrylic bone cement: State of the art review. J Biomed Mater Res. 1997;38(2):155–82.

22. Bridgens J, Davies S, Tilley L, Norman P, Stockley I. Orthopaedic bone cement: DO WE KNOW WHAT WE ARE USING? J Bone Jt Surg Br. 2008 May 1;90-B(5):643–7.

23. Wilkinson JM, Eveleigh R, Hamer AJ, Milne A, Miles AW, Stockley I. Effect of mixing technique on the properties of acrylic bone–cement. J Arthroplasty. 2000 Aug;15(5):663–7.

24. Jiranek WA, Hanssen AD, Greenwald AS. Antibiotic-Loaded Bone Cement for Infection Prophylaxis in Total Joint Replacement. J Bone Jt Surg Am. 2006 Nov 1;88(11):2487–500.

25. Linden U. Mechanical-Properties of Bone-Cement - Importance of the Mixing Technique. Clin Orthop. 1991 Nov;(272):274–8.

26. Macaulay W, DiGiovanni CW, Restrepo A, Saleh KJ, Walsh H, Crossett LS, et al. Differences in bone–cement porosity by vacuum mixing, centrifugation, and hand mixing. J Arthroplasty. 2002 Aug;17(5):569–75.

27. Mau H, Schelling K, Heisel C, Wang JS, Breusch SJ. Comparison of various vacuum mixing systems and bone cements as regards reliability, porosity and bending strength. Acta Orthop Scand. 2004 Apr;75(2):160–72.

28. Boger A, Bisig A, Bohner M, Heini P, Schneider E. Variation of the mechanical properties of PMMA to suit osteoporotic cancellous bone. J Biomater Sci Polym Ed. 2008;19(9):1125–42.

29. Fries IB, Fisher AA, Salvati EA. Contact dermatitis in surgeons from methylmethacrylate bone cement. J Bone Joint Surg Am. 1975 Jun;57(4):547–9.

30. Kuehn K-D, Ege W, Gopp U. Acrylic bone cements: composition and properties. Orthop Clin North Am. 2005 Jan;36(1):17–28.

31. Nieuwenhuijse MJ, Muijs SPJ, van Erkel AR, Dijkstra SPD. A clinical comparative study on low versus medium viscosity polymethylmetacrylate bone cement in percutaneous vertebroplasty: viscosity associated with cement leakage. Spine. 2010 Sep 15;35(20):E1037–1044.

32. Nieuwenhuijse MJ, Van Erkel AR, Dijkstra PDS. Cement leakage in percutaneous vertebroplasty for osteoporotic vertebral compression fractures: identification of risk factors. Spine J Off J North Am Spine Soc. 2011 Sep;11(9):839–48.

33. Muijs SPJ, van Erkel AR, Dijkstra PDS. Treatment of painful osteoporotic vertebral compression fractures A BRIEF REVIEW OF THE EVIDENCE FOR PERCUTANEOUS VERTEBROPLASTY. J Bone Jt Surg-Br Vol. 2011 Sep;93B(9):1149–53.

34. Hasenwinkel JM, Lautenschlager EP, Wixson RL, Gilbert JL. A novel high-viscosity, two-solution acrylic bone cement: effect of chemical composition on properties. J Biomed Mater Res. 1999 Oct;47(1):36–45.

35. Hasenwinkel JM, Lautenschlager EP, Wixson RL, Gilbert JL. Effect of initiation chemistry on the fracture toughness, fatigue strength, and residual monomer content of a novel high-viscosity, two-solution acrylic bone cement. J Biomed Mater Res. 2002 Mar 5;59(3):411–21.

36. Revell P, Braden M, Freeman M. Review of the biological response to a novel bone cement containing poly(ethyl methacrylate) and n-butyl methacrylate. Biomaterials. 1998 Sep;19(17):1579–86.

37. Santin M, Motta A, Borzachiello A, Nicolais L, Ambrosio L. Effect of PMMA cement radical polymerisation on the inflammatory response. J Mater Sci-Mater Med. 2004 Nov;15(11):1175–80.

38. He S, Scott C, Higham P. Mixing of acrylic bone cement: effect of oxygen on setting properties. Biomaterials. 2003 Dec;24(27):5045–8.

39. Heraeus Palacos R Instructions for use. Heraeus medical GmbH; 2008.

40. Stryker Simplex P Instructions for use. Stryker Howmedica Osteonics Corp.; 2009.

41. Kuehn K, Ege W, Gopp U. Acrylic bone cements: composition and properties. Orthop Clin North Am. 2005 Jan;36(1):17–+.

42. Gilbert JL, Hasenwinkel JM, Wixson RL, Lautenschlager EP. A theoretical and experimental analysis of polymerization shrinkage of bone cement: A potential major source of porosity. J Biomed Mater Res. 2000 Oct;52(1):210–8.

43. Kwong F, Power R. COMPARISON OF BONE CEMENT SHRINKAGE BETWEEN DIFFERENT POLYMETHYLMETHACRYLATE COMMERCIAL PREPARATIONS IN USE. J Bone Joint Surg Br. 2006 May 1;88-B(SUPP II):237–237.

44. Orr JF, Dunne NJ. Measurement of Shrinkage Stresses in PMMA Bone Cement. Appl Mech Mater. 2004;1-2:127–32.

45. Kinzl M, Boger A, Zysset PK, Pahr DH. The mechanical behavior of PMMA/bone specimens extracted from augmented vertebrae: a numerical study of interface

properties, PMMA shrinkage and trabecular bone damage. J Biomech. 2012 May 11;45(8):1478–84.

46. Buruiana T, Melinte V, Jitaru F, Aldea H, Buruiana EC. Photopolymerization Experiments and Properties of Some Urethane/Urea Methacrylates Tested in Dental Composites. J Compos Mater. 2012 Feb 1;46(4):371–82.

47. Skrtic D, Stansbury J., Antonucci J. Volumetric contraction and methacrylate conversion in photo-polymerized amorphous calcium phosphate/methacrylate composites. Biomaterials. 2003 Jun;24(14):2443–9.

48. Lopez A, Unosson E, Engqvist H, Persson C. Direct and interactive effects of three variables on properties of PMMA bone cement for vertebral body augmentation. J Mater Sci-Mater Med. 2011 Jun;22(6):1599–606.

49. Kane RJ, Yue W, Mason JJ, Roeder RK. Improved fatigue life of acrylic bone cements reinforced with zirconia fibers RID A-9398-2008. J Mech Behav Biomed Mater. 2010 Oct;3(7):504–11.

50. Moszner N, Salz U. New developments of polymeric dental composites. Prog Polym Sci. 2001 May;26(4):535–76.

51. National Toxicology Program U.S. Department of Health and Human Services. NTP-CERHR Monograph on the Potential Human Reproductive and Developmental effects of BisPhenol A. Center for the Evaluation of Risks to Human Reproduction; 2008 Sep. Report No.: NIH 08-5994.

52. Soderholm KJ, Mariotti A. BIS-GMA-based resins in dentistry: Are they safe? J Am Dent Assoc. 1999 Feb;130(2):201–9.

53. Teeguarden JG, Hanson-Drury S. A systematic review of Bisphenol A “low dose” studies in the context of human exposure: A case for establishing standards for reporting “low-dose” effects of chemicals. Food Chem Toxicol Int J Publ Br Ind Biol Res Assoc. 2013 Jul 16;62.

54. Lewis A. Drug Device Combination Products: Delivery Technologies and Applications. Lewis A, editor. Woodhead Publishing Ltd; 2009. 560 p.

55. Karmaker A, Prasad A, Sarkar N. Characterization of adsorbed silane on fillers used in dental composite restoratives and its effect on composite properties. J Mater Sci Mater Med. 2007 Jun 1;18(6):1157–62.

56. Xu H, Eichmiller F, Antonucci J, Schumacher G, Ives L. Dental resin composites containing ceramic whiskers and precured glass ionomer particles. Dent Mater. 2000 Sep;16(5):356–63.

57. Petersen R. Discontinuous fiber-reinforced composites above critical length. J Dent Res. 2005 Apr;84(4):365–70.

58. Gao Y, Sagi S, Zhang L, Liao Y, Cowles DM, Sun Y, et al. Electrospun nano-scaled glass fiber reinforcement of bis-GMA/TEGDMA dental composites. J Appl Polym Sci. 2008 Nov 15;110(4):2063–70.

59. Pomrink GJ, DiCicco MP, Clineff TD, Erbe EM. Evaluation of the reaction kinetics of CORTOSS, a thermoset cortical bone void filler. Biomaterials. 2003 Mar;24(6):1023–31.

60. Söderholm KJ, Mariotti A. BIS-GMA--based resins in dentistry: are they safe? J Am Dent Assoc 1939. 1999 Feb;130(2):201–9.

61. Gonçalves F, Kawano Y, Pfeifer C, Stansbury JW, Braga RR. Influence of BisGMA, TEGDMA, and BisEMA contents on viscosity, conversion, and flexural strength of experimental resins and composites. Eur J Oral Sci. 2009 Aug 1;117(4):442–6.

62. Chen L, Yu Q, Wang Y, Li H. BisGMA/TEGDMA dental composite containing high aspect-ratio hydroxyapatite nanofibers. Dent Mater. 2011 Nov;27(11):1187–95.

63. Lewis G, Xu H, Madigan S, Towler MR. Influence of strontia on various properties of Surgical Simplex (R) P acrylic bone cement and experimental variants. Acta Biomater. 2007 Nov;3(6):970–9.

64. Mehdawi I, Neel EAA, Valappil SP, Palmer G, Salih V, Pratten J, et al. Development of remineralizing, antibacterial dental materials. Acta Biomater. 2009 Sep;5(7):2525–39.

65. Garoushi S, Vallittu P, Lassila L. Short glass fiber reinforced restorative composite resin with semi-inter penetrating polymer network matrix. Dent Mater. 2007 Nov;23(11):1356–62.

66. Puska MA, Lassila LV, Närhi TO, Yli-Urpo AUO, Vallittu PK. Improvement of Mechanical Properties of Oligomer-modified Acrylic Bone Cement with Glass-fibers. Appl Compos Mater. 2004 Jan;11(1):17–31.

67. Annual Report Pursuant to Section 13 or 15(d) of the securities Exchange Act of 1934: Orthovita Inc. United States Securities and Exchange Commission; 2008. Report No.: 0-24517.

68. Imazato S, Torii M, Tsuchitani Y, McCabe JF, Russell RR. Incorporation of bacterial inhibitor into resin composite. J Dent Res. 1994 Aug;73(8):1437–43.

69. Merkhan IK, Hasenwinkel JM, Gilbert JL. Quantitative analysis of monomer vapor release from two-solution bone cement by using a novel FTIR technique. J Biomed Mater Res B Appl Biomater. 2005 Jul;74(1):643–8.

70. Rodrigues DC, Gilbert JL, Hasenwinkel JM. Two-solution bone cements with cross-linked micro and nano-particles for vertebral fracture applications: effects of zirconium dioxide content on the material and setting properties. J Biomed Mater Res B Appl Biomater. 2010 Jan;92(1):13–23.

71. Barszczewska-Rybarek IM. Quantitative determination of degree of conversion in photocured poly(urethane-dimethacrylate)s by Fourier transform infrared spectroscopy. J Appl Polym Sci. 2011 Aug 19;123(3):1604–11.

72. Antonucci JM, Regnault WF, Skrtic D. Polymerization shrinkage and stress development in amorphous calcium phosphate/urethane dimethacrylate polymeric composites. J Compos Mater. 2010 Feb 1;44(3):355.

73. Leung D, Spratt D, Pratten J, Gulabivala K, Mordan N, Young A. Chlorhexidine-releasing methacrylate dental composite materials. BIOMATERIALS. 2005 Dec;26(34):7145–53.

74. Sideridou I, Tserki V, Papanastasiou G. Effect of chemical structure on degree of conversion in light-cured dimethacrylate-based dental resins. Biomaterials. 2002 Apr;23(8):1819–29.

75. Sideridou ID, Achilias DS, Kostidou NC. Copolymerization kinetics of dental dimethacrylate resins initiated by a benzoyl peroxide/amine redox system RID B-7985-2010. J Appl Polym Sci. 2008 Jul 5;109(1):515–24.

76. Lewis G, Koole LH, van Hooy-Corstjens CSJ. Influence of powder-to-liquid monomer ratio on properties of an injectable iodine-containing acrylic bone cement for vertebroplasty and balloon kyphoplasty. J Biomed Mater Res B Appl Biomater. 2009 Nov 1;91B(2):537–44.

77. Antonucci J, Regnault W, Skrtic D. Polymerization Shrinkage and Stress Development in Amorphous Calcium Phosphate/Urethane Dimethacrylate Polymeric Composites. J Compos Mater. 2010 Feb;44(3):355–67.

78. Miyazaki CL, Medeiros IS, Matos J do R, rio, Rodrigues Filho LE. Thermal characterization of dental composites by TG/DTG and DSC. J Therm Anal Calorim. 2010;102(1):361 – 367.

79. Basaran C, Nie S, Hutchins CS, Ergun H. Influence of Interfacial Bond Strength on Fatigue Life and Thermo-Mechanical Behavior of a Particulate Composite: An Experimental Study. Int J Damage Mech. 2008 Mar 1;17(2):123–47.

80. Ormsby R, McNally T, Mitchell C, Dunne N. Incorporation of multiwalled carbon nanotubes to acrylic based bone cements: Effects on mechanical and thermal properties. J Mech Behav Biomed Mater. 2010 Feb;3(2):136–45.

81. Zhang H, Zhang M. Effect of surface treatment of hydroxyapatite whiskers on the mechanical properties of bis-GMA-based composites RID F-8331-2011. Biomed Mater. 2010 Oct;5(5).

82. Lucksanasombool P, Higgs WA., Higgs RJE., Swain MV. Toughness of glass fibres reinforced glass-ionomer cements. J Mat Sci. 2002;37:101–8.

83. Jancar J, Hynstova K, Pavelka V. Toughening of denture base resin with short deformable fibers. Compos Sci Technol. 2009 Mar;69(3-4):457–62.

84. Tacir I, Kama J, Zortuk M, Eskimez S. Flexural properties of glass fibre reinforced acrylic resin polymers. Aust Dent J. 2006 Mar;51(1):52–6.

85. Dodiuk-Kenig H, Lizenboim K, Roth S, Zalsman B, McHale WA, Jaffe M, et al. Performance Enhancement of Dental Composites Using Electrospun Nanofibers. J Nanomater. 2008;2008:1–6.

86. Puska M, Narhi T, Aho A, Yli-Urpo A, Vallittu P. Flexural properties of crosslinked and oligomer-modified glass-fibre reinforced acrylic bone cement. J Mater Sci-Mater Med. 2004 Sep;15(9):1037–43.

87. May-Pat A, Herrera-Kao W, Cauich-Rodríguez JV, Cervantes-Uc JM, Flores-Gallardo SG. Comparative study on the mechanical and fracture properties of acrylic bone cements prepared with monomers containing amine groups. J Mech Behav Biomed Mater. 2012 Feb;6:95–105.

88. Ho S, Young A. Synthesis, polymerisation and degradation of poly(lactide-co-propylene glycol) dimethacrylate adhesives. Eur Polym J. 2006 Aug;42(8):1775–85.

89. Young AM, Rafeeka SA, Howlett JA. FTIR investigation of monomer polymerisation and polyacid neutralisation kinetics and mechanisms in various aesthetic dental restorative materials. Biomaterials. 2004 Feb;25(5):823–33.

90. Hagan C, Orr J, Mitchell C, Dunne N. Real time monitoring of the polymerisation of PMMA bone cement using Raman spectroscopy. J Mater Sci Mater Med. 2009;20(12):2427–31.

91. Morgan DR, Kalachandra S, Shobha HK, Gunduz N, Stejskal EO. Analysis of a dimethacrylate copolymer (bis-GMA and TEGDMA) network by DSC and 13C solution and solid-state NMR spectroscopy. Biomaterials. 2000 Sep;21(18):1897–903.

92. Lovestead TM, Burdick JA, Anseth KS, Bowman CN. Understanding multivinyl monomer photopolymerization kinetics through modeling and GPC investigation of degradable networks. Polymer. 2005 Jul 25;46(16):6226–34.

93. Rojas SS, Frigo GJM, Bernardi MIB, Rastelli AN de S, Hernandes AC, Bagnato VS. Thermal and structural properties of commercial dental resins light-cured with blue emitting diodes (LEDs). J Therm Anal Calorim. 2010 Jan 1;99(1):263–8.

94. Larkin P. Infrared and Raman spectroscopy: principles and spectral interpretation. Amsterdam [etc.]: Elsevier; 2011.

95. Hofmann MP, Young AM, Gbureck U, Nazhat SN, Barralet JE. FTIR-monitoring of a fast setting brushite bone cement: effect of intermediate phases. J Mater Chem. 2006;16(31):3199–206.

96. Li J, Li H, Fok ASL, Watts DC. Multiple correlations of material parameters of light-cured dental composites. Dent Mater Off Publ Acad Dent Mater. 2009 Jul;25(7):829–36.

97. Rueggeberg F, Tamareselvy K. Resin cure determination by polymerization shrinkage. Dent Mater. 1995 Jul;11(4):265–8.

98. Obukuro M, Takahashi Y, Shimizu H. Effect of diameter of glass fibers on flexural properties of fiber-reinforced composites. Dent Mater J. 2008 Jul;27(4):541–8.

99. Chung SM, Yap AUJ, Chandra SP, Lim CT. Flexural strength of dental composite restoratives: Comparison of biaxial and three-point bending test. J Biomed Mater Res B Appl Biomater. 2004;71B(2):278–83.

100. Ban S, Anusavice KJ. Influence of test method on failure stress of brittle dental materials. J Dent Res. 1990 Dec;69(12):1791–9.

101. Palin W, Fleming G, Burke F, Marquis P, Randall R. Monomer conversion versus flexure strength of a novel dental composite. J Dent. 2003 Jul;31(5):341–51.

102. Marquis PM, Palin WM, Fleming GJP, Burke FJT, Randall BC. The relative reliability of biaxial and 3-point bend flexure testing of the strength of brittle light setting dental biomaterials. J Dent Res. 2003 Jun;82:B37–B37.

103. Palin WM, Fleming GJP, Marquis PM. The reliability of standardized flexure strength testing procedures for a light-activated resin-based composite. Dent Mater. 2005 Oct;21(10):911–9.

104. Pick B, Meira JBC, Driemeier L, Braga RR. A critical view on biaxial and short-beam uniaxial flexural strength tests applied to resin composites using Weibull, fractographic and finite element analyses. Dent Mater. 2010 Jan;26(1):83–90.

105. Byrne WP, Morrell R. Results of the UK Interlaboratory Strength Test Exercise (NPL report). National Physical Laboratory.Great Britain, Centre for Materials Measurement and Technology;

106. Kutz M. Handbook of Materials Selection. John Wiley & Sons; 2002. 1524 p.

107. Morrell R. Biaxial Flexural Strength Testing of Ceramic Materials, Measurement Good Practice Guide No. 12. National Physics Laboratory; 1999.

108. Lakes RS. Viscoelastic Solids. CRC Press; 1999. 494 p.

109. NAKAYAMA W, HALL D, GRENOBLE D, KATZ J. ELASTIC PROPERTIES OF DENTAL RESIN RESTORATIVE MATERIALS. J Dent Res. 1974;53(5):1121–6.

110. Versluis A, Tantbirojn D, Douglas W. Do dental composites always shrink toward the light? J Dent Res. 1998 Jun;77(6):1435–45.

111. PhD KJAD. Phillips' Science of Dental Materials, 12e. 12th ed. Saunders; 2012. 592 p.

112. Chung S, Yap A, Koh W, Tsai K, Lim C. Measurement of Poisson's ratio of dental composite restorative materials. BIOMATERIALS. 2004 Jun;25(13):2455–60.

113. Higgs W, Lucksanasombool P, Higgs R, Swain M. A simple method of determining the modulus of orthopedic bone cement. J Biomed Mater Res. 2001;58(2):188–95.

114. Sakaguchi RL, Wiltbank BD, Murchison CF. Prediction of composite elastic modulus and polymerization shrinkage by computational micromechanics. Dent Mater. 2004 May;20(4):397–401.

115. Hashin Z, Shtrikman S. A variational approach to the theory of the elastic behaviour of multiphase materials. J Mech Phys Solids. 1963 Mar;11(2):127–40.

116. Mechanics of composite materials. Taylor & Francis Group; 1999. 546 p.

117. Abou Neel E, Palmer G, Knowles J, Salih V, Young A. Chemical, modulus and cell attachment studies of reactive calcium phosphate filler-containing fast photo-curing, surface-degrading, polymeric bone adhesives. ACTA Biomater. 2010 Jul;6(7):2695–703.

118. Yuan F, Huang L. Molecular dynamics simulation of amorphous silica under uniaxial tension: From bulk to nanowire. J Non-Cryst Solids. 2012 Dec 15;358(24):3481–7.

119. Porto ICC de M, Soares LES, Martin AA, Cavalli V, Liporoni PCS. Influence of the photoinitiator system and light photoactivation units on the degree of conversion of dental composites. Braz Oral Res. 2010 Dec;24(4):475–81.

120. Willis H., Zichy VJ., Hendra P. The laser-Raman and infra-red spectra of poly(methyl methacrylate). Polymer. 1969;10:737–46.

121. Liang CY, Krimm S. Infrared spectra of high polymers. VI. Polystyrene. J Polym Sci. 2003 Mar 10;27(115):241–54.

122. Degen IA, Newman GA. Raman spectra of inorganic ions. Spectrochim Acta Part Mol Spectrosc. 1993 May;49(5–6):859–87.

123. Bell IM, Clark RJH, Gibbs PJ. UCL Chemistry - Chemistry Resources - Raman Spectroscopic Library [Internet]. [cited 2013 Jul 17]. Available from: http://www.chem.ucl.ac.uk/resources/raman/

124. Rehman I, Harper EJ, Bonfield W. In situ analysis of the degree of polymerization of bone cement by using FT-Raman spectroscopy. Biomaterials. 1996 Aug;17(16):1615–9.

125. Barberis P, Merle-Méjean T, Quintard P. On Raman spectroscopy of zirconium oxide films. J Nucl Mater. 1997 Aug 2;246(2–3):232–43.

126. Miletic V. Micro-Raman spectroscopic studies on the adhesive-dentine interface and the degree of conversion of dental adhesives [Internet]. 2010 [cited 2012 May 21]. Available from: http://www.era.lib.ed.ac.uk/handle/1842/4415

127. Carmona N, Ortega-Feliu I, Gómez-Tubío B, Villegas MA. Advantages and disadvantages of PIXE/PIGE, XRF and EDX spectrometries applied to archaeometric characterisation of glasses. Mater Charact. 2010 Feb;61(2):257–67.

128. Tiba A, Culbertson B. Development of visible light-cured multi-methacrylates for dental restorative materials. J Macromol Sci-PURE Appl Chem. 1999;A36(4):489–506.

129. Karacaer O, Polat T, Tezvergil A, Lassila L, Vallittu P. The effect of length and concentration of glass fibers on the mechanical properties of an injection- and a compression-molded denture base polymer. J Prosthet Dent. 2003 Oct;90(4):385–93.

130. Lee JK, Choi J-Y, Lim B-S, Lee Y-K, Sakaguchi RL. Change of properties during storage of a UDMA/TEGDMA dental resin. J Biomed Mater Res B Appl Biomater. 2004 Feb 15;68(2):216–21.

131. Tai H, Wang W, Vermonden T, Heath F, Hennink W, Alexander C, et al. Thermoresponsive and Photocrosslinkable PEGMEMA-PPGMA-EGDMA Copolymers from a One-Step ATRP Synthesis. BIOMACROMOLECULES. 2009 Apr;10(4):822–8.

132. Abou Neel EA, Salih V, Revell PA, Young AM. Viscoelastic and biological performance of low-modulus, reactive calcium phosphate-filled, degradable, polymeric bone adhesives. Acta Biomater. 2012 Jan;8(1):313–20.

133. Zhao X, Olsen I, Li H, Gellynck K, Buxton P, Knowles J, et al. Reactive calcium-phosphate-containing poly(ester-co-ether) methacrylate bone adhesives: Chemical, mechanical and biological considerations. ACTA Biomater. 2010 Mar;6(3):845–55.

134. Sohn HY, Moreland C. The effect of particle size distribution on packing density. Can J Chem Eng. 1968;46(3):162–7.

135. Du M, Zheng Y. Degree of conversion and mechanical properties studies of UDMA based materials for producing dental posts. Polym Compos. 2008 Mar 24;29(6):623–30.

136. Qin C, Xu J, Zhang Y. Spectroscopic investigation of the function of aqueous 2-hydroxyethylmethacrylate/glutaraldehyde solution as a dentin desensitizer. Eur J Oral Sci. 2006 Aug;114(4):354–9.

137. Sideridou ID, Achilias DS, Karava O. Reactivity of Benzoyl Peroxide/Amine System as an Initiator for the Free Radical Polymerization of Dental and Orthopaedic Dimethacrylate Monomers: Effect of the Amine and Monomer Chemical Structure. Macromolecules. 2006;39(6):2072–80.

138. Rosentritt M, Shortall AC, Palin WM. Dynamic monitoring of curing photoactive resins: A methods comparison. Dent Mater. 2010 Jun;26(6):565–70.

139. Young RJ, Lovell PA. Introduction to Polymers. 2nd ed. CRC Press; 1991.

140. Turi EA. Thermal characterization of polymeric materials. Academic Press; 1997. 1200 p.

141. Sandner B, Kammer S, Wartewig S. Crosslinking copolymerization of epoxy methacrylates as studied by Fourier transform Raman spectroscopy. Polymer. 1996 Oct;37(21):4705–12.

142. Vallittu P. Oxygen inhibition of autopolymerization of polymethyl methacrylate-glass fibre composite. J Mater Sci-Mater Med. 1997 Aug;8(8):489–92.

143. Shi L, Shi L, Wang L, Duan Y, Lei W, Wang Z, et al. The Improved Biological Performance of a Novel Low Elastic Modulus Implant. PLoS ONE. 2013 Feb 21;8(2):e55015.

144. Belkoff S, Mathis J, Erbe E, Fenton D. Biomechanical evaluation of a new bone cement for use in vertebroplasty. Spine. 2000 May 1;25(9):1061–4.

145. Boger A, Heini P, Windolf M, Schneider E. Adjacent vertebral failure after vertebroplasty: a biomechanical study of low-modulus PMMA cement. Eur Spine J. 2007 Aug 23;16(12):2118–25.

146. Boger A, Bohner M, Heini P, Verrier S, Schneider E. Properties of an injectable low modulus PMMA bone cement for osteoporotic bone. J Biomed Mater Res B Appl Biomater. 2008 Aug 1;86B(2):474–82.

147. Calais J, Soderholm K. Influence of Filler Type and Water Exposure on Flexural Strength of Experimental Composite Resins. J Dent Res. 1988 May;67(5):836–40.

148. Rahaman MN, Day DE, Bal BS, Fu Q, Jung SB, Bonewald LF, et al. Bioactive glass in tissue engineering. Acta Biomater. 2011 Jun;7(6):2355–73.

149. Soderholm K. Degradation of Glass Filler in Experimental Composites. J Dent Res. 1981;60(11):1867–75.

150. Ferracane JL, Berge HX, Condon JR. In vitro aging of dental composites in water - Effect of degree of conversion, filler volume, and filler/matrix coupling. J Biomed Mater Res. 1998 Dec 5;42(3):465–72.

151. Robinson V. Finding alternatives: an overview of the 3Rs and the use of animals in research. Sch Sci Rev. 2005 Dec;87(319):111–4.

152. Buckwalter JA, Grodzinsky AJ. Loading of healing bone, fibrous tissue, and muscle: implications for orthopaedic practice. J Am Acad Orthop Surg. 1999 Oct;7(5):291–9.

153. Vats HS, McKiernan FE. Infected vertebroplasty: case report and review of literature. Spine. 2006 Oct 15;31(22):E859–862.

154. Eriksson RA, Albrektsson T. The effect of heat on bone regeneration: An experimental study in the rabbit using the bone growth chamber. J Oral Maxillofac Surg. 1984 Nov;42(11):705–11.

155. Gruen T, Markolf K, Amstutz H. Effects of Laminations and Blood Entrapment on Strength of Acrylic Bone Cement. Clin Orthop. 1976;(119):250–5.

156. Majkowski R, Bannister G, Miles A. The Effect of Bleeding on the Cement-Bone Interface - an Experimental-Study. Clin Orthop. 1994 Feb;(299):293–7.

157. Benjamin JB, Gie GA, Lee AJ, Ling RS, Volz RG. Cementing technique and the effects of bleeding. J Bone Joint Surg Br. 1987 Aug 1;69-B(4):620–4.

158. Majkowski R, Miles A, Bannister G, Perkins J, Taylor G. Bone Surface Preparation in Cemented Joint Replacement. J Bone Jt Surg-Br Vol. 1993 May;75(3):459–63.

159. Togawa D, Bauer T, Lieberman I, Takikawa S. Histologic evaluation of human vertebral bodies after vertebral augmentation with polymethyl methacrylate. Spine. 2003 Jul 15;28(14):1521–7.

160. Piattelli A, Scarano A, Piattelli M, Matarasso S. Cellular colonization and bone formation into expanded polytetrafluoroethylene membranes: a light microscopical and histochemical time course study in the rabbit. J Periodontol. 1996 Jul;67(7):720–5.

161. Erbe EM, Clineff TD, Gualtieri G. Comparison of a new bisphenol-a-glycidyl dimethacrylate-based cortical bone void filler with polymethyl methacrylate. Eur Spine J Off Publ Eur Spine Soc Eur Spinal Deform Soc Eur Sect Cerv Spine Res Soc. 2001 Oct;10 Suppl 2:S147–152.

162. Verlaan JJ, Oner FC, Slootweg PJ, Verbout AJ, Dhert WJA. Histologic changes after vertebroplasty. J Bone Joint Surg Am. 2004 Jun;86-A(6):1230–8.

163. Urrutia J, Bono CM, Mery P, Rojas C. Early histologic changes following polymethylmethacrylate injection (Vertebroplasty) in rabbit lumbar vertebrae. Spine. 2008 Apr 15;33(8):877–82.

164. Kobayashi N, Togawa D, Fujishiro T, Powell KA, Turner AS, Seim HB 3rd, et al. Histological and radiographic evaluation of polymethylmethacrylate with two different concentrations of barium sulfate in a sheep vertebroplasty model. J Biomed Mater Res A. 2005 Oct 1;75(1):123–7.

165. Khan MA, Young A, Main K. Low Monomer Content, High Strength Composite Bone Cements. ACTAPRESS; 2013 [cited 2013 Aug 8]. Available from: http://www.actapress.com/PaperInfo.aspx?paperId=454953

166. Shim J, Warner S, Hasenwinkel J, Gilbert J. Analysis of the shelf life of a two-solution bone cement. BIOMATERIALS. 2005 Jul;26(19):4181–7.

167. ASTM F1980 -07 Standard Guide for Accelerated Aging of Sterile Barrier Systems for Medical Devices [Internet]. [cited 2010 Nov 8]. Available from: http://www.astm.org/Standards/F1980.htm

168. Cook W, Chen F, Pattison D, Hopson P, Beaujon M. Thermal polymerization of thiol-ene network-forming systems. Polym Int. 2007 Dec;56(12):1572–9.

169. Achilias D, Sideridou I. Study of the effect of two BPO/amine initiation systems on the free-radical polymerization of MMA used in dental resins and bone cements RID B-7985-2010. J Macromol Sci-Pure Appl Chem. 2002;A39(12):1435–50.